# Regeneration of decellularised tendon by human mesenchymal stem cells in response to uniaxial tensile strain

Normalina Sandora

Submitted in accordance with the requirements for the degree of

Doctor of Philosophy (PhD)

The University of Leeds

School of Mechanical Engineering

School of Biomedical Sciences

September 2016

The candidate confirms that the work submitted is her own and that appropriate credit

has been given where reference has been made to the work of others

This copy has been supplied on the understanding that it is copyright material and that

no quotation from the thesis may be published without proper acknowledgement

# Acknowledgement

I would like to thank my supervisor, Professor Eileen Ingham and Professor John Fisher, for whom that without them, I would not be what I am today. No words to describe how grateful I am, by showing me how hard work and delicate approach make things worked. This training has shaped me, and changed my view of science and life! Your words will forever be remembered. I also would like to thank Professor Joanne Tipper, for always believes in me, stands by me..

Also to Daniel Thomas, my lab buddy, thank you for always being so helpful. I think those machines were just listened you! To Gemma Jones who showed me how to decellularise the scaffolds, to Blessing for being a PCR teacher, to Iraklis for training me in cell handling, to Amisha Densai to show me the biomechanical testing, to Andrew Aldrige, I love those MSCs, they are so cute, thanks! For everyone in the lab, Ruth, Ash, Jenny, Emily, Helen, Lindsey.., thanks for laughing together and listened to my tears! Especially for Fatima, Jayna, and Saurabh, thanks for being my friends. For all of the technicians in Biology; Fiona, Sha, Natalie, thanks! For the engineering technicians; Phil, thanks for helping me to design the dissection clamp, for Irvin; the Mr Load-Cell, and thanks for those pig legs, for Lee; the Mr TenCell, thanks. For Rhys Moore to draw my dissection clamp in details and everyone that I could not name one by one, thanks..

To my Natasha and Kevin, my daughter and son, thanks for being such a beautiful life for me! Every single second with you is so darlingly sweet, and we had had such a precious moment in the UK! To Karim, my husband, thanks for keep supporting me! My Mom to whom had made this happened, thanks!! To my Dad, Elly, Emilia, and Ruby; thanks to make this PhD easier, sorry for being so selfish and so out of mind.. And most of all; thanks to the Higher Education of the Indonesia for sponsoring me and the EPRSE to pay my research! Thank you so much.

# Abstract

Injury of ligaments is very common, and a total tear of the anterior cruciate ligament (ACL) demands replacement. Ideally, a graft for ligament replacement should be able to regenerate into a native like ligament, and restore physiological and anatomical function immediately after transplantation. The University of Leeds has developed a protocol to generate an acellular tendon scaffold derived from allograft/ xenograft using decellularisation technology. The aims of the study were to study the differentiation of human bone marrow derived multipotential stromal cells (BM-MSC) seeded onto the decellularised porcine patella tendon scaffold in response to cyclic tensile strain.

Porcine patellar tendons were harvested and decellularised using the Leeds protocol. The decellularised tendon scaffolds were then characterised to determine their: (i) acellularity, (ii) histoarchitecture, (iii) extracellular matrix components (iv) levels of DNA (v) sterility, and (vi) biocompatibility. The decellularisation protocol was found to have minimal effect on the tissue histoarchitecture, and consistently generated sterile, non-toxic acellular scaffolds among different batches, with 98 – 99 % DNA removal compared to native tissue. Both porcine and human BM-MSCs were characterised using a range of antibodies to CD markers and trilineage differentiation and shown to have properties consistent with multipotential stromal cells.

Human BM-MSCs were seeded directly onto appropriately sized samples of porcine patella tendon scaffolds at $1 \times 10^5$ cells.cm$^{-2}$ for 12 hours, and then transferred to culture wells of TenCell-1 (a physically interactive rig for delivery of cyclic tensile strain). The cell-seeded tendon scaffolds were cultured either statically or with 4, 6 or 8 % cyclic tensile strain for 4/24 hours at 1 Hz, for 7 days. The response of the cells to cyclic tensile strain was investigated using viability assays (Live/Dead assay and ATPlite™ assay), histology, immunohistochemistry and gene expression analysis (RT-qPCR and gel electrophoresis). The mechanical properties of the scaffolds before and after incubation with cells were determined using uniaxial tensile testing. Under 4, 6 and 8 % cyclic tensile strain, the cell seeded scaffolds had a histological appearance of tendon-like tissue. When cultured under 6 and 8 % cyclic tensile strain, there was evidence that the MSCs were differentiating into tenogenic cells by expressing scleraxis, tenascin C, collagen I and collagen III genes. Cell-seeded scaffolds cultured under 6 % cyclic tensile strain had the highest viability and the matrix stiffness, was significantly increased compared to cell-seeded scaffolds cultured at 4 or 8 % cyclic tensile strain. The cell-seeded scaffolds incubated statically for 7 days showed matrix disorganization, had lower cell viability and less cell infiltration compared to samples incubated with cyclic strain.

# Table of Contents

# List of Tables

# List of Equations

# List of Figures

# List of Abbreviations

| | |
|---|---|
| (v/v) | Volume per volume |
| (w/v) | Weight per volume |
| ACL | Anterior cruciate ligament |
| ANOVA | Analysis of variance |
| ATP | Adenosine triphosphate |
| BM-MSCs | Bone marrow mesenchymal stem cells |
| BMP | Bone morphogenic protein |
| bp | Basepair |
| CD | Cluster of differentiation |
| cDNA | Coding DNA |
| CFU-F | Colony forming unit-fibroblasts |
| CPS | Count per second |
| DAPI | 4',6-diamidino-2-phenylindole |
| DMEM | Dulbecco's modified Eagles medium |
| DMSO | Dimethyl suphoxide |
| DNA | Deoxyribonucleic acid |
| ECM | Extracellular matrix |
| EDTA | Disodium ethylenediaminetetraacetic acid |
| FACS | Fluoresecence-activated cell sorting |
| FBA | Fresh blood agar |
| FCS | Fetal calf serum |
| FDA | Food and drug administration |
| FITC | Fluorescein isothyocyanate |
| GADPH | Glyceraldehyde 3-phosphate dehydrogenase |
| GAGs | Glycosaminoglycans |

| | |
|---|---|
| GMEM | Glasgow's minimum essential medium |
| h | Hour |
| H&E | Haematoxylin and eosin |
| HLA | Human leukocyte antigen |
| hMSCs | Human mesenchymal stem cells |
| Ig | Immunoglobulin |
| IGF | Insulin like growth factor |
| IL | Interleukin |
| ISCT | International Society of Cellular Theraphy |
| ITS | Insulin, transferrin, and selenium |
| MAPK | Mitogen-activated protein kinases |
| MHC | Major histocompatibility |
| min | Minute |
| mRNA | Messenger ribonucleic acid |
| MSC | Mesenchymal stem cell |
| NBF | Neutral buffered formalin |
| ns | Not significant |
| p | Passage |
| PAA | Peracetic acid |
| PBS | Phosphate buffer saline |
| PCL | Posterior cruciate ligament |
| PTFE | Polytetrafluoro-ethylene |
| pMSCs | Porcine mesenchymal stem cells |
| PPARγ | Peroxisome proliferator-activated receptor gamma |
| PPT | Porcine patellar tendon |
| qRT-PCR | Quantitative reversed transcription polymerase chain reaction |
| RDD | DNA extraction buffer (Qiagen) |

RLT   Lysis buffer (Qiagen)

RNA   Ribonucleic acid

ROM   Range of motion

RPE   Retinal pigment epithelial cells

Runx2   Runt-related transcription factor 2

SDS   Sodium dodecyl sulphate

T-0   Time zero

TGF-α   Transforming growth factor alpha

TGF-β   Transforming growth factor beta

TPB   Tryptose phosphate broth

XTT   2,3-Bis-(2-Methoxy-4-Nitro-5-Sulfophenyl)-2*H*-Tetrazolium-5-

Carboxanilide

# Chapter 1 General Introduction

The word ligament comes from *ligare,* in Latin this means to bind, as ligaments attach to bones at two ends in articulating joints in order to guide and maintain joint movement in congruency (Chen et al., 2003a). Injury to ligaments is extremely common, which occurs mostly in the extremities. Annually, there are more than 800,000 patients hospitalised with ligament and tendons injuries across the world (Butler et al., 2003). About 400,000 hospital visits for ligament injuries were recorded in the USA in 2005 (Hing et al., 2006). Generally, about 90 % of knee injuries involve the anterior cruciate ligament (ACL), with or without injury of the medial collateral ligament (MCL) (Miyasaka et al., 1991, MacLean and Gratzer, 2011). Injuries to the ACL have been reported to occur in 1,147/100,000 of the population in New Zealand (Gianotti et al., 2009), and about 350,000 ACL reconstructions annually are performed in the US (Hing et al., 2006), while in the UK, there were about 13,941 ACL reconstructions in 2012 (annually 13.5% incidence per 100,000 English population) (Jameson et al., 2012). In the younger population, ligament injury occurs mainly as a result of sports or daily activities, and this trend is also seen among the eldery.

Ligaments possess a poor intrinsic healing capacity after or without clinical intervention due to their low cellularity and vascularity (Frank et al., 1985, Doroski et al., 2007). A tear or rupture of the ligament causes pain and joint instability, and leads to premature osteoarthritis if not replaced. The current gold standard for knee ligament replacement is still the use of autograft of patellar or hamstring tendon. Nevertheless, harvesting the autograft causes secondary surgical morbidity of the harvest site and increases the risk of infection. The healing of the patella donor site requires six months to one year to recover (Yazdanshenas et al., 2015). Allografts offer excellent clinical outcomes, but their use is limited by the potential for immunological rejection, insufficient supply and lack of ideal sterilization methods. Hence, neither autografts nor allografts are the ideal options for ligament substitution. Different surgical procedures have also been introduced to increase the success rate of ligament reconstruction, although the techniques to repair or replace the ACL or MCL were reported not to fully satisfy either surgeons or

patients. About 20 – 25 % of post reconstruction patients, return for other tissue damage of the knee caused by the unstable knee joint (Aglietti et al., 1997, Vieira et al., 2009). In order to overcome these limitations, alternative sources of ligament replacements such as synthetic and biological materials are increasingly sought.

## 1.1. Ligament function and properties; characteristics of the ACL

### 1.1.1. Anatomy of the knee joint

#### 1.1.1.1. Embryology of the knee

Understanding of knee development during the embryological and foetal stages can provide knowledge of the physiological and pathological processes that can be found in later life.

Lower limb buds start to appear during the embryonic period from the scleroblastema at 4 weeks after fertilization (Gardner and O'Rahilly, 1968), differentiate into complete infantile limbs within two weeks, then undergo maturation until birth [Figure 1.1 A] (Watanabe, 1974). Gray and Gardner (1950) believed that the cruciate ligaments develop from blastemal derivates, whilst Haines (1953) concluded that they differentiate from extra blastemal sites. Nevertheless, Haines agreed that the human articular system is formed by the condensation of the blastemata into a primitive articular cavity. They both reported that strands of knee ligament collagen could be clearly identified 14 and 19-weeks after fertilization, orientated in a similar direction to the adult and parallel to vascular and nerve circuits (Gray and Gardner, 1950, Haines, 1953). The ACL, meniscus and peripheral knee joint blood vessels can be identified approximately 7½ to 8 weeks post fertilization and the arrangement resembles that found in the adult knee joint by the end of the 8th week [Figure 1.1. B]. The patella ligament can be identified as early as 6 weeks after fertilization and becomes obvious at 7 weeks. During the 7th week of gestation, the fibular collateral ligament and patellar bone condense and can be observed and distinguished after 18 weeks [Figure 1.1. C] (Gardner and O'Rahilly, 1968). The condensation of the ACL begins before the knee joint cavitation and it is surrounded by the mesentery-like synovial fold, that

originates from the posterior capsule, therefore the ACL remains extra-synovial (Duthon et al., 2006).
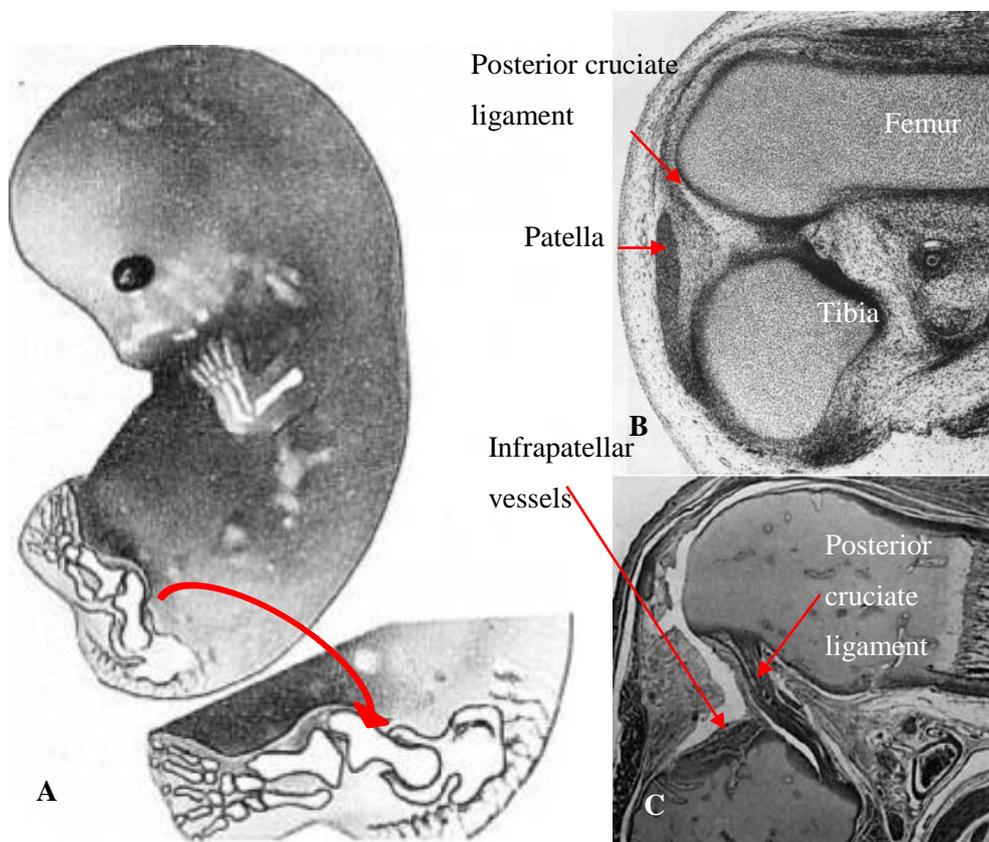


**Figure 1.1 Human embryo of a 7½ - 8-week gestation.** (A) at 8 weeks has all the differentiated components including limb details. This image is taken from Watanabe (1974). (B) Sagittal sections of a 7½ - 8-week embryonic knee, femur and tibia. The cruciate ligaments can be identified as cellular and oriented structures. This image is taken from Gardner and O'Rahilly (1968). (C) Parasagittal section of the right knee from an 18-week foetus, the posterior cruciate ligament (PCL) is shown from its origin and insertion. Blood vessels can be seen at the tibia attachment of the ACL to the infrapatellar region. This image is taken from Gray and Gardner (1950).

Generally, the critical period of human limb development is between 3 and 6 weeks of gestation, when the limb buds start to emerge. At this time, the embryo is very sensitive to any teratogenic agents, for example Thalidomide that caused the devastating effects of epidemic phocomelias, shocked Germany and the world between 1959-1962 (Gray and Gardner, 1950, Gardner and O'Rahilly, 1968). Complete agenesis of the ACL is a very rare anomaly, due to genetic errors, that can be found in several diseases such as femur-fibula-ulna (FFU) syndrome

(Fuhrmann et al., 1980), thrombocytopenia absent radius (TAR) syndrome (Heron et al., 2001), and femur shortness (Ergun et al., 2008).

### 1.1.1.2. Anatomy of the knee

Anatomical knowledge is fundamental for the tissue engineer to develop an anatomically correct substitute tissue replacement that is able to function and incorporate into its surroundings.

The knee joint is a synovial joint articulation involving the femur, tibia, fibula and patella [Figure 1.2]. In normal healthy adults, each bone surface is covered by 4 mm thickness of articular cartilage, and the joint is enclosed by a synovial membrane. The shape of the lateral and medial menisci in the articulation, compensates for the anisotropic nature of the tibial plateau to facilitate the gliding movement of the tibia over the femur (Kapandji, 1970). The lower limb muscles (quadriceps, sartorius, gracilis, tensor fasciae latae, hamstring and gastrocnemius) and the knee ligaments (ACL, PCL, medial and lateral collateral ligament) provide knee stabilization (Al-Turaiki, 1986).
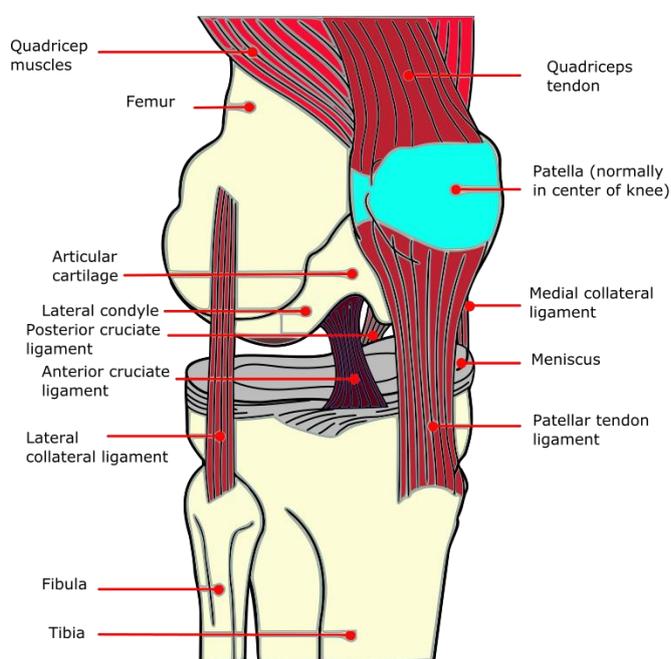


**Figure 1.2 ACL of the right knee joint from the anterior view with other knee components.** Reproduced from https://commons.wikimedia.org/wiki/File:Knee_diagram-fr_ACL_PCL.svg

The ACL and PCL cross each other, where the ACL originates from the anterior tibiae intercondylar notch and inserts upwards and backwards to the lateral femoral condyle, whilst the PCL emanates from the posterior intercondylar notchs of the tibia and inserts upwards and forwards into the lateral part of the medial femoral condyle [Figure 1.2].

The average length of the ACL is $31 \pm 3$ mm, the thickness is $5 \pm 1$ mm and width is $10 \pm 2$ mm. As the knee is flexed to 90 degrees, the angle between the ACL and the long axis of the femur is approximately $28 \pm 4$ degrees. At $0^0$ knee flexion, the ACL is elongated 10 mm on average from flexion to extension and twists $90^0$ as the knee undergoes $90^0$ of flexion (Odensten and Gillquist, 1985).

### 1.1.2. The vascular and lymphatic supply of the ACL

A blood supply is crucial to feed knee tissue and the fibroblasts of the ligaments, in order to maintain its function. Understanding of vascularisation in the knee is important for improving the success of tissue replacement therapies in the knee joint as the vascular networks along with the lymphatic system play an important role in tissue repair and the healing process (Greenfield, 1993).

The ACL is predominantly supplied by the middle geniculate, whist the distal part is fed by the inferior branch [Figure 1.3 A] (Arnoczky et al., 1979). The lateral and medial superior genicular branches are anastomosed, such that both terminals form a peri-ligamentous network to supply the synovial fold around the ligament. No vascularisation or lymphatic network can be identified at the bone-ligament interface with the femur or tibia, and up to 0.5 cm proximal from the tibiae insertion. The microvasculature was detected using immunohistochemical staining for laminin in the basal membrane of blood vessels and by the reaction to 5'-nucleotidase in the lymphatic endothelium. For the lymphatics labelling, the ACL was isolated within 48 hr after death, frozen sectioned and fixed with 10 % NBF (neutral buffered formalin), followed by incubation in medium modified after Heusermann, containing 2 mM Adenosine-mono-

phosphate (AMP) and the lymphatic endothelium was visualised by a dark precipitation of lead

sulphide [Figure 1.3. B] (Petersen and Tillmann, 1999).
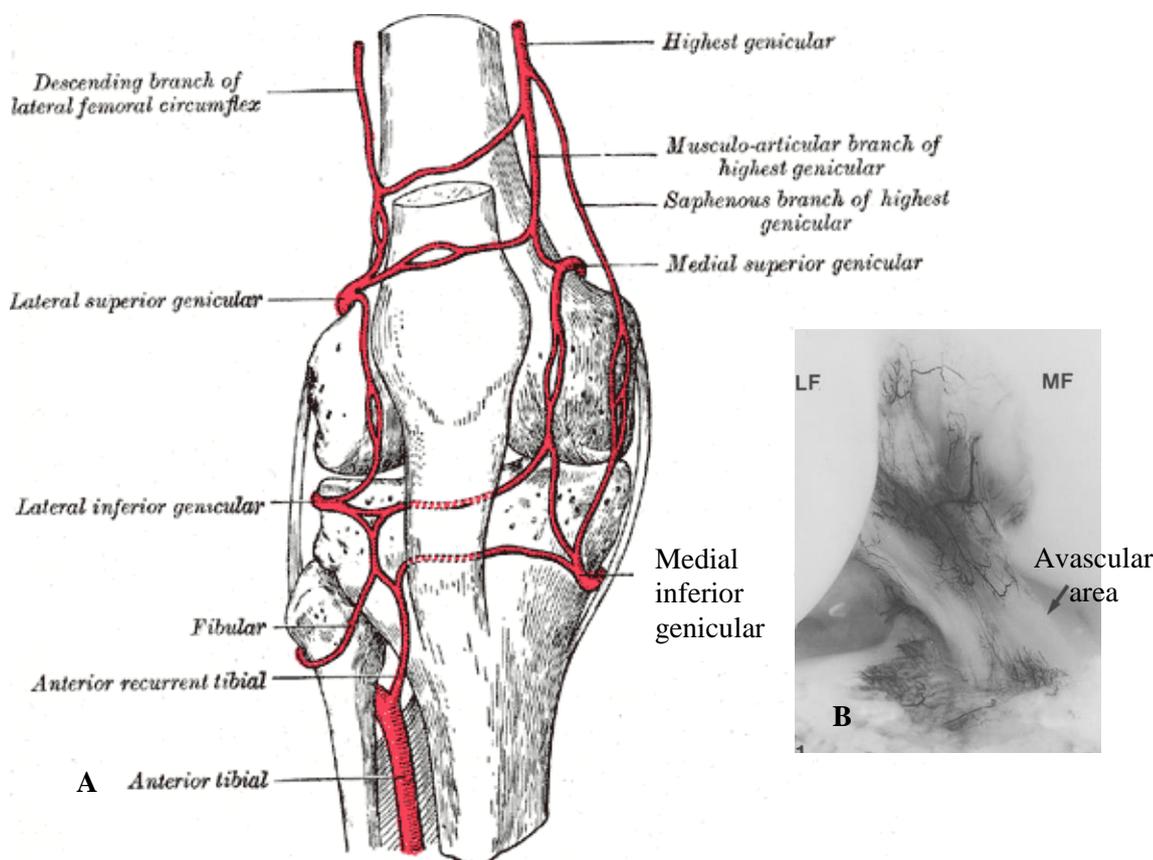


**Figure 1.3 Knee vascularisation** (A) Circum-patellar anastomoses of the right knee, from the anterior view. This image was derived from https://en.wikipedia.org/wiki/Knee. (B) ACL vascularisation imaging using India ink injection through the femoral artery into a cadaveric right knee. The arrow indicates the avascular area at 0.5 cm proximal to the origin at the tibial interface and has been confirmed by a lack of laminin labelling of that area. This image is taken from Petersen and Tillmann (1999).

### 1.1.3. Neuro-anatomy of the knee

Understanding innervation in the knee is important to guide accurate diagnosis of injured area

of the knee, while understanding the neuro-histology can enhance the success of tissue

replacement therapies in the knee joint. Knee joint innervation follows Hilton's law, which

states that the efferent motor neurons control knee movement in response to afferent stimulation

from the knee capsule (Hilton, 1891), ligaments (Gardner, 1948), retinaculum and bone head

(Horner and Dellon, 1994). Knee innervation is classified into the anterior part (anterior branch

of the femoral, common peroneal and saphenous nerve) and the posterior part (posterior

articular and obturator nerve) (Kennedy et al., 1982). The medial cutaneous femoral nerve branches into the prepatellar plexus to innervate the skin of the lateral knee and also to the medial retinaculum and patella. The saphenous nerve branches into the infra patella, whilst the common peroneal nerve innervates the knee capsule from the inferior. From the posterior of the knee, the terminal branch of the obturator nerve, namely the medial retinacular nerve branches to the MCL (Horner and Dellon, 1994). These nerves are responsible for the active and passive six-degrees of motion of the knee joint and react strongly to impending injury to protect the knee components. Any block or disruption in the proximal lower limb innervations that supply the knee joint nervous system can cause both cellular and mechanical dysfunction.

Kennedy et al. (1982) demonstrated the relationship between the neuro-histology of the ACL and knee joint function. The tortuosity of the vascular and para-vascular nerves [Figure 1.4 A] facilitates their penetration into different regions of the ligament and allows complex direction of ligament movement.

Nerve location towards the vascular plexus serves a different function; the para-vascular nerves are believed to provide vasomotor control, whilst the nerve fibres away from the vascular plexus act as slow pain receptors. It has also been found that the knee capsule has complex types of mechanoreceptor innervations to maintain knee stability and provide peripheral sensory input. Both capsular and ligament nerves contribute to initiate protection loop reflexes during abnormal stress and muscular splinting. Neither axons [Figure 1.4 B] nor receptors [Figure 1.4 C] are present in the deep layers of the cruciate ligaments or meniscus (Kennedy et al., 1982). Schutte et al (1984) described the three morphologic types of mechanoreceptors in the ACL; Ruffini endings for light tension, Ruffini (Golgi tendon) for slow adaptation and Pacinian corpuscles for rapid mechano-reception. These mechanoreceptors are critical for proprioceptic perception (Schutte et al., 1987). When the nervous system is impaired and unable to evoke proprioceptive reflexes of the protective muscles to protect the ligament, then this causes the ligament to injure (France et al., 1987, Cailliet, 1992).
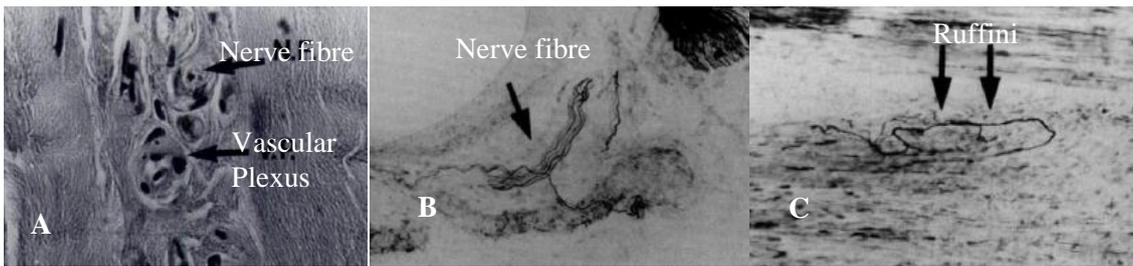
**Figure 1.4 Neuro-histology of the ACL.** (A) Afferent receptor indicated by the arrow, (B) the axon and (C) the Golgi-like, tension receptor that has been identified in the PCL. Images are taken from Kennedy et al. (1982).

Moreover, Dye et al. (1998) believe that the intra articular innervation is crucial for homeostasis of the knee joint components. Their study had successfully mapped the conscious pain sensation of the knee joint components, using electrical stimulation through arthroscopic palpation. Neuro-sensation of the knee joint components varied from no sensation (0) to severely painful (4 A-B) [Figure 1.5 A&B].
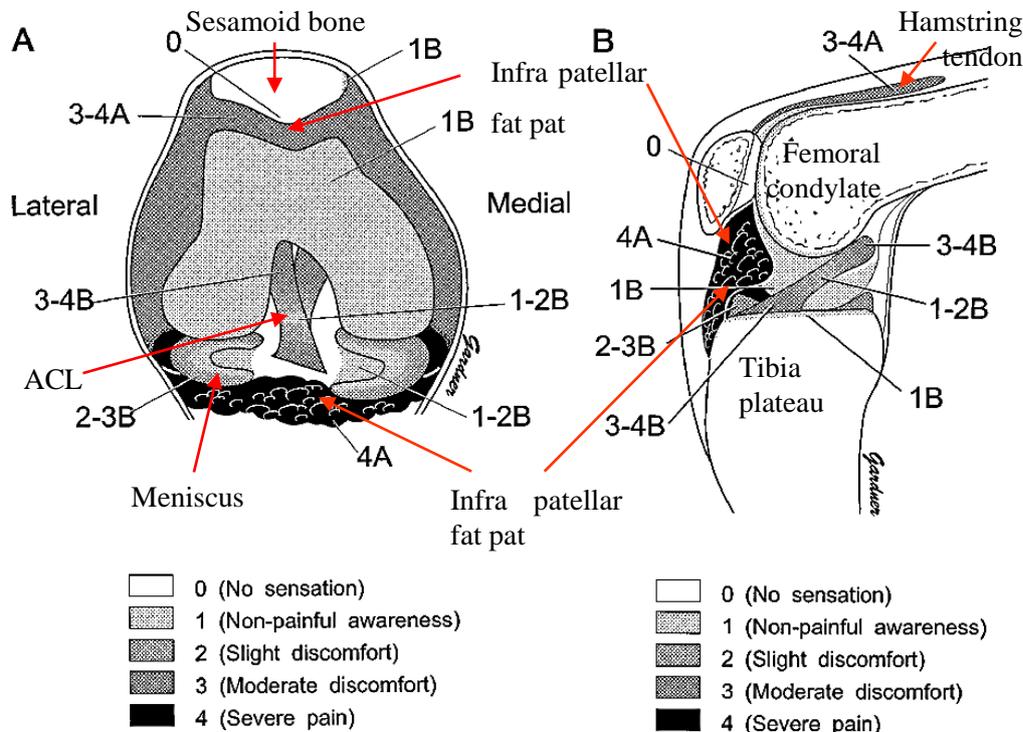


**Figure 1.5 Conscious neuro-sensory mapping of the knee intra-capsular structures.** (A) The coronal section and (B) the sagittal section of the right knee. The pain sensation grading is represented by 0 to 4, where 0 means no pain and 4 severe pains. The proprioceptive perception is indicated by A (accurate spatial) and B (poor spatial) localization. Images are taken from Dye et al. (1998).

The cruciate ligaments showed less sensation in the middle part, which increased significantly at the bone interface, as well as the capsular margins of the menisci (Dye et al., 1998). Dye et al's (1998) findings of severe pain in the tibiae origin are in agreement with Kennedy et al`s findings where this area has rich innervations.

Beside the ligaments, the infra patellar fat pat is also rich in pain receptors, and has been reported to have a high sensitivity to pain, and acts as a protective mechanism. Hoff disease with infra patellar fat pat impingement gives a persistent pain (Ogilvie-Harris and Giddens, 1994). The infra patellar fat pat is also a source of adipose derived stem cells that are responsible during patellar tendon injury for releasing the SDF-1 (stromal cell-derived factor-1) to recruit inflammatory cells and to direct the stem cells homing (Liu et al., 2011).

## 1.1.4. Histoarchitecture of the tendon

The hierarchy of the assembly of collagen molecules in ligamentous tissues consists of three levels. Tropocollagen is the basic structural unit of collagen consisting of three polypeptide alpha chains (two α1 chains and one α2 chain), which each chain forms a left-handed helix (level 1). This level 1 chain is heterotypic, which molecules between the three chains are unidentical. They are composed of repeating triplet Gly-X-Y, that the X or Y can be any amino acids (most often is proline or hydroxyproline). The three alpha chains are weaved into a superhelical cable (level 2) into a tropocollagen with right-handed helix (level 3), which consists of 1014 amino acid residues. Subsequently, five tropo-collagens build a microfibril followed by a subfibril, a fibril and finally a fibre [Figure 1.6] (Danylchuk et al., 1978, Kastelic et al., 1978, Pradhan et al., 2012).

Another important aspect of the structure of ligaments is the transitional bone-ligament interface. It consists of: (1) the crimped collagen fibres; (2) the unmineralized fibrocartilage tissue; (3) the mineralized ground substance; and (4) the lamellar bone (Cooper and Misol, 1970). In the ACL, this transitional zone is induced by the compressive stress which accumulates at the end of the avascular notch, as this point serves as the bone pulley for the ACL when the knee is in full extension (Petersen and Tillmann, 1999).

tropocollagen    microfibril    subfibril    fibril     fibre

1.5nm      3.5nm      10-20nm    50-500nm    50-300mm
X-ray      X-ray, EM    X-ray, EM    X-ray, EM, SEM    EM, SEM, OM

staining      periodicity      crimp
35nm      64nm      45-50mm
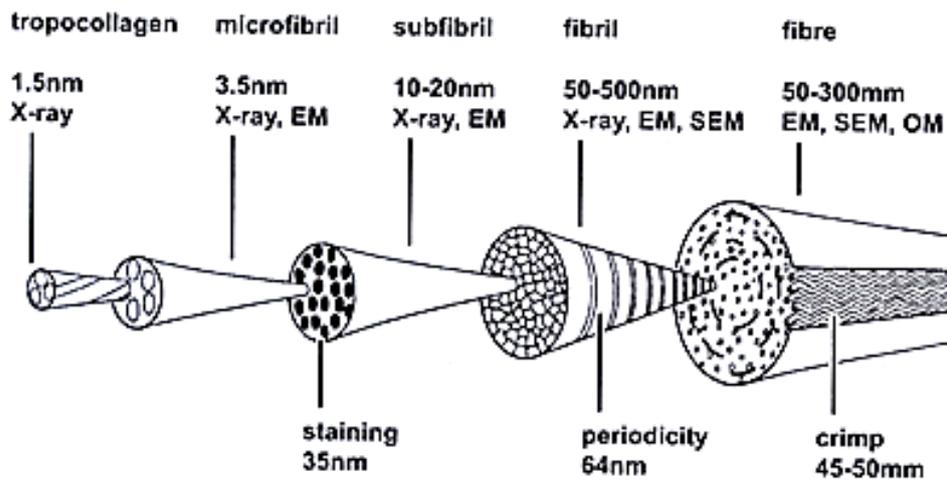
**Figure 1.6 Arrangement of the collagen fibres;** the tropocollagen to the tendon fibre. The image is taken from (Kastelic et al., 1978).

## 1.1.5. Components of the extracellular matrix of the ACL

The non-cellular part of the ligament is its extracellular matrix (ECM), which is mainly comprised of collagen fibres. Collagen type I is the major constituent, accounting for 70 – 80 % of the ECM dry weight and it is responsible for endowing the ligament with tensile strength. The remaining collagens are type III (12 %) and types IV (8 %) dry weight (Birk and Mayne, 1997). The two thirds of ligament wet weight is water, that is needed to; (i) sustain viscoelastic behaviour by hydration of the fibres (inter-fascicular sliding) (Amiel et al., 1990), (ii) provide nutrient exchange, (iii) induce hydrodynamic pressure gradients (Laurencin and Freeman, 2005) and (iv) support cell metabolism (Woo et al., 2006). Elastin accounts for only 1.5 % of the dry weight, and endows the ligament with some elasticity by straightening under load and recoiling back to the coiled globular elastin molecular complexes when unstressed. Other important components of the ligament ECM are proteoglycans, glycosaminoglycans (GAG**s**) and fibronectin. GAGs, the ground substance, are hydrophilic and highly negative charged. GAGs hold water provide cushion effect and enhance the viscoelasticity of ligament. Fibronectin is important for cell adhesion, cell communication and provides for a cell-matrix feedback mechanism (Thornton, 2006).

The effects of aging to the structure and composition of the bone-ligament interface in the ACL were demonstrated by histological and immunocytochemical studies. Bovine ACL of neonates (1-7 days), immature (2-6 months), and mature (2-5 years old) age groups showed that the bone interface in the neonatal group had (i) more cartilage, (ii) the lowest GAG concentration, (iii) was thicker and (iv) had fewer cell numbers compared to the bone and (v) ligamentous area, the collagen fibres were shown to lie in parallel to the bone interface. In contrast, the bone interface in the mature group had more fibrocartilage and the collagen fibres were inserted perpendicular to the interface region (Wang et al., 2006).

### 1.1.6. Cellular components of ACL; the cells and cell adhesion molecules

Essentially, cells determine their environment by producing their surrounding ECM according to the need (Nerem, 2000). Ligament cells are mainly fibroblasts, known as "connective tissue workhorses", synthesizing macromolecules to form the ECM (Pollard et al., 2008, Tamada and Ikada, 1994). Fibroblasts are varied in shape, size, orientation and number and located in between the collagen fibres. The growth of the fibroblasts is specific to the types of mechanical force applied; static uniaxial tensile strain has cells proliferate longitudinally following the axis, while the cyclic strain induces proliferation and infiltration of the cells (Russell et al., 2000, Frey et al., 2009). Ligament has a very low number of macrophages, endothelial cells and smooth muscle cells (Doroski et al., 2007).

The ACL has three different zones as determined by the shape of the fibroblastic stromal cells, which adapt to different mechanical loads across the ligament [Figure 1.7 A]. The (postero-lateral) quarter of the ACL, at the femoral insertion is loaded with the highest tension and the cells develop a fusiform morphology. Loading stress is gradually lower towards the medial portion of the ligament, and cells in this region take on an ovoid shape and become more spherical to form chondroid shape until the end portion of the ligament (Murray and Spector, 1999).
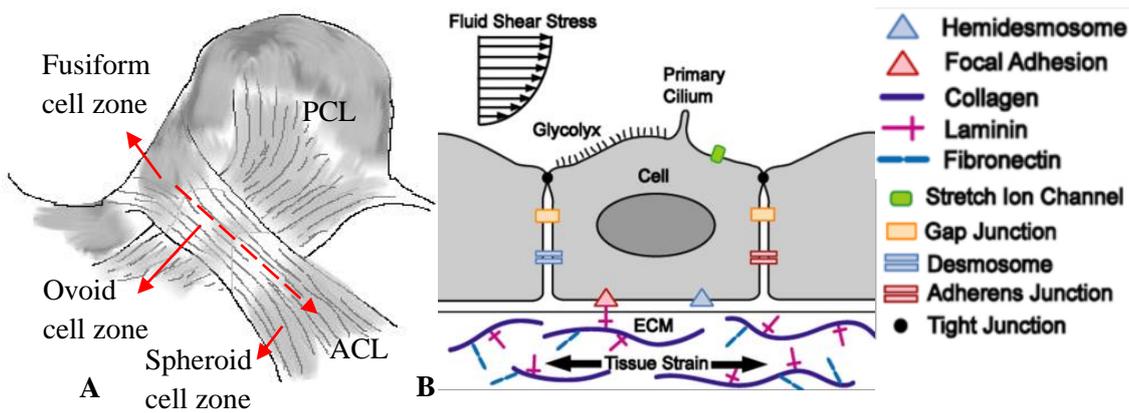
**Figure 1.7 ACL cells and the surface molecules.** (A) Different fibroblast shapes along the ACL is dependent on the loading magnitude. Dashed red arrow refers to the loading magnitude, from the higher to the lower. Reproduced from Murray and Spector (1999). (B) Cell adhesion molecules for cell to cell and cell to matrix interaction. The image is taken from Rodriguez et al. (2013).

Cells attach to the ECM through the expression of receptors, known as the cell adhesion molecules (CAMs) on their membranes [Figure 1.7 B]. Examples of the integrin family of adhesion receptors are described in Table 1.1.

| CAMs | Structure | Extracellular ligands | Intracellular ligands | Expressed by | Function |
|---|---|---|---|---|---|
| Fibronectin receptor | α5β1 | Fibronectin | Talin, paxillin | Fibroblasts | Cell-matrix adhesion |
| Tenascin-C | Hexamer | Tenascin-C - Integrin | αVβ3, α7β1, α9β1 | Nerve, ligaments/ tendon, wound healing, tumour | Weak adherent without cytoskeletal rearrangements |

**Table 1.1 Examples of the integrin family with their ligands and functions.** Summarised from Mackie (1997), Polland et al. (2008), Tucker and Chiquet-Ehrismann (2015).

Tenascin C is an adhesion glycoprotein in the ECM that is expressed in the nervous system and connective tissues including bone, tendon and ligament. It is over expressed during inflammation, wound healing and tumour genesis (Mackie, 1997).

Tenocytes create multicellular communication networks throughout the collagen fibril bundles in tendon, through the binding of hemi-channels between the adjacent cells membrane (hexamer complex of connexion 32 and 43). This pore allows a permeate of ions, small molecules and metabolites less than 1 kDa, and enables a synchronization of cell responses (McNeilly et al., 1996, Waggett et al., 2006, Levin, 2007). The mechano-chemicals are transported in vesicles as the messenger between neighbouring cells are transferred through a gap junction on each cell (Schneider et al., 2011). The messengers will be transferred through the actin filaments, focal adhesion complexes (talin-vinculin, paxillin) to the nucleus once they have reached the intracellular environment. These will regulate gene transcriptions followed by protein translation to initiate signals for cellular adhesion, migration or gene expression (Hynes, 1999, Pollard et al., 2008).

## 1.2. Mechanical function of the ligaments in the knee joint

### 1.2.1. Physiological function of the knee

Understanding the function of the knee is important to recognise how injuries occur, accurately justify the injuries for an appropriate provision of therapies.

The knee joint movement is a result of complex interactions among various components. The knee joint is the most complex joint in the human body, capable to maintain stable congruent movement and motor transmission. It allows transmission and dissipation of load amongst the femur, tibia, fibula and patella, provides six degrees of freedom including translation in three planes (medio-lateral; antero-posterior; proximo-distal) and rotation in three planes (flexion/extension; internal/external; varus/ valgus) [Figure 1.8]. The knee flexion-extension manoeuvre is a combination of rotation around the sagittal axis of the femoral condyle to the vertical axis of the tibia that glides simultaneously. The tibia rotates towards the femoral condyle. The first 20º of flexion causes a rocking motion (as the tibia moves posteriorly) and starts to rotate in the longitudinal axis of the tibia. The tibia is parallel to the femoral condyles at 30º of flexion and starts to rotate internally after 45º until full flexion at 90º (Daniel and Stone, 1988). The in-congruency of the tibial plateau and the length differences of the lateral and

medial femoral condyles play a role in the internal and external rotation. Knee flexion-extension causes external rotation at 0º, becomes parallel at 30º and rotates internally from 45º to 90º full flexion (Cailliet, 1992).
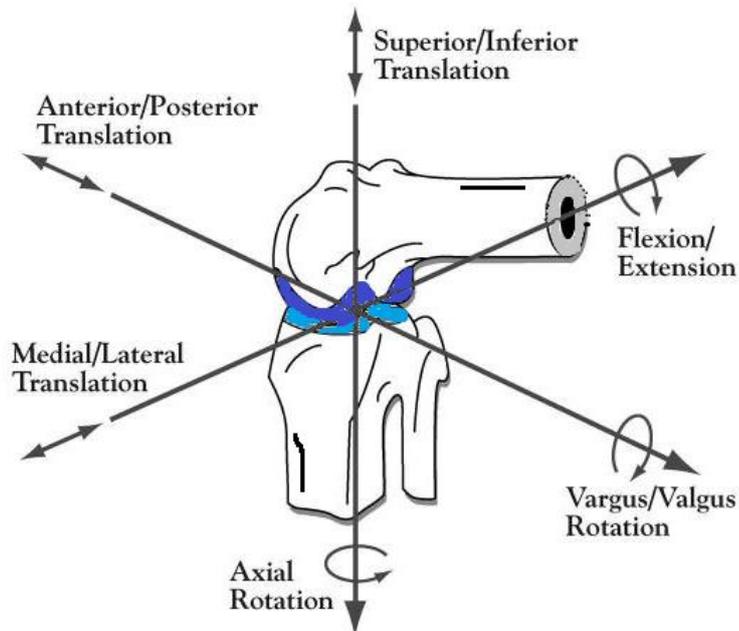


**Figure 1.8 Knee kinematics; the 6-degrees of freedom.** Image was reproduced from (Komdeur et al., 2002).

Dynamic stability is provided as external forces are in balance with the internal forces, achieved by the balance of imposing load from the ground (external force) versus the resultant reaction of the muscles, ligaments and the joint contact geometry. Knee ligaments act as adaptive linkages whilst the menisci facilitate mobility and load distribution of the bearing (Al-Turaiki, 1986).

### 1.2.2. The role of ligament in knee motion

Some components of the knee joint sustain knee joint stability in the static or dynamic state. The menisci and knee joint capsule support static stability while the muscles maintain the dynamic movement. Ligaments contribute to both static and dynamic joint stabilization, through the signals modulated from the ligament mechano-sensitive receptors to give proprioception information and generate muscle coordination (Sjölander et al., 2002). In addition to the ligaments; the joint geometry, the low friction properties of the articular cartilage surfaces and

the compressive forces of the body weight in the synovial joint also play role to maintain knee joint stability (Sjölander et al., 2002).

Each ligament has specific properties according to its anatomical location and geometry. Knee joint stability is provided centrally by the ACL and PCL, medially by the medial collateral ligament and the semimembranosus, and laterally by the lateral collateral ligament, antero-lateral femorotibial ligament and the popliteus (Larson, 1993). The ACL restrains the knee joint from hyperextension and external rotation [Figure 1.9 A&B]. The ACL is taut while the knee is in full extension at 5º - 20º and 70º - 90º degrees of knee flexion and most relaxed at 40º - 50º (Kennedy et al., 1974, Cailliet, 1992). The ACL is comprised of two functional bundlies (the antero-medial and postero-lateral bundle), the antero-medial bundle has a higher elastic modulus, tensile strength and strain energy compared to the postero-lateral bundle (Butler et al., 1992). Both bundles respond non-uniformly to tensile stress as well as to torsion, while the bony part of the ligament has to deal with stress transfer (Sakane et al., 1997, Thornton, 2006). The neurological system plays a crucial role in providing stability of the knee joint through a neuromuscular reflex. Sensory and motor loop in spinal system loop explains how the internal force is produced (Cailliet, 1992).
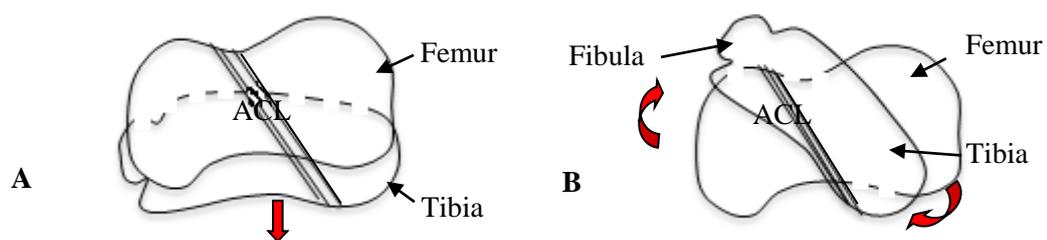


**Figure 1.9 The role of ligaments in knee motions**. ACL restricts the knee joint (A) hyperextension and (B) the external rotation. The images were reproduced from Cailliet (1992).

Tensile stimulation acts on the knee ligaments, tendons, intrafusal and extrafusal muscles as proprioceptic. Impulses are accepted by the receptors and transmitted throughout the Ia and Ib nerve fibre to the dorsal ganglia root into the anterior horn of the spinal cord. Efferent reflexes are generated from this anterior horn through the motor nerve fibre into the muscles around

knee. The ACL and PCL provide this mechanical and proprioceptive control of the knee motion (Cailliet, 1992).

## 1.2.3. Viscoelastic properties of ligament

Ligaments exhibit a non-linear force deformation curve, a unique response to the strain due to their composition and crimped pattern of the collagen fibres. This response leads to a smooth joint movement under normal loading and restrains excessive joint displacement under high tension (Woo et al., 2006).

In the stress–strain curve [Figure 1.10 A], a toe region is shown as strain is transferred to collagen fibrils (as referred to the symbols at the top of the graph as I), straightening all the crimps (II) (Nordin, 2001b). The fibres are compressed laterally; this causes water to escape, thus the amount of stress applied per unit strain is low. After all of the fibrils are recruited, the amount of stress accepted by each fibre per unit increases sharply. At this linear region, the collagen triple helix is stretched and the inter-fibrillary crosslinks are broken (III) (Young Iii and Toth, 2006). Finally, when it reaches its yield point, no more stress can be endured and the ligament becomes plastic, causing defibrillation and failure (IV) (Laurencin and Freeman, 2005).

The interaction of proteoglycans (GAGs), water, collagen and elastin gives rise to the viscoelastic behaviour of ligaments, which exhibit stress relaxation and creep responses (Woo et al., 2006). In stress relaxation, under a lower single or cyclic stress, the viscoelastic elements of ligament will immediately respond to the loading and decay, showing a non-linear line until a steady state has been achieved [Figure 1.10 B]. Rapid loading rate causes the ligament to become stiffer and stronger compared to a slow load application. Analogous to the stress relaxation, creep is an increase in length over time after constant loading, in which the tissue is elongated even though the stress has been removed [Figure 1.10 C]. However, after being exposed to cyclic loading, ligaments are not able to totally recover immediately (ligament hysteresis) [Figure 1.10 D]. Time is needed for water influx, collagen crimp formation and for

elastin to recoil into its granule formation and reach a state of equilibrium. This is approached

after a few hours under relaxed conditions (Nordin, 2001a, Thornton, 2006).
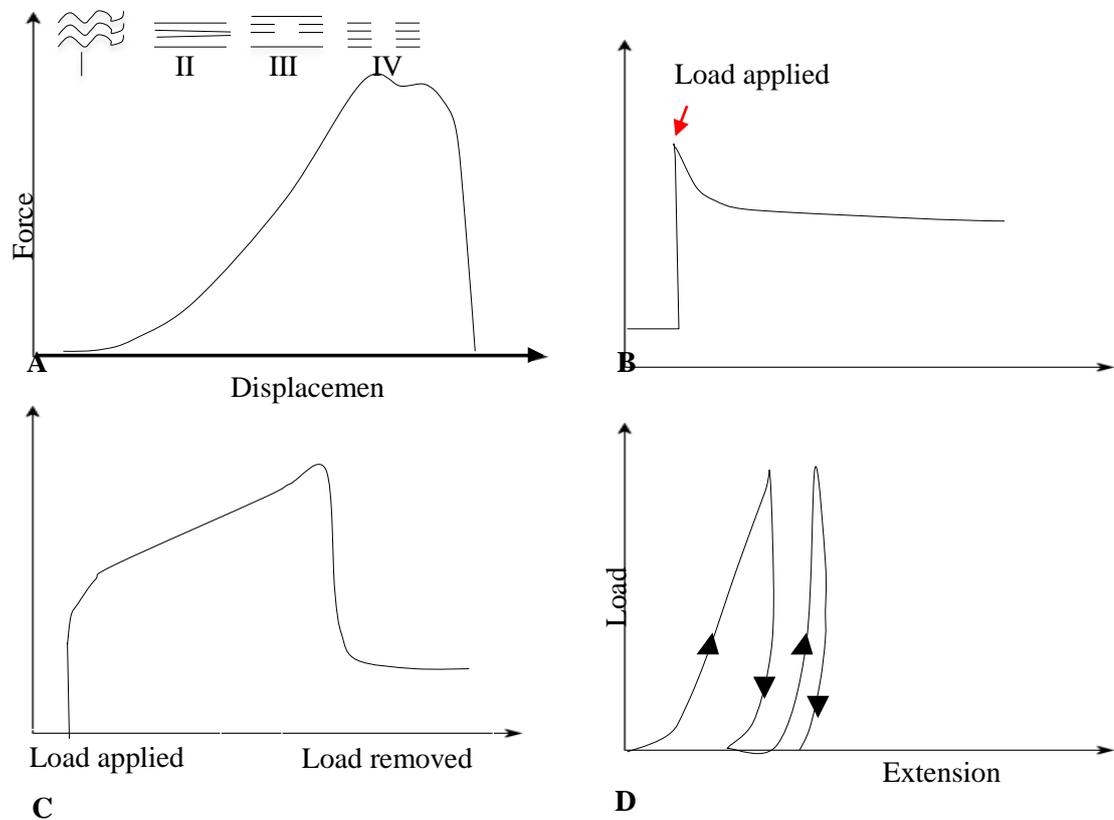


**Figure 1.10 Ligament mechanical properties**. (A) Ligament normal loading curve, the top
figure is showing the collagen fibre condition, (B) curve of stress relaxation and (C) creep of
ligament. (D) Ligament hysteresis after being exposed to two cycles of loading. Images were
reproduced from Nordin (2001).

There are several factors affecting ligament properties; (i) aging, as the diameter of collagen

fibres shrink after 60 years, the mechanical properties were superior in the younger age [Table

1.2] (Woo et al., 1991, Ainsworth and Chaudhuri, 2005). (ii) Metabolic diseases such as

diabetes mellitus increase ligament stiffness, pregnancy and regular haemodialysis cause hyper-

laxity of ligaments decrease tensile strength. (iii) Medications, such as regular usage of steroids

and oestrogens block collagen synthesis, whilst therapeutic doses of non-steroidal anti-

inflammatory drugs (NSAID) can increase collagen cross-linking (Oatis, 2004).

| ACL mechanical properties | 22-35 years | 40-50 years | 60-97 years |
|---|---|---|---|
| Ultimate load (N) | 2160 | 1530 | 658 |
| Linear stiffness (N.mm$^{-1}$) | 242 | 220 | 180 |
| Energy absorption (N.m) | 11.6 | 6.1 | 1.8 |

**Table 1.2 Differences in ACL mechanical properties related to age.** Summarised from Ainsworth and Chaudhuri (2005).

Joint immobilisation for up to 8-weeks decreases ligament stiffness, causes contracture of ligaments, however the capability to absorb energy can never be restored (Nordin, 2001b, Oatis, 2004, Woo et al., 1987).

## 1.3. Knee ligament injury and treatments

### 1.3.1. Mechanism of injury, signs and symptoms of knee ligament injuries

Knee ligament injury can be isolated or associated with other knee tissue injuries. The knee joint loses its stability immediately after a torn ACL and causes other components such as the menisci and other ligaments to experience additional friction forces. It really depends on the mechanism of the trauma (Louboutin et al., 2009).

Females tend to suffer ACL injuries four to six times more often than males during non-contact sport such as cutting and jumping actions (Arendt and Dick, 1995). Oestrogen has been reported to increase ligament laxity and lax ligaments cannot provide joint stability (Liu et al., 1996). Oestrogen (17-β-estradiol) affects collagen production throughout the menstrual cycle. Collagen production has been shown to be reduced by 40 % at the normal physiologic level of the (0.025 to 0.25 ng.mL $^{-1}$) and by 50 % at the 2.5 to 25 ng.mL $^{-1}$ (Liu et al., 1997). Oestrogens have also been shown to down regulate the proliferation and ECM production of rabbit ACL fibroblasts (Pollard et al., 2006).

The classic cause of the ACL tear is tendon overuse when the knee is suddenly twisted inward to the femur, while the foot, ankle and leg are fixed and tight as well as the pelvis are spun violently, or vice versa, causing avulsion of the bony part of the femur/ tibia attachment and

ACL mid-region rupture. The force direction can also be emanating from the medial direction with excessive external rotation, hyperextension or shear stress from the tibia (Lewin, 1952a, Kennedy et al., 1974). Rotation combined with abduction or adduction of the knee causes a range of knee injuries (menisci, cruciates, capsule and joint surfaces). About 10 - 25 % of the meniscal injuries are associated with rupture of the cruciate ligaments (Kennedy et al., 1982). Soccer and skiing are the most common causes of ACL injuries in the UK; soccer represented 54 %, whilst skiing was less (Kapoor et al., 2004).

Minor ACL injuries that damage the afferent nerve circuit result in inadequate feedback responses to maintain knee stability and cause progressive ligamentous laxity [Figure 1.11] (Kennedy et al., 1982). In addition, the pain of damaged cartilage is elicited from the transmission of the load from the tibia, femur or patellar plateaus to the subchondral bone (Dye et al., 1998). This agrees with previous findings of Dye et al. that painful sensation appears significant when the intraosseous pressure is increased (Dye and Boll, 1986).
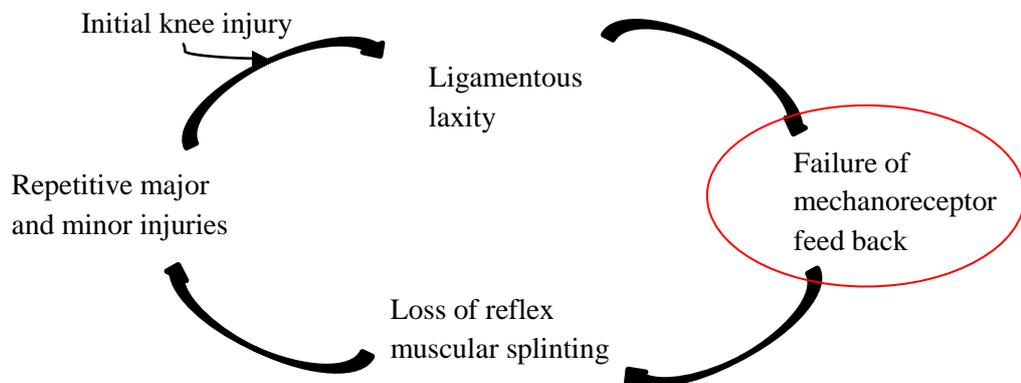


**Figure 1.11 Mechanism of knee ligament injuries.** The hypothesis that the afferent neurons contribute to knee instability due to ligamentous laxity after injuries. Figure is adapted from Kennedy et al. (1982).

Typical sign of a major ACL tear is a sharp pain with disability following a knee twist. ACL rupture gives various rotator knee instabilities such as positive Lachman test and pivot shift test/ Drawer sign. Accurate history-taking and physical examination can highlight a torn ACL in an acute knee injury or chronic knee instability (Al-Turaiki, 1986, Burnett and Fowler, 1985, Odensten and Gillquist, 1985).

Different from ACL injuries, medial collateral ligament (MCL) tears occur by direct excess external valgus forces of the medial part of the knee when it is semi-flexed or by rotational trauma. In the classic solitary MCL injuries, the patient experiences more knee weakness rather than pain. Tenderness of the medial knee can be identified by careful physical diagnosis with pain valgus stress 30º or laxity valgus stress 30º. The cruciate signs, Lachman, Loose or Drawer sign, as well as the pivot shift should be negative (Cailliet, 1992, Kastelein et al., 2008). Lateral collateral ligament (LCL) is usually associated with other ligament injuries and knee dislocation as a result of severe forces of abrupt abduction force with external rotation, whilst a severe isolated LCL injury is very rare (Krukhaug et al., 1998).

### 1.3.2. Complications of ACL injuries

The complication of an untreated ACL tear is clear. It leads to progressive tibiofemoral joint degeneration and end stage osteoarthritis within ten years. The pathogenesis of osteoarthritits following ACL injury can be primarily through direct damage of articular cartilage and/ or the meniscus or secondary as a result of the failure of cartilage and the meniscus to withstand chronic friction forces which result from the alteration of knee joint biomechanics (Louboutin et al., 2009).

Patients with ACL injuries will lose their knee joint proprioception as they can no longer locate the joint position and suffer kinaesthesia (Barrett, 1991), as well as losing the efferent activities that regulate knee muscle stiffness that is required for the reflex responses. Objective assessment of knee functional instability can be performed by measuring the reflex time of the hamstring and frequency in giving way (Beard et al., 1993). Muscle atrophy of the affected leg such as the quadriceps following the ACL injury or post reconstruction is widely reported.

Numerous findings have shown a significant relationship between non-surgical restorations of ACL tears to the development of further knee joint damage. About 63 % of patients with ACL tears have been shown to develop osteoarthritis after conventional therapy, while the other 37 % experienced joint space narrowing, 12 years post injury (Segawa et al., 2001). Menisectomy was unavoidable in 79 % of German Olympic athletes, 10 years after ACL injury without reconstruction and this rose to 95 % after 20 years (Nebelung and Wuschech, 2005). Moreover, 100 % athletes with ACL injury were reported to develop osteoarthritis after 35 years of conservative treatment; among them 42 % went on to total knee replacement. In contrast, a lower risk of osteoarthritis was found at 20 years following ACL reconstruction; about 14 - 26 % post reconstruction patients developed osteoarthritis, meanwhile a higher incidence was found in the post meniscectomy patients (Louboutin et al., 2009). Complications of ACL tears over time are represented in Figure 1.12.

|  | ACL rupture |  |
|---|---|---|
| Time 0 | Meniscal tears 10 -20 % |  |
|  | Chondral lesions 16 % |  |
|  |  |  |
| Month 6 |  | Meniscal tears 63 % |
|  |  | Degeneration 29 % |
|  | Untreated ACL rupture | ACL reconstruction |
|  |  | Meniscectomy |
| Year 10 | Osteoarthritis 60 % | Osteoarthritis |
|  |  | In normal/repaired ACL:10% |
|  |  | In pre-ACL rupture  : 60 % |
|  |  | In total ACL rupture : 30 % |
|  |  | In partial ACL rupture: 20 % |
| Year 20 | OA 60 -100 % | Osteoartritis |
|  |  | In normal ACL : 14% |
|  |  | In repaired ACL: 26 % |
|  |  | In post meniscectomy: 37 % |
| Year 30 | OA 86 – 100 % |  |
|  | Total knee replacement 42 % |  |

**Figure 1.12 Summary of ACL tear complication over time.** This figure is adapted from Louboutin et al. (2009).

### 1.3.3. Wound healing capacity of the ACL

Generally, ligament healing takes several years, which is too slow to re-establish its biomechanical function. Hence, ligament healing is a major clinical issue to be addressed (Woo et al., 2008).

Bleeding is usual following an acute ACL rupture, and within a few hours, neutrophils will infiltrate to the wound and release mediators to attract more inflammatory cells. Later on, a sequence of leucocytes will be recruited, monocytes can be found after 18 hours, T-cells and macrophages after 36-48 hours (Akeson, 2003). In short, the ligament healing process of an incomplete torn ligament is characterised by the inflammatory stage (1-7 days), proliferative phase (7-21 days) and remodelling (three weeks to years) (Kader et al., 2002). During injury, the healing process of the ACL is supported by the blood supply from the infra-patellar fat pad and synovial membrane (Arnoczky et al., 1979). Naturally, the optimum distance of blood vessels to supply the fibroblasts adequately is within a range of 200 μm. However, the ACL has lack of vascularisation thus the healing process is not complete (West et al., 1985, Petersen and Tillmann, 1999).

Hyaluronan is believed to promote cellular differentiation, adhesion and migration, increase fibroblast proliferation and induce angiogenesis. Radial vascularisation with a spoked-wheel pattern was found 3 days after application of hyaluronic acid dried powder on the chick chorioallantoic membrane (West et al., 1985). Wigg et al. (2005) injected 0.4 mL (10 mg.mL$^{-1}$) hyaluronan into a surgical tear of the rabbit ACL and found that this injection improved healing by increasing the collagen III production, compared to a saline control injection. Numerous fibroblasts were found in the area injected with the hyaluronan which agreed with another finding of an increase in proliferation and cell migration as a result of the swelling effect of the hyaluronan injection (Wiig et al., 2005). Moreover, hyaluronan gives rise to a more controlled inflammatory response, with better fibroblast and collagen organization (O'Donoghue et al., 1971, Wiig et al., 2005).

Macrophages support the healing process. Inhibition of macrophage migration inhibitory factor (MIF) causes poor MMP-2 and 13 mRNA expression, that interrupt the wound healing process. Kitayama et al. (2011) observed the healing process of the MCL taken from wild type and MIF knock out type mice. The healing process in the MIF knock out type was shown to be delayed with fibrosis and lower mechanical properties (tensile strength and elasticity) (Kitayama et al., 2011).

### 1.3.4. Synovial fluid in the wounded joint

Synovial fluid supports the healing process by providing an appropriate environment for the injured knee. Matinez et al. isolated the synovial fluid from three groups of patients; those with torn ACLs, chondral and meniscus injuries. The levels of IL-1, IL-6 and IL-10 were found to be higher in all groups, but TNF-β was significantly higher in the synovial fluid of patients with ACL tears, with mild increases in IL-2 and TNF-α levels.

In summary, synovial fluid provides an anabolic and inflammatory environment in patients with ACL tears, whilst it provides catabolic factors in patients with chondral and meniscus injuries (Martínez de Albornoz Torrente and Forriol, 2012). Cytokines in the synovial fluid of patients with chronic untreated ACL tears with osteoarthritis were found to be similar to the inflammatory factors released by cartilage degradation only. IGF-1 and TGF-β act as anabolic factors that induce proteoglycan, collagen II and integrin synthesis and inhibit ECM destruction. These factors are also found in chronic degenerative inflammation. Acute ACL tears are usually associated with hemartosis (knee bleeding), which promotes the joint repair process as it releases growth factors such as IL-1, IL-2, IL-6 and TGF-α. IL-2 is needed for cellular immune memory (Higuchi et al., 2006).

## 1.4. Clinical practice for ACL injuries

During the last 40 years, approaches to the reconstruction of the ruptured ACL have developed enormously. A range of different grafts or substitute materials have been used together with a variety of surgical techniques and rehabilitation regimens in order to restore knee joint stability

and to reduce secondary damage to the articular cartilage. Clinical treatment of ligament injuries in the knee joint depends on the severity of the injury. It is necessary to make an appropriate decision to apply supportive therapies with or without surgical treatment immediately after diagnosis of a torn ligament in order to avoid further knee joint complications. Thorough awareness of the patient history, mechanism of injury and symptoms aids correct diagnosis of ACL injury. Physical examination such as neurologic status (Beard et al., 1993), cruciate tests (positive Drawer sign, Lachman manoeuvre and Lewin test) and radiologic evidence is used by clinicians to guide diagnosis (Lewin, 1952b, Cailliet, 1992). In addition, the patient's age and occupation should be taken into consideration in order to determine the course of treatment (Fu and Schulte, 1996, Levy, 2010).

Aspiration of hemarthrosis in the knee is crucial in both the diagnosis and therapy during the acute phase after a knee ligament tear, 48-72 hours post injury, since up to 66% of ACL tears are associated with knee joint swelling (Feagin and Curl, 1996). This procedure decompresses the swelling, decreases pain and allows accurate knee joint examination. Moreover, the aspirate can be used for histological examination (Lewin, 1952b, Cailliet, 1992, Kapoor et al., 2004).

### 1.4.1. Historical approaches

Surgeon skill is important to achieve long life implants as the implant should be fixated in the right position to reduce wear and optimize its function. There are two surgical methods to apply the knee ligament substitute: the intra and extra-articular techniques. Historically, the extra-articular technique was the first surgical intervention for ACL repair reported by Mayo in 1895. The intervention involved suturing with wire and silk, however, this approach soon failed (Burnett and Fowler, 1985). Catgut ligatures were later used to repair a torn cruciate ligament and were reported to provide a "perfectly strong" knee joint after 6 years fixation in one patient (Robson, 1903). Hey Groves described a method to replace the ACL using an ilio-tibial band [Figure 1.13] (Hey Groves, 1917), this technique formed the basis of modern ACL intra-articular reconstruction (Snook, 1983).

Alwyn Smith (1918) implanted the first silk-ACL substitute by using eight ply of No. 3 silk connected with a wire loop. However, this substitute was rejected after nine weeks. The knee joint became swollen with severe ankylosis and developed a sinus. Smith (1918) was also the first to use an autograft taken from fascia lata, which was reported to satisfy the patient eight weeks after transplantation (Smith, 1918).

MacIntosh introduced the use of the lateral third of the patellar tendon as the ligament source for ACL replacement in 1974 and this was known as Marshall-MacIntosh technique. Intra-articular surgical methods were then introduced using: arthroscopy, open reconstruction (miniarthrotomy) or transpatellar tendon. Miniarthrotomy was reported to cause decrease of tight circumference due to the quadriceps atrophy (Noyes et al., 1987), while others claimed no significant difference in the outcomes compared to the arthroscopy group (Fu and Schulte, 1996). Others preferred arthroscopy as it had less tissue destruction and better visualization of the ligament femoral insertion (al-Zarahini et al., 1997).
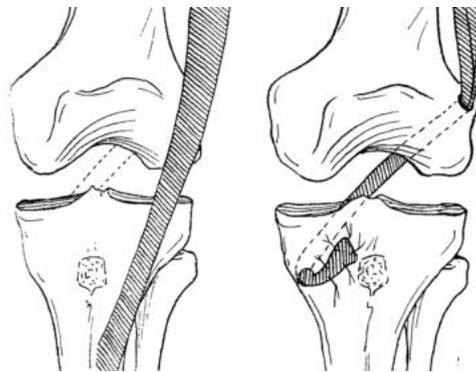


**Figure 1.13 The first ACL reconstruction technique** by rerouting the ilio-tibial band through the external condyle of the femur down to the tibial tubercle and drilling the condyle of the femur to the tubercle of the tibia. This became the principle of the modern ACL reconstruction. The images are taken from Hey Groves (1917).

Later, a technique was introduced to produce less wear. The implant should be placed at $28^0$ towards the femoral axis, and the femoral insertion point at 31 mm from the tibial origin. The substitute should be linear to the tibia, joint space and femur when it is flexed at 90 degrees, and the central point of the implant to the tibial and femoral attachment that should be isometric at flexion and extension (Odensten and Gillquist, 1985).

## 1.4.2. Biological grafts for ACL replacement

Until recently, the gold standard for ACL replacement was the use autograft or allograft of patellar tendon/ BPT-B or hamstring. A national survey conducted among surgeons in the UK and Canada to determine their preferences in ACL replacement revealed that most surgeons preferred autografts/ allografts rather than synthetic ligament, and the BPT-B was more favourable compared to hamstring (32 %) in Canada (Mirza et al., 2000) or semitendinosus and gracilis (33 %) in the UK (Kapoor et al., 2004). This finding is in agreement with Salgado et al. (2004) who reported that autografts and allografts accounted for 90 % of ligament repairs, whilst synthetic materials accounted for about 10 % of replacements (Salgado et al., 2004). Moreover, patient size should match to the graft size for example: male patient with more than 80 kg body weight is more likely to have BPTB as the graft source rather than hamstring (Larson, 1993).

There are different sources of autograft/ allograft tissue used for ACL replacement; such as the middle third of patellar tendon (Clancy et al., 1981), patellar tendon with bone plug (BPT-B) (Christian and Indelicato, 1993) or four-strand hamstring (semitendinosus and gracilis) (Trojani et al., 2009). In chronic cases, patellar tendon gave higher success rate compared to the semitendineous (85 % vs 50 %), however if patients were treated within 6-days post injury, the semi-tendineous gave as high as 85 % good result (Holmes et al., 1991).

There are advantages and disadvantages to the use of both autograft and allograft. Autograft causes secondary surgical morbidity of the harvest site (Zavras et al., 1995, Petersen and Laprell, 2000), and in the case of BPT-B may cause fracture of the patellar bone (Papageorgiou et al., 2001) or the proximal tibia (Anderson and Smith, 2009), but no fear of disease transmission or rejection (Petersen and Laprell, 2000). In contrast, the use of allograft is less invasive, more readily available and provides properties similar to autograft, but raises some concerns; such as immunological rejection (Sabiston et al., 1990), transplant contamination and disease transmission (Vacanti and Langer, 1999, Young Iii and Toth, 2006).

Allograft should ideally be sterilized such as through the physical or chemical methods. Gamma irradiation at 4 MRad was reported to disrupt matrix mechanical properties by causing collagen cross linking; decreasing graft stiffness by 12% and its ultimate strength by 26% (Rasmussen et al., 1994). Viral transmissions has been reported to occur in several transplanted patients using this sterilization method (Conrad et al., 1995). Thus recently, peracetic acid (PAA) has been extensively used to sterilize medical devices and biological grafts. It kills bacteria, fungi and virus through the free radical reactions which were reported in different doses, such as 0.1% (v/v) (Kemp, 1995), 0.18% (v/v) (Hodde and Hiles, 2002) and 5 % (v/v) (Raghavan et al., 2012).

Sun et al. (2011) compared the result of using allograft and autograft hamstring transplantation, by measuring the side-to-side discrepancy using an arthrometer. They found only 32.3% post hamstring allograft patients reached the normal range side-to-side discrepancy (less than 3 mm) compared to 86.1% of patients who received autografts. Moreover, patients receiving allografts had longer durations of post-operative fever without infections (Sun et al., 2011).

### 1.4.3. Synthetic grafts for ACL substitute or replacement

In the past, there have been many different synthetic materials introduced as an alternative for ACL replacements/ substitutes. Proplast® (Vitex-Inc, Houston, TX, USA) was the first permanent ACL substitute used in 1973, made of Teflon-carbon and embedded with aluminium oxide. This was reported to fail after less than one year (Ahlfeld et al., 1987). Integraft® TM (Osteonics Biomaterials, Livermore, CA, USA), other carbon fibre substitutes, produced large amounts of wear debris that was found in regional lymph nodes and the synovium (Jenkins, 1978, Jenkins and McKibbin, 1980), and failed 12 months after implantation (Thomson et al., 1994). The carbon fibre also caused persistent synovitis and non-conjunction post implantation (Grafil® type A-S) (Rushton et al., 1983, Amis et al., 1988). Eventually, carbon fibre substitute for ligament replacements were withdrawn from the market due to the high rupture rate and inflammatory reaction (Legnani et al., 2010).

Approved by the FDA, a permanent ACL replacement made from Dacron (Meadox Medicals, Oakland, NJ, USA; Stryker Corp., Kalamazoo, MI, USA), has been reported to induce cell infiltration, however it has also been reported that the implant material frequently tears at the femoral and tibia insertion (Lopez-Vazquez et al., 1991). A Dacron ligament prosthesis developed by Stryker® Dacron (E.I. DuPont de Nemours and Co., Wilmington, DE) failed to reach post reconstruction restoration criteria. Forty percent were found to fail in 40 patients after 4 years follow up, and 27.5% patients had serious complications mainly due to synovitis. This product had a failure rate of approximately 60% (Barrett et al., 1993).

Permanent implants made of poly-tetra-fluoro-ethylene (PTFE) such as Gore-Tex® (W.L. Gore, Flagstaff, AR, USA) were initially used in vascular surgery but later the PTFE was woven into multiple loops to create ligament substitutes. These exhibited the highest ultimate tensile strength of synthetic ACL replacements of close to 5.3 kN (DM et al., 1993, Bolton and Bruchman, 1985). However, this substitute has also been shown to fail gradually over time. In 82 patients after 18 months follow up, the Gore Tex® was reported to improve patient pain and knee function in the early post-operative period, however 5 % of patients suffered later ruptures, 17 % needed re-operations and 18% had other complications (Glousman et al., 1988). Wear debris (10 μm particulates) produced by the implanted material caused aseptic loosening and was also found in the ipsilateral lymph nodes (Miller et al., 2006). Satisfactory outcomes were reported after 28 months in 80 patients (Lukianov et al., 1989), however the failure rate increased to 47.5 to 60 % among 40 patients after 4 years follow up (Barrett et al., 1993).

Polyester ligaments such as the Leeds-Keio® (Neoligaments Ltd, UK) were implanted into over 50,000 patients worldwide (Legnani et al., 2010). This substitute works as a temporary scaffold to support the injured ligament and allow fibrous tissue ingrowth for new ligament formation. Histologically, mature ligamentization was achieved after 60 months implantation (Nomura et al., 2005). However, there are unsatisfying reports of graft failure, for example 25 % out of 20 patients implanted with the Leeds-Keio® suffered implant rupture (Macnicol et al., 1991, Schindhelm et al., 1991, Guidoin et al., 2000). This result was comparable to 18 patients

followed for up to 16 years who showed 27.7 % complete rupture and required partial meniscectomy 6 years after implantation. Only 11 % of implants remained stable in patients undertaking high impact sports activities (Murray and Macnicol, 2004). Another study reported that Leeds-Keio® ligament possessed similar properties to patellar tendon (laxity score, subjective knee function, and functional ability) after 5 years in vivo (Ghalayini et al., 2010a).

The ligament advance reinforcement system (LARS®) is fabricated from PET, and has a structure that mimics the structure of the ACL and good porosity to induce tissue ingrowth. Use of the LARS device was reported to show no difference to B-PBT autografts after 24 month implantation (Nau et al., 2002). The LARS® system has also been used successfully in four sports medical centres in China for 5 years. It was reported to have only a 4.4 % failure rate and 5.7 % complication rate (Gao et al., 2010). The LARS system can also be used to augment short (less than 15 cm length) and small gracilis autograft (3 – 4 mm) or hamstring autografts (4 – 5 mm) for ACL replacement. After 5 years use in this application in 112 patients, no patients developed synovitis, graft rupture or loosening (Hamido et al., 2011). Another study reported graft rupture (29.4%), degenerative osteoarthritis (100 %), and functional impairment (29.4 %) 19 years after ACL augmentation using PET in 126 patients (Ventura et al., 2010).

The Kennedy ligament augmentation device (LAD; 3M, St Paul, MN, USA) is used mostly as an augmentation device to support ACL reconstruction. Again, different centres have reported varying results. The LAD device showed no additional advantages compared to patients undergoing ACL reconstruction with the Marshall-MacIntosh technique (Moyen et al., 1992). On the other hand, the LAD device was reported to be comparable to B-PTB autograft (Muren et al., 1995), although others have reported complications in patients treated with this device such as muscle dysfunction, osteoarthritis (Marumo et al., 2000) and synovitis cyclops syndrome (Kim et al., 2003).

### 1.4.4. Disadvantages of current grafts for ACL substitute or replacement

The literature states that none of the graft materials are ideal for ACL replacement. Autografts and allografts do not satisfy either the patient or the clinician. Whist synthetic prostheses provide adequate mechanical properties in the short term, however, cyclic stress causes creep and fatigue that decays the materials strength over time. Abrasion of synthetic prostheses rubbing against bone and friction between the fibres has been shown to generate wear debris that accumulates in synovial membranes causing inflammatory reactions. Woven materials have been shown to split under axial stress, have low rates of cell infiltration as well as low extensibility (Olson et al., 1988). The development of scar tissue following implantation of the synthetics reduced the graft' mechanical strength (Larson, 1993). The fibre elasticity of several synthetic scaffolds such as PTFE, PET has also been reported to decay due to fatigue (Laurencin et al., 1999) and lose their structural integrity by the infiltration of phagocytic cells (Guidoin et al., 2000). Moreover, none of the current ACL substitutes are able to restore the neuro-sensory system thus loading of non-sensate ACL constructs beyond the ultimate failure point can cause further structural damage (Dye et al., 1998). Similar conditions are also found in various degenerative and inborn diseases that sensory output of the knee joint components as a defence mechanism that eventually leads to structural failure of the intra-articular system (Koshino, 1991, O'Connor et al., 1992). The synthetic materials such as Leeds-Keio® are not used today due to many reports of insufficiency, while LARS and LAD are still being used, mostly only for ACL augmentation (Ventura et al., 2010).

## 1.5. Tissue engineering of the ligament

To address these limitations mentioned above, 'Tissue engineering'; a recent and integrated science has been developed in an attempt to generate solutions which can be designed, constructed, modified and will integrate and function in the patient (Vacanti and Langer, 1993). This branch of science has increased in popularity since the name was firstly introduced by Prof. Y.C. Fung in 1987 at the National Science Foundation Meeting (Eugene, 2000). Biomaterials for tissue engineering applications should be biodegradable and biocompatible,

provide appropriate mechanical properties and be capable of integration into the host (Badylak et al., 2009).

### 1.5.1. Aspects of Tissue Engineering in general

Cells, scaffolds, signalling factors and mechanical stimuli are believed to be the four major components required for the tissue engineering process in order to mimic nature. It has been suggested that each component should be synchronized since they may influence the behaviour of each other. The safety and function of the scaffold should be investigated using the right animal model [Figure 1.14] (Nerem, 2000, Badylak, 2002a).
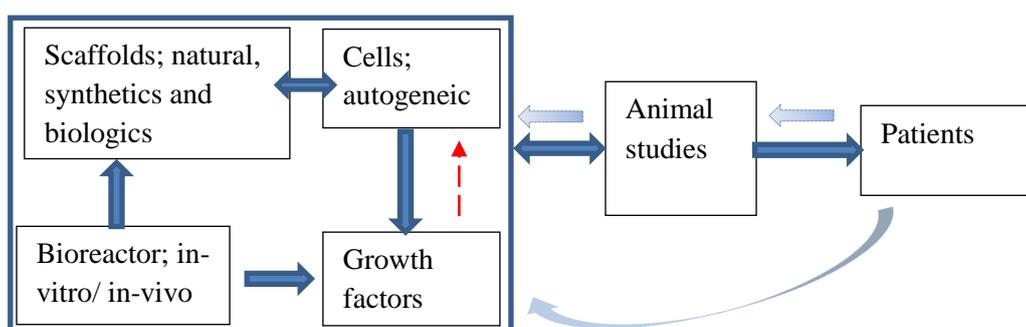


**Figure 1.14 Tissue engineering flowchart; from the bench to the bed**. The flowchart is summarised from different sources (Badylak, 2002b, Chue et al., 2004, Song et al., 2010). The double pointing arrow indicates a two-way interaction whilst the one-way dash arrow indicates a one-way interaction. Light blue arrow indicates a reverse back of the experiment to trouble shoot when problems arise. The one-way dash red arrow indicates adding growth factor.

The extra cellular matrix (ECM) is a vital and essential natural scaffold for cells of all tissues and organs in the process of morphogenesis, tissue maintenance and healing from injury (Badylak, 2002a, Badylak et al., 2009). It provides an environment for cells to live in and divide, as well as chemical stimuli important for cellular communication (Hubbel, 2000). The interaction between cells and the ECM is dynamic and reciprocal. The ECM and cells influence each other's behaviour through signalling, growth factors and enzymes, creating a suitable microenvironment for cells to continuously remodel their environment in response to external factors such as mechanical stimulation (Roskelley et al., 1995).

For tissue engineering applications, the optimal source of cells is autologous, whilst scaffolds can be generated from natural (allogeneic and xenogeneic), synthetic or biological materials. External growth factors may be added when the endogenous factors are not adequate. Mechanical stimulation can be applied to drive cell behaviour through the use of in-vitro or in-vivo bioreactors. However, in-vitro bioreactors are not responsive to changes in the properties of the tissue engineered constructs as they develop (in Figure 1.13, this is shown as a direction dash arrow), whilst being incubated in an in-vivo bioreactors (animal study), there will be two-way interaction between scaffolds and the environment (Chue et al., 2004, Song et al., 2010).

## 1.5.2. Scaffolds for ligamentous tissue engineering

As the major surrogate for the ECM, the scaffold must be perfectly designed as it plays a major role in providing ligament mechanical function. An artificial scaffold should be able to replace the ECM both structurally and functionally (Badylak, 2002a). Later, the scaffold will be absorbed and replaced by the new tissue formation, and should not release toxic molecules. This process should be developed gradually over time, in order to give the replaced ligament time to restore its full capacity to resist high tensile stress in normal activities or sports. During the remodelling process, the scaffold will gradually lose its ultimate tensile strength and suffer from fatigue or creep (Vieira et al., 2009).

Tissue engineering for ligament replacement involves research of tissue-based or tissue-inducing scaffolds. It offers an additional advantage such as the restoration of joint kinematics and an improvement of knee mechanics while the implants are remodelled (Mascarenhas and MacDonald, 2008). It has been suggested that ideally, scaffolds for tissue engineering should be (i) 3D matrices that have physiochemical and mechanical properties that resemble those of the host tissue to be replaced, (ii) provide an environment that mimics the ECM, (iii) contain growth factors and adhesion factors, (iv) the material and its degradation products should be non-toxic (Koutsopoulos, 2012). Moreover, the biomaterial should be amenable to design and modification, not induce an immune response and be easy to scale up (Holmes, 2002).

There are numerous materials currently being considered as candidates for the manufacture of scaffolds for ligament tissue engineering; natural materials such as silk and collagen, synthetics such as PEFT or PET, and acellular biological scaffolds derived from allografts or xenografts. Silk has been used for centuries as a suture biomaterial and has also been used for ligament substitution. Silk can be woven in a hierarchical architecture similar to the histological structure of the ligament. This arrangement has been shown to exhibit the three phases of native ligament mechanical properties; the toe region, elastic linear and yield point. In addition, silkworm scaffolds are biodegradable (Altman et al., 2002a) and non-toxic (Chen et al., 2003b). They have also been reported to express trypsin-inhibitor on the surface, that slows down trypsin degradation once implanted (Kurioka et al., 1999).

Scaffolds prepared using pure collagen are not ideal for tissue engineering of the ACL since they exhibit poor mechanical properties and degrade very quickly. In a study designed to mimic the composite nature of the ACL, a collagen type I hydrogel scaffold was prepared with two bony ends, implanted into goat knees and terminated after 6-months implantation due to failure. The explants were found to have adjacent synovial cell infiltration into both insertion points and into the outer region of the middle part ($500 \pm 46$ cells.mm$^{-2}$ and $270 \pm 30$ cells.mm$^{-2}$, respectively) but the centre of the scaffold remained acellular (Robayo et al., 2011).

Biological scaffolds prepared by decellularisation of natural mammalian tissues have been engineered by nature. They provide natural ECM and can be prepared using optimal processes to be use for clinical needs (Holmes, 2002). In theory, once implanted they should be remodelled and restore their structure and function to adapt to the new implanted environment (Badylak et al., 2009). Natural tissues contain foreign cells that lead to the rejection of allogeneic and xenogeneic tissues. Removing the cells using physical or chemical methods during a decellularisation process may produce acellular biological scaffolds. Nowadays, studies investigating the utility of acellular biological scaffolds are widely reported. Many different techniques have been used in the decellularisation processes with different tissue sources, allograft or xenograft. Xenograft is most often used to produce biological scaffolds and the best

option to be employed in tissue engineering strategies for ligament replacement is the porcine patellar tendon because it has the right size, possesses the mechanical properties and also it is a ligament.

Chemicals such as detergents; SDS (sodium dodecyl sulphate), Triton-X 100, tri-nitro-buthyl-phosphate (TnBP) have been used to solubilise cellular membranes and have been used to decellularise tissues such as heart valve, tendon or organs; such as liver. Porcine aortic and pulmonal roots have been shown to be decellularised with minimal ECM disruption using 0.5 % (w/v) Triton-X100, 0.25 % (w/v) SDS, but not with 0.5 % (w/v) SDS and trypsin treatment. Trypsin at a very low concentration (0.1 %) (w/v) combined with SDS 0.5 % (w/v) were found to damage the matrix (Kasimir et al., 2003). For the porcine heart valve, N-lauronylsarcosinate and lactated Ringer`s altered the matrix structure whilst retaining a small number of cells in the arterial wall (Hilbert et al., 2004). Porcine diaphragm has been decellularised using TnBP (1 %) with minimal disruption of the structure and tissue composition (Deeken et al., 2011).

SDS is one of the negatively charged sulphate group of detergents and has an amphipathic molecule with a hydrophilic head and a hydrophobic carbon chain. It can solubilise hydrophobic molecules in water including the lipid bilayers of cell membranes, which are disintegrated and form mixed micelles (Bhairi and Mohan, 1997). SDS has been used widely to decellularise different tissues using various concentrations for each specific tissue; such as 0.1 % (w/v) for human ACL (Ingram et al., 2004) and human flexor tendon (Raghavan et al., 2012), 1 % (w/v) SDS for human umbilical vein (Abousleiman et al., 2008), 0.5 % (w/v) for porcine cornea (Du and Wu, 2011) and 1 % (w/v) for human flexor tendon (Pridgen et al., 2011). SDS 0.1 % (w/v) has been shown to be superior and the optimal concentration to remove cells from the intrasynovial tendons, compared to the application of Triton X-100 1 % (w/v), TnBP 1 % (w/v) or 1 % (w/v) SDS following 0.1 % (w/v) EDTA treatment. The superiority of SDS 0.1 % (w/v) treatment was shown due to no changes in the mechanical properties compared to the fresh tendons (Pridgen et al., 2011). Human flexor tendons decellularised using 0.1 % (w/v) EDTA, 0.1 % (w/v) SDS and 5 % (v/v) peracetic acid were implanted in the rats for four weeks showed

no B-cell (CD20) and macrophage (CD68) infiltrations, no change in the UTS but decrease of elastic modulus into half (Macnicol et al., 1991, Raghavan et al., 2012).

The levels of SDS in acellular biological scaffolds have been shown to affect the cellular in growth rate. Gratzer et al., used 1 % (w/v) SDS to decellularise bone-patella tendon bone and demonstrated that an alkaline (pH 9) and 70 % (v/v) alcohol washes following their decellularization process reduced the SDS residual levels 8 and 23 times lower, respectively, compared to the reported cytotoxic threshold level (10 $\mu$g.mg$^{-1}$ SDS in dry tissue) (Arechabala et al., 1999, Gratzer et al., 2006).

Sterilization is crucial to ensure the safety of scaffolds for tissue engineering applications. However, the sterilisation method must, ideally, not change the mechanical and biological properties of the scaffold. The use of the chemical sterilant, peracetic acid 0.1 % (v/v) in PBS for three hours has been shown to sterilize biological material such as human skin without cytotoxic effects or matrix disruption (Lomas et al., 2003). It has also been used to successfully sterilise human bone (Pruss et al., 2001). Ethylene oxide gas can be used as a sterilant however; it has been shown to produce cytotoxic, teratogenic, mutagenic and genotoxic residuals (Roberts et al., 1991, Silvaggio et al., 1993).

The University of Leeds has been studying decellularisation of tissues for over a decade. Numerous patents have been generated based upon an underpinning decellularization method using 0.1% (w/v) SDS in the presence of proteinase inhibitors (Booth et al., 2002) and the application of ultrasonification to increase tendon scaffold porosity (Ingram et al., 2004). Decellularised technique to produce tendon scaffolds proprietary by the University of Leeds has been published and undergone different validations (Ingram et al., 2004, Ingram et al., 2006). The decellularised PPTs can be used as a scaffold if they have fulfilled the criteria as an acellular scaffold; such as being free from cells/ DNA and any cellular remnants, have retained their histoarchitecture, are sterile and biocompatible, and have retained their biomechanical properties.

| Agent/ techniques | Mode of action | Effects on ECM |
|---|---|---|
| **Chemical agents** | Solubilise cytoplasmic components of cells, disrupt nucleic acids and tend to denature protein. | |
| 1. Acids and bases | | Damage collagen, GAG and growth factor |
| 2. Hypotonic and hypertonic solution | Lyse cells by osmotic shock and disrupt DNA protein interaction. | Effective to lyse cells however it cannot remove cell remains. |
| 3. Non-ionic detergents | | |
| - Triton X-100 | Disrupt DNA-protein, lipid-lipid and lipid-protein interactions, however less in between protein. | Mixed results with efficacy dependent on tissue; more effective cell removal from thin tissue. However, it causes ultrastructure disruption, GAG removal and less effective than SDS. |
| 4. Ionic detergents | | - Effectively removes nuclear remnants and cytoplasmic proteins from dense tissue, tends to disrupt ultrastructure, removes GAGs and growth factors, damages collagen. |
| - Sodium dodecyl sulphate (SDS) | Solubilizes cell and nucleic membranes, tends to denature proteins | |
| - Sodium deoxycholate | | - Mixed results with efficacy depend on tissue thickness, some disruption of ultrastructure and removal of GAGs. |
| -Triton X-200 | | - More effectively remove cells from thin tissue but with greater disruption of ultrastructure compared to other detergents. |
| 5. Zwitterionic detergents -CHAPS, Sulfobetaine-10 (SB-10) and -16 (SB-16) | Exhibit properties of non-ionic and ionic detergents | - Effectively removes cells with mild disruption of ultrastructure in thin tissues. |

| 6. Solvent | | - Effectively removes cells from dense tissue and inactive pyrogens but crosslinks and precipitates proteins, including collagen. |
|---|---|---|
| - Alcohols or acetone | Cell lysis by dehydration, solubilised and removes lipids. | |
| - Tri(*n*-butyl) phosphate (TnBP) | Forms stable complexes with metal, disrupts protein-protein interactions | Mixed results with efficacy dependent on tissue, dense tissues lost collagen but impact on mechanical properties was minimal. |
| **Biological agents** | | |
| 1. Enzymatic | Catalyse the hydrolysis of ribonucleotide and deoxyribonucliotide chains | |
| - Nucleases | | Difficult to remove from tissue and could evoke immune response. |
| - Trypsin | Cleave peptide bonds on the C-side of Arginine and Lysine. | Prolonged exposure can disrupt ECM ultrastructure, removes ECM constituents such as collagen, laminin, fibronectin, elastin and GAG (slower removal of GAG compared to detergents). |
| - Dispase | Cleave specific peptides, mainly fibronectin and collagen IV. | Prolonged exposure can disrupt ECM, removes ECM components such as fibronectin and collagen IV. |
| 2. Chelating agent (EDTA, EGTA) | Chelating agents bind metallic ions thereby disrupting cell adhesion to ECM. | Typically used with other enzymatic methods, ineffective when used alone. |
| **Physical methods** | Disrupt cell membrane by forming intracellular ice crystals. | |
| 1. Freeze and thaw | Removal of tissue eliminated cells and force | Ice crystals may disrupt and fracture ECM |

| | | |
|---|---|---|
| 2. Mechanical force | can burst remaining cells. | Force can damage ECM |
| 3. Pressure | Pressure can burst cells and aid in removal of cellular material. | Pressure can damage ECM |
| 4. Electroporation | Pulsed electrical fields disrupt cell membranes. | Electrical field oscillation can disrupt ECM. |
| **Techniques to apply agents** | | |
| 1. Perfusion | Facilitate chemical exposure and removal of cellular material | Pressure associated with perfusion can disrupt ECM |
| 2. Pressure gradient across tissue | Pressure can burst cells | Pressure gradient can disrupt ECM. |
| 3. Supercritical fluid | Supercritical fluid facilitates chemical exposure and removal of cellular material | Pressure associated with the supracritical phase can disrupt ECM. |
| 4. Agitation | Lyse cells and facilitate chemical exposure and removal of cellular material | Aggressive agitation or sonification can disrupt ECM |

**Table 1.3 Basic techniques to decellularise tissues.** This table is adapted from Crapo et al. (2011).

### 1.5.3. Cells sources for ligamentous tissue engineering

In tissue engineering, the aim is to manipulate cells to grow on scaffolds in an effort to produce neo-tissues, which are as close as possible to the natural tissue to be replaced. Cells can be stimulated to grow appropriately in the artificial microenvironment and reproduce the reciprocal interaction between the cells and the scaffold. Promotion of cell differentiation to the desired phenotype will be dependent upon the matrix having the appropriate physical properties and by facilitating communication of cells to cells and cells to matrix (Chen et al., 2003b, Serban et al., 2008).

Autologous cells are the ideal choice for seeding onto the scaffold, using mature differentiated cells (ACL fibroblasts, tenocytes) or progenitor cells (stem cells). Human fibroblasts, however, have a limited lifespan (Hayflick and Moorhead, 1961) and only limited cell numbers can be harvested from a patient without a major operative procedure. Human mesenchymal stem cells (human MSCs), however, can be derived from adipose tissue or bone marrow (5-10 mL) and have an extended lifespan. Human MSCs are multipotential cells that may be differentiated into a range of mesodermal cell types (Chen et al., 2003b). They can be cryopreserved as stock, expanded and derived into many cell types. In addition, it has been shown that MSCs seeded into a ligament scaffold can produce collagen (Sahoo et al., 2010). Human bone marrow stem cells (human BM-MSCs) have been shown to function significantly better in ligament scaffolds compared to ACL fibroblasts when seeded on an RGD-modified silk scaffold. The human BM-MSCs had better capability to attach to the RGD-silk matrix and as a result, it had higher cell density and ECM production. Both cell types were seeded and cultured for six days in both static and dynamic conditions (1 Hz tensile loading associated with 0.5 mm linear and 45° rotational displacement) (Chen et al., 2003b).

Other cellular sources, such as adipocyte stem cells, although more abundant, however, they have more adipogeneic tendency during differentiation. Tendon-specific MSCs isolated from the ACL possess a higher tendency to express tenocyte markers such as collagen I, collagen III

and tenascin-C (Huang et al., 2008), lead to tenogenesis in response to mechanostimulation (Zhang and Wang, 2010). Tendon-specific MSCs isolated from injured tendon tends to differentiate into a chondrogeneic derivation (Asai et al., 2014).

In general, cells exhibit several behaviours when seeded into scaffolds such as cell adhesion, migration, proliferation, differentiation and aggregation. Initially, cell adhesion to the scaffold is a weak transient bonding to allow cell migration in between the fibres. Adhesion initiates cell differentiation, protein secretion, receptor activation, cell movement, cell division or gene expression in response to the environment (Pollard et al., 2008). Cell adhesion to the scaffold surface can be easily quantified by measuring the cell number on the surface (Saltzman, 2000). Cell migration into the scaffold or association with other cells is essential in forming tissue architecture (Trinkhaus, 1984). Cell aggregation influences cell differentiation, viability and migration (Landry et al., 1984), and plays an important role in reconstructing an engineered tissue (Vacanti and Langer, 1993). Moreover, optimal nutrition achieved by perfusion into the scaffold is crucial to successful tissue engineering. Necrotic cores have been found in cell aggregates of more than 1 mm diameter in-vitro (Altman et al., 2002b).

Cells to cells contact and cell shape are reported to drive the MSC's commitment to differentiate into osteocytes or adipocytes. After 4-weeks culture in an adipogenic medium, human MSCs at higher cell density ($21,000$ cells.cm$^{-2}$ and $25,000$ cells.cm$^{-2}$) formed fat drops, but no fat drops could be found at lower cell densities ($1000$ and $2000$ cells.cm$^{-2}$). In contrast, human MSCs cultured in osteogenic medium expressed more alkaline phosphatase at the lower density than at the higher density. Low-density cells had a flat and spread cell shape, which switched on the endogenous Rho and derived the human MSCs into osteocytes. On the other hand, Rho inhibition resulted in a rounded shape and drove the human MSCs to differentiate into adipocytes (McBeath et al., 2004).

Growth factors are also believed to aid cell proliferation and migration. An optimal concentration of external doses of the right growth factor delivered at the right time may be the

key to success and to improve cell growth in-vitro. However, this type of intervention is very subjective, and inaccuracy of dosage or timing may cause significant errors. To deal with this, genetically engineered cells that can produce their own growth factors and can adjust their needs in response to interactions with the scaffold can be implemented. Steinert et al. seeded ACL fibroblast cells as a monolayer onto hydrogels scaffolds. The cells were transfected with adenovirus to deliver insulin like growth factor gene (IGF-1 cDNA). They showed that IGF-1 increased fibroblast proliferation, as well as the collagen type I and III, elastin, tenascin-C and vimentin production (Steinert et al., 2008). Bone morphogenic protein (BMP) is also believed to increase Achilles cell proliferation and collagen production (Majewski et al., 2008).

### 1.5.4. Mechanotrasduction; in the knee and in the bioreactor

The control of the loading stress to direct the tissue structure is demonstrated early in the developmental process in which foetal movement determines articular structure (Watanabe, 1974). The knee joint is a highly active joint with about 2 - 4 million flexions and extensions per year, or nearly 8 million in an active athlete (Olson et al., 1988). This highly repetitive loading strain is transmitted to the mechanosensitive knee ligament and tendon cells that are aligned within the tissue matrix. The strain stress drives the cells to express defined genes (Garvin et al., 2003). The distribution of mechanical force transduction is translated into chemical information and gene expression that influences cell shape and even determines cells apoptosis (Chen et al., 1997, Chiquet et al., 2009). This process is needed to maintain tendon homeostasis through the balance of ECM turnover and matrix degragation (Killian et al., 2012).

Loaded ECM fibres contract isometrically and generate dense arrays of microfilaments, and the construct is disintegrated when tension is released (Burridge and Chrzanowska-Wodnicka, 1996). Later, these forces are translated into chemical signals and transported to cell nucleus to promote translocation and transcription to regulate the cell cycle, cell phenotype and movement, as the responses to the environment stimulation (Orr et al., 2006, Miralles et al., 2003). Integrins are linked to the cell cytoskeleton through the vitronectin receptor $\alpha v\beta 3$ to form a "focal complex" (less than 1 μm). When tension is increased, more integrin molecules are recruited

(fibronectin receptor α5β1, vinculin, thalin, paxillin and α-actinin) and form a "focal adhesion".

Fibrillar adhesion has fibronectin receptor α5β1 that resists parallel tension [Figure 1.15]. The

cascade of the cell response to strain stimulation is described in Figure 1.16.
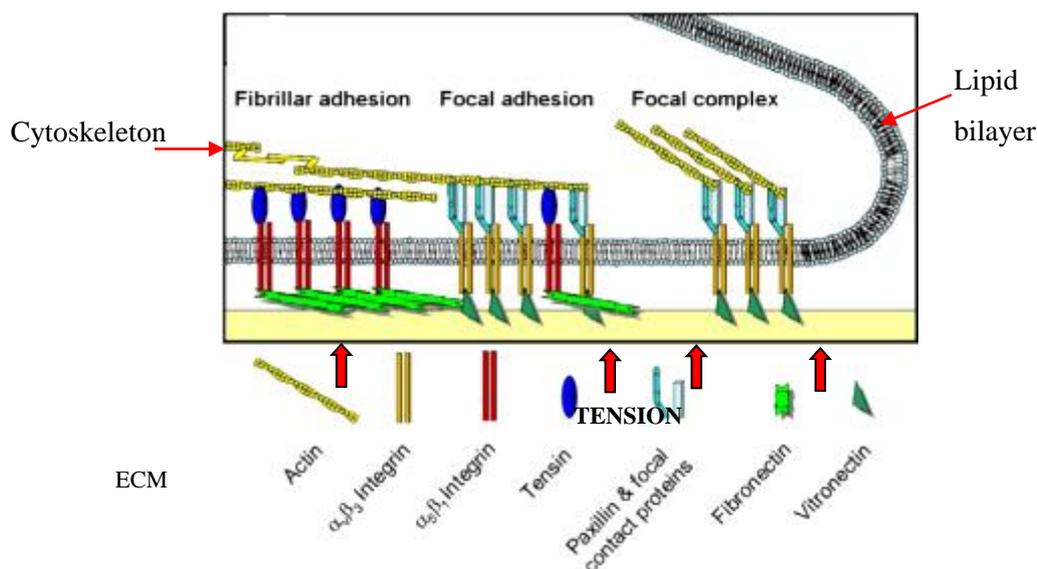


**Figure 1.15 Cell responses to mechanotransduction**. Fibroblast cell membrane, tensile loading is mediated mostly by the integrin family of molecules which form focal complexes (< 1 μm). When the tension is increased, this complex becomes more complex and larger. It forms focal adhesions. Fibrillary adhesion is a different complex formed under parallel tension. Images was taken from Chiquet et al. (2009).
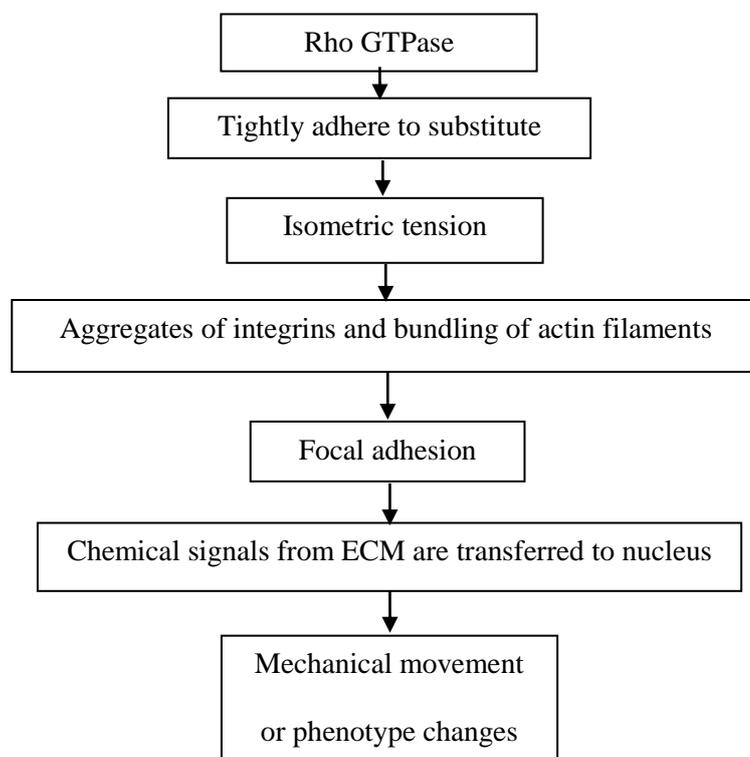


**Figure 1.16 Cascade of an external tensile stimulation to cells.** Figure is adapted from Miralles et al. (2003).

Progenitor cells have also been shown to express different responses to tensile loading. MSCs cultured in a collagen type I hydrogel have been shown to express collagen type I and III, fibronectin and elastin at significantly higher levels when subjected to 10 % strain, 1 Hz uniaxial tensile culture for 14 days, compared to the static group (Stehle et al., 2006). Beta-actin and decorin were also found to be more highly expressed in BAT (bio-artificial tendon) compared to unstimulated scaffolds (Garvin et al., 2003), as well as tenascin-C after 21 days culture under 10 %-1 Hz tensile loading in poly(ethylene glycol) based hydrogel scaffolds (Doroski et al., 2010).

## 1.8. Overall aim and objectives

The aim of this study was to investigate the responses of human BM-MSCs seeded onto decellularised porcine patellar tendon (PTT) and cultured under 4, 6 and 8 % cyclic uniaxial tensile strain in-vitro in the TenCell-1 bioreactor.

The objectives were:

1. To generate decellularised PPTs using the University of Leeds proprietry process

2. To characterise human BM-MSCs following the criteria of the ISCT and develop suitable culture conditions for the cells

3. To develop a method for seeding the BM-MSCs onto the decellularised PPT scaffolds

4. To culture the human BM-MSCs seeded onto the decellularised PPT scaffolds under 4, 6 and 8 % cyclic uniaxial tensile strain in the TenCell-1 bioreactor and determine the expression of genes indicative of tenogenesis, chondrogenesis, osteogenesis and adipogenesis.

## 1.9. Experimental design

Porcine patellar tendons (PPTs) were decellularised using the decellularisation protocol of the University of Leeds. Porcine PT is the best candidate to study a regeneration the decellularised ligamentous scaffolds using human BM-MSCs because it has an appropriate size (Dahlin et al., 1991), has similar micro architechture (Derwin et al., 2006, Valentin et al., 2006), has a comparable mechanical properties (Barber et al., 2006) to the ACL, and had been used extensively in musculoskeletal research (Stone et al., 2007). Pig is also the favourable animal, since its knee is anatomically similar with human, pigs are also widely available and the pig maturity can be consistent (Kwan et al., 1993). There are numerous porcine extracellular matrices that have been used clinically, such as the dermal matrix; cross-linked and non cross-linked (Permacol™ and Strattice™) (Cheng et al., 2014a, Caviggioli et al., 2014), the small intestinal submucosal (SIS); Restore™ (DePuy Orthopaedics), Cuffpatch™ (Organogenesis Inc.) (Coons and Barber, 2006), the heart valves; Prima™ (Edward Lifesciences), and bladders; Acell Vet (Acell Inc).

The decellularised PPT scaffolds were analysed for their biological and biomechanical properties to ensure that the decellularisation process had not damaged the properties of the tendon matrix. Their collagen fibre was analysed using Pico Sirius red and Miller's elastin staining to show the collagen structure, following the protocol described by Junqueira et al. (1979). Scaffold acellularity and ECM histoarchitechture were analysed using H&E and DAPI. Further assay to assure that no genomic materials remain in the matrix was to quantify the DNA extracted from the matrices (ng.mg$^{-1}$ dry weight tissue). DNA remnants in the implant constructs may cause an inflammatory reaction (Zheng et al., 2005), therefore it is important to trace removal of DNA residue in the decellularised matrices.

Investigations of ECM components in the decellularised tendon of collagen I, III and tenascin C were carried out using immunohistochemistry techniques specific to those proteins, described by Hsu et al. (1982); (Hsu and Soban, 1982). Collagen I and collagen III proteins in the ECM were observed due to their mechanical roles in tendon (Amiel et al., 1983). Dry weight tendon

contains high compositions of collagen I (78%) and collagen III (19%) (Tsuzaki et al., 1993). Tenascin-C, the macromolecule hexameric glycoprotein is highly expressed in the tensile-subjected tissue such as tendon, and its expression indicates tenocyte activities (Jarvinen et al., 1999).

The sterilisation technique to sterilise the decellularised PPT was following a method described by Lomas (Lomas et al., 2003). To determine the sterility of the decellularised matrices, nutrient broth and agar plates were used. Contact biocompatibility assay is needed to ensure that the decellularised products are not toxic.

Human BM-MSCs were prepared and seeded onto the tendon scaffolds, and the responses of the cell-seeded tendon scaffolds when incubated under mechanical strains in the TenCell-1 bioreactor were investigated. Porcine BM-MSCs were initially used to learn different techniques such as for cell handling and to develop several methods before using human BM-MSCs.

The responses of human BM-MSCs seeded onto decellularised PPT scaffolds were determined by viability analysis (Live/Dead assay and ATPlite™ assay), histological (H&E, DAPI staining) and immunohystochemical analysis of the ECM components, and transcript gene expressions indicating tenogenesis. Gene expressions of the adipogenesis, chondrogenesis and osteogenesis were used as the controls.

The experimental design of this study is summerised in Figure 1.17.
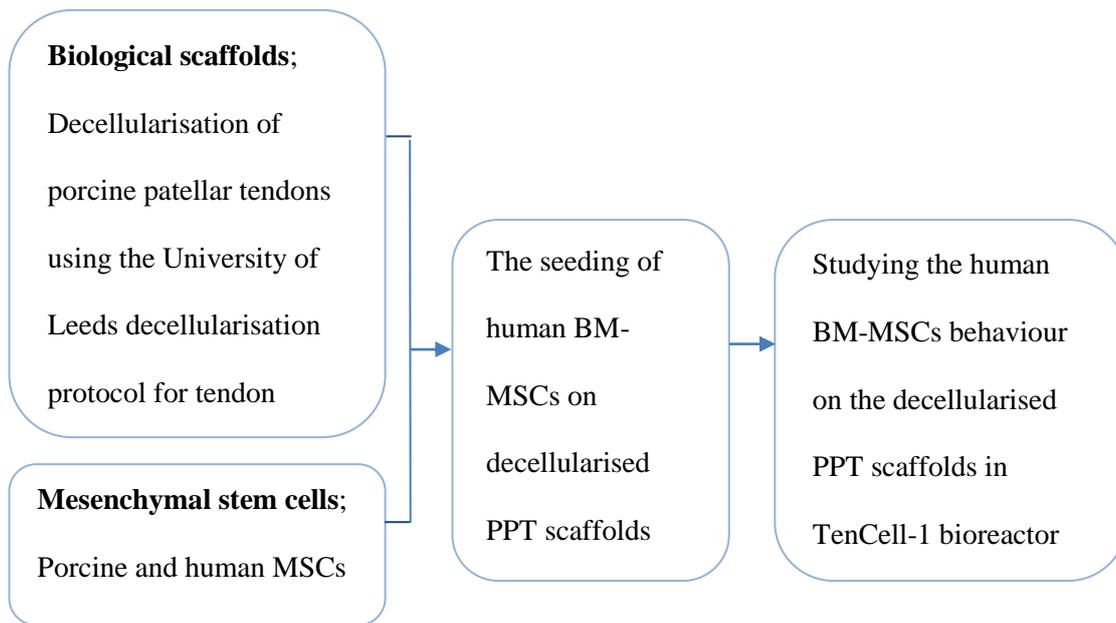
**Figure 1.17 Experimental design of the regeneration of decellularised tendon by human MSCs in response to uniaxial tensile strains.**

# Chapter 2 Materials and Methods

## 2.1. General Materials

### 2.1.1. Consumables

#### 2.1.1.1. Sterile plastic-ware

Details of plastic-ware used throughout this study are listed in Table 2.1

| Sterile plastic ware | Size | Supplier |
|---|---|---|
| Bijous | 5 mL | Scientific Laboratory Supplies (SLS) Ltd |
| Conical tubes | 15 mL | Thermo Fisher Scientific Ltd |
| Cryovials | 2 mL | Sigma Aldrich Ltd |
| Multi-well plates, Nunc® (flat and round bottomed) | 6-well, 12-well, 24-well, 48-well, 96-well | Thermo Fisher Scientific Ltd |
| Optiplate™-white | 96 well | Perkin Elmer Ltd |
| Petri dish | 90 mm | Thermo Fisher Scientific Ltd |
| Pipette tips (non-filtered and filtered) | 2 μL, 20 μL, 200 μL, 1000 μL | Star Labs |
| Plastic containers | 60 mL, 150 mL, 250 mL | SLS Ltd |
| Stripette ™ (disposable pipettes) | 1 mL, 2 mL, 5 mL, 10 mL, 25 mL | Sigma Aldrich Ltd |
| Syringe filter unit | 0.22 μm, 33 mm | Merck Millipore |
| Syringes | 1 mL, 5 mL, 10 mL, 15 mL, 25 mL | SLS Ltd |
| Syringes needles | 25 G, 21 G | SLS Ltd |
| Tissue/slide culture plate | 4-well | VWR International |
| Universals | 25 mL | SLS Ltd |

**Table 2.1 Sterile plastic-ware used during the study including the suppliers**

## 2.1.1.2. Miscellaneous consumables

Consumables used throughout this study are listed below;

| Items | Model/Size | Supplier |
|---|---|---|
| Cover slips | 22 mm$^2$, 22 x 64 mm | SLS Ltd |
| Filter paper | Whatman® Grades 1-5 | Whatman International Ltd |
| Histology cassettes | Histocette® | VWR International |
| Microscope slides | Superfrost, Superfrost Plus® | VWR International |
| Microtome blades | - | Raymond A Lamb |
| Parafilm M | - | Sigma Aldrich Ltd |
| Scapel blades | No 22 | Thermo Fisher Scientific Ltd |
| Superfrost plus® slides | - | SLS Ltd |
| TopSeal | - | Perkin Elmer Ltd |

**Table 2.2 Other consumables used in this study**

## 2.1.1.3. Chemicals

Details of general chemicals and reagents used throughout this study are listed in Table 2.3.

| Chemical/ Reagent | Supplier |
|---|---|
| 1,4-diazobicyclo-(2, 2, 2)-octane (DABCO) | Sigma-Aldrich Ltd |
| 1,9 dimethylene blue | Sigma-Aldrich Ltd |
| 1.5 M sodium chloride | Fisher Scientific |
| 3M Steri-Strip® SkinClosure 3 x 75 mm | Medisave |
| 4',6-Diamidino-2-phenylindole dihydrochloride (DAPI) | Thermo Fisher Scientific Ltd |
| Acetic acid | VWR International |
| Aceton | European Bios |
| Ammonium sulphate | VWR International |
| Aprotinin (10,000 KIU.mL$^{-1}$) | Mayfair house, Leeds Teaching |

| | hospital |
|---|---|
| Ascorbic acid | Sigma-Aldrich Ltd |
| Ascorbic-2-phosphate | Sigma-Aldrich Ltd |
| ATPlite™ assay kit | Perkin Elmer Ltd |
| Benzonase nuclease, purity > 99 % (250 U.$\mu$L$^{-1}$) | G Biosciences |
| Bovine serum albumin | Sigma-Aldrich Ltd |
| Calcium acetate (anhydrous/dried) | Thermo Fisher Scientific Ltd |
| Calcium chloride | VWR International |
| Camptothecin | Sigma-Aldrich Ltd |
| Citric acid monohydrate | VWR International |
| Cyanoacrylate adhesive | VWR International |
| Dexamethas1 | Sigma-Aldrich Ltd |
| Dimethyl sulphoxide (DMSO) | Invitrogen |
| Disodium ethylenediaminetetraacetic acid (EDTA) | Thermo Fisher Scientific Ltd |
| DNeasy blood and tissue kit | Qiagen |
| DPX mountant | Thermo Fisher Scientific Ltd |
| Dulbecco's modified Eagle's medium (DMEM) | Gibco Life Technologies Ltd |
| Dulbecco's PBS solutions without MgCl$_2$ and CaCl$_2$ | Sigma-Aldrich Ltd |
| Dulbecco's phosphate buffered saline (PBS) solutions with MgCl$_2$ and CaCl$_2$ for cell culture | Sigma-Aldrich Ltd |
| Eosin | VWR International |
| Ethanol 100 % (v/v) | Thermo Fisher Scientific Ltd |
| Ethanol 100 % (v/v) molecular biology grade | Thermo Fisher Scientific Ltd |
| Foetal bovine serum (FBS) | Biosera |
| Giemsa solution | WVR International |
| Glasgow minimum essential medium (GMEM) | Sigma-Aldrich Ltd |
| Glycerol 100 % (v/v) | Thermo Fisher Scientific Ltd |

| | |
|---|---|
| Haematoxylin | Thermo Fisher Scientific Ltd |
| Histo-clear III | National Diagnostics |
| Horse serum 10 % (v/v) | Lonza |
| Hydrochloric acid | WVR International |
| Hydrocortisone | Acros-Organics |
| Hydrogen peroxide 30 % (v/v) | Sigma-Aldrich Ltd |
| ImmEdge hydrophobic barrier pen | Vector Laboratories |
| Indomethacin | Sigma-Aldrich Ltd |
| Intrastatin, fixation and permeabilisation kit for Flow Cytometry | Dako Ltd |
| Insulin transferring selenium (ITS) | Gibco Life Technologies Ltd |
| L-glutamine (200 mM) | Gibco Life Technologies Ltd |
| Liquid nitrogen | BOC Edwards |
| LIVE/DEAD® assay kit | Invitrogen Ltd |
| Magnesium chloride | Thermo Fisher Scientific Ltd |
| Magnesium sulphate | Acros Organics |
| Magnifying lamp | Daylight company |
| Mayer's haematoxylin | Bios Europe Ltd |
| Methanol | Vickers Laboratories |
| Methylated spirits | Biostains Ready Reagents |
| Miller`s stain | Raymond A Lamb |
| N-(2-hydroxyethyl) piperazine N;-(2-ethansulphonic acid) [HEPES] (1 M) | Lonza |
| Neutracon® | SLS Ltd |
| Neutral buffered formaldehyde (NBF) 10 % (v/v) | Atom Scientific |
| N-Lauryl sarcosine sodium salt | Sigma-Aldrich Ltd |
| Nutrient Broth | N/A |

| | |
|---|---|
| Oxalic acid | Fisher Scientific |
| Paraffin wax pellets | Bios Europe Ltd |
| Penicillin 5000 U.mL$^{-1}$ - Streptomycin 5 mg.mL$^{-1}$ | Lonza |
| Peracetic acid | Sigma-Aldrich Ltd |
| Percoll | Sigma-Aldrich Ltd |
| pH standards (4, 7, 10) | SLS Ltd |
| Phosphate buffered saline (PBS) tablets | Oxoid |
| Phytohaemagglutinin | Sigma-Aldrich Ltd |
| Picric acid | Sigma-Aldrich Ltd |
| Potassium permanganate | Thermo Fisher Scientific Ltd |
| Proteinase K | Dako Ltd |
| RNase A (100 mg.mL$^{-1}$) | Qiagen |
| Scott's tap water | Atom Scientific |
| Sheath Fluid (FASC instrument) | Becton & Dickenson |
| Sirius red | Sigma-Aldrich Ltd |
| Sodium acetate | Thermo Fisher Scientific Ltd |
| Sodium azide 1 % (w/v) solution | G Biosciences |
| Sodium bicarbonate | Sigma-Aldrich Ltd |
| Sodium chloride | Thermo Fisher Scientific Ltd |
| Sodium dodecyl sulphate (SDS) | Sigma-Aldrich Ltd |
| Sodium hydrogen carbonate | VWR International |
| Sodium hydroxide | Thermo Fisher Scientific Ltd |
| Sodium pyruvate | Sigma-Aldrich Ltd |
| Streptavidin biotin blocking reagent | Vector Laboratories |
| Transforming growth factor β3 (TGF β3) | Sigma-Aldrich Ltd |
| Trigene® | SLS Ltd |
| Trizma® base | Sigma-Aldrich Ltd |

| | |
|---|---|
| Trypan blue (0.4 %) (v/v) | Sigma-Aldrich Ltd |
| Trypsin 0.5 % (v/v) with EDTA (10 x) | Invitrogen |
| Trypsin porcine pancreas | Sigma-Aldrich Ltd |
| Tryptose phosphate broth (TPB) | Sigma-Aldrich Ltd |
| Tween 20® | Sigma-Aldrich Ltd |
| Tyrode's solution | Sigma-Aldrich Ltd |
| Ultra-Vision DAB plus substrate system | Thermo Fisher Scientific Ltd |
| Ultra-Vision 1 detection system, HRP polymer | Thermo Fisher Scientific Ltd |
| Virkon | Bios Europe Ltd |
| Xylene | Biostains Ready Reagents |
| Zinc acetate | Sigma-Aldrich Ltd |
| Zinc chloride | Fluka |
| β-mercaptoethanol | Sigma-Aldrich Ltd |

**Table 2.3 Chemicals and reagents used throughout this study including suppliers**

## 2.1.2. Equipment

All equipment was obtained from reputable suppliers, maintained according to the manufacturer`s instructions and periodically calibrated. A full list of equipment used during this study is presented in Table 2.4.

| Equipment | Model | Supplier |
|---|---|---|
| 5 % (v/v) $CO_2$ incubator | MCO-20AIC | Sanyo Biomedical Europe BV |
| Automatic pipettes | Gilson P2-P500 | Anachem Ltd |
| Balance | GR200/ GX2000 | Jencons Plc |
| BD FACS Flow | BD | Becton Dickson |
| BioBath | Model 3130-100 | Instron |
| Centrifuge | Harrier 15/80 | Sanyo Biomedical Europe BV |
| Centrifuge-Micro | MSE Micro Centaur I | Sanyo Biomedical Europe BV |

| | | |
|---|---|---|
| Class II safety cabinet | Heraeus 85 | Kendro |
| Constant power supply | LKB2301 | Bio-Rad Laboratories |
| Counting chamber Improved Neubauer | HAE2012 | SLS Ltd |
| Digital camera (hand held) | DX6490 | Kodak Ltd |
| Digital camera (microscope) | Evolution™ MP (Olympus CK40) | Media Cybernetics Olympus |
| Digital camera (microscope) | AxioCam MRc5 (Axio - Imager M2) | Zeiss |
| Digital colour camera (microscope) | Evolution™ MP5 colour (Olympus IX71) | Media Cybernetics Olympus |
| Digital vernier calliper | 150 mm | Bargain Universe |
| Dissection clamp | N/A | Mech-Eng, University of Leeds |
| Dissection kit | N/A | Stewart Thackray Instrument |
| Dry heated oven | Sanyo OMT225 | Sanyo Biomedical Europe BV |
| Freeze dryer | Savant ModulyoD | Thermo Fisher Scientific Ltd |
| Freezer -20 °C | Electrolux 3000 | Jencons PLC |
| Freezer -80 °C | MDF-U72V | Sanyo Biomedical Europe BV |
| Fridge | Electrolux ER8817 C | Jencons Plc |
| Fume hood | - | Whiteley |
| High speed centrifuge | Evolution RC | Sorvall® Evolution RC |
| Histology water bath | 3 L histology bath | Leica Microsystems |
| Hot air oven | Sanyo OMT225 | Sanyo Biomedical Europe BV |
| Hot wax dispenser | E66 wax dispenser | Raymond A Lamb |
| Hot wax oven | Windsor E18/31 | Raymond A Lamb |
| Hot plate | E18.1 hot plate | Raymond A Lamb |
| ImmEdge hydrophobic | H-4000 | Vector Laboratories |

| barrierpen | | |
|---|---|---|
| Incubator | Sanyo4808 | Sanyo Biomedical Europe BV |
| Laminar flow cabinet | Bassaire 06HB | Jencons Plc |
| Liquid nitrogen dewar | BIO 65 | Jencons Plc |
| Luminescence counter and liquid scintillation counter | Packard TopCount NX | Perkin Elmer Ltd |
| Magnetic stirrer | Stuart SB161 | SLS Ltd |
| Microplate reader | Multiscan spectrum | Thermo Electronic Corporation |
| Microscope inverted | Olympus IX71 | Olympus Optical Co (UK) Ltd |
| Microscope upright | Axio-Imager M2 | Zeiss |
| Microscope upright | Olympus CK40 | Olympus Optical Co (UK) Ltd |
| Microscope upright | Olympus BX71 | Olympus Optical Co (UK) Ltd |
| Microtome | RM2125 RTR | Leica Microsystem |
| Microwave | SI50 | Stuart Scientific |
| Nanodrop Spectrophotometer | ND-1000 | Labtech Int |
| Orbital shaker | POS 300/ PSU-10i | Grant-bio |
| pH meter | Jenway 3510 | VWR International |
| Pipette boy | Accu-classic | SLS Ltd |
| Plate shaker | IKA KS 130 basic | Jensons Plc |
| Ruler | - | Products Engineering |
| Slide holder | E102 | Raymond A Lamb |
| Spatula | Fisherbrand | Thermo Fisher Scientific Ltd |
| Tensile testing machine | Model 3365 | Instron |
| Thermocouple | T type (IT-21) | Physitemp Instruments Inc |
| Thermocouple (WATLOW) | T type | WATLOW |
| Thickness gauge | J-40-T | Schmidt |
| Tissue processor | Leica TP 1020 | Leica Mycrosystems |

| | | |
|---|---|---|
| Tube-strip PicoFuge™ | Model 137859 | Stratagene |
| Ultrahigh speed centrifuge | Sorvall Discovery 100 SE | Thermo Electronic Corp. |
| Vortexer | Clifton CM-1 | SLS Ltd |
| Vacuum pump | RV8 | Edwards |
| Water bath | Grand | Jencons Plc |
| Water purifier | Option 7 | ELGA |

**Table 2.4 Equipment used during this study including the model and supplier**

### 2.1.2.1. Glassware

Bottles, measuring cylinders, beakers (100 mL, 1000 mL, and 2000 mL), Pyrex hybridization bottles (300 x 35 mm, 250 x 35 mm, 150 x 35 mm) and Pyrex glass Petri dishes (90 mm x 16.2 mm) were purchased from Thermo Fisher Scientific Ltd. Glass troughs were purchased from Raymond A Lamb. The glassware was cleaned by soaking overnight in 1 % (v/v) Neutracon®, washed thoroughly in tap water and subsequently three times in distilled water. Glassware was sterilised by dry heat in an oven at 190 °C for 4 hours.

### 2.1.3. Antibodies

The antibodies and isotype controls used during these studies for immunohistochemistry are shown in below.

| Antibody | Antigen retrieval | Host | Concentration ($\mu g.mL^{-1}$) | Supplier |
|---|---|---|---|---|
| Collagen I/ IgG1 | Proteinase K | Mouse/ Rat | $10 \ \mu g.mL^{-1}$ | Milli Pore/ Dako Ltd |
| Collagen III/ IgG1 | Proteinase K | Rabbit/ Rat | $20 \ \mu g.mL^{-1}$ | Abcam/ GenTech |
| Tenascin-C/ IgG2b | Trypsin | Mouse/ Rabbit | $10 \ \mu g.mL^{-1}$ | Nova/ Dako Ltd |

**Table 2.5 Details of primary antibodies and isotype controls used throughout this study**

## 2.1.4. Cells

Details of cell lines which were purchased from commercial suppliers are presented in Table 2.6.

| Cell | Type | Lot number | Supplier |
|---|---|---|---|
| 3T3 Swiss albino INFORM L055 O | Fibroblast | 04L007 | HPA culture collections |
| BHK 21 Strain 31 | Epithelial | 04H011 | HPA culture collections |
| L929 | Fibroblast | 04102001 | HPA culture collections |

**Table 2.6 Cell lines used throughout this study**

## 2.1.5. General solutions

All solutions were autoclaved and stored at room temperature, unless otherwise stated.

a) Phosphate buffered saline (PBS) solutions

   1 tablet of Oxoid PBS was dissolved into 100 mL of distilled water and the pH was adjusted to 7.3 to 7.4. The solution was stored for up to 1 month.

b) Hydrochloric acid solutions (6 M)

   Hydrochloric acid (250 mL) was mixed with 250 mL of distilled water. The solution was stored up to 3 months.

c) Sodium hydroxide solution (6 M)

   Sodium hydroxide (120 g) was dissolved into 500 mL of distilled water. The solution was stored up to 3 months.

d) Tris solution (2 M)

   Trizma base (242.26 g) was dissolved into 500 mL of distilled water and the pH was adjusted to 7.6. After the pH adjustment, the solution was made up to 1000 mL with distilled water and stored for 1 month.

e) Tris buffered saline (TBS)

Tris solution (25 mL, 2 M) was added to 50 mL of 3 M sodium chloride and the pH was adjusted to 7.6. The solution was then made up to 1000 mL with distilled water.

f) Tryptose phosphate broth (TPB) stock solution

TPB (7.38 g) was dissolved into 250 mL distilled water and filtered through a 0.22 μm filter unit. The sterile solution was stored at $-20^0$ C in 20 mL aliquots for 6 months.

## 2.2. Methods

### 2.2.1. General methods

#### 2.2.1.1. Measurement of pH

The pH of solutions was measured using a Jenway 3020 pH-meter, which was calibrated daily by using standard solutions of pH 4, 7 and 10. The desired pH was achieved by adding 6 M hydrochloride or 6 M sodium hydroxide drop wise.

#### 2.2.1.2. Sterilisation

(a) Dry heat sterilisation

Glass or metal containers to be sterilised were placed in a 190 ℃ oven for four hours.

(b) Moist heat sterilisation

Solutions were sterilised by autoclaving at 121 ℃, 15 psi for 20 min. The lids of containers were loosened during the process to allow steam to escape during the process.

(c) Filter sterilisation

Solutions that were unsuitable to be autoclaved were sterilised by filtering through a 0.22 μm pore size filter. This procedure was performed in a class II safety cabinet.

### 2.2.1.3. Microscopy

(a) Bright-field microscopy

Sections of stained tissues were visualized using an Olympus BX40 microscope. For image capture, an Olympus BX51 microscope with an Evolution MP Colour digital camera was used. This camera was connected to a computer using cell^B® imaging software with correct Kohler illumination. Cells in tissue culture flasks were routinely visualized using an inverted microscope (Olympus CK40) and imaged using an Olympus X71 microscope using the same camera and software.

(b) Fluorescence microscopy

Sections of tissues with fluorescence staining were visualized using an upright fluorescence microscope Zeiss Aixo-Imager 2 and imaged using a Zeiss AxioCam MRc5 camera with Zen Blue software.

## 2.2.2. Basic histological techniques

### 2.2.2.1. Tissue processing and paraffin embedding

Samples prepared for the haematoxylin and eosin (H&E) staining were fixed using NBF 10 % (v/v) (Atom scientific) and for the immunohistochemistry using zinc fixative solutions.

**Zinc fixative solution for tissue fixation**

Calcium acetate (0.5 g) was dissolved into 1000 mL of 0.1 M Tris solution and the pH was adjusted to 7.0 – 7.4. Zinc acetate (5.0 g) and zinc chloride (5.0 g) were then dissolved into the solution. This solution was stored at room temperature up to 3 months.

**Methods**

Tissue samples were placed in histological cassettes (Histocette®) and immersed in the zinc fixative solution (30 to 60 mm3 sample size per mL) for 72 h at room temperature. The cassettes were then dehydrated and infused with wax automatically in the tissue processor using programme 9 for 23 h. Briefly, the cassettes were subjected to 10 steps; 1 h in 70 % (v/v)

ethanol, 1 h in 90 % (v/v) ethanol, 2 h 20 min in 100 % (v/v) ethanol, 3 h 20 min in 100 % (v/v) ethanol, 4 h 20 min in 100 % (v/v) ethanol, 1 h in xylene, 1 h 30 min in xylene, 2 h in xylene, 1 h 30 min in molten wax, 2 h in molten wax, and 2 h in molten wax. After completion, the samples were immersed into molten wax in a wax oven, and each sample was placed into a histology mould, covered with molten wax and left to solidify.

### 2.2.2.2. Sectioning of tissue blocks and slide preparation

The wax blocks were trimmed of any excess wax and left on ice for 10-20 min. The microtome was set at a $5^0$ cutting angle and 6 μm thick sections were cut for all staining methods, except for haematoxylin and eosin (H&E) and Sirius Red – Miller's elastin staining when sections were cut at 10 μm. Sections were floated on a 40 $^0$C water bath and then transferred onto Superfrost plus® slides. The slides were heated on a hot plate (40 $^0$C) to dry the slides and to bake the tissue sections onto the slides.

### 2.2.2.3. Dewaxing and rehydration of paraffin embedded sections

Sections were cleared from the wax by immersion into two separate pots of Histo-clear III for 10 min each and rehydrated in 100 % (v/v) ethanol for 3, 2 and 2 min, respectively, followed by 70 % (v/v) ethanol for 2 min. Slides were rinsed under running tap water for 3 min.

### 2.2.2.4. Haematoxylin and eosin staining

Sections were immersed into haematoxylin for 1 min and rinsed 3 times in running tap water. The sections were then immersed in eosin for 3 min. Sections were dehydrated through a gradient of ethanol; 70 % (v/v) (1 min) to three steps of 100 % (v/v) (2 min twice and 3 min respectively). Sections were immersed in Histo-clear III for 10 min twice, mounted in DPX mountant and covered with a cover slip. The sections were imaged using bright-field upright microscope Zeiss Aixo-Imager M2, captured using a Zeiss AxioCam MRc5 camera with Zen Blue software. Haematoxylin and eosin staining was used to visualize cell nuclei and tissue

histoarchitecture. The haematoxylin will stain the chromatin in blue and the eosin will stain the protein (cytoplasma filaments, extracellular fibres) in pink.

## 2.2.2.5. Sirius Red and Miller's elastin staining

**Solutions**

a) Potassium permanganate 5 % (w/v)

Potassium permanganate (15 g) was added into 300 mL of distilled water and stored at room temperature for 6 months. This solution was filtered before used.

b) Sirius red 0.1 % (w/v)

Sirius red dye (0.1 g) was added into 100 mL of aqueous saturated picric acid solution, filtered and stored at room temperature for six months.

c) Weigerts haematoxylin

Solution A of the Weigerts haematoxylin was mixed equally with the solution B and stored at 4 $^0$C for 1 month.

d) Oxalic acid 1 % (w/v)

Oxalic acid (2 g) was dissolved into 200 mL of distilled water and used immediately.

e) Acid alcohol 1 % (v/v)

Hydrochloric acid (5 mL) was mixed with 495 mL of 70% (v/v) ethanol and used immediately.

**Methods**

Sections were immersed into 5 % (w/v) potassium permanganate for five min, rinsed in distilled water, immersed in 1 % (w/v) oxalic acid for two min, de-stained in 70 % (v/v) and 95 % (v/v) ethanol for 1 min each. Elastin was stained by immersing the sections in Miller's dye for 1 hour, followed by washing in 95 % (v/v) and 70 % (v/v) ethanol for 1 min each and running tap water (two min). Sections were then stained with Weigerts haematoxylin for ten min and rinsed under running tap water for 1 min. The sections were then differentiated in 1 % (v/v) acid alcohol for 1 min followed by a 30 sec wash using distilled water. The sections were stained using picro-

Sirius red dye for 1 h, washed in distilled water and dehydrated by using 70 % (v/v) ethanol (five sec) and three steps of 100 % (v/v) ethanol (one, two, three min respectively). The sections were finally immersed in the two steps of xylene (10 min each), mounted using DPX mountant and covered with a cover slip. The images were visualised using an upright microscope with normal Koehler illumination and polarised light. Collagen fibres were stained using Sirius red into bright orange colour and the elastin fibres were stained using Miller's elastin into blue.

### 2.2.2.6. DAPI staining

**Solutions**

a) DAPI dye stock solution (1 mg.mL$^{-1}$)

   DAPI (10 mg) was dissolved into 10 mL of nuclease free water and stored in 100 μL aliquots at -20 $^{0}$C, wrapped in aluminium foil. This solution was stable for 6 months.

b) DAPI dye buffer (10 mM Tris, 1 mM Na2EDTA, 1 mM NaCl)

   Trizma base (1.211 g), EDTA (0.3724 g) and NaCl (0.058 g) were dissolved into 1000 mL of distilled water and the pH was adjusted to 7.4.

c) The DAPI working dye solution

   DAPI dye stock solution (1 mg.mL $^{-1}$) was added into 200 mL of dye buffer solutions, covered in aluminium foil and used immediately.

d) Sodium hydrogen carbonate buffer (0.1 M)

   Sodium hydrogen carbonate (4.2 g) was dissolved into 500 mL of distilled water and the pH was adjusted to 9. This solution was stored at room temperature for 3 months.

e) DABCO 2.5 % (v/v)

   DABCO (2.5 mg) was dissolved into 100 mL of sodium hydrogen carbonate buffer (0.1 M) and the pH was adjusted to 9.

f) DABCO glycerol mountant

   DABCO 2.5 % (w/v) (10 mL) was mixed with 90 mL glycerol and stored at 4 $^{0}$C wrapped in aluminium foil for 3 months.

**Methods**

Following dewaxing and rehydration [Section 2.2.2.3], staining was carried out in the dark at room temperature. The sections were immersed in DAPI working solution for 10 min, washed in PBS for 10 min three times and mounted in DABCO fluorescence mounting medium. Slides were stored at 4 $^0$C, wrapped in aluminium foil and imaged within 48 h using a fluorescence microscope (Olympus BX51) with DAPI filter. The double stranded DNA associated with cell nuclei was visualised as the bright blue.

### 2.2.2.7. Immunohistochemical staining

Immunohistochemistry was performed using the Ultravision antibody detection kit reagents supplied by Thermo Fisher Scientific Ltd. A proper positive control and a negative control specific to the antigen of interest were always included during each procedure.

**Solutions**

All solutions were autoclaved and stored at room temperature, unless otherwise stated.

a) Sodium chloride solution (3 M)

   Sodium chloride (175.32 g) was dissolved into 1000 mL of distilled water.

b) Tris buffered saline (TBS)

   25 mL of 2 M Tris solution was added with 50 mL of 3 M sodium chloride and the pH was adjusted to 7.6. The solution was then added with distilled water to make 1000 mL of total volume.

c) TBS solution with 0.05% (w/v) Tween 20 (TBS-Tween)

   Tween 20 (500 μL) was added into 1000 mL and the pH was adjusted to 7.6.

d) Bovine serum albumin (BSA) solutions (5 % (w/v))

   BSA (2.5 g) was dissolved into 50 mL of PBS and sterilised through a 0.22 μm filter unit. This solution was stored at room temperature for 3 months.

e) Antibody diluent (TBS, 0.1% (w/v) BSA, 0.1% (w/v) sodium azide)

Sodium azide 1 % (6 mL) was added to 300 μL of BSA 5 % (w/v) and 40 mL of TBS. The pH was adjusted to 7.6 and then the solution was added with TBS solution to make up to 60 mL of total volume. This solution was stored at $4^0$ C for 3 months.

f) Trypsin solutions

Trypsin (2 g) and calcium chloride (0.2 g) were dissolved into 200 mL of TBS solution. The pH was adjusted to 7.8 and pre-warmed in a 37 °C incubator before used.

g) Citrate buffer (0.01 M)

Anhydrous citric acid (3.84 g) was dissolved into 1.8 L distilled water and pH was adjusted to 6.0. The solution was made up to 2 L and pre-warmed in a 37 °C incubator before used.

**Methods**

All of the immunohistochemistry steps were performed in four well plates at room temperature and sections were washed with TBS and TBS-Tween by mild agitation on a rocking table, unless otherwise stated.

After dewaxing and rehydration of the sections [Section 2.2.2.3] each section was carefully circled using a hydrophobic marker and subjected to an appropriate antigen retrieval method following the protocols of each antibody. There were two methods to retrieve antigen that used throughout this study;

a) Enzymatic method

The proteolytic enzyme used was Proteinase K ($20\mu g.mL^{-1}$). Sections were unmasked using 50 μL of Proteinase K for 10 min at room temperature and washed thoroughly using tap water followed by an incubation of hydrogen peroxide 3% (v/v) in PBS for 10 min at room temperature.

b) Heat-induced method

Sections for heat-induced antigen retrieval were incubated with hydrogen peroxide 0.5% (v/v) in methanol for 10 min at room temperature before starting the unmasking

procedure. The sections were then immediately washed under tap water and incubated with 0.01 M citrate buffer (pH 6.0) at high heat microwave for 10 min. After that, sections were then immersed in 37 $^{0}$C distilled water for 5 min and in the trypsin solution for 30 sec at 37 °C.

After the antigen retrieval step, the sections were washed for three min by a tap water and followed by a ten min TBS wash. The sections were incubated with 25 µL dual endogenous enzyme block (Ultra vison kit) for 10 min. The primary antibodies and their isotypes were diluted using antibody diluents as indicated in Table 2.4 and 2.5. The sections were then labelled with 35 µL primary antibody for 1 h at room temperature, in the dark, in a moist atmosphere. Sections were washed twice in TBS and TBS-tween alternately for 10 min each and incubated with Polymer-HRP (Ultra vision kit) (20 µL) at room temperature for 10 min in dark. Substrate chromagen (Ultra vision kit) was prepared by adding 20 µL DAB chromagen in 1 mL of substrate buffer. After a subsequent TBS-Tween and TBS washes (twice for 10 min each), 15 µL of substrated chromagen was added to the sections and incubated for 10 min in the dark and at room temperature. The sections were then washed four times in distilled water and immersed in haematoxylin for 10 sec, rinsed under tap water prior to dehydration and mounting as described above. Sections were visualised using bright-field upright microscope (Zeiss Aixo-Imager M2), imaged using a Zeiss AxioCam MRc5 camera through Zen Blue software. The negative control slide should have purple-blue background and the positive control slide should stain brown. Any specific staining occurred in the negative control or negative staining in the positive control resembled to an invalid result.

## 2.2.3. Cell culture techniques

### 2.2.3.1. Tissue culture medium

All procedures were performed aseptically in a class II cabinet and all media or solutions were pre- warmed in a 37 $^{0}$C incubator before used. General culture medium used;

   a) DMEM (Dulbecco's modified Eagle's medium) complete medium

The standard cell culture medium used in this study were DMEM with 4.5 g.L$^{-1}$ glucose for the 3T3 cells and porcine MSCs or 1.0 g.L$^{-1}$ glucose for human MSC, supplemented with 10 % (v/v) FBS, 100 U.mL$^{-1}$ penicillin, 100 mg.mL$^{-1}$ streptomycin and 2 mM L-glutamine. The medium was stored at 4 $^0$C for 1 week.

b) GMEM (Glasgow`s minimal essential medium) complex medium

This medium was used to culture the BHK cells. To make up 200 mL stock; 20 mL TPB solution, 10 % (v/v) FBS, 4 mL of 100 u.mL$^{-1}$ penicillin- 100 mg.mL$^{-1}$ streptomycin, and 2 mL of 200 mM L-glutamine was added to 164 mL of GMEM. This solution was stored at 4 $^0$C for 1 week.

## 2.2.3.2. Cell resurrection and maintenance

Frozen cells were removed from liquid nitrogen and thawed quickly in a 37 $^0$C incubator. The cells were transferred into a universal container and 10 mL DMEM complete medium was added drop-wise. DMSO was removed by centrifugation for 10 min at 150 g for the 3T3, BHK cells, PMSC and the human MSC. The cell pellet was resuspended in 1 mL of the medium appropriate for the cell type and seeded at 5000 cells.cm$^{-2}$ in a T75 tissue culture flask. A further 9 mL of culture medium was added and the cultures were incubated at the 37 $^0$C in 5 % (v/v) CO$_2$ in air. The culture medium was changed with fresh cell culture medium every 3 days.

## 2.2.3.3. Cell passage

The cells were passaged when the cells reached 85 % to 90 % confluence. The medium was carefully removed and the cell layer was washed twice with 10 mL of PBS without Ca$^{++}$/ Mg$^{++}$. Trypsin/EDTA solution (3 mL) was added and the flasks incubated at 37 $^0$C in 5 % (v/v) CO$_2$ in air for 5 min. The flask was gently rocked to detach the cells and disrupt cell clumps. Detachment was confirmed by inverted microscopy (Olympus CK40) and the trypsin was neutralized by adding 9 mL of culture medium.  The cell suspension was centrifuged at 150 g (3T3, BHK cells, PMSC and human MSC) for 10 min and the pellet was resuspended in 5 mL

culture medium. The number of viable cells was counted [Equation 1]. Cells were seeded at 5000 cells.cm$^{-2}$ in a new T75 tissue culture flask and maintained as described above [Section 2.2.3.2].

## 2.2.3.4. Viable cell counting; Trypan blue dye exclusion method

The membrane of the dead cells is compromised and this allows penetration of dyes such as Trypan blue. Dead cells appear blue whilst viable cells are unstained. Cells were counted using an Improved Neubauer counting chamber [Figure 2.1]. The cell suspension was diluted with 0.4 % (v/v) Trypan blue solution at a ratio of 1:1. The cover slip was placed firmly on the chamber until Newton's rings were visible. The cell suspension was loaded into the counting chamber using a pipette at a $45^0$ angle. The number of cells per 1 mm$^2$ square was estimated [black circle in Figure 2.1]; if the total cells were between 30 to 300, the whole cells in the 25 triple ruled squares were counted; however if less than 30 cells were estimated presented in 1 mm$^2$, the cell dilution was decreased; if more than 300 cells were estimated, the cells in 5 small squares [red crosses in Figure 2.4. B] were counted. Using this area, the volume of the square was 0.1 mm$^3$, thus to obtain the number of cells per 1 mL suspension, the formula below was used (Guillard and Sieracki, 2005).

Equation 1:

$$Viable\ cells = \frac{(total\ cell\ - dead\ cell\ )}{Number\ of\ 1\ mm^2\ counted} \times 2\ (dilution\ factor) \times 10^4$$
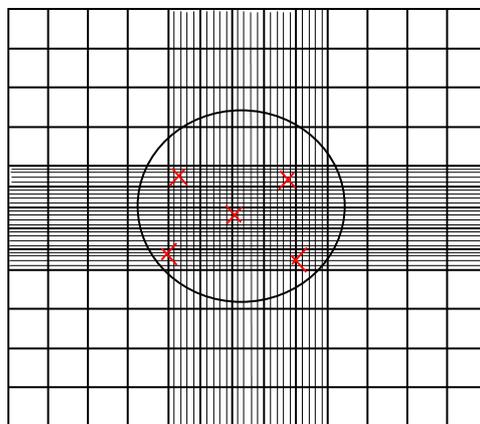


**Figure 2.1 Grid layout of the Improved Neubauer hemocytometer** for **cell counting**

### 2.2.3.5. Cryopreservation of cells

The cell lines and primary cells for future use were stored as frozen stock in liquid nitrogen (-196 $^0$C). Cells were pelleted [Section 2.2.3.3], resuspended in culture medium and enumerated (Section 2.2.3.4). The cells were centrifuged for 10 min at 150 g (3T3, BHK, L929 cells, PMSC and human MSC) and adjusted to $1 \times 10^5$ - $3 \times 10^5$ cells.mL$^{-1}$. The cryoprotectant medium was prepared prior to use by adding 10 % (v/v) DMSO in DMEM complete medium. 1 mL of the cryoprotectant medium was added to the pellet of the cells which were then resuspended and aliquots dispensed into cryovials, 1 mL each vial. The cryovials were placed into a Mr Frosty and left at -80 ℃ for a minimum of 4 h (cooling rate -1 $^0$C per min). The cryovials were then immediately transferred into liquid nitrogen for long term preservation.

### 2.2.4. Assays of cell viability for cells and tissues

### 2.2.4.1. LIVE/DEAD® Assay

Viable cell can be distinguished from the dead cell by staining intracellular esterase activity in living cell using Calcein-AM (green fluorescence). Dead cells are stained red using Ethidium homodimer-1 that binds to cellular DNA in cells which have a disrupted plasma membrane (Petronilli et al., 1999).

**Reagent**

LIVE/DEAD® working solution (3 µM Calcein-AM and 3 µM Etidium homodimer-1); Calcein-AM stock (4 mM; 1.5 µL) and Ethidium homodimer-1 (2 mM; 3 µL) were added to 2 mL of PBS solution and wrapped with aluminium foil. This working solution should be made just before use.

**Method**

A cell-seeded scaffolds tendon scaffold (25 x 10 mm$^2$) was cut in the middle as well as its 2.5 mm end. This gave a final sample size of a 10 x 10 mm$^2$ construct. Each sample was placed into the well of a 24-well plate with the cell seeded surface uppermost and incubated with 500 µL of

LIVE/DEAD® working solution for 1 h, followed by three of 10 min washes in PBS. The procedure was performed at 37 $^0$C in the dark with agitation at 90 rpm on an orbital shaker. Finally, the sample was placed on a microscope slide, wet mounted with PBS solution and covered with a cover slip to be visualised using an upright fluorescence microscope Zeiss Aixomager M2. The green fluorescence is captured using a 38 green fluorescence filter at a 494 nm wavelength and the red fluorescence is captured using a 20 rhodamine filter at a 592 nm wavelength. The percentage of live cell was determined by counting the number of live cells over the total live and dead cells from nine fields of observation in each sample using Image J software.

**Data processing**

Nine fields of observation were captured at 5 x magnification and processed through Image J. Live cell was determined by intact green cell shape and dead cells by a red dot. Cells that had both red and green were counted dead. Total of live and dead cells were counted first and followed by the viable cells only. Percentage of the live cells from each view was determined by the number of live cells over the total cells and presented as a mean from 9 fields with 95% C.I. Seeded cells were assumed to well dispersed, therefore to estimate total cell number found on the scaffolds after being seeded was by multiplying the average of live and the dead cell from 9 fields of observation to 19.13 (ratio of 9 field (0.88 x 0.66 mm$^2$ for each view area of 5 x magnification) to the total sample size; 10 x 10 mm$^2$), using the equation below;

Equation 2:

$$Total\ live\ cells\ in\ one\ sample = \frac{\sum live\ cells\ counted}{9}\ x\ 19.13$$
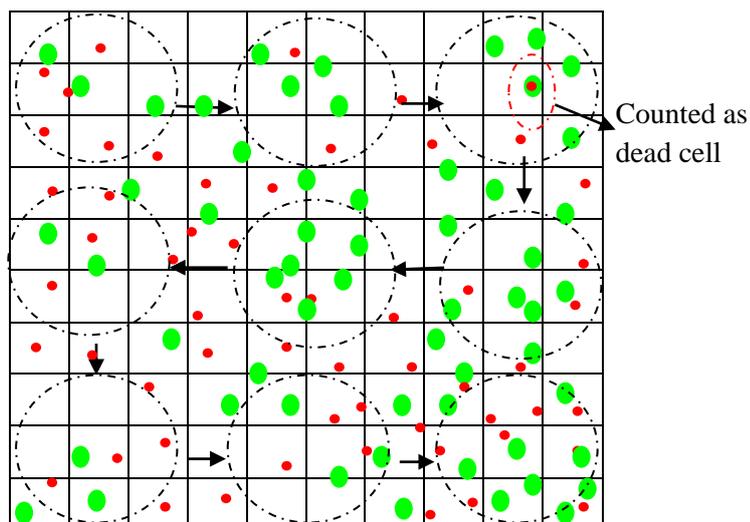
**Figure 2.2 Scheme of the enumeration techniques to determine the percentage of viable and dead cell from one sample.** The sample size was 10 x 10 mm$^2$ and the size of each field of observation was 1.76 mm x 1.32 mm (scaled in grid).

### 2.2.4.2. ATPlite™ assay

The measurement of cellular ATP levels is a sensitive indicator of cell viability. In order to assess cellular ATP levels in tissue samples, the ATPlite™ assay kit (PerkinElmer) was used. ATPlite™ assay analyses ATP levels in living cell, converted by luciferase into light [Figure 2.3] as described below (Elmer, 2013). The luminescence was quantified using a Top Count (PerkinElmer) luminescence reader and Chameleon software.

$$\text{ATP} + \text{D-Luciferin} + O_2 \xrightarrow[\text{Mg}^{++}]{\text{luciferase}} \text{Oxyluciferin} + \text{AMP} + \text{PPi} + CO_2 + \text{light}$$
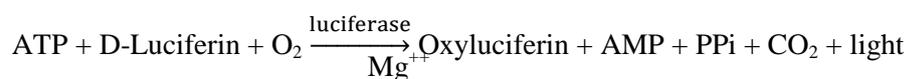
**Figure 2.3 Quantification of ATP level by converting the ATP to light**

**Solutions**

ATPlite-M™ working solution was prepared by reconstituting the lyophilized ATPlite following the manufacturer instruction and stored at -20 $^0$C in 5 mL aliquots glass pots wrapped with aluminium foil.

**Methods**

Culture medium of each monolayer cells were aspirated from each well of the 96-well plate, and replaced with 150 µL of new cell culture medium, added with 150 µL of mammalian lysis solution. The plate was agitated on an orbital shaker at 700 rpm, 5 min. After that, three of 100 µL aliquots from each sample were transferred into each wells of a 96-well Optiplate, added with 100 µL of substrate solution was then added into each well and incubated in the dark for 5 min with agitation at 700 rpm. Three aliquots of cell culture medium only were included as the negative control. Air-bubbles in the wells were eliminated by briefly swept the wells with blue flame of a Bunsen. The plate was then covered with Top-Seal and sample's luminescence was counted using TopCount and ATP2007 software. The counts per second (CPS) were normalised by subtracting the average CPS of 3 measurements from each sample to the background (the cell culture medium only). The final calculations were presented per mg tissue weight with standard curves of the means between samples and the control.

## 2.3. Statistical analysis

The collected data were initially analysed for their normality distribution by Q-Q plot. Non-normal data were transformed before being analysed. All numerical data were calculated using Microsoft Excel (Version 2003 VIand 2007, Microsoft), analysed and presented as a graph using GraphPad Prism® version 6 (GraphPad Software Inc, California, USA). Parametric data were presented as mean ± 95 % CL. Student t-test was used to compare two means, one-way ANOVA was used to compare more than two means, while when two or more variants were compared, a two-way ANOVA was used, followed by T-method to determine the minimum significant difference (MSD) for an equal sample size (Sokal and Rohlf, 1981). The difference was considered significant when the p value was smaller than 0.05 (Sokal, 1995). Data were mostly expressed with mean ± 95 % C.l.

Standard deviation was calculated using the equation below,

Equation 3:

$$SD = \sqrt{\frac{(\Sigma x)^2}{n}}$$

Where the $\Sigma(x)$ is the total value and n is total sample number.

Standard error (SE) was calculated by divided the SD over the square root of total sample number;

Equation 4:

$$SE = \frac{SD}{\sqrt{n}}$$

The 95% confidence limit was calculated by

Equation 5:

$$95\ \%\ C.l. = SE\ x\ t - value$$

Data expressed in percentage were arcsine e transformed in order to fulfil the assumption of data normally distributed. The arcsine transformation of the percentages values followed:

Equation 6:

$$y = \frac{180^0}{\pi}\ x\ arcsin \sqrt{\frac{x}{100}}$$

Where the x is the percentage value and the y is the arcsine data. The lower and upper limits were then calculated using the equation below;

Equation 7:

$$Upper\ limit = mean + 95\ \%\ C.I.$$

$$Lower\ limit = mean - 95\ \%\ C.I.$$

The values were then back transformed for presentation.

Equation 8:

$$y = sin\left(\frac{\pi}{180^0}\ x\ \frac{mean^2}{100}\right)$$

Then for the upper and lower error bars calculated as follows:

Equation 9:

$$Upper\ error\ bar = upper\ limit - mean$$

$$Lower\ error\ bar = mean - lower\ limit$$

# Chapter 3

# Preparation of acellular porcine patellar tendon scaffolds

## 3.1. Introduction

The ECM of a tissue or organ acts as a home for the resident cells that generate and remodel the matrix in response to microenvironmental stimuli, so that the matrix forms an important component of the functional tissue or organ (Bissell and Aggeler, 1986). The ECM of tendon or ligament tissues mainly consists of collagen I, which is highly conserved throughout evolution. Collagen I has low antigenic potential when transplanted between animals of different species (Badylak, 2002b). To enable utilisation of the ECM for tissue transplantation, the cells, DNA and damage associated molecular patterns (DAMPs) in the ECM should be removed completely while preserving the histoarchitecture and major structural components (Bianchi, 2007). This approach is known as a decellularisation process (Badylak et al., 2009, Crapo et al., 2011). Many tissue-engineering centres across the world apply different decellularisation techniques using a variety of chemical, physical, enzymatic and or mechanical approaches.

### 3.1.1. Decellularisation protocols

Basic approaches to the decellularisation of tissues are presented in Table 3.1. The University of Leeds developed a novel decellularisation process, that has been patented (Booth et al., 2001) and applied to a range of tissues, some of which have been commercialised through the University of Leeds spinout company, Tissue Regenix Group PLC. The process for the decellularisation of porcine tendons presented in this chapter has been published and it comprises chemical, physical and enzymatic processes (Ingram et al., 2007). In this study, the source material for producing the acellular tendon scaffold was the porcine patella tendon (PT) due to its size, anatomical and physiological similarities to human patella tendon (Sachs, 1994, Yamada et al., 2005). Porcine patellar tendon has an appropriate size (Dahlin et al., 1991), has similar micro architechture (Derwin et al., 2006, Valentin et al., 2006), has a comparable

mechanical properties (Barber et al., 2006) and had been used extensively in musculoskeletal research (Stone et al., 2007). The process developed by Booth et al. (2002) utilised hypotonic buffer to lyse the cells in the presence of proteinase inhibitor (Aprotinin) to prevent proteolytic degradation of the ECM. The cell membranes were then solubilised using low concentration SDS in the presence of proteinase inhibitors followed by treatment with nucleases to cleave the DNA and RNA. The acellular tissue was washed extensively between treatments and finally sterilised using peracetic acid (Booth et al., 2002). Sterilization is crucial to ensure the safety of scaffolds for tissue engineering applications. However, the sterilisation method must ideally not change the mechanical and biological properties of the scaffold. Peracetic acid (PAA) has been extensively used to sterilize porcine-derived medical devices, used in low concentration and neutral or high ionic strength to sterilize collagen matrices without causing structural damage (Kemp, 1995, Lomas et al., 2003). It releases free radicals which kills microorganisms by causing microbial enzyme oxidation (Marquis et al., 1995, Pruss et al., 1999). PAA is effective to eradicate common viruses found in pigs such as porcine reovirus, murine leukemia retrovirus (LRV) and pseudorabies virus (PRV) (Hodde and Hiles, 2002), porcine parvovirus (PPV), porcine pseudorabies (herpes) (Scheffler et al., 2007).

### 3.1.2. Quality assurance of decellularised porcine patella tendon scaffolds

Ideally, a decellularised biological scaffold should conform to minimum criteria; such as contain less than 50 ng dsDNA per mg ECM dry weight, have less than 200 bp DNA fragment length and lack of visible nuclear material visualised by DAPI and H&E staining (Gilbert et al., 2006a, Crapo et al., 2011). The acellularity and matrix histoarchitecture of the scaffolds produced in this study were therefore investigated using histology with H&E staining of tissue sections, and dsDNA was studied in tissue sections using DAPI staining. The residual DNA present in the scaffolds was quantified following extraction, using nanospectrophotometry and presented as $ng.mg^{-1}$ dry weight. The ECM component, sterility and biocompatibility of the scaffolds were also verified.

## 3.2. Aim and objectives

The aim of this chapter was to produce the acellular matrices, intact, sterile and biocompatible tendon scaffolds. Those decellularised tendons were prepared so they could eventually be used as scaffolds for this study.

The objectives were:

1. To procure and dissect the porcine patellar tendon
2. To decellularise the harvested porcine patellar tendon
3. To determine the quality assurances of the decellularisation products in terms of their acellularity, histoarchitectural, DNA quantity, ECM component of collagen I, collagen III and Tenascin-C, sterility and contact biocompatibility.

**Experimental Design**

Fresh porcine PTs were collected and stored at $-80\ ^{0}$C. Four tendons were decellularised as batch (1) for decellularisation training purposes. There were twelve porcine patellar tendons decellularised in batch (2) and (3), and twenty porcine patellar tendons were decellularised in batches (4), (5) and (6). PPTs decellularised in batches (1) until batches (5) were used to characterise the scaffolds and to develop methods for cell seeding and determination of subsequent cellular viability. The sixth batch was used to investigate the regenerative capacity of the human MSCs under different regimes of uniaxial tensile stimulation. Three samples from each decellularisation batch were chosen randomly and used for evaluation of acellularity and quality.

## 3.3. Material and methods

### 3.3.1. Procurement and dissection of porcine PTs

Right hind legs were procured from Large White pigs (75 – 85 kg), aged 4 to 6 months, which had been slaughtered within 24 h at the local abattoir (J Penny & Sons). The skin was excised to expose the knee joint and identify the patellar tendon. Fat and connective tissue was removed from the tendon, taking care not to damage the fibres. The fat pat was trimmed carefully in order to leave enough fat for the tendon fibres not to disintegrate during decellularisation. The patellar tendons were harvested by cutting straight through the tendon tibial interface, and the through the patellar interface. The tendons were stored individually at -80ºC in sterile universals, with filter paper soaked with PBS. The tendon in situ and following dissection is shown in Figure (3.1).
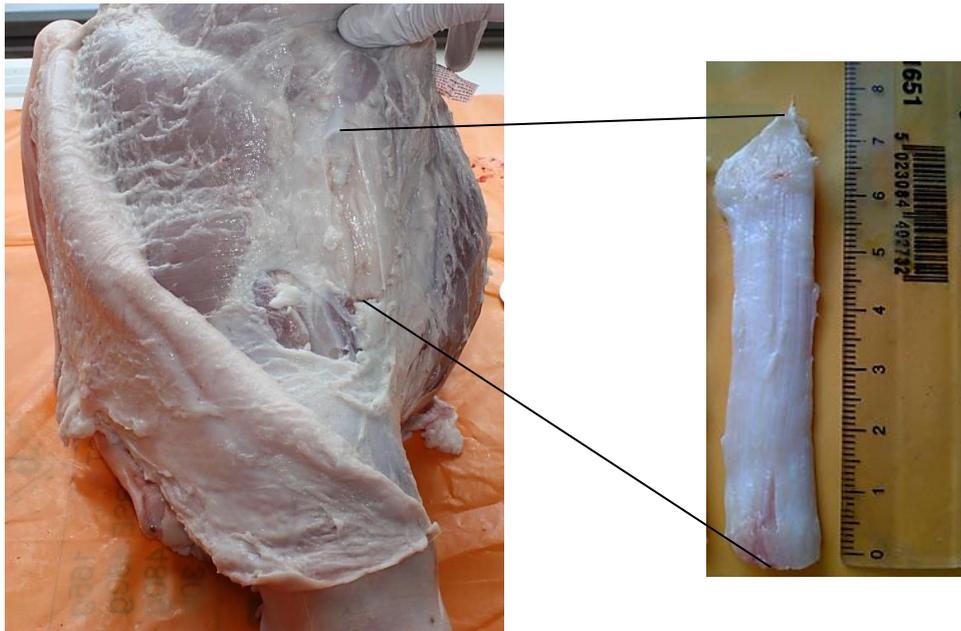


**Figure 3.1 Harvesting of the porcine PT**. (A) Porcine PT in situ in the porcine right knee joint. (B) Porcine PT after dissection.

## 3.3.2. Decellularisation of the porcine PTs

### 3.3.2.1. Solutions

All solutions were autoclaved before use, and stored at room temperature for up to one month, unless otherwise stated. The pH of the solutions was adjusted drop wise using 6 M hydrochloric acid or 6 M sodium hydroxide.

a) Sodium hydroxide solution (6 M)

Sodium hydroxide (120 g) was dissolved in 500 mL of distilled water and used for up to three months.

b) PBS solution

One tablet of PBS was dissolved in 100 mL of distilled water, the pH was adjusted to 7.2 – 7.4.

c) PBS-Aprotinin (10 KIU.mL$^{-1}$ Aprotinin)

To sterile PBS solution (1000 mL) was added 1 mL of 10,000 KIU.mL$^{-1}$ Aprotinin just before use.

d) PBS-EDTA (2.7mM; 0.1 % (w/v))

EDTA (1 g) was dissolved in 1000 mL of PBS, the pH was adjusted to 7.2 – 7.4.

e) PBS-EDTA (2.7 mM) containing 10 KIU.mL$^{-1}$ Aprotinin

One mL of Aprotinin (10 KIU.mL$^{-1}$) was added into 1000 mL of sterile PBS-EDTA solution (2.7mM; 0.1%; w/v) just before use.

f) Hypotonic buffer (10 mM tris, 2.7 mM EDTA, 10 KIU.mL$^{-1}$ Aprotinin)

Trizma base (1.21 g) and EDTA (1 g) were dissolved into 900 mL distilled water, the pH was adjusted to 8.0 – 8.2, and the solution topped up to 1000 mL. Aprotinin (1 mL; 10,000 KIU.mL$^{-1}$) was added just before use.

g) Sodium docecyl sulphate (SDS) hypotonic buffer (0.1% (w/v) SDS, 10 mM Tris, 2.7 mM EDTA, 10 KIU.mL$^{-1}$ Aprotinin)

SDS (10 g) was dissolved into 100 mL distilled water to make a 10% (w/v) SDS solution which was sterilised by passing through a 0.2 μm filter (this stock was stored at

room temperature for up to 6 months). Ten mL of the sterile 10% (w/v) SDS stock was added to 990 mL sterile hypotonic buffer to make 0.1% (w/v) SDS. The solution was dispersed by inverting the bottle and was stored at 4-8ºC for one week.

h) Nuclease solution (50 mM tris; 20 mM magnesium chloride; Benzonase 1U.mL$^{-1}$)

Trizma base (6.1 g) and magnesium chloride (2.0 g) were dissolved into 80 mL distilled water. The volume was made up to 1 L after adjusting the pH to 7.5 -7.7. Benzonase (250 U.µL$^{-1}$) was added just before use, at 4 µL per 1 L buffer solution.

i) Hypertonic solution (50 mM tris, 1.5 M sodium chloride)

Sodium chloride (87.66 g) and tris (6.06 g) were dissolved into 900 mL distilled water. The pH was adjusted into 7.5 – 7.7 and the volume was topped up to 1000 mL.

j) Peracetic acid (PAA) solution (0.1%; v/v) (1.57 mL) was added into 500 mL sterile PBS, the pH was adjusted to 5.9 – 6.2 and the solution used within one hour.

### 3.3.2.2. Method

Each step was carried out at 37 $^0$C on an orbital shaker (Grant) at 110 rpm with one porcine PT in 100 mL of solution unless otherwise stated.

The decellularisation process began with three freeze-thaw cycles. Each time the tendon was thawed at room temperature and immersed in hypotonic buffer, before being frozen again at -80ºC. Tendons were transferred to hybridisation bottles and 200 mL acetone was added and agitated at room temperature for one h. This was repeated twice, (three washes in total) each time with fresh acetone. After the acetone washes, the tendons were washed in PBS solution five times for five min each. The tendons were transferred to 150 mL pots and washed in hypotonic buffer for 24 h, and then hypotonic buffer plus 0.1 % (w/v) SDS for 24 h. These two steps were repeated. The tendons were washed in PBS plus Aprotinin, three times for 30 min followed by a 70 h wash in PBS plus Aprotinin. The PBS-Aprotinin solution was then replaced with fresh PBS-Aprotinin solution and agitated for 30 min. Each tendon was then treated with 60 mL of nuclease solution, and incubated for two h with the agitation reduced to 90 rpm. This

step was repeated twice (three nuclease washes in total). The tendons were washed three times in PBS-Aprotinin for 30 min each, and then washed in hypertonic solution for 20 h.  After the incubation in hypertonic solution, the tendons were washed in PBS-Aprotinin three times for 30 min and once for 20 h followed by sterilization in 0.1% (v/v) PAA for three h. After this step, the tendons were treated as sterile materials and all manipulations were performed in a class II cabinet. Finally, the tendons were washed in PBS-Aprotinin three times for 30 min, twice for 80 h and then for 170 h to remove any residual chemicals. This protocol is presented in Figure 3.2.
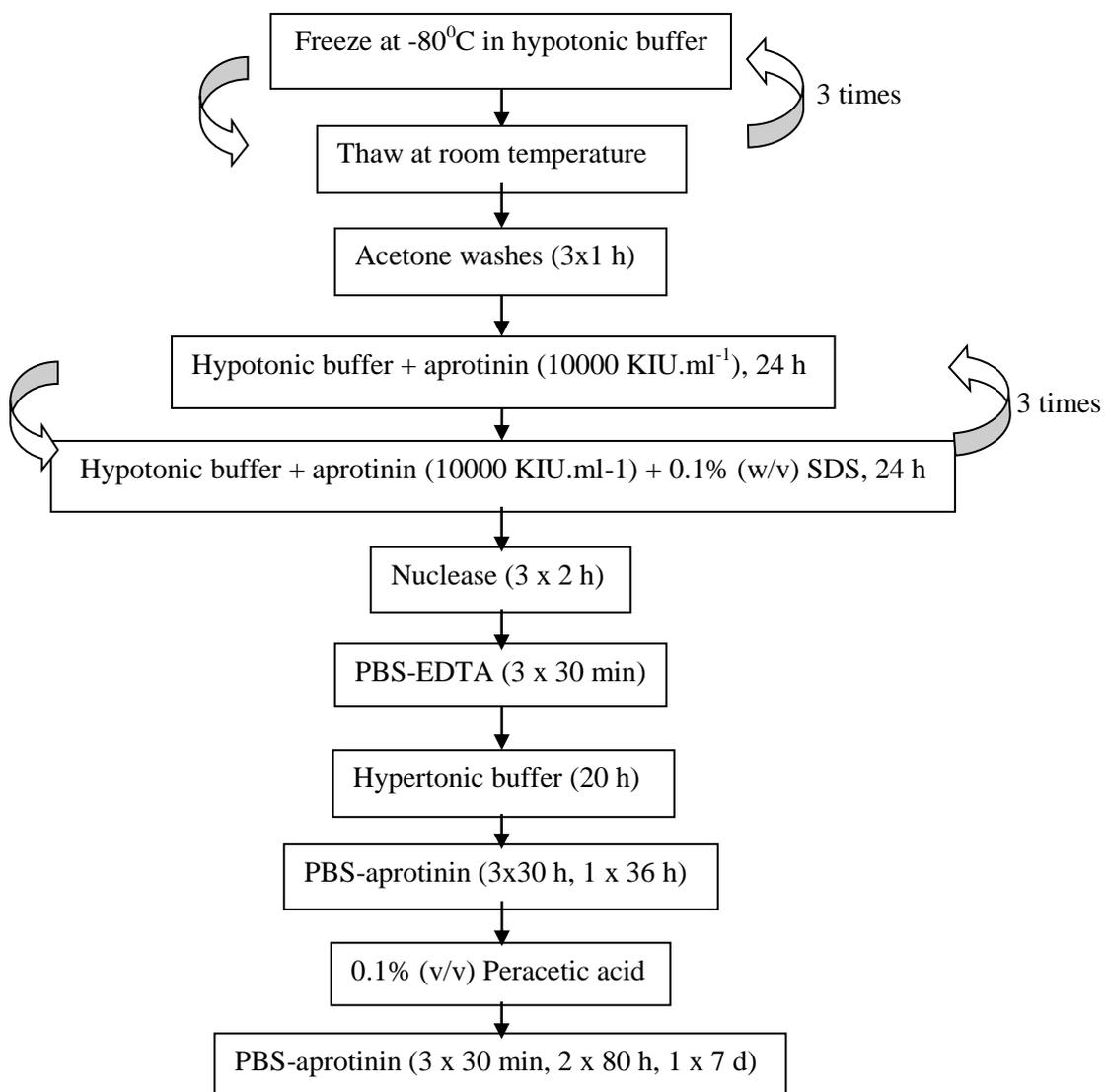


**Figure 3.2 Method used for decellularisation of porcine PTs;** all steps were performed at 37ºC with agitation at 110 rpm or 90 rpm (nuclease).

### 3.3.3. Characterisation of the decellularised porcine PTs

On completion of decellularisation, using native tendons as control tissue, the tendon was cut into 3 sections for analysis [Figure 3.3]: the patellar interface (PI); intermediate (IM); and tibial interface (TI). Each section was cut into 2 mm width samples, and each sample was cut into two equal samples, which were then placed into histological cassettes for fixation in 100 mL either 10% (v/v) NBF or zinc fixative for 4 days.
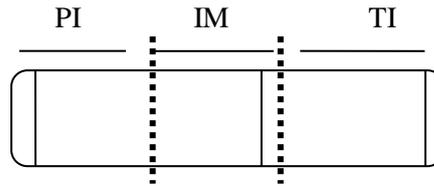


**Figure 3.3 Each porcine PT was divided into three parts**: the patellar interface (PI), the intermediate (IM) and the tibial interface (TI). The dashed lines indicate the cutting line for each tendon.

The materials and methods describing the basic histological techniques to prepare samples for histological staining and immunohistological labelling can be found in Chapter 2; Section 2.2.2 and the antibodies used in Chapter 2; Section 2.1.3, Tables 2.5.

### 3.3.3.1. Sterility assessment

Sterility assays were assessed from each batch of the decellularised PPTs, using:

- Nutrient broth was used to assess the cultivation of the aerobic bacterial contamination.

- Agar plates. Nutrient agar (NA) was used to detect non-fastidious bacteria, fresh blood agar (FBA) for more fastidious microorganisms. Sabouraud agar (SAB) which has a lower pH was used to detect any fungal contamination.

**Method**

Each sample of the decellularised porcine PTs (n=3) was cut into 5 x 5 x 5 mm$^3$, immersed individually into nutrient broth and incubated at 37 $^0$C for 21 days. The sterility was observed on the second, seventh and 21$^{st}$ day of the incubation. Solutions that remained clear showed no

bacterial growth. Further observation was continued by plating 100 µL of each stage of observation onto NA, FBA and SAB agar plates. The NA and FBA plates were kept at $37^0$C, and the SAB plates were incubated at $30^0$C. Any growth was observed on the second, seventh and 21st day of incubation.

### 3.3.3.2. Contact biocompatibility assay

**Cells**

Cells used for this test were the mouse fibroblast (3T3) and the baby hamster epithelial cells (BHK) as shown in Chapter 2; Section 2.1.4, Table 2.6.

**Culture media**

Culture media used were the high glucose DMEM complete medium for 3T3 cells, and GMEM complex medium for the BHK cells [Chapter 2; Section 2.2.3.1].

**Method**

Contact assays were conducted to determine the contact biocompatibility of the acellular porcine PTs using BHK and 3T3 cell lines. Steri-Strip (3M) was used as a negative control and cyanoacrylate as the positive control. All procedures were performed aseptically in a class II cabinet. Using a 6-well plate, a sample of tissue (5 mm²) was placed into the centre of each well, and fixed with Steri-Strip®. Steri-Strip® alone was placed in a single well to be used as the negative control. Cyanoacrylate (10 µL) was added to the centre of another well to be used as the positive control [Figure 3.4]. Each well was washed twice for 10 min with PBS without $Ca^{++}/Mg^{++}$. BHK and 3T3 cells were passaged and counted [Chapter 2; Section 2.2.5.2 and 2.2.5.3] and resuspended in the appropriate medium to give a cell density of 250,000 cells.mL$^{-1}$. The cell suspension (2 mL) was added to each well and the plates were incubated for 48 h at 37 ºC in 5% (v/v) $CO_2$ in air. The cell layers were washed with PBS without $Ca^{++}/Mg^{++}$, and fixed with 10% (v/v) NBF for 10 min in the fume hood, then stained with Giemsa for 5 min and imaged after being air-dried overnight.

**Data analysis**

Cell growth up to and in contact with the samples, cell morphology, detachment and lysis were used to assess the contact biocompatibility of the samples.
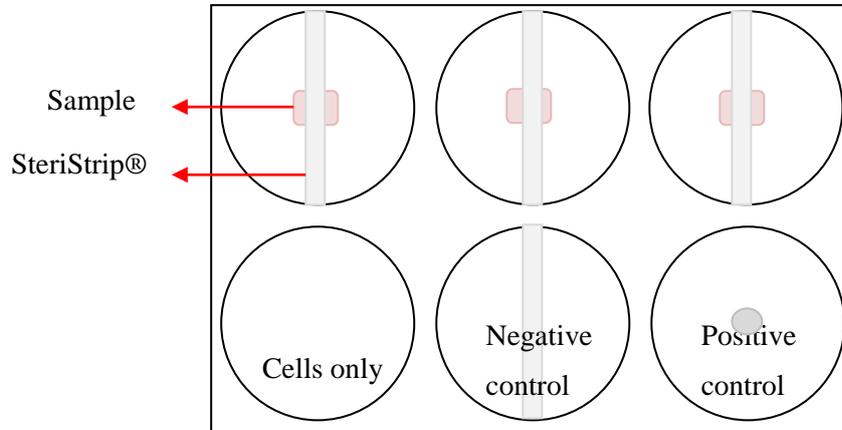


**Figure 3.4 Contact biocompatibility assay using 6-well plate**; each sample was attached to the plate using Steri-Strip®. The top row was used for samples (n=3) and the bottom was the controls.

**3.3.3.3. DNA quantification of the decellularised porcine PTs**

**Preparation**

Under aseptic conditions, fresh (25 mg) and the decellularised (250 mg) porcine PTs was weighted three times, macerated and placed individually in a dried bijou. The bijous were placed in a Freeze dryer (ModulyoD) with loosened lid to allow the water to escape. The samples were weighted every 24 h, three times each to determine the mass until a constant weight was attained.

**Method**

DNA was extracted from the tissues using a column system from the DNeasy kit (Qiagen), following the manufacturer`s protocol. All vortexing using pulse vortexing was carried out for less than 10 sec and all centrifugation was performed at room temperature using a microcentrifuge. The freeze-dried samples were placed in a sterile 1.5 mL microcentrifuge tube, and processed for tissue lysis using 10% (v/v) of Proteinase K in Buffer ATL (200 μL into the native and 400 μL to the decellularised PT samples). This digestion process was enhanced by a constant mixing in a Thermomixer set at 56 $^0$C for 3 h, and pulse vortexting every 30 min to

enhance the dispersion. Samples were then treated to remove RNA using 4 μL or 8 μL of RNase inhibitor (100 mg.mL$^{-1}$) into the native or the decellularised samples respectively and incubation for 2 min at room temperature. Following this, each sample was pulse vortexed for 5 sec and 200 μL of 100% (v/v) of absolute molecular grade ethanol in Buffer AL was added to the native and 400 μL to the decellularised samples, and mixed thoroughly by vortexing. After this, the DNA was extracted using the column system. All solutions from each sample were bound to the DNeasy Mini spin column in a 2 mL collection tube; 600 μL of the solution was filtered each time at 6000 g for one min. The flow through was discarded and the collection tube was changed between each centrifugation. Next, two wash steps were performed using Buffer AW1 (500 μL), centrifuged for 1 min at 6000 g and using Buffer AW2 (500 μL) centrifuged for 3 min at 20,000 g. Finally, after the wash steps, the DNA was ready to collect by eluting the column using 200 μL Buffer AE, centrifuged at 6000 g for one min. It was important to dry the column before the collection step to avoid ethanol carry-over. This elution was repeated twice to obtain a maximum yield of DNA. The DNA solution was stored at -20 $^{0}$C up to 6 months. The collected DNA was measured using a Nanodrop spectrophotometer at 260 nm absorbance using Buffer AL as the blank. Three readings were taken for each sample and the average DNA content was calculated as ng.μL$^{-1}$.

**Data analysis**

Data were exported into Microsoft Excel and the DNA concentration was normalised for total elution volume (200 μL or 400 μL) and presented as the DNA concentration per mg tissue dry weight (ng.mg$^{-1}$), as indicated below;

Equation 10:

$$\text{DNA weight (ng) per tissue dry weight (mg)} = \frac{\text{mean absorbance x 400 or 200}}{\text{mg dry weight}}$$

The mean ± 95% C.l of total DNA weight per tissue dry weight (ng.mg$^{-1}$) is presented for each of the native and decellularised batches and the percentage reduction in DNA content after decellularisation was calculated.

## 3.4. Results

### 3.4.1. Decellularised porcine PTs

Six batches of decellularised tendons were produced; and four, twelve or twenty native tendons were processed in each batch, following the University of Leeds decellularisation protocol [Section 3.3.2]. All histology and immunohistochemistry images presented in this chapter were taken from the decellularised PPTs batch (6).
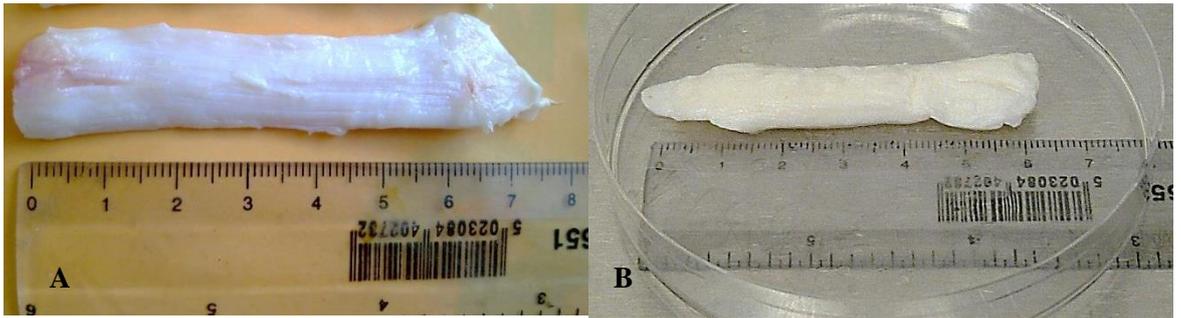


**Figure 3.5 Porcine PTs**: (A) a native porcine PT after dissection, and (B) a decellularised porcine PT, white in colour.

Grossly, no morphological differences were found between the native [Figure 3.5 A] and the decellularised tendon [Figure 3.5 B], except that the decellularised tendon was white in colour.

### 3.4.2. Scaffold acellularity

The goal of the decellularisation process is to eliminate cells and nuclear remnants from the tissue, without damaging the scaffold. Histological staining of tissue sections was used with the aim of highlighting any nuclei and the scaffold histoarchitecture.

#### 3.4.2.1. Haematoxylin & eosin stained tissue sections

H&E staining of tissue sections was used to demonstrate the tissue histoarchitecture and cell nuclei. Native tendon tissue sections stained using H&E showed numerous nuclei arranged in order between fibres and around blood vessels [Figure 3.6 A]. No nuclei could be identified in the H&E stained sections of the decellularised tendons, neither in between fibres nor around the blood vessels. The area where the blood vessels are located is highlighted in Figure 3.6 B to demonstrate the acellularity. No histoarchitectural differences were found between the native

and decellularised tendons however, the spaces between fibres in the decellularised tissue sections were slightly widened. Further assessment for nuclear remnants in the decellularised tissue was performed using DAPI staining of histological sections. No positive staining was observed in the sections of the decellularised tissue stained using DAPI [Figure 3.6 D] compared to numerous nuclei found in the native tendon sections [Figure 3.6 C].
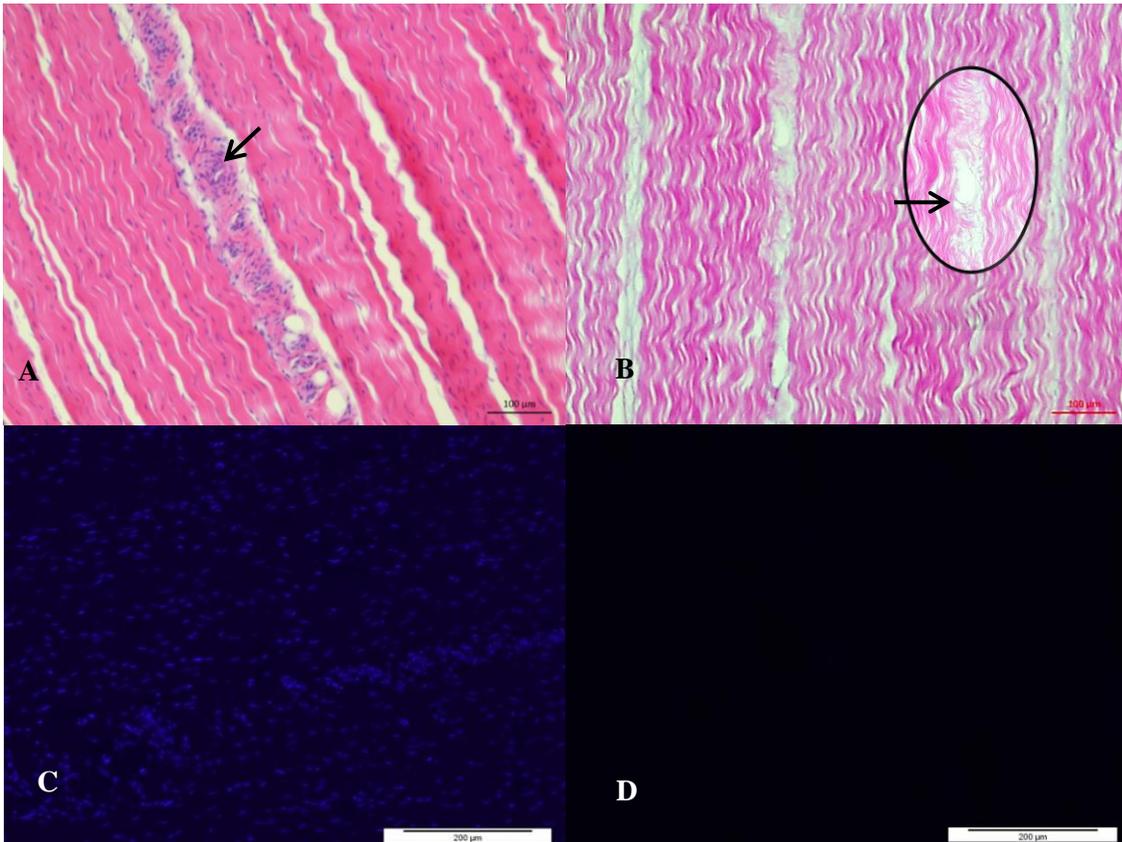


**Figure 3.6 Histology of fresh (A,C) and decellularised (B,D) porcine PTs** at 100x magnification. (A,B) H&E stained sections of the native (A), and the decellullarised tissues (B), scale bars represent 100µm. (C, D) DAPI stained sections of the native endon (C) and the decellularised tendon (D), scale bars represent 200µm. Arrows indicate the presence of blood vessels.

### 3.4.3. Visualisation of components of the ECM

### 3.4.3.1. Sirius red and Miller`s elastin stained tissue sections

Tissue sections from the same samples of tendon were stained with Sirius red and Miller's elastin dye and imaged at 100x magnification using bright light microscopy [Figure 3.7 A, B] and under polarised light [Figure 3.7 C, D] to visualise the collagen crimp and orientation.

Grossly, sections viewed under both bright light and polarised light showed that the crimp amplitude of the fibres in the native [Figure 3.7 A, C] and decellularised tissue sections [Figure 3.7 B, D] had no major differences, although there was minor loosening of the crimp waveform seen in the decellularised tissue sections [Figure 3.7 B]. Elastin was evident in the wall of the blood vessels of native tissue sections, no difference in the appearance of the elastin fibres was found between the native [Figure 3.7 A] and the decellularised tissue sections [Figure 3.7 B].
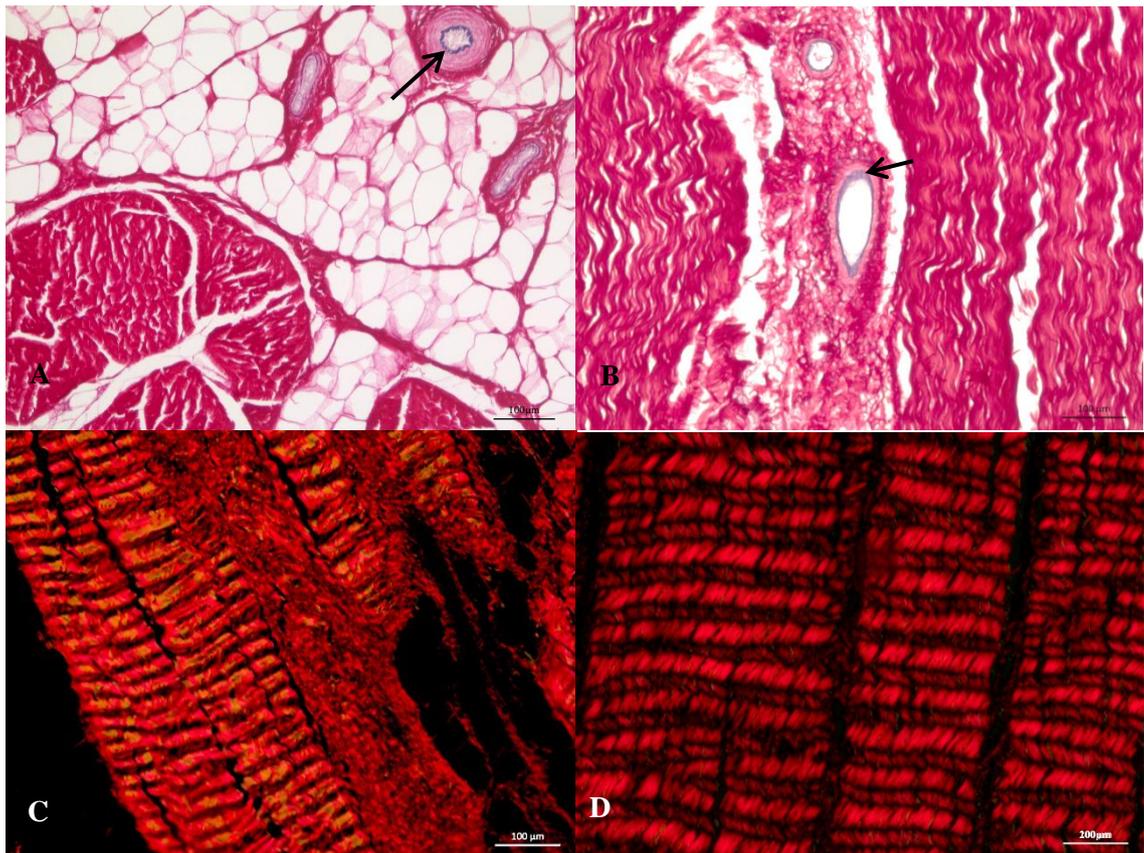


**Figure 3.7 Sirius red-Miller's elastin stained sections at 100x magnification.** (A, B) using bright light microscopy and (C, D) polariation channel to the native (A, C) and decellularised sections (B, D). The native section (A) was observed to contain fatty tissue, the decellularised section (B) was observed to have loosened fibres. Arrows indicate the presence of elastin fibres. Scale bars of (A, B, and C) indicate 100µm, scale bar of (D) indicates 200µm.

Both H&E and Sirius red stained sections showed that the decellularised tendons were not damaged during the process as indicated by the retention of collagen fibre alignment and endotenon regions between the fibre bundles. The H&E stained sections gave more distinct information on the histoarchitecture compared to the Sirius red-Miller`s elastin stained sections.

### 3.4.3.2. Immunohistochemical evaluation of the native and decellularised porcine PTs

The immunohistochemical staining technique required the inclusion of an isotype control, a negative control and a positive control in order for the presence of the antigen of interest to be concluded accurately.

### 3.4.3.2.1. Collagen I

Antibody labelling of the decellularised tissue sections for collagen I using the antibody at a 1 in 100 dilutions is displayed in Figure 3.8 A.
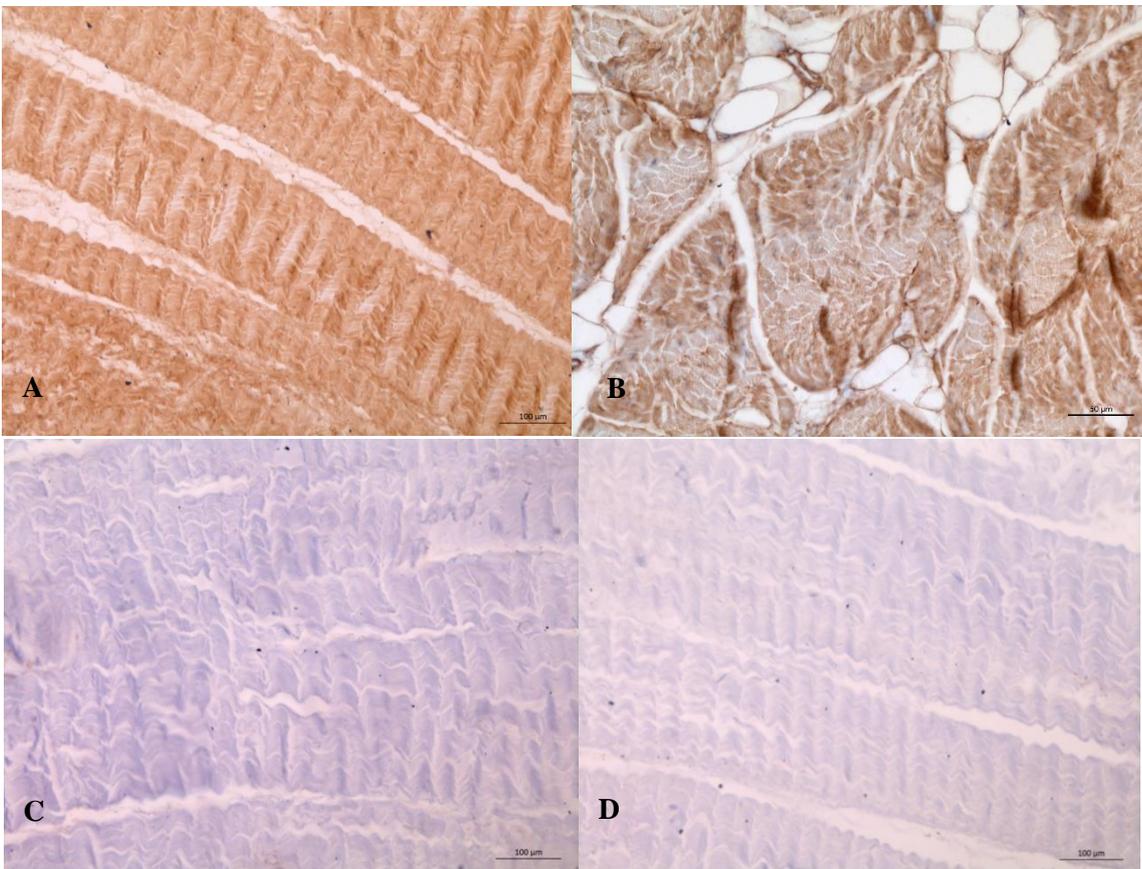


**Figure 3.8 Immunohistochemical staining for the collagen I at 100x magnification (A,B) and 40x magnification (C,D)**; (A) decellularised tissue section stained with antibody to collagen I (1:100) (B) native tissue section stained with antibody to collagen I (1:100) (C) decellularised tissue section stained with the IgG1 isotype control antibody (1:100) and (D) no antibody negative control. Scale bars represent 100µm.

Collagen I was detected throughout the native tendon [Figure 3.8 B] and the decellularised tendon sections section [Figure 3.8 A]. No positive staining was found in the sections stained with isotype control antibody [Figure 3.8 C] and the negative control [Figure 3.8 D].

### 3.4.3.2.2 Collagen III

An image of a decellularised tissue section labelled with an antibody to collagen III (1: 50) is shown in Figure 3.9 A.
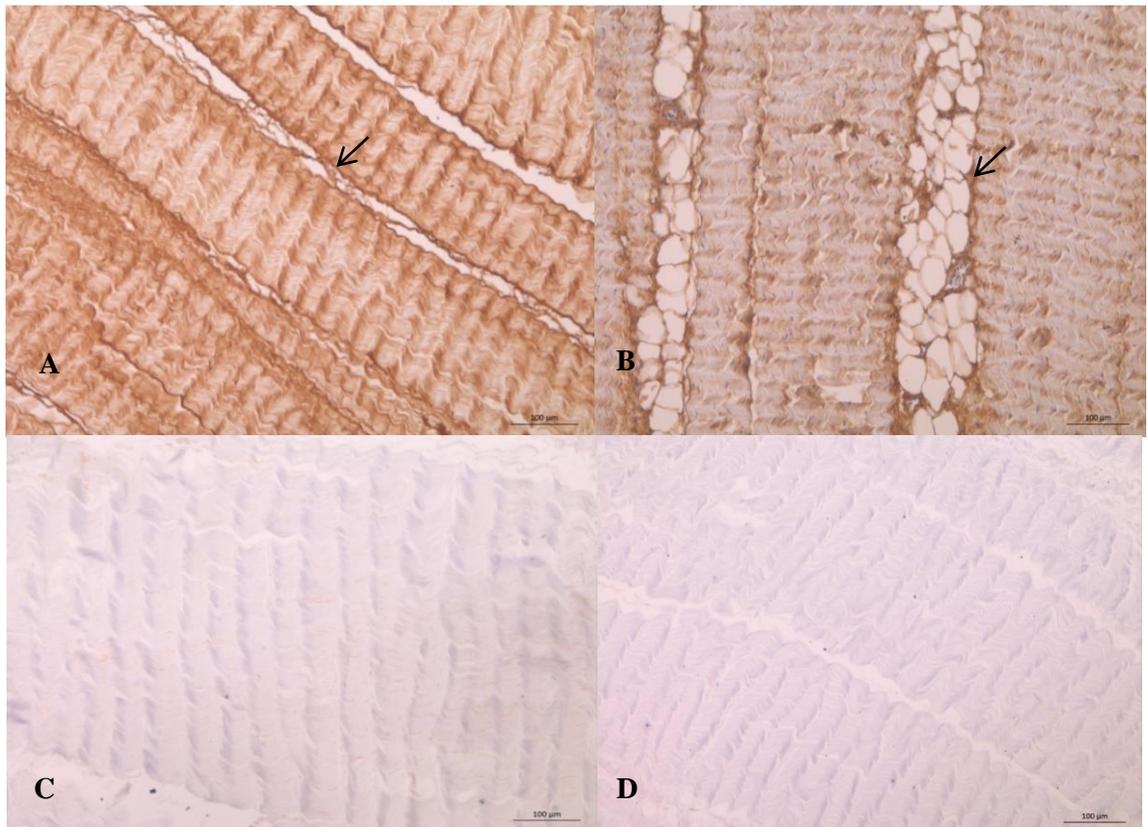


**Figure 3.9 The immunohistochemical staining for collagen III,** at 100 x magnification (A,B) and 40 x magnification (C,D); (A) the decellularised section (1:50), (B) the native section (1:50), (C) incubated with IgG1, the isotype control (1:50) and (D) the negative control. Arrows indicate the epitenon and endotenon. Scale bars represent 100µm.

Collagen III was present throughout the decellularised [Figure 3.9 A] and the native [Figure 3.9 B] tendon sections. Both sections had a similar appearance with a denser brown staining found surrounding the fibres.

**3.4.3.2.3. Tenascin-C**

Antibody labelling for tenascin-C showed that this glycoprotein was no longer stained in the tissue sections after the decellularisation process. There was no positive staining [Figure 3.10 A] compared to the native tendon [Figure 3.10 B], the isotype control (IgG2B (1:100)) [Figure 3.11 C] and the negative control [Figure 3.10 D].
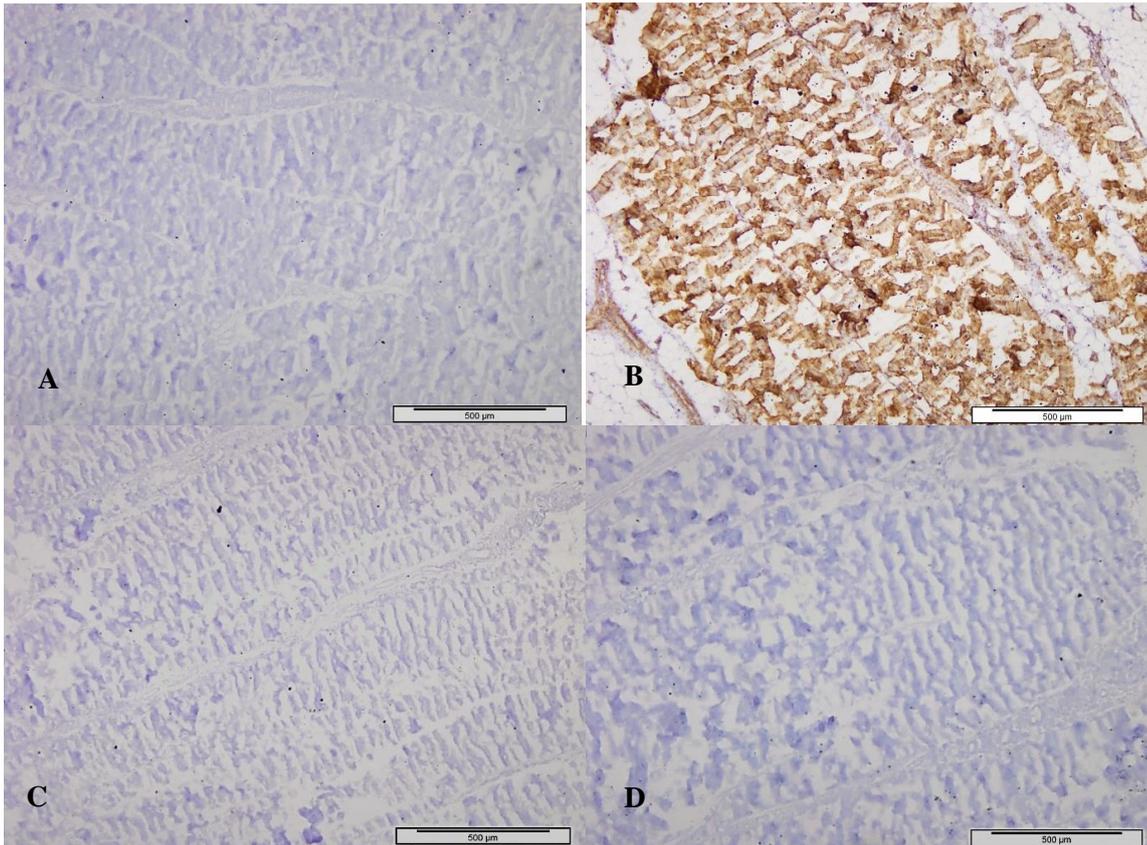


**Figure 3.10 Immunohistochemical staining for tenascin-C** at 40x magnification to (A) the decellularised section (1:100), (B) the native section (1:100), (C) incubated with IgG2b, the isotype control (1:100), and (D) the negative control. Scale bars represent 500 µm.

**3.4.4. Sterility assessment**

All batches of the decellularised porcine PTs (n=3; taken randomly from each batch) had no bacterial growth in the nutrient broth solutions. The NA, FBA and SBA plates also showed no growth of any colonies.

### 3.4.5. Contact biocompatibility assay

Three decellularised tendons were assessed for their contact biocompatibility, taken randomly from each batch of decellularised tissue. About 5 mm² of the tissue was cut from three parts (PI, IM, TI) of each decellularised tendon. The results presented here are taken from the batch (6). The contact biocompatibility assay using BHK [Figure 3.11] and 3T3 [Figure 3.12] cells showed that the decellularised tendon tissue was biocompatible. The morphology of the BHK and 3T3 cells, after being cultured for 48 h in the presence of the decellularised tendon tissue [Figure 3.11/12 A, D] showed no differences compared to the morphology of the cells in the negative control [Figure 3.11/12 B, E] or the cells only control [Figure 3.11/12 C, F]. Significantly, the Cyanoacrylate killed the cells [Figure 3.11/12 G] as no cells could be found after Giemsa staining [Figure 3.11/12 H].
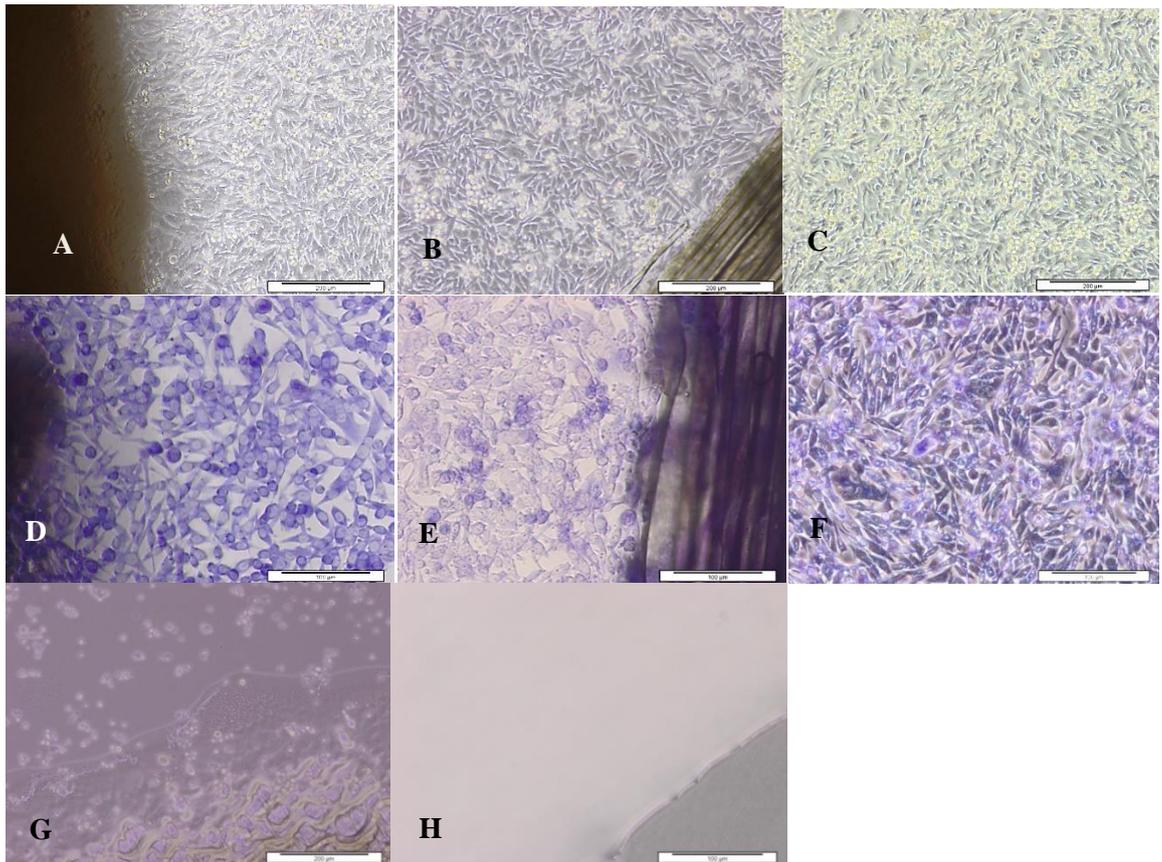


**Figure 3.11 BHK contact cytotoxicity assay**, imaged at 200x magnification. (A, D) the decellularised tendon, (B, E) the negative control, (C, F) the cells only, and (G, H) the positive control. A, C, E, G are the direct imaging and B, D, F, H are the Giemsa staining images. Scale bars represent 200 µm.

The images of the contact biocompatibility assay of the decellularised PPT batch (6) to 3T3 cells and its controls [Figure 3.12].
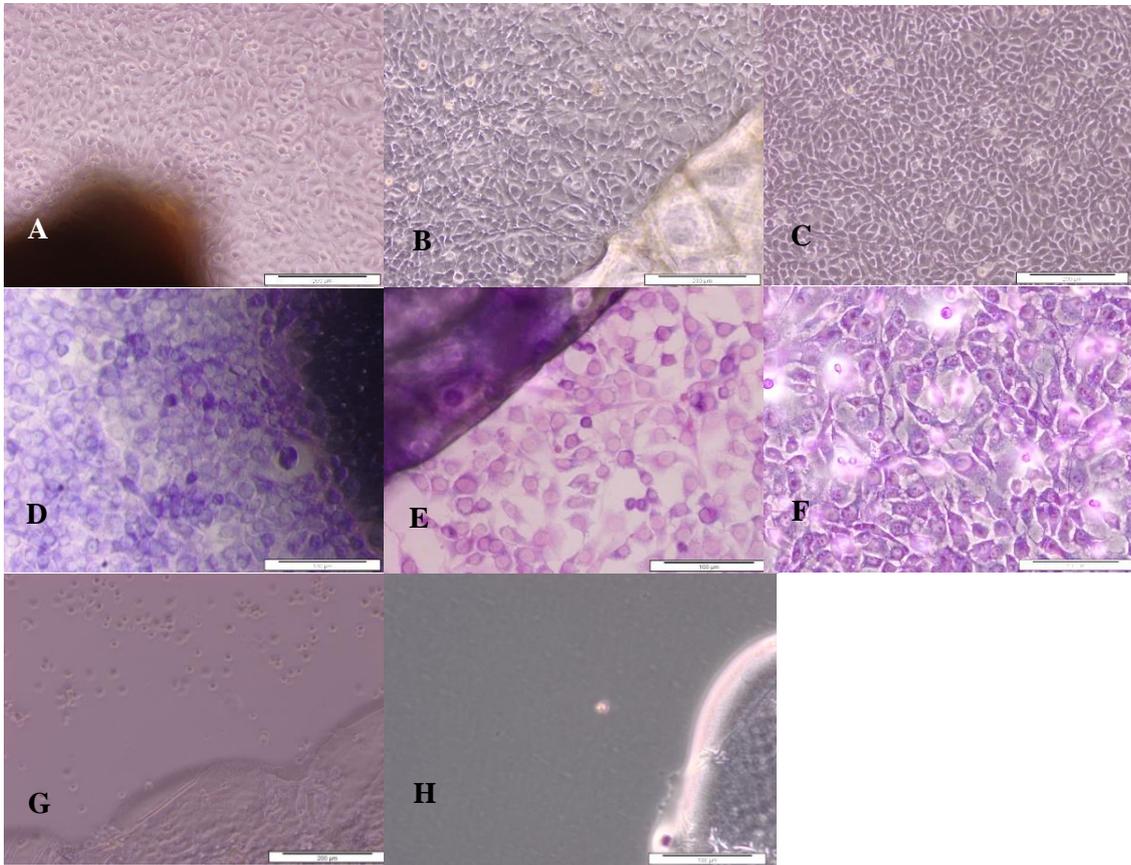


**Figure 3.12 3T3 contact cytotoxicity assay**, imaged at 200x magnification. (A, D) the decellularised tendon, (B, E) the negative control, (C, F) the cells only, and (G, H) the positive control. A, C, E, G are the direct imaging and B, D, F, H are the Giemsa staining images. Scale bars represent 200 μm.

### 3.4.6. DNA quantification of decellularised porcine PTs

The DNA content per mg dry weight of the native PT (n = 6) was $557 \pm 80$ ng.mg$^{-1}$ dry weight (mean $\pm$ 95% Cl) for the tissue from the PI, $480 \pm 118$ ng.mg$^{-1}$ dry weight (mean $\pm$ 95% Cl) for the tissue from the IM and $460 \pm 101$ ng.mg$^{-1}$ dry weight (mean $\pm$ 95% Cl) for the tissue from the TI. The DNA content of the decellularised PT batch (2) (n=6) was $4.9 \pm 2.3$, $4.8 \pm 2.3$ and $3.9 \pm 1.6$ ng.mg$^{-1}$ dry weight (mean $\pm$ 95 % Cl) for the tissue from the PI, IM and TI respectively [Figure 3.13]. This represented a reduction of DNA content as a result of the

decellularisation process of 98.82 %, 98.85% and 99.24% for the tissues from the PI, IM and TI respectively [Figure 3.14].
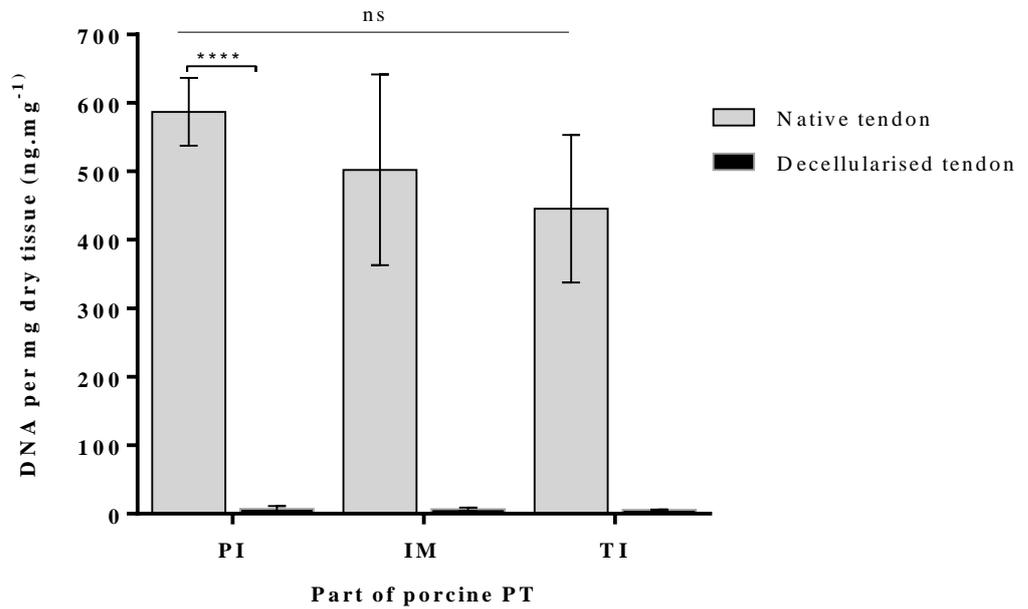


**Figure 3.13 DNA content of native and decellularised porcine PT from batch (2).** The data was analysed by two-way ANOVA with post- multiple comparisons test. Bars denote mean ± 95% Cl. **** indicates significantly different ($p < 0.0001$).

No differences in the DNA content were found between the three areas of the decellularised PTs ($p > 0.05$), however there were obvious differences between the native and the decellularised groups ($p < 0.0001$).
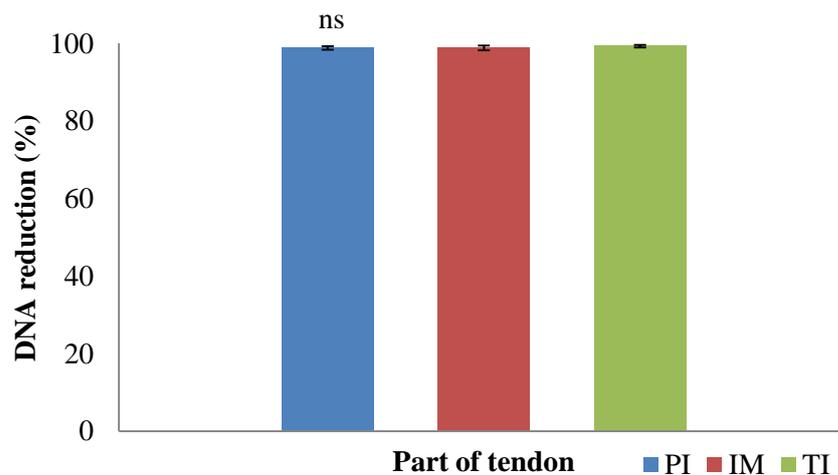


**Figure 3.14 Percentage reduction in DNA content among different parts of the decellularised porcine PTs from batch (2) compared to native PTs**. Bars denote mean ± 95% Cl after arcsine transformation of the data and back-transformation to percentages.

The percentage of DNA reductions among different parts of a decellularised PPT were found to have no differences.

### 3.4.7. Summary of the analysis of all batches of the decellularised porcine PTs

All images shown in this chapter were taken from the decellularised PTs batch (6). The DNA quantification was taken from the batch (2) as this was the first batch that quantified the DNA from three parts of tendon. In summary, the analyses of the decellularised PTs were found to be consistent from batch to batch and are presented in the Table 3.2.

| Batch no | Acellularity | Histo-architecture | ECM component | DNA assay ($ng.mg^{-1}$) mean ± 95% Cl | Bio-compatibility | Sterility |
|---|---|---|---|---|---|---|
| 1 (n=4) | No cells | Not altered | Collagen I + Collagen III + Tenascin-C - | - | Compatible | No growth |
| 2 (n=12) | No cells | Not altered | Collagen I + Collagen III + Tenascin-C - | 7.1±2.1 | Compatible | No growth |
| 3 (n=12) | No cells | Not altered | Collagen I + Collagen III + Tenascin-C - | 6.5±3.9 | Compatible | No growth |
| 4 (n=20) | No cells | Not altered | Collagen I + Collagen III + Tenascin-C - | 2.2±1.3 | Compatible | No growth |
| 5 (n=20) | No cells | Not altered | Collagen I + Collagen III + Tenascin-C - | 1.9±1.7 | Compatible | No growth |
| 6 (n=20) | No cells | Not altered | Collagen I + Collagen III + Tenascin-C - | 5.5±7.8 | Compatible | No growth |

**Table 3.2 Summary of the analyses of all batches of the decellularised porcine PTs**.

## 3.5. Discussion

The decellularisation process applied to porcine PTs and reported in this chapter, had successfully produced acellular, sterile, biocompatible batches of decellularised PPT scaffolds that retained their histoarchitecture and major structural ECM components.

Macroscopically, the decellularised PPTs had no morphological differences compared to the native tendons, but were white in colour. However, the histology of the decellularised scaffolds showed complete nucleus elimination across the samples, without any indication of double stranded DNA fragments. In contrast, the native tendons had numerous cell nuclei arranged in order in between fibres and around blood vessels. DNA fragments may, however stick to the scaffold ECM and hence it was important to quantify the residual DNA content. The acellular porcine PTs from batch (2) had less than 10 $ng.mg^{-1}$ total DNA per dry weight, and there was no difference among the three parts of the tendons (PI, IM or TI) analysed. This confirmed that the decellularisation process had effectively and consistently removed DNA from all areas of the patellar tendon. Assessment of decellularised batches (3) to (6), DNA quantification was therefore not carried out on all areas of the tendon but on pooled tissue.

Both H&E and Sirius red stained tissue sections showed that the decellularised tendons were not damaged during the process, as indicated by the retention of collagen fibre alignment and endotenon regions between the fibre bundles compared to native tendon sections. Although a few sections of decellularised tissues showed some fibres that appeared slightly widened, in majority, the crimp of the collagen fibres appeared unchanged between the native and decellularised tissue sections. This crimp arrangement of the collagen fibres was in agreement with the original findings of the nature of tendon collagen fibres (Dale et al., 1972).

It is difficult to visualise elastin fibres in tendon tissue since it represents only up to 1 - 2% of total dry mass (Kannus, 2000). Nonetheless, elastin fibres were obviously seen in the walls of blood vessels in the native and the decellularised tissue sections stained using Sirius red – Miller`s elastin, and visualised using bright field microscopy. Hence, the decellularisation

protocol retained not only the structural components of the ECM but also the blood vessel structure. It is possible that "empty" blood vessel networks in the decellularised scaffolds might offer an advantage to the scaffold if used as an implant. An in-vivo study using poly(glycerol sebacate) scaffolds, fabricated with a multilayer of 100 μm tunnels to mimic the microvasculature, showed an endothelial-cell lining over the micro-vessel surface after 7 days' implantation intra-peritoneally in rats (Ye et al., 2013).

Qualitative assessment of the collagen I and III content of the tendon before and after decellularisation using immunohistochemical labelling showed no differences, as had been previously reported (Ingram et al., 2007). Collagen I staining was very intensive throughout the fascicles, whereas the collagen III labelling showed that layers surrounding the fascicles were more intensively stained compared to the fascicles. The outer layer of the tendon fascicles might have been endotenon and epitenon that have been reported to have predominantly collagen III composition (Tsuzaki et al., 1993, Kielty and Grant, 2003). These findings showed that major structural ECM components of collagen I and III were preserved during the decellularisation process.

In contrast, tenascin-C immunostaining of the tissue was diminished after the decellularisation process. Tenascin-C is a large hexameric ECM glycoprotein (Figure 3.15) present constantly in tissues that are subjected to tension such as tendons and ligaments (Jarvinen et al., 1999, Mehr et al., 2000). It is also expressed in organogenesis and inflammation processes as well as in pathologic situations such as cancer (Bartsch, 1996). In tendon, tenascin-C is produced by the fibroblasts into the ECM to facilitate cell-matrix adhesion (Mackie, 1997). Each tenascin-C monomer is 180-250 kDa in size and binds weakly to the ECM (Pas et al., 2006). Therefore, it was not surprising that tenascin-C was removed during the decellularisation process. This finding may be advantageous for comparing between the decellularised scaffold and cell-seeded regenerated scaffolds, which is a major objective of this study.
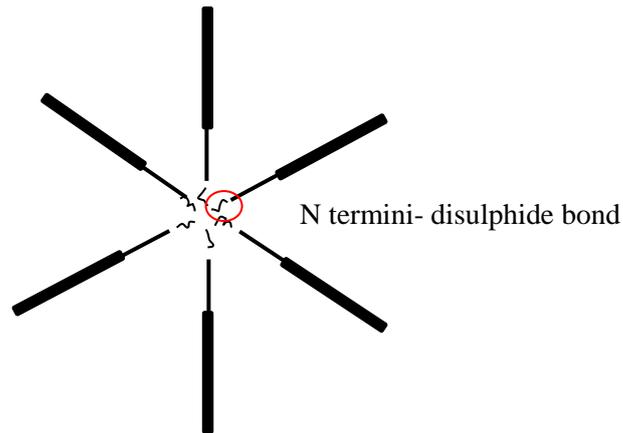
**Figure 3.15 Structure of a large molecule hexameric monomer of tenascin-C.** Reproduced from Mackie (1997).

The contact biocompatibility assays showed that the decellularised porcine PTs were biocompatible. During this study, two cell lines (BHK 21 Strain 31 and 3T3 Swiss albino INFORM L055 O) were used to determine any toxicity of the decellularised tendons. Cell lines such as BHK, 3T3 and L929 are commonly used because they are easy to cultivate, stable (not changing from passage to passage) and cheap. Compared to the use of cell lines for this type of assessment, the use of primary differentiated cells is preferable to show organ specific reactions (Ekwall, 1983) such as studies to reveal toxicity effects (liver or kidney cell) (Zhang et al., 2007). The use of standard cell lines can overcome the issue of variability between different laboratories.

The results showed that none of the decellularised tendons affected the growth of the two cell lines; the cell morphology was no different while growing in contact with or without the scaffolds. Therefore, all batches of the decellularised tendons produced in this project were biocompatible. Previous studies of the biocompatibility of tendons decellularised using this protocol also tested the viability of L929 cells and porcine tenocytes cultured in soluble extracts from the scaffolds (Glover, 2010), human tenocytes and A549 cells (Ingram et al., 2007), and human PTs (Huang et al., 2013a).

To summarise, the decellularised porcine PTs were shown to fulfil the criteria for an acellular scaffold for tissue engineering applications that have less than 50 ng dsDNA per mg ECM dry weight, and lack of visible nuclear material visualised by DAPI and H&E staining (Gilbert et

al., 2006a, Crapo et al., 2011). They also passed all of the quality assurance assessments stated above.

This protocol began with three cycles of freeze-thaw in hypotonic buffer, which caused osmotic shock and intracellular ice formation that damaged the cell membranes and released all intracellular materials such as protease enzymes into ECM. Protease enzymes can digest ECM, therefore a protease inhibitor was needed. In this protocol, Aprotinin was used from the very beginning to inhibit serine proteases, and EDTA to inhibit matrix metalloproteases (Booth et al., 2002). EDTA also blocks cell adhesion through the binding to the fibronectin-RGD receptor and chelates metal ions (Crapo et al., 2011). The use of these chemicals successfully protected the major components of the ECM.

The concentration of SDS used in this protocol (0.1% (w/v)) has been shown by others to have no adverse effects on the mechanical properties of the porcine tendon tissues (Pridgen et al., 2011, Herbert et al., 2015). Higher concentrations of SDS such as 1 % (w/v) followed by 70 % (v/v) ethyl alcohol sterilisation has been shown to effectively remove cells but caused minor inter-fibre disintegration when applied to rat tail tendons (Cartmell and Dunn, 2000). In addition, porcine ACL washed with SDS 1% (w/v) was also shown to be less receptive to porcine fibroblasts compared to Triton X-100 (2 % (w/w)) and the TnBP (2 % (w/w)) treated tissue. Scaffolds receptivity to cells was not improved by augmenting the culture medium using EGF (epidermal growth factor) (33 ng.mL$^{-1}$), or even by expanding the culture duration to 56 days (Harrison and Gratzer, 2005). Another study also confirmed that higher concentrations of SDS (0.5% (w/v)) cause matrix alterations (Kasimir et al., 2003). Residual SDS in decellularised matrices has also been shown to affect cellular growth rate (Arechabala et al., 1999).

In conclusion, 0.1% (w/v) SDS concentration is considered an optimal dose to produce an acellular tendon. This agrees with the general consideration to apply the mildest protocol possible to yield an acellular material without structural and biomechanical disruption (Gilbert et al., 2006b, Badylak, 2002a).

The sterilant used in this study was 0.1% (w/v) PAA in PBS at pH 7.0 incubated for three hours, and assessment of the decellularised porcine PTs using a sterility assay showed no bacterial or fungal growth. Other studies, using similar concentrations, have reported successfully sterilising human bone (Pruss et al., 2001) with no damage to dermis structure and no cytotoxic effects (Lomas et al., 2003), and showed no impact on the biomechanical properties of decellularised human patellar tendon (Lomas et al., 2004).

However, it has recently been reported that peracetic acid at 0.1% (v/v) significantly reduced the tangent modulus of the toe region in porcine supraflexor tendons compared to native tissue (Herbert et al., 2015). Higher concentrations of PAA (5% (v/v)) after 4 and 20 hour washes have been shown to extensively increase the fibre porosity of human acellular supraflexor tendons (Woon et al., 2011).

Compared to PAA, other sterilisation techniques had several limitations. Ethylene oxide gas produces cytotoxic, teratogenic, mutagenic and genotoxic residuals (Roberts et al., 1991, Silvaggio et al., 1993). Gamma irradiation has been shown to disrupt the mechanical properties of ligamentous grafts by causing collagen cross-linking, also decreasing graft stiffness by 12% and 26% of its ultimate strength (Rasmussen et al., 1994). For DNA removal, Benzonase (1 $U.mL^{-1}$), an endonuclease digestion, was used to hydrolyse the interior bonds of the DNA or RNA chains (Freyman, 2005, Gilbert et al., 2006b). This decellularisation protocol used here also involved the use of a hypertonic solution to remove the residual hydrophobic glycoproteins such as (α Gal).

## 3.6. Conclusions

This work described in this chapter has demonstrated that the native porcine PTs had successfully been harvested, and used to produce acellular porcine PTs through an established decellularisation process. The decellularised tendons from different batches were acellular, had little residual DNA, and were sterile and biocompatible. The scaffolds retained their histoarchitecture and structural ECM components, however, Tenascin-C was diminished by the end of the protocol, suggesting that the glycoprotein molecule in the ECM had been washed away. These decellularised PTs had therefore fulfilled the quality assurance as the acellular scaffolds to be used to study the regeneration capacity using human BM-MSCs.

# Chapter 4

# Isolation and characterisation of the MSC

## 4.1. Nomenclature of mesenchymal stem cells

Adult progenitor cells have been extensively studied over 40 years, since they were introduced by Friedenstein (1966) with his initial description of stromal cells as colony forming, spindle-shaped cells with multipotent differentiation potential, isolated from bone marrow (Friedenstein et al., 1974). Subsequently, stromal cells were also identified from other sources, such as embryonic chick limb mesenchymal cells (day 4.5), that could be derived into chondroblasts and osteoblasts (Caplan, 1991).

Studies of mesenchymal stem cells (MSCs) are now established across the world, however different laboratories have used different sources, methods and culture conditions. This has made comparison between studies difficult therefore, the International Society for Cellular Therapy (ISCT) developed a term for the fibroblastic-like plastic adhered cells, regardless of their source as multipotent mesenchymal stromal cells. The term 'MSC' should follow the general considerations of the Mesenchymal and Tissue Stem Cells Committee of the ISCT; that is the cells should be plastic-adherent, should express surface molecules such as CD 73, CD 90, and CD 105, and be negative for CD 45, CD 34, CD 14, CD 11b, CD 79α, CD 19 and HLA-DR. The cells should be able to differentiate into osteoblasts, adipocytes and chondroblasts in vitro (Horwitz et al., 2005, Dominici et al., 2006).

**MSC source**

MSCs have been identified in the pre-natal tissue such as the placenta (Battula et al., 2007), umbilical cord blood (Perdikogianni et al., 2008), amnion epithelium (Pirjali et al., 2013), and the post-natal tissues such as peripheral blood (Sniecinski, 1991), bone marrow (Bianco et al., 2001) and indeed, most organs and tissues. Regardless of the source of MSCs, they are self-

renewing and pluripotent, serve as a reservoir to replace dead cells and repair wounds (Pittenger et al., 1999, Phinney and Prockop, 2007).

Bone marrow derived MSCs are multi-lineage cells located within marrow tissue, with the purpose of supporting the surrounding tissue. In addition to their capacity for tri-lineage differentiation into bone, cartilage and fat cells, bone marrow MSC have been reported to differentiate into myocytes (Ferrari et al., 1998) or even to cross their embryonic lineage-fate and form astrocytes (Kopen et al., 1999) or hepatocytes (Lagasse et al., 2000).

Bone marrow is sparsely populated with MSC; they have been reported comprise about 0.001 to 0.01% of the total marrow of human tissue (Pereira et al., 1995). Bone marrow tissue is easy to harvest, and the MSC are relatively easy to isolate and expand with preservation of their differentiation capacity (Pittenger et al., 1999). In this chapter, the mesenchymal properties of porcine and human bone marrow derived MSCs (BM-MSC) were validated. Different methods to analyse cellular viability and to extract the RNA for RT-qPCR analysis were developed.

## 4.2. Aims and objectives

Aim: to isolate and characterise the BM-MSCs for subsequent studies of their response to mechanical strain when seeded onto decellularised porcine PT scaffolds

Objectives:

1. To isolate porcine BM-MSCs and to determine their characteristics

2. To utilise porcine BM-MSCs to determine the cell density required to isolate a sufficient concentration of mRNA for analysis of gene expression.

3. To characterise donated human BM-MSCs using tri-lineage differentiation assay and analysis of lineage gene expression

4. To determine the culture conditions required to support the expansion of human BM-MSCs in-vitro.

## 4.3. Material and methods

### 4.3.1. Porcine BM-MSCs

#### 4.3.1.1. Isolation and culture of porcine BM-MSC

The bone marrow MSCs were isolated using a Percoll gradient since this method has been reported to yield a high number of MSC with no effect on the differentiation capacity of the cells compared to the classical method (Bourzac et al., 2010).

**Solutions**

a) Percoll

b) NaCl 1.5M

c) Tyrode's solution

A Percoll gradient was prepared the day before the isolation of the MSC from porcine bone marrow. Percoll (22.05 mL) was added to 2.45 mL of 1.5 M NaCl and 10.5 mL Tyrode's solution in a 50 mL centrifuge tube. This was centrifuged at 20,000 g for 15 min, and stored at 4 °C. Porcine bone marrow was isolated from the porcine femoral heads of Large White pig (75 – 85 kg), aged 4 to 6 months that had been slaughtered no more than 24 h previously. All procedures were performed in a class II safety cabinet.

The bone marrow was exposed using a sterile bone saw and harvested using spatulas. The bone marrow was dispersed in 25 mL DMEM complete medium and centrifuged at 600 g for 5 min. The supernatant and the fat layer were carefully removed, and the pellet was layered carefully on the Percoll gradient. The gradient was centrifuged for 15 min at 460 g and 14 cm of the upper fraction was harvested. To this, 35 mL DMEM complete medium was added and centrifuged at 600 g for 5 min. The pellet was resuspended in 5 mL culture medium and incubated for 5 days in a T25 flask at 37 $^0$C in 5% (v/v) $CO_2$ in air. The porcine BM-MSCs were maintained, passaged and cryopreserved as described in Section 2.2.3.

**4.3.1.2. Porcine BM-MSC characterisation using flow cytometry**

The porcine BM-MSCs at p7 were analysed for the expression of a panel of markers commonly

used to characterize MSC by flow cytometry [Table 4.1].

| Primary antibody | Type | Isotype | Dilution | Supplier |
|---|---|---|---|---|
| CD29 (+) | Mouse anti human | IgG2a-RPE | 1:5 | AbD Serotec |
| CD44-FITC (+) | Rat anti pig | IgG1-FITC | Neat | AbD Serotec |
| CD45 (-) | Mouse anti pig | IgG1-FITC | 1:10 | AbD Serotec |
| CD90-RPE (+) | Mouse anti human | IgG1-RPE | 1:5 | BD Pharmigen |
| SLA ClassII DR (-) | Mouse anti pig | IgG2b-RPE | Neat | AbD Serotec |
| **Secondary antibody** | | **Conjugate** | **Dilution** | **Supplier** |
| Rabbit anti mouse | | RPE | 1:10 | Dako |
| Anti-mouse | | FITC | 1:10 | Biologend |
| **Isotype** | **Host** | | **Dilution** | **Supplier** |
| IgG2a-RPE | Mouse | | 1:10 | AbD Serotec |
| IgG1-FITC | Mouse | | 1:10 | MBL |
| IgG1-RPE | Mouse | | 1:10 | Dako |
| IgG2b-RPE | Mouse | | 1:10 | AbD Serotec |

**Table 4.1 Primary and, secondary antibodies and the isotype controls,** used for flow
cytometry analysis of porcine MSC.

**Buffers and solutions**

The following reagents were prepared and stored at 4 $^{0}$C, unless otherwise stated.

a) 2x FACS blocking buffer

PBS (5 tablets) were dissolved into 500 mL distilled water, EDTA (0.465 g) was added,

and the solution was autoclaved, stored at 4 °C. FBS (20 mL) was added prior to use.

b) Antibody diluent

This was prepared by adding 1% (w/v) sodium azide (6 mL) and 5% (w/v) BSA (300 µL) in 40 mL of PBS. The pH was adjusted to 7.6 and the volume was topped up to 60 mL using PBS.

c) PBS solution

One tablet of PBS was dissolved into 100 mL of distilled water and the pH was adjusted into 7.2 – 7.4.

**Method**

Cells were harvested at approximately 80 – 90 % confluence and counted [Chapter 2; Section 2.2.3]. The cell suspension was centrifuged at 600 g for 10 min and the pellet was resuspended using ice cold PBS to obtain a cell density of 2 x 10$^6$ cells per mL. Cell suspensions (100 µL) were aliquoted into 1.5 mL Eppendorf tubes. The cell suspensions were incubated with 100 µL of FACS blocking buffer for 20 min, followed by incubation with 100 µL of antibody, isotype control or antibody diluent alone for 1 h on ice in the dark. The antibodies and isotypes were prepared just before use, diluted with antibody diluent following the dilution factor described in Table 4.1. After incubation, the suspensions were washed in 300 µL ice cold PBS, centrifuged at 600 g for 5 min at 4 $^0$C. The pellet was resuspended in 200 µL ice cold PBS, 100 µL of the secondary antibody was added and incubated on ice in the dark for 1 h. Subsequently, the cells were washed twice for 5 min using 300 µL ice cold PBS at 600 g and the pellets were resuspended in 200 µL ice cold PBS. The intensity of cells fluorescence was analysed using FACSCalibur (Becton Dickinson). Data was collected (10,000 events per sample) using CellQuest™ v.3.1 flow cytometry data acquisition software (Becton Dickinson), and analysed using FlowJo™ v.7.6.5 flow cytometry analysis software (Tree Star Inc).

Initially, a template for FACs analysis was set by loading the correct information into the software (CellQuest™v.3.1 flow cytometry data acquisition software (Becton Dickson)). Cells of interest taken from the scatter plots produced by sorting the untagged cells were gated

[Figure 4.1]. The gating grouped the cells of interest and excluded dead cells or debris. After setting up the template, cells with labelled antibody were sorted and the data were recorded. These data were later analysed and converted into histograms using FlowJo software. Using the histograms, the maximum fluorescence intensity of the appropriate isotype control was used to determine the cut-off point for determining the percentage of cells that were stained positive with the test antibody. Graphs of fluorescence intensity of the cells stained with the test antibody and appropriate isotype control were overlapped and the value was derived from the comparison. Generally, positive staining was categorised as cells with fluorescence intensity above $10^2$.
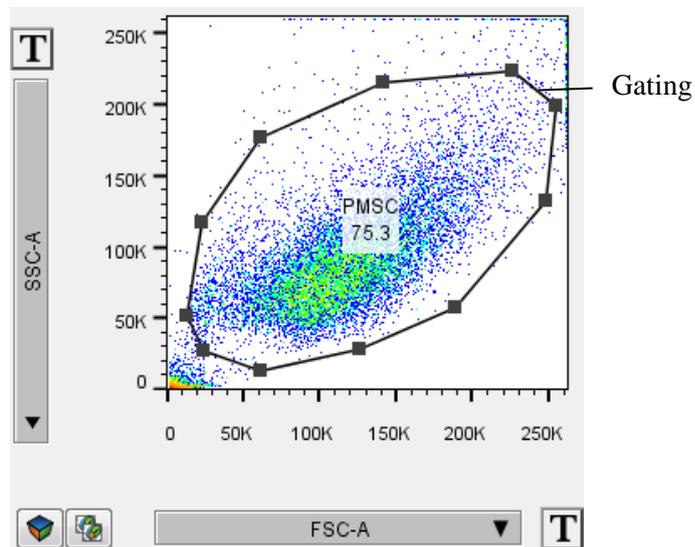


**Figure 4.1 Gating of the cell of interest and exclusion of dead cells and debris.**

### 4.3.1.3. MSC characterisation using tri-lineage differentiation

The capability of MSC to differentiate into adiphocytes, chondroblasts and osteoblasts is used to determine whether the cells are MSC or not. The trilineage differentiation assay used was according to the methods of Bosch et al. (2006) (Bosch et al., 2006).

All additives for the differentiation media were filtered through a 0.2 µm pore size filter and stored as stocks at – 20 $^0$C, whilst the differentiation media were prepared using standard culture medium [Chapter 2; Section 2.2.3.1] and stored at 4 $^0$C for up to one week, unless otherwise stated.

### 4.3.1.3.1. Differentiation Medium

**Adipogenic differentiating medium**

a) IBMX (Isobuthylmethylxantine; Sigma-Aldrich) 0.5 M stock:

This was prepared by dissolving IBMX (100 mg) into 0.9 mL of 100 % (v/v) methanol. The stock was aliquot into 100 µL amounts.

b) Indomethacin 0.6 M stock:

Indomethacin (100 mg) was dissolved into 467 µL 100% (v/v) methanol. The solution was aliquoted into 10 µL amounts.

c) Hydrocortisone 0.1 mM stock:

Hydrocortisone (4.854 mg) was dissolved in 100 mL PBS. The stock was aliquoted into 500 µL amounts.

d) Horse serum 10 % (v/v) was added to 89.39 mL DMEM complete medium.

Adipogenic medium was made by adding IMBX (0.5 mM), Indomethacin (60 µM), hydrocortisone (0.5 mM) and horse serum 10 % (v/v) into DMEM complete medium to make up to 100 mL total medium.

**Osteogenic differentiation medium**

a) Dexamethasone 50 mM stock:

Dexamethasone (25 mg) was dissolved into 1,280 µL of 100 % (v/v) methanol. The stock was aliquoted into 10 µL amounts.

b) Ascorbic-2-phosphate 200 mM stock:

Ascorbic-2-phosphate (2.57 g) was dissolved into 50 mL of distilled water. The stock was aliquot into 50 µL amounts.

c) Beta-2-glycerophosphate 2 M stock:

Beta-2-glycerophosphate (10 g) was dissolved into 23 mL of distilled water. The stock was aliquoted in 500 µL amounts.

Osteogenic culture medium was made by adding dexamethasone (100 nM), ascorbic-2-phosphate (100 µM) and beta-2-glycerophosphate (10 mM) into DMEM complete medium to make up to 100 mL of total medium.

**Chondrogenic differentiation medium**

a) Ascorbic-2-phosphate 200 mM stock:

Ascorbic-2-phosphate (2.57 g) was dissolved into 50 mL of distilled water. The stock was aliquot into 75 µL amounts.

b) Sodium pyruvate 100 mM stock:

Sodium pyruvate (1.1 g) was dissolved in 100 mL of distilled water. The stock was aliquoted into 1 mL amounts.

c) Insulin transferrin selenium (ITS, 6.25 $\mu g.mL^{-1}$) and TGF β3 (250 $\mu g.mL^{-1}$).

Chondrogenic medium was prepared by adding insulin (6.25 $\mu g.mL^{-1}$), ascorbic-2-phosphate (0.3 mM), pyruvate (1 mM) and TGF β3 (0.01 $\mu g.mL^{-1}$) into DMEM complete medium to make up to 100 mL of total medium.

**4.3.1.3.2. Differentiation Method**

Three groups (adipogenesis, osteogenesis, and chondrogenesis) of five 6-well-plates per group (Day 0, Day 3, Day 7, Day 14 and Day 21) were prepared. The cell density for adipogeneic differentiation was 4000 $cells.cm^{-2}$, for osteogeneic differentiation; it was 3000 $cells.cm^{-2}$ and 6000 $cells.cm^{-2}$. MSC cell suspension in standard culture medium (2 mL) was added to each well of the six well plates, and left overnight at 37 $^0C$, 5 % (v/v) $CO_2$ in air to allow the cells to adhere. The standard culture medium was then replaced with the appropriate differentiation medium by the next day. Chondrogenic differentiation was studied using microdrop culture (10 µL), at a cell density of 1 x $10^7$ $cells.mL^{-1}$. The microdrops were incubated for 3-4 h to allow the cell pellet to adhere to the plate followed by the addition of the chondrogenic medium. The plates were incubated at 37 °C, 5% (v/v) $CO_2$ in air and the differentiation media were replaced with the fresh differentiation media every three to four days.

**4.3.1.3.3. Assessment of MSC differentiation**

Differentiation of the MSC was assessed using different staining methods as described below, and the staining solution was stored at room temperature up to one week.

**Adiphogeneic staining solution**; Oil-Red-O dye working solution

Oil-Red (50 mg) was added into 10 mL of isopropanol to produce an Oil red stock solution (0.5% (w/v)). The working solution was prepared by adding three parts of Oil red stock solution to two parts distilled water. This was left at room temperature for 20 min and filtered through a 0.2 μm filter.

**Adipogeneic staining method**

Throughout this procedure, the cell monolayer was washed using PBS without $Ca^{++}Mg^{++}$ twice between every step. After the first wash, the cell layer was fixed using 10 % (v/v) NBF for 10 min, stained with Oil-Red-O working solution for 10 min at room temperature. After being air dried, the cell layer was visualized as described below.

**Osteogenic staining solutions**

   a) Ammonium hydroxide (10 % (v/v))

   Ammonium hydroxide 28 % (v/v) was mixed with 60 mL of distilled water.

   b) Alizarin red solution (40 mM)

   Alizarin red (2 g) was dissolved in 100 mL of distilled water. The pH was adjusted to 4.1 by adding 10 % (v/v) ammonium hydroxide.

**Osteogenic staining method**

The cell monolayer was washed twice using distilled water in between each step of the procedure and four times at the end of the process. The cell monolayer was fixed using 10 % (v/v) NBF for 15 min and stained using Alizarin red solution for 20 min with gentle agitation at room temperature. After being air dried, the cell monolayer was visualized as described below.

**Chondrogenic staining solution**

Alcian blue working solution; 1% (w/v) alcian blue in acetic acid

**Chondrogenic staining method**

The cell pellet was washed using distilled water between each step throughout the procedure. The cell pellet was fixed using 10 % (v/v) NBF for 15 min and stained with Alcian blue working solution for three min at room temperature. To determine the differentiation capacity of the MSC, each plate (Day 0, Day 3, Day 7, Day 14 and Day 21) was stained at each time point using the three staining procedures. The cells were visualised using inverted microscope, Olympus IX71 and the images were captured using an Evolution MP Colour digital camera connected to the computer using cell^B® imaging software with correct Kohler illumination.

### 4.3.1.4. RNA extraction from different densities of porcine BM-MSCs for PCR

The aim of these studies was to determine the quantity of RNA extracted from different densities of porcine BM-MSCs.

Four groups of porcine BM-MSCs at p5 (n=4) at cell densities of 500, 1000, 10000 and 20000 cells per 100 µL PBS solutions were prepared for RNA extraction using RNeasy mini kit (Qiagen). The work station used to extract the RNA was cleaned using RNase OUT. The water and consumables used throughout these experiments were RNA/DNase-free, and the ethanol 100% (v/v) was molecular grade (ThermoFisher Scientific). All centrifugation steps were performed at room temperature unless otherwise stated.

**Solutions (prepared just before use)**

a) DNase I stock solution; lyophilized DNase I (1500 KU) was dissolved in Nuclease water using a syringe and mixed by inversion to make a 2.5 KU.µL$^{-1}$ stock. The dissolved DNase I was aliquoted into 20 µL volumes and stored at -20 $^{0}$C for 9 months. The working solution for DNase I incubation mix (0.34 KU.µL$^{-1}$) was prepared by adding RDD buffer (Qiagen).

b) RLT lysis buffer was prepared by adding β-mercaptoethanol (10 µL.mL$^{-1}$).

**Method**

Porcine BM-MSCs at 80% confluence were trypsinized following the method outlined in Chapter 2; Section 2.2.3 and the cells were prepared at the desired densities in 1 mL of PBS solutions in 2 mL sterile Eppendorfs. The cell suspensions were then centrifuged at 5000 g for five min to harvest the cell pellet, followed by removing the PBS solutions, leaving the pellet undisturbed. The pellets were flicked, lysed with 350 µL of RLT lysis buffer plus β-mercaptoethanol (10 µL.mL$^{-1}$). The lysate was vortexed for one sec to homogenize, followed by adding 175 µL of 70% (v/v) ethanol.

The RNA was then collected by filtering 700 µL of the lysate by each centrifugation, through an RNeasy spin column, at 8,000 g for 15 sec. Once all lysate were were filtered, the membrane was then washed using 350 µL of RW1 buffer at 8,000 g for 15 sec. The DNA was eliminated on the column using 80 µL of DNase I incubation mix at room temperature for 15 min. The membrane was washed using 350 µL RW1 buffer, followed by 500 µL RPE buffer; each at 8000 g centrifugation for 15 sec. The membrane was then dried at 8000 g for 1 min. Finally, the RNA was harvested using 30 µL of RNAase free water to elute at 8000 g for 1 min. The collected RNA was quantified using Nanodrop 1000-V3.7 spectrophotometer (Thermo Scientific) at 260 nm. Samples (2 µL) were measured three times and a mean value was taken. The purity of the RNA was determined through the ratio of A260/280 generated for each reading, a reading between 1.9-2.1 was considered as pure RNA. Before using, the cuvette was cleaned using Nuclease-free water and the reading was set to zero by using the Nuclease-free water that was used to elute the RNA. The RNA was aliquoted and stored at − 80 $^{0}$C (Qiagen, 2012a).

**Data presentation**

The concentration of mRNA isolated from each of the cell densities used is presented as ng.µL$^{-1}$. The quantity of mRNA per cell is presented as pg per cell, by calculating the total RNA

extracted from each sample group and dividing by 30 µL (total elution volume) then dividing by the total number of cells. The A260/280 is presented as the mean value (n=4) ± 95 % Cl.

## 4.3.2. Determination of the porcine BM-MSC differentiation by identification of lineage specific gene expressions

### 4.3.2.1. Primer Selections

The primer pairs (forward and reverse) were designed using Primer-BLAST primer design software (Ye et al., 2012) to target the sequence of an exon (gene of interest/ GOI). The primer-pair sequences were selected following the guidelines showed in the Table 4.2 and their specificity to the target gene was evaluated using the BLAST tool (nucleotide; www.ncbi.nlm.nih.gov/blast/Blast). Primer pairs to target the βactin, S28R, GADPH (glyceraldehyde-3-phosphate dehydrogenase) genes were used as a loading control as these genes are consistently expressed at the same level (reference genes) (Thellin et al., 1999).

### Method

Specific information (species, protein) was uploaded in the NCBI library (http://www.ncbi.nlm.nih.gov/) to obtain the relevant mRNA sequences. The oligonucleotide sequence then appeared in a Graphic file, a sequence was then chosen, followed generation of the primer pairs using Primer-BLAST software. The primer sequences were then selected. The primer pair properties such as melting temperature, size and target sequences were re-evaluated using OligoCalculator software (Sigma). Primer pairs were synthetized and supplied by OligoSigma. Each primer was diluted into 100 µM stocks using Nuclease-free water following the manufacturer's instructions and stored in the 20 µL aliquots at -20 $^{0}$C to avoid repeated freeze/thaw. The aim of this study was to investigate the tenogenesis differentiation of human BM-MSC in the decellularised PPTs in response to mechanical strain. The gene markers to identify the tenogeneic differentiation were the collagen I, collagen III, tenascin-C and scleraxis. The markers for adipogenesis (PPARγ), chondrogenesis (Sox9, collagen II), and osteogenesis

(Runx2 and osteopontin) were also identified to emphasis the mechanotransduction responses of the human BM-MSCs. The reference genes used in this study were βactin, GADPH and S28R. The primer pair of S28R was adapted from the published paper (Chuan et al., 2014).

### 4.3.2.2. Polymerase Chain Reaction (PCR)

The transcript gene expressions were identified using a two-tube method, which has a separated reaction; to reverse transcript mRNA to its complimentary DNA/ cDNA, and to amplify the cDNA using PCR. The amplified DNA were labelled using a DNA dye (SYBR®Green) that binds double stranded DNA and gives fluorescence signals at 497 – 520 nm absorbance. Each reaction had the PCR negative controls; a no DNA control (water) and an internal control (no template control and no primer control) and was visualised using gel electrophoresis. All primer pairs that were selected following the Table 4.2, were used throughout the study, and are listed in Table 4.3.

| Parameter | Optimum value |
|---|---|
| Unique oligonucleotide sequence | Obtained from DNA library (FASTA) |
| Primer length | 18 – 25 bases |
| G-C clamp at the 3' end | 1-2 G/C nucleotides |
| No self-complementarity (primer dimers) | Less than 3 contiguous bases |
| No complementarity to antisense (hair pin) counterpart | Less than 3 contiguous bases |
| Random base distribution and composition | 45-55 % G/C content |
| Match primer $T_m$ (melting temperature) | Less than 3-5 $^0$C discrepancy |
| Distance and composition of intra primer sequence | 100-600 bases apart |
| Amplicon size | Less than 200 bp |

**Table 4.2 Guidelines to design a primer pair.** This table was summarised from Sharrocks (1994), Bustin et al. (2011), Ye et al. (2012).

| GOI<br><br>Accession number | References and the sequence | Product<br><br>length |
|---|---|---|
| Collagen I<br><br>NM_000089.3 | (F) 5' GCTCTGCGACACAAGGAGTC 3'<br><br>(R) 5' ACAAAGTCCGCGTATCCACA 3' | 71 bp |
| Collagen II<br><br>NM_001844.4 | (F) 5' GGAAGAGTGGAGACTACTGGATTGAC 3'<br><br>(R) 5' TCCATGTTGCAGAAAACCTTCA 3' | 76 bp |
| Collagen III<br><br>NM_000090.3 | (F) 5' CTTCCCCGGTCCTAAAGGAAAT 3'<br><br>(R) 5' CCTGAGGTCCAGTTTCACCATT 3' | 116 bp |
| PPAR γ<br><br>NM_138712.3 | (F) 5' GCTCCGTGGATCTCTCCGTA 3'<br><br>(R) 5' ATCTGCAACCACTGGATCTGT 3' | 140 bp |
| Runx2<br><br>NM_001024630.3 | (F) 5' CAGCGTCAACACCATCATTC 3'<br><br>(R) 5' CAGACCAGCAGCACTCCATA 3' | 174 bp |
| Osteopontin<br><br>NM_001251830.1 | (F) 5' ACACATATGATGGCCGAGGT 3'<br><br>(R) 5' GTGTGAGGTGATGTCCTCGT 3' | 116 bp |
| Scleraxis<br><br>XM_006716616.1 | (F) 5' CGCACCAACAGCGTGAAC 3'<br><br>(R) 5' GCGTCTCAATCTTGGAGAGCTT 3' | 91 bp |
| Sox9<br><br>NM_000346.3 | (F) 5' CCCATGTGGAAGGCAGATG 3'<br><br>(R) 5' GAAGGTTAACTGCTGGTGTTCTGA 3' | 69 bp |
| Tenascin-C<br><br>NM_002160.3 | (F) 5' GAGATATGGGGACAATAACCACAG 3'<br><br>(R) 5'ATTTCTGAAGTTGCTTGGTCTCAG 3' | 102 bp |
| β-actin<br><br>NM_001101.3 | (F) 5' CAGCACAATGAAGATCAAGATCATT 3'<br><br>(R) 5' GGACAGCGAGGCCAGGAT 3' | 85 bp |
| GADPH<br><br>NM_001289745.1 | (F) 5' AACATCATCCCTGCCTCTACTG 3'<br><br>(R) 5' CTCCGACGCCTGCTTCAC 3' | 189 bp |
| S28R<br><br>(Chuan et al., 2014) | TTGAAAATCCGGGGGAGAG<br><br>ACATTGTTCCAACATGCCAG | 100 bp |

**Table 4.3 List of the selected primer pairs**.

### 4.3.2.2.1. Converting mRNA to its complementary DNA (cDNA)

The Omniscript RT kit (Qiagen) was used to convert the mRNA to cDNA. Briefly, the mRNA (100 ng) was incubated with 2 μL Oligo(dT) (Qiagen), 2 μL dNTP mix, 2 μL of 10x RT buffer, 10 U.μL$^{-1}$ of RNase inhibitor (Qiagen), 1 μL of Omniscript reverse transcriptase (Qiagen) and the volume of Nuclease-free water was adjusted to give a total reaction volume of 20 μL. The reaction was incubated in a 5Prime thermal cycler (Techne) at 37 $^{0}$C for 1 hour and stored at -20 $^{0}$C for months.

### 4.3.2.2.2. Quantitative PCR (qPCR)

DNA polymerase was used to amplify the nucleotides; QuantiFast SYBR® Green (Qiagen) to label the amplified DNA and the ROX® was used as the passive reference dye to normalise the fluorescence level between the wells. The reaction was performed in the Mx3000 (Stratagen) thermal cycler and data were collected using MxPro3000 software. All plastic ware, filter pipette tips and water were RNA/DNase free, all reactions were prepared in a PCR-UV cabinet (VWR) and the work-station was cleaned using RNAse Zap® (Thermo Fisher). All template, primers and reagent were kept on ice during preparation. The PCR tubes were flat X-clear cap (SLS). In the PCR-UV cabinet, each reaction was prepared in an individual tube; the reaction mixture was prepared by mixing QuantiFast (12.5 μL) with up to 1.0 μM of each primer (forward and reverse), a maximum of 10% cDNA template and water to make up to 25 μL [Table 4.4].

| Component | Volume (μL) | Final concentration |
|---|---|---|
| 2x QuantiFast SyberGreen | 12.5 | 1x |
| Forward primer (10 μM) | 1.25/ 2.5 | 0.5/ 1.0 μM |
| Reverse primer (10 μM) | 1.25/ 2.5 | 0.5/ 1.0 μM |
| Template cDNA | 2.5 | No more than 10% (v/v) total reaction |
| RNase-free H2O | 5 | - |

**Table 4.4 Standard qPCR reaction mixture**

The template used to test the primers was prepared from the cells or tissue known to express the gene of interest. The template and primer concentration used in this study are listed in Table 4.5.

| Source of template | GOI | Primer concentration (μM) |
|---|---|---|
| Day 21 human BM-MSCs derived adipocytes | PPARγ | 0.5 |
| Day 21 human BM-MSCs derived osteoblasts | Osteopontin | 1.0 |
| Day 21 human BM-MSCs derived chondroblasts | Collagen II<br>Sox9 | 1.0<br>0.5 |
| Human BM-MSCs at p6 | Collagen I<br>βactin<br>GADPH | 0.5<br>0.5<br>0.5 |
| Human tenocytes at p7 | Tenascin-C<br>Scleraxis<br>Collagen III | 0.5<br>1.0<br>0.5 |

**Table 4.5 List of templates and primer pairs concentrations**.

The reaction mixture was amplified in a thermal cycler (Mx3000, Stratagene) following the steps described in Table 4.6.

| Step | Temperature ($^0$C) | Duration (sec) | Number of cycles |
|---|---|---|---|
| Stage 1; Denaturation | 95 $^0$C | 5 min | 1 |
| Stage 2; Denaturation<br>Annealing/ extension | 95 $^0$C<br>60 $^0$C | 10 sec<br>30 sec | 35 |
| Stage 3; Denaturation<br>Annealing<br>Final extension | 95 $^0$C<br>55 $^0$C<br>95 $^0$C | 1 min<br>30 sec<br>30 sec | 1 cycle |

**Table 4.6 Standard qPCR thermal cycling program**

The protocol for the PCR followed the Minimal Information Quantitative RT-qPCR Experiments (MIQE) guidelines (Bustin et al., 2009, Bustin et al., 2010).

### 4.3.2.2.3. qPCR data acquisition and analysis

The FAM filter was used to quantify the level of fluorescence recorded from the total SYBR®Green dye that tagged the DNA products during the annealing and extension steps. ROX filter was used to quantify the reference dye (ROX® dye). The number of DNA amplicons increased exponentially until it exceeds the threshold (background fluorescence level); this is known as the Ct value. Ct value is defined as the 'number of cycles' needed to produce a sufficient amount of fluorescence to reach a specific threshold of detection. Each sample had three replicates and mean of Ct value (cycle threshold) was calculated. Using the MxPro3000 software, data are presented as the amplification curve (the amplification of the product versus the number of cycles) and the melting temperature curve (dissociation curves).

A standard curve for the Ct value versus the relative quantity of the target gene and the reference gene was used to demonstrate the efficiency of the amplification. This was generated by the software. The standard curve should have a slope between -3.1 to -3.6 and the amplification efficiency should be around 90-110 %. This standard curve was used to interpolate the relative level gene expression of the GOI and the reference gene.

### 4.3.2.2.4. Gel electrophoresis

The DNA products were then separated using 3.5% (w/v) agarose gels stained using Syber®Safe DNA dye (Invitrogen) run at 110 V for 45 min. Tris borate EDTA (TBE) 1x (Fisher) was used as the buffer as the target DNA size was less than 200 bp. The DNA ladder used was Hyperladder 25 bp (Bioline).

Briefly, the agarose cast was sealed using autoclave tape with an eight-well comb on place. The agarose powder (Sigma) was dissolved in the 1 x TBE solution to make a 3.5% (w/v) agarose gel by heating in a microwave and gently mixing until it boiled. Each cast was filled with 25 mL agarose gel to make a 3 - 5 mm thick gel. When the gel had cooled, SYBR®Safe DNA gel stain

($1 \, \mu L.mL^{-1}$) was added (1: 10,000 dilution) which had a fluorescence excitation at~280 and~502 nm. The agarose gel was left to set and the tape was released. The cast was then placed into a DNA gel running tank. TBE solution (1 x) was added into the tank until it flooded over the gel. The comb was removed, and finally each well was loaded with 20 µL sample; 18 µL of sample was added with 2 µL of Blue Juice™ Gel loading buffer (10x). Once all samples were loaded, 10 µL of the DNA ladder was added to the first lane. The tank was connected to the gel power control unit, set at 110 V and run for 45 min. The gel was then imaged using a gel imaging system (LOGIC 1500, Kodak).

### 4.3.3. Human BM-MSCs

The human BM-MSCs at p3 were generously provided by Andrew Aldridge. The human BM-MSCs were isolated from the bone marrow of a male donor of 8 years. The cells were isolated using plastic adherence method and had been previously showed to fulfil the criteria for an MSC phenotype defined by the ISCT. The cells had fibroblastic morphology and plastic adhered. They were positive to CD 73, CD 90, CD 105, HLA DR and did not express CD14, CD 19, CD 34, CD 45 and HLA ABC (Aldridge., 2011).

### 4.3.3.1. Culture, expansion and characterisation of human BM-MSCs using tri-lineage differentiation

The techniques used for the culture, expansion and cryopreservation of the human BM-MSCs were as described in Chapter 2; Section 2.2.3. The protocol for the tri-lineage differentiation assay was as described in Section 4.3.1.3 using p6 human BM-MSCs. Passage 6 was used as the cell number generated from this passage was enough for MSC characterisations; for both flow cytometry and tri-lineage differentiation. The following cell densities were used: for adipogenesis 4,000 $cells.cm^{-2}$, for osteogenesis 3,000 $cells.cm^{-2}$ and for chondrogenesis $10^7$ $cells.mL^{-1}$ in a 10µL cell pellet (n=3). The cells were stained on Day 3, Day 7, Day 14 and Day 21. The RNA was extracted from the Day 14 and 21, obtained from each differentiated group of cells as described in Section 4.3.1.4, and cDNA synthesis and PCR techniques were carried out

as described in Section 4.3.3.2. Human tenocytes (p7) were taken from the cell stocks from the previous researcher of the group, James Glover (Glover, 2010). The human tenocytes were incubated for 10 days in a DMEM 4.5 g.L$^{-1}$ glucose complete culture medium [Chapter 2; Section 2.2.3.1].

## 4.3.3.2. Investigation of the growth curve of human BM-MSCs incubated in different culture medium conditions

The viability of human BM-MSCs incubated in DMEM culture medium with low (1.0 g.L$^{-1}$) and high (4.5 g.L$^{-1}$) glucose concentrations supplemented with four different concentrations of FBS (1, 2, 5 and 10% (v/v)) (n=3) was investigated. The aim was to determine which condition of the standard culture medium was able to maintain cellular viability as high as the proprietary culture medium, when used to incubate human BM-MSCs. A commercial culture medium; MesenCult® (StemCell technology) added with 10% (v/v) of the provided commercial serum was used as the control. All culture media were supplemented with 100 U.mL$^{-1}$ penicillin, 100 mg.mL$^{-1}$ streptomycin and 2 mM L-glutamine. The growth of the human BM-MSC's was observed on the Day 1, Day 3, Day 5, Day 11 and Day 17 of culture by qualitative observations using light microscopic imaging and quantitatively analysed using the ATPlite™ assay.



**Figure 4.2 Plate set up for assessment of the growth of human BM-MSCs in different culture media (48-well plate).** Shading indicates a well with cells and no shading indicates an empty well.

The human BM-MSCs (p6) were seeded into each well of a 48-well plate at a density of 3,000 cells.cm$^{-2}$. Five plates were prepared for harvesting on the relevant days. Three replicates of BM-MSC in each of the culture media to be assessed were prepared in each plate as showed in Figure 4.2. Initially, the human BM-MSCs cell pellet was diluted in 1 mL of MesenCult® without supplements and the cell density determined as described in Section 2.2.3.4. The cell suspension was adjusted to ten times the required density in MesenCult®. Total volume of cell suspension prepared was 5 mL, and approximately 50 µL was added to each well of each plate [Figure 4.2]. The culture medium to be tested was then added to make up the volume to 500 µL. The plates were incubated at 37 $^{0}$C in an atmosphere of 5% (v/v) $CO_2$ in air. The culture medium was replaced every three days. At each time point, the confluence of the human BM-MSCs was monitored and imaged, and one plate was used to determine the viability of the cells using ATPlite™ assay as described in Chapter 2; Section 2.2.6.2.

**Data presentation**

The confluence of the cells at each time point was recorded as a percentage and the data was arcsin transformed, means and 95 % confidence limits calculated and analysed using two-way ANOVA with Tukey's multiple comparison tests (p< 0.05). Data was back transformed for presentation purposes. The ATP counts were analysed using two-way ANOVA with Tukey's multiple comparison tests (p< 0.05).

**4.3.3.3. Viability assay of human BM-MSCs at different cellular densities**

In order to determine the relationship between ATP levels and numbers of human BM-MSC at different densities, the ATPlite™ assay was conducted on the following cell numbers: 0.25, 0.5, 1.0, 2.0 and 4.0 x 10$^5$ cells (n=4). Cell suspensions of human BM-MSCs at p6 were prepared at the cell densities (per mL) stated above. The cells were centrifuged at 300 g for 10 min. The supernatants were removed and 500 µL of lysis buffer (ATPlite™) was added to the cell pellets. The suspensions were shaken at 700 rpm for 5 min. Substrate buffer (500 µL) was added and the cell suspensions were shaken at 700 rpm 5 min in the dark. Each sample (100 µL) was transferred into a white 96-well Optiplate (Perkin Elmer), then the luminescence counts were recorded (counts per second) using a Top Count plate-reader (Perkin Elmer).

## 4.4. Results

### 4.4.1. Porcine BM-MSCs expansions and characterisation

#### 4.4.1.1. Culture and expansion of porcine BM-MSCs

Porcine bone marrow was obtained from a femoral bone and the mononuclear cell fraction was isolated and cultured from the bone marrow using Percoll gradient centrifugation. The initial mononuclear cell culture (primary culture), designed p0 was predominantly non-adherent cells, including red blood cells, mononuclear cells and marrow debris. The cell suspension was cloudy, red, very dense and heterogeneous. Following the first medium change, the culture became clear and the cells less rounded and heterogeneous [Figure 4.3 A].
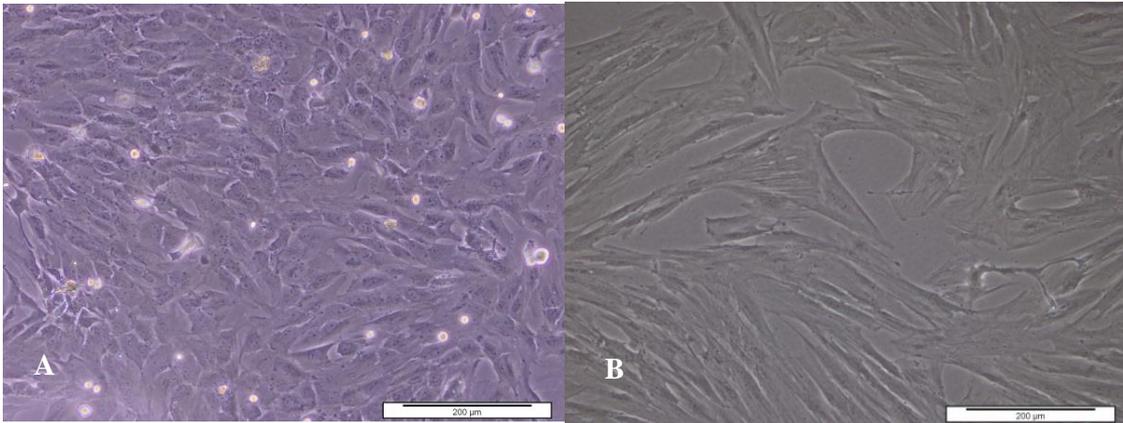


**Figure 4.3 The porcine MSC, plastic adherent cells** at 100x magnification. (A) p0 at 90% confluent, (B) the porcine MSC colony with radial growth pattern, (C) fibroblastic shape of porcine BM-MSCs (p3) at 80% confluence. Scale bars represent 200 µm.

After the subsequent medium change, sparse spindle-shaped bipolar fibroblastic-like cells and dendritic-like cells were seen individually adhered to culture flasks at p0. These were detected on the third day and became dense and reached 90 % confluences in the T25 flask 10-days post-isolation [Figure 4.3 A]. The cells formed into discreet colonies and formed a radial pattern after 14-days culture. This growth pattern was less obvious after serial passages. The fibroblastic-like cells became more homogeneous after passage 2 [Figure 4.3 B]. This trend indicated that the MSC dominated the cultures and expanded into colony forming units-fibroblasts (CFU-F) form.

The porcine BM-MSCs were expanded in culture until sufficient cells were obtained for characterisation. Cell morphology did not alter over subsequent passage.

**4.4.1.2. Porcine BM-MSCs characterisation using flow cytometry**

Porcine BM-MSCs at p5 were analysed for the expression of CD 29, CD 44, CD 45, CD 90 and MHC II using flow cytometry. Isotype controls appropriate for each antibody were used as controls to confirm the specificity of the test antibodies.
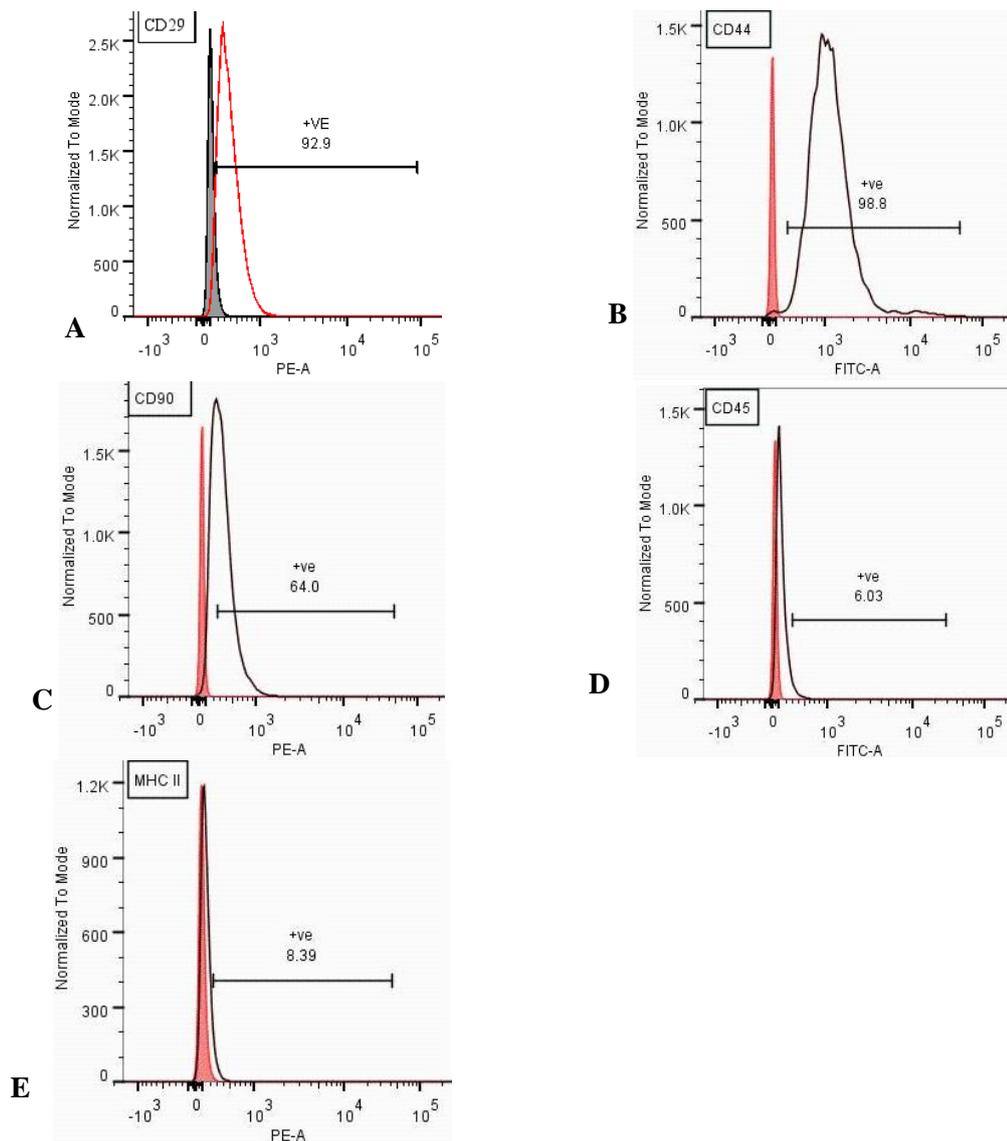


**Figure 4.4 Phenotype of p5 porcine BM-MSCs analysed using BD LSR Fortessa.** The red peaks indicate staining with the isotype control and the black peaks indicate labelled with the antibody. (A) CD 29, (B) CD 44, (C) CD 90, (D) CD 45 and (E) MHC II.

The data generated from the FACs analysis were converted into histograms using FlowJo software and the results are shown in Figure 4.4. The porcine BM-MSCs were found to express CD 29$^+$ (92.9 %), CD 44$^+$ (98.8 %), CD 90$^+$ (64.0 %) and CD 45$^-$ (6.03 %) and MHC Class II$^-$ (8.39 %).

**4.4.1.3. Porcine BM-MSC characterisation by tri- lineage differentiation**

Porcine MSC at p7 were cultured in adipogenic, osteogenic and chondrogenic media for 21 days and stained using lineage specific staining methods to determine their differentiation capacity. The results are shown in Figure 4.5, 4.6 and 4.7. Adipogenesis was identified after seven days culture in the adipogenic medium [Figure 4.5 D]. The number of the fat drops in the adipogenic culture increased over time [Figure 4.5 D,F,H]. The control cells in standard culture medium are shown on the left and the cells in differentiated medium on the right.
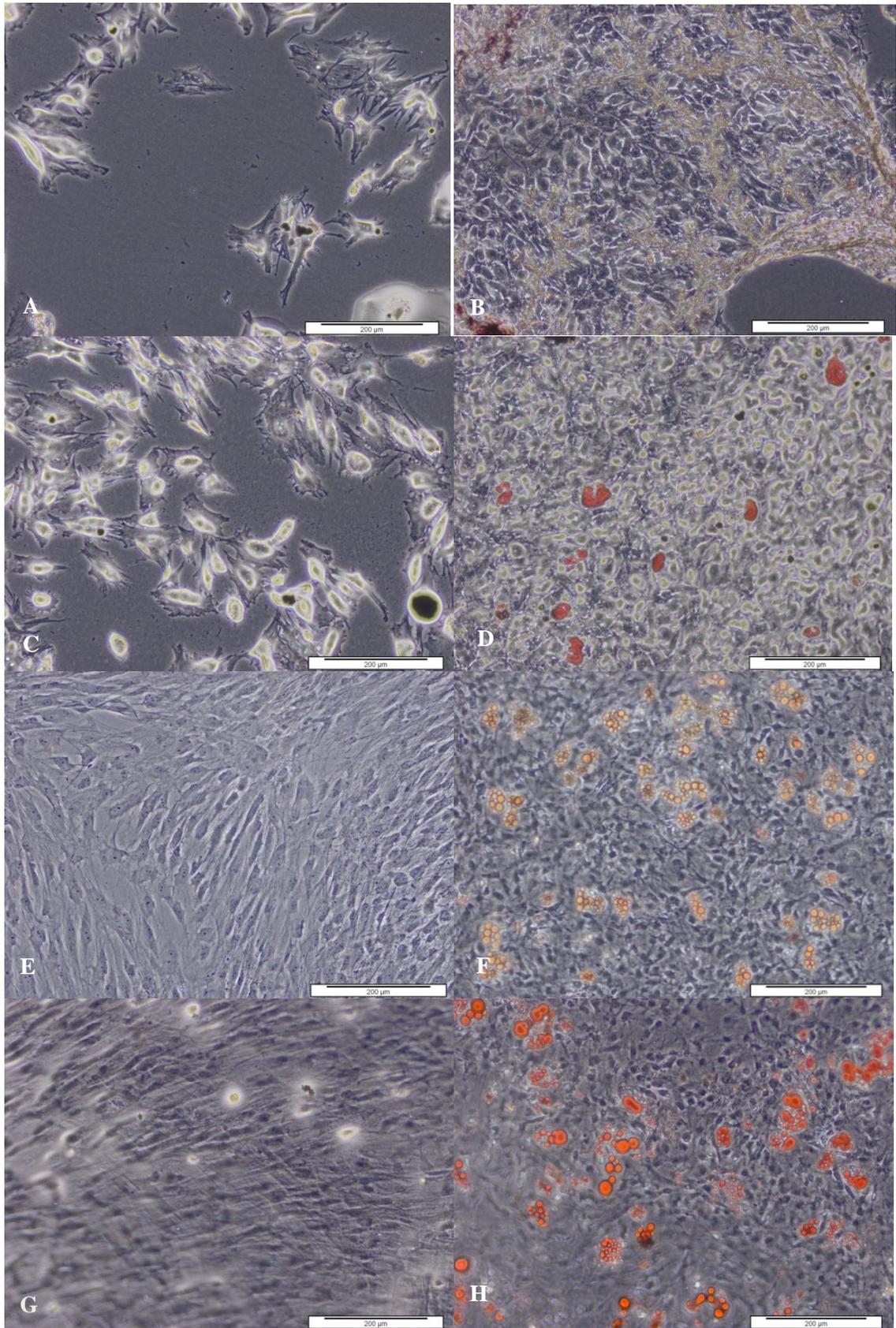
**Figure 4.5 Adipogeneic differentiation of porcine BM-MSC.** (A,B) Day 3, (C,D) Day 7, (E,F) Day 14 and (G,H) Day 21. The control cells in standard culture medium are shown on the left and the cells in differentiation medium on the right. The cell monolayers were stained with Oil red. Images captured at 100x magnification. Scale bars represent 200 µm.

The porcine MSC p7 took longer to differentiate into osteocytes, that was first identified after 14 days of culture in the osteogenic medium [Figure 4.6 H,I].
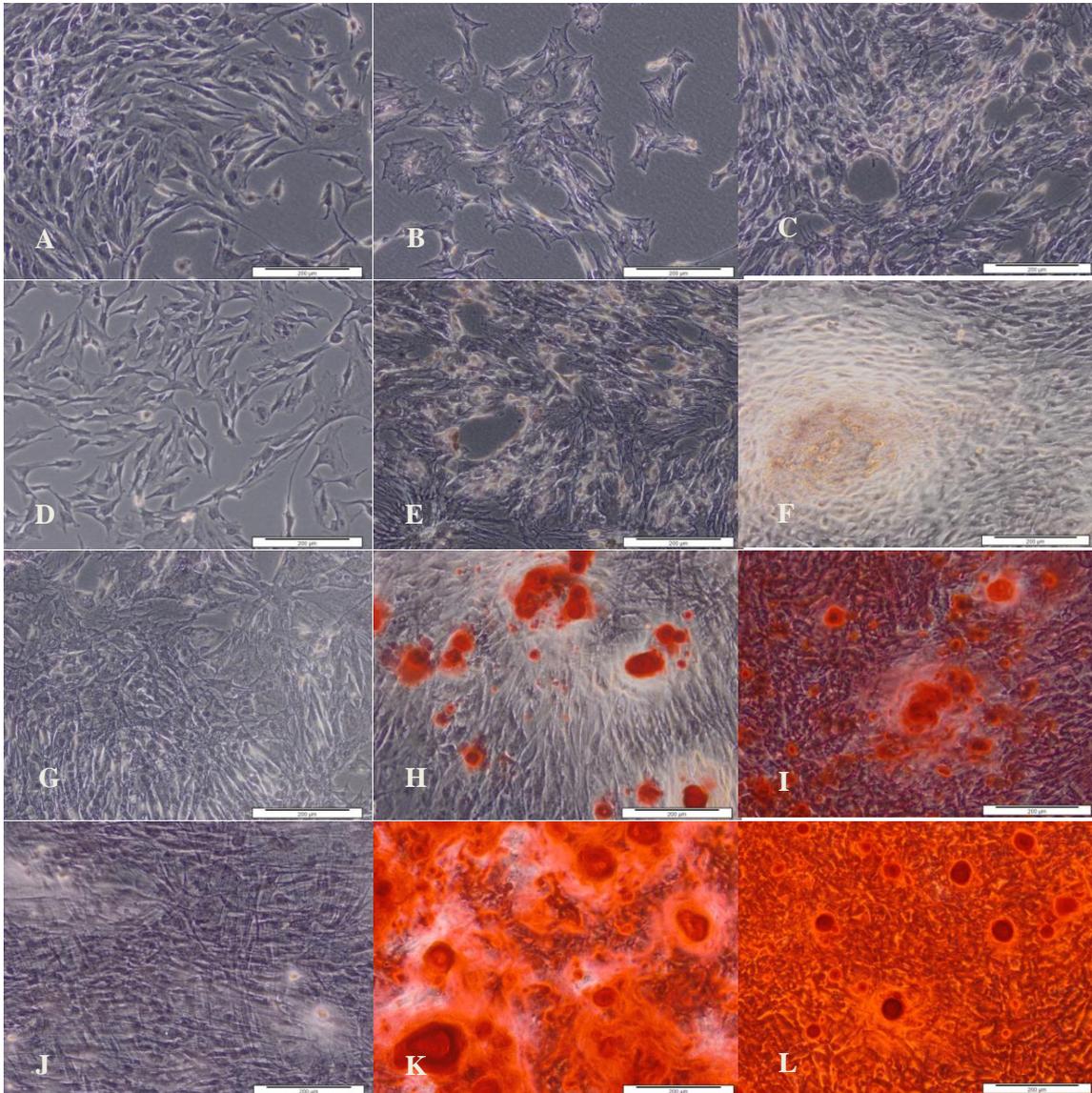


**Figure 4.6 Osteogeneic differentiation of porcine BM-MSC.** (A,B,C) Day 3. (D,E,F) Day 7. (F) The cells started to form an aggregates. (G,H,I) Day 14, increasing number of nodules and aggregates. Calcium deposition was found (I). (J,K,L) Day 21, both cell density groups had calcium deposition. Cells in standard culture medium (controls) are showen on the left (A,D,G,I). The images in the centre are cells seeded at 3000 cells.cm$^{-2}$ in osteogeneic differentiation medium (B,E,H,K). Images on the right are cells seeded at 6000 cells.cm$^{-2}$ (C,F,I,L). The orange colour indicates positive staining with Alizarin red indicative of calcium deposition. Images captured at 100 x magnification. Scale bars represent 200 μm.

Osteogenesis of the porcine BM-MSC was influenced by cell seeding density. On Day 7, the cells seeded at 6000 cells.cm$^{-2}$ started to develop aggregates [Figure 4.6 F], whilst this was not found in the cells seeded at 3000 cells.cm$^{-2}$. In the osteogenic cultures, the presence of

aggregates and nodules increased over time, and the osteogenesis activities were more intensive in the higher cell density cultures (6000 cells.cm$^{-2}$) [Figure 4.6 F,I,L] compared to the lower cell density cultures (3000 cells.cm$^{-2}$) [Figure 4.6.B,E,H,K].

In the chondrogenic differentiation assay, only the Day 21 cell pellet of porcine BM-MSC is presented [Figure 4.7], as the cells pellets of the Day 3, Day 7 and Day 14 were lost during the staining procedure with alcian blue. Importantly, GAGs were identified after the Alcian blue staining [Figure 4.7 B] of the cultures at 21 days, however not in the control cultures [Figure 4.7]. This indicated that the BM-MSC had differentiated along a chondrogenic lineage.
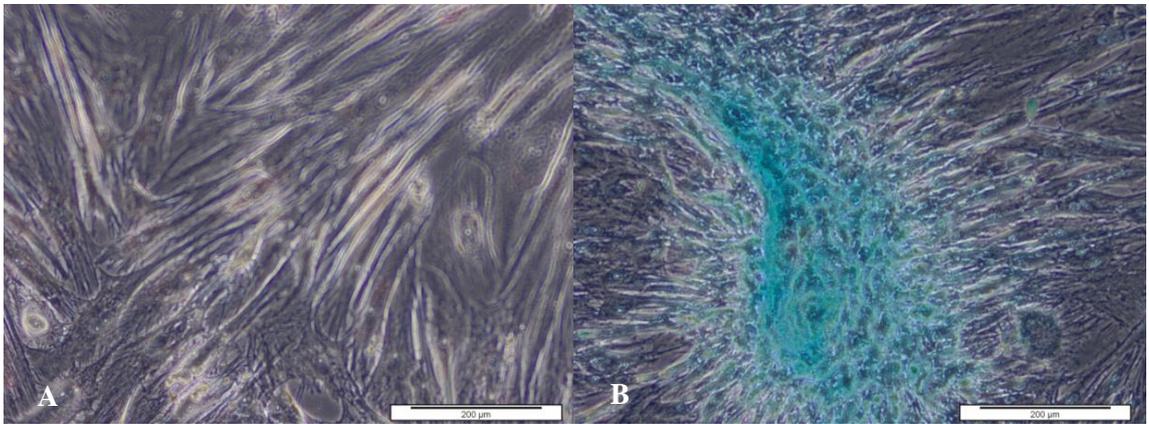


**Figure 4.7 Chondrogenic differentiation of porcine BM-MSC at 21 days of culture** (A) BM-MSCs in standard culture medium (control) and (B) BM-MSC in chondrogenic differentiation medium. The blue colour indicates presence of GAGs, stained by Alcian blue. Images captured at 100 x magnification. Scale bars represent 200 µm.

#### 4.4.1.4. Extractions of mRNA from different densities of porcine BM-MSCs

In order to determine the number of BM-MSCs required to extract sufficient RNA for subsequent studies of gene expression analysis, the RNA was extracted from different numbers of porcine BM-MSCs at p4 (500, 1000, 10000 and 20000 cells.mL$^{-1}$ (n=4)).

The RNA concentration was measured using nanospectrophotometry. The results were presented for each cell number in Figure 4.8. The purity of each sample of extracted RNA was also investigated by measuring the ratio of absorbance at 260/280 nm [Figure 4.8].
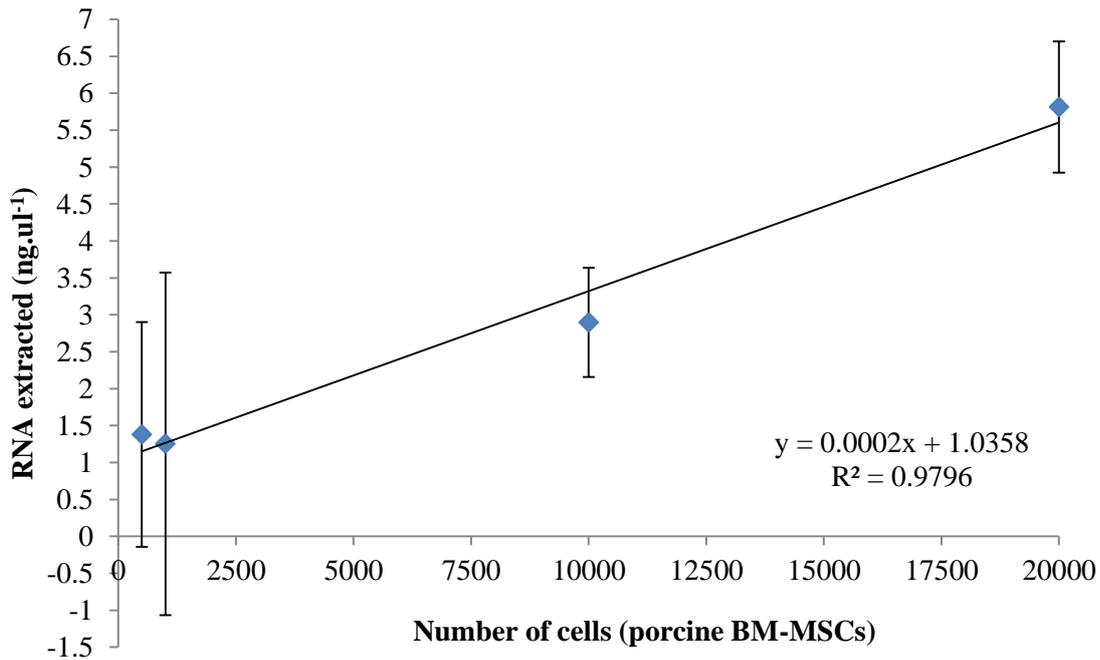
**Figure 4.8 Quantities of RNA extracted from different numbers of porcine BM-MSCs.**

The levels of RNA extracted from different numbers of cells were roughly proportionate to the cell number. However, the data indicated that extraction of RNA from cell numbers below 1000 was highly variable and therefore not reliable. The levels of RNA extracted from 1000 and 500 cells were not proportional to the 20000 and 10000 cells.
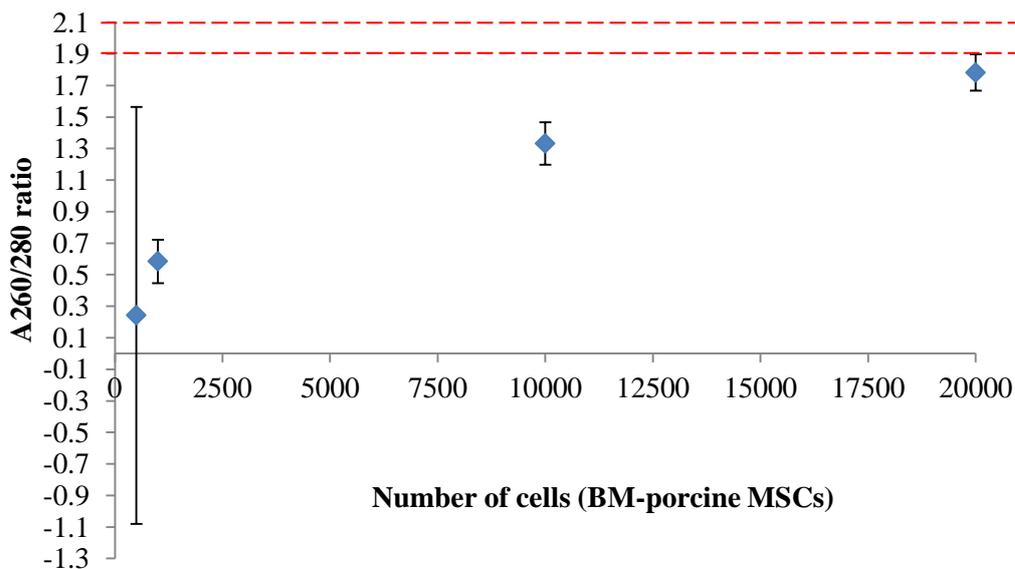


**Figure 4.9 The A260/280 ratios from the RNA measurement.** Data is presented as the mean (n=4) ± 95 % Cl. Dash red lines indicate the normal range of purity value of RNA (1.9 – 20) (Gallagher and Desjardins, 2001).

None of the A260/280 ratios recorded for the extracted RNA gave a reading of 2.0 indicating that the RNA was not pure. In order to determine whether the extraction method was working adequately, the RNA content per cell was calculated, the 20000 and 10000 cells had $17.44 \pm 2.68$ pg.cell$^{-1}$ and $17.38 \pm 4.45$ pg.cell$^{-1}$ (mean (n=4) $\pm$ 95 % Cl), respectively which was within the range expected from the literature [Figure 4.10].
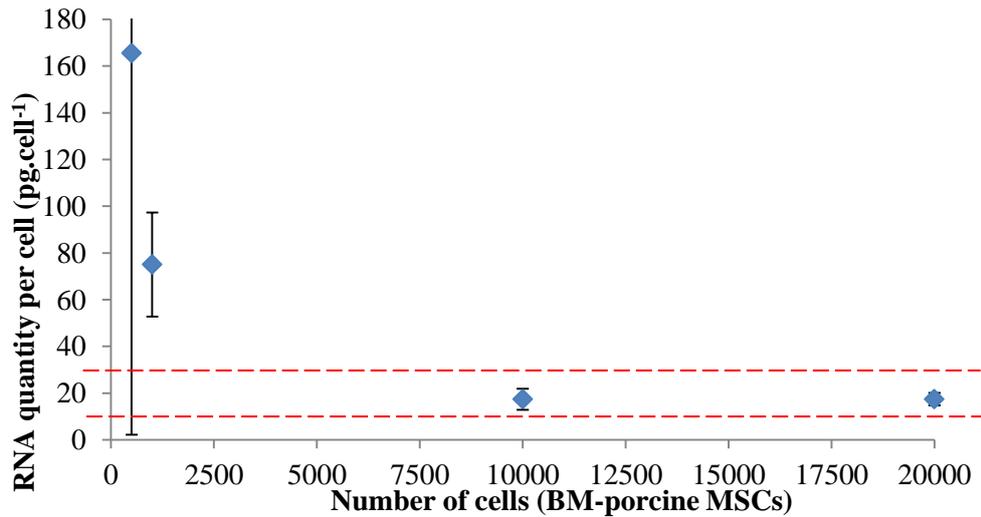


**Figure 4.10 Estimation of RNA quantities per cell.** Data is presented as mean (pg per cell) (n=4) $\pm$ 95 % Cl. Dash red lines indicate the normal range of the quantity of RNA (pg) per each mammalian cell (10 – 30 pg per cell).

## 4.4.2. Culture of human BM-MSCs

### 4.4.2.1. Human BM-MSCs culture and expansion

The human BM-MSCs used in this study were found to be plastic adherent, had a spindle-fibroblastic shape and were capable of differentiation along adipogenic, chondrogenic and osteogenic lineages.
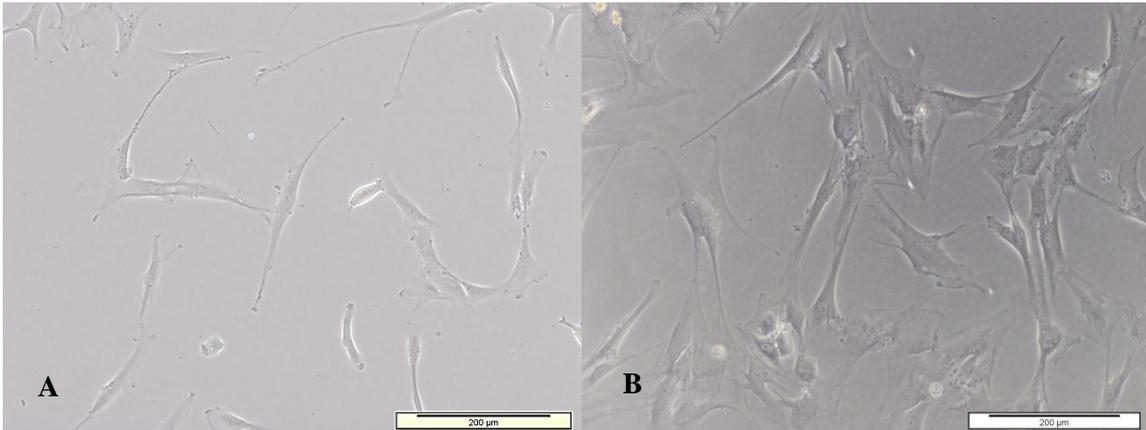


**Figure 4.11 Images of human BM-MSC in culture,** (A) at p5 with 2 % confluence. Cells had a spindle like morphology, and (B) cells at p7 with 10% confluence. Cells were more varied in morphology, flatter and wider. Images captured at 100x magnification. Scale bars represent 200 μm.

### 4.4.2.2. Trilineage differentiation assay

When human BM-MSCs were initially incubated in differentiation media, the cells exhibited no difference in cellular morphology compared to human BM-MSCs incubated in the standard culture medium. Over time, human BM-MSCs in adipogenic medium began to differentiate and the cells accumulated fat in the cytoplasm after 3-days induction. This became more obvious after 7 days and beyond. Cells in the osteogenic medium began to form calcium nodules and aggregates identified by Alizarin red staining after 14 days of culture; however, they were small, solid and solitary, and found sparsely in the cells. Only a few nodules remained in the cultures after 21-days incubation. Human BM-MSCs became rounded in the chondrogenic culture medium after 7-days incubation and GAG accumulations were visible after 14 days, stained by Alcian blue [Figure 4.12].
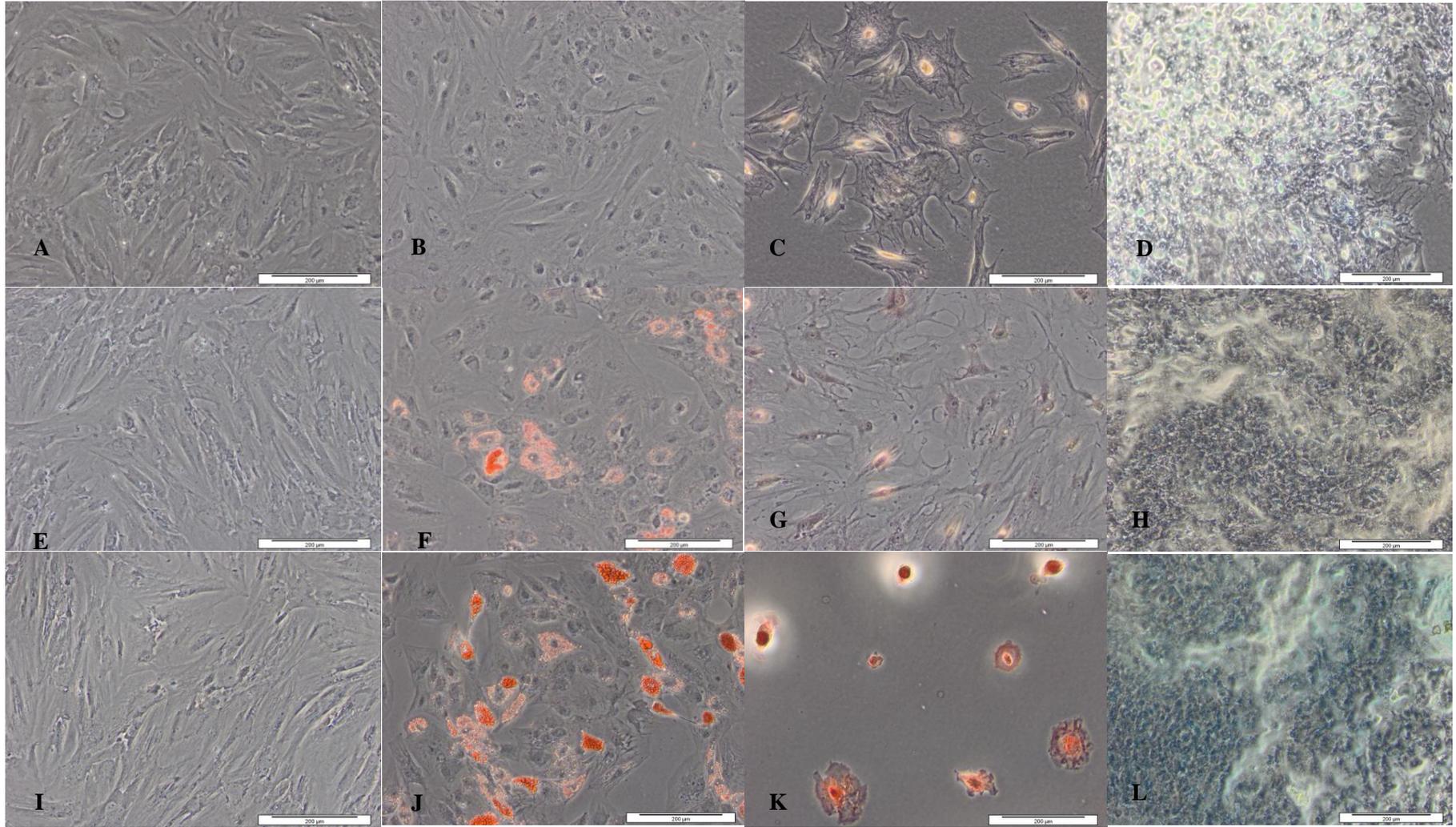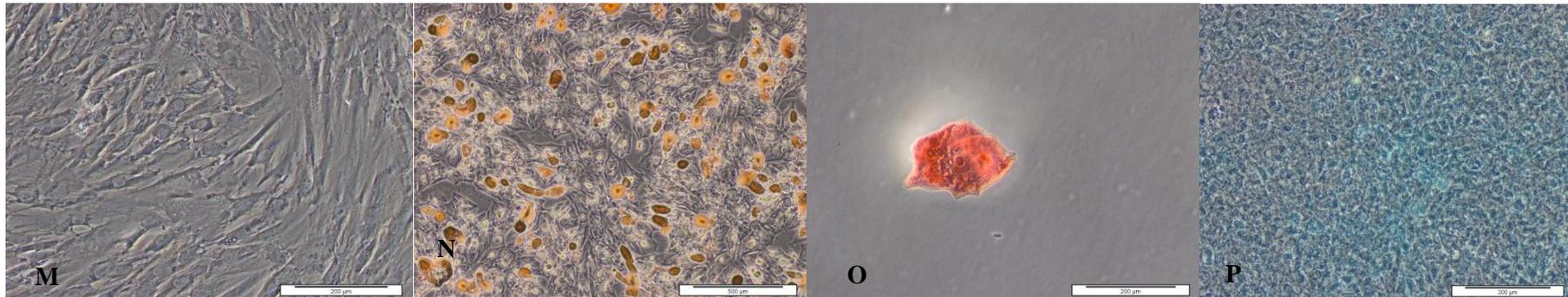
**Figure 4.12 Trilineage differentiation of human BM-MSCs passage 6.** Images from the first row down show Day 3, Day 7, Day 14 and Day 21 cultures, respectively, of the cells in standard culture medium (A, E, I, M), adipogenic medium (B, F, J, N), osteogenic medium (C, G, K, O) and chondrogenic medium (D, H, L, P). Cells were stained with Oil red (adipogenesis), Alizarin red (osteogenesis), or Alcian blue (GAGs indicative of chondrogenesis). All images were taken at 100 x magnification. Scale bars represent 200 µm.

**4.4.2.3. Growth of human BM-MSC in different culture medium conditions**

The growth and viability of human BM-MSCs (p6) in DMEM culture medium with high glucose (4.5 g.L$^{-1}$) and low glucose (1.0 g.L$^{-1}$) supplemented with 1, 2, 5, or 10 % (v/v) FBS and 100 U.mL$^{-1}$ penicillin-streptomycin, 2 mM L-glutamine was observed and compared to the commercial medium (MesenCult®) complete medium. Data of cell confluence is presented in Figure 4.13 and the ATP level indicating cell viability is presented in Figure 4.14.
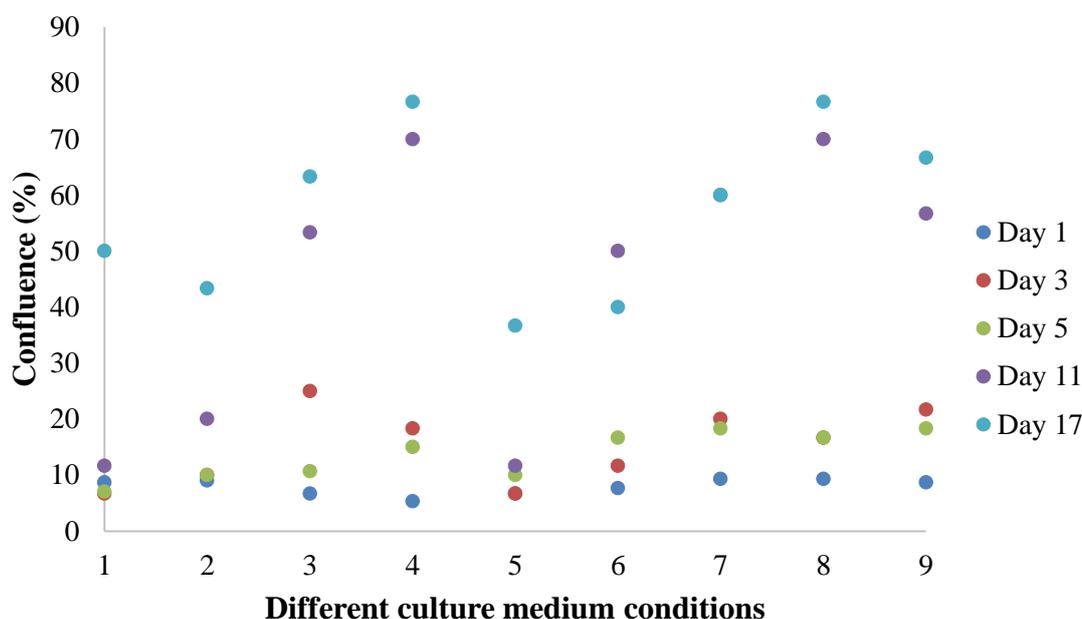


**Figure 4.13 Percentage confluences of human BM-MSCs (p6) in different culture medium conditions over time.** The confluence of the cells was observed using inverted microscopy at 100x magnification. Legend (1) Low glucose 1 % (v/v) FBS, (2) Low glucose 2 % (v/v) FBS, (3) Low glucose 5 % (v/v) FBS, (4) Low glucose 10 % (v/v) FBS, (5) High glucose 1 % (v/v) FBS, (6) High glucose 2 % (v/v) FBS, (7) High glucose 5 % (v/v) FBS, (8) High glucose 10 % (v/v) FBS, (9) MesenCult® (control). Data was analysed by two-way ANOVA followed by the Turkey test, and is expressed as the mean (n=3) ± 95 % Cl. The data were compared at each time point.

No significant differences were found among all groups after 24 h incubation. After 3 days, cells in the Low and the High glucose medium with 5 % and 10 % (v/v) FBS, and the MesenCult® medium had higher percentage confluence than the cells in 1 and 2 % (v/v) FBS (Low and High glucose) (p<0.05).
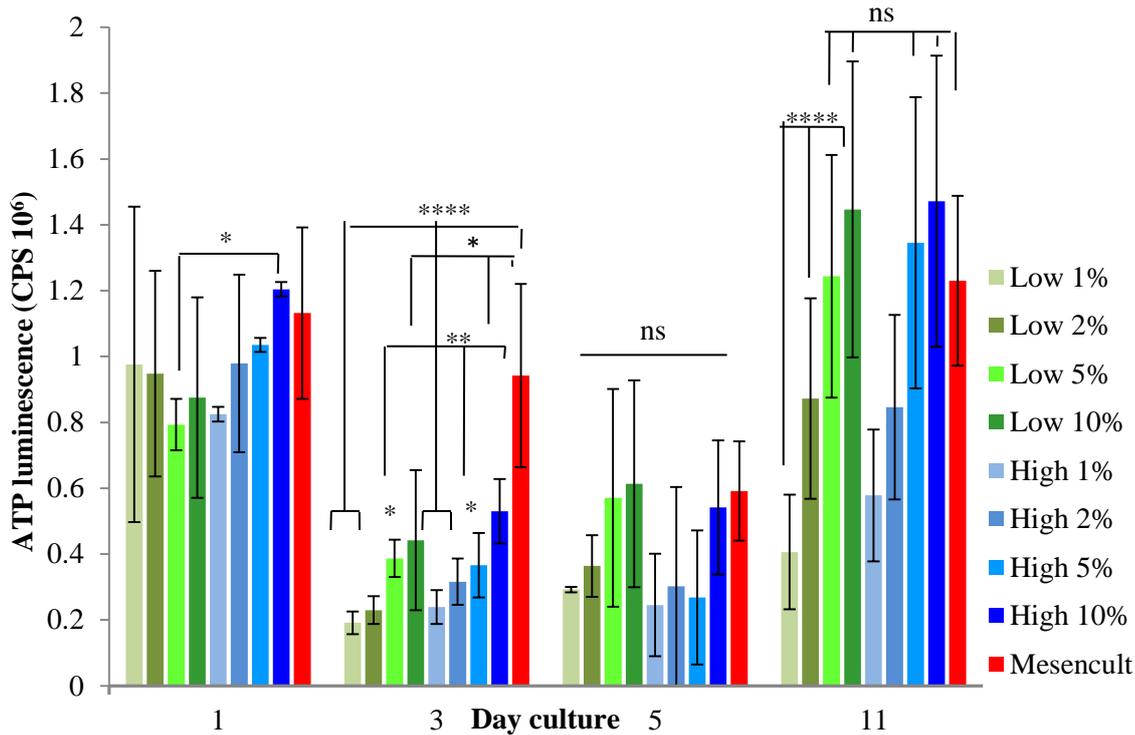
**Figure 4.14 ATP counts per second of human BM-MSCs p6 incubated in different medium conditions using ATPlite™ assay.** Low glucose media (1.0 g.L$^{-1}$) supplemented with 1, 2, 5, 10 % (v/v) FBS were compared to high glucose media (4.5 g.L$^{-1}$) supplemented with 1, 2, 5, 10 % (v/v) FBS and the commercial culture medium (MesenCult®, StemCell) added with 10 % (v/v) commercial serum provided was used as the control. Data was analysed using two-way ANOVA followed by calculation of the MSD (p<0.05) by the Tukey test. T method was also used to statistically determine the individual differences of ATP luminescence between different culture medium conditions. Data were compared at each time point. Data is presented as the mean of ATP counts (n=3) ± 95 % Cl.

During the first day culture, the ATP counts of the human BM-MSCs in all groups showed no significant differences to the control, with the exception of the Low glucose 5 % (v/v) FBS compared to the High glucose 10 % (v/v) FBS (p<0.05). By the Day 3, cells incubated in the MesenCult® medium had significantly higher ATP levels compared to all other groups (p<0.05), while there were no significant differences between the other culture media. The ATP counts in all of the culture media dropped at Day 5 and there were no significant differences between the counts obtained in any of the culture media. The ATP counts in all the culture media increased by Day 11, the Low and the High glucose media with 1 and 2 % (v/v) FBS had ATP counts significantly lower compared to the Low and the High glucose media with 5 and 10

% (v/v) FBS, also was significantly lower then the MesenCult® culture medium ($p < 0.05$). The Day 17 luminescence results, however, could not be presented due to technical faults.

### 4.4.2.4. ATP levels of human BM-MSCs at different densities

The relationship between the numbers of human BM-MSCs and their ATP levels was investigated using ATPlite assay™. Data is presented in Figure 4.15.
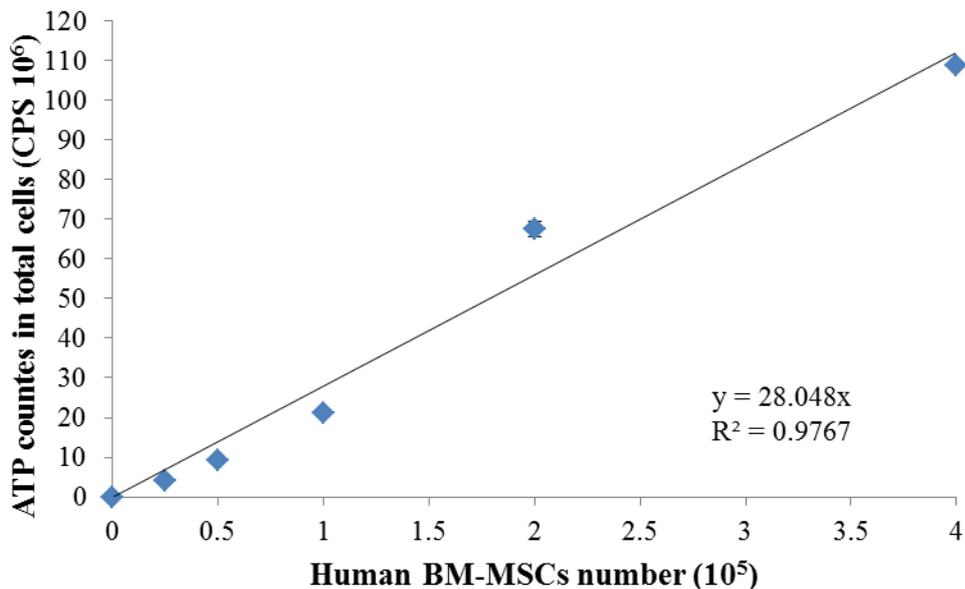


**Figure 4.15 ATP levels (CPS) of human BM-MSCs at different densities.** Error bars denote the mean (n=4) ± 95% Cl.

A linear regression was found between the ATP counts and the number (cell density) of human BM-MSCs ($R^2 = 0.977$).

### 4.4.2.5. RNA extraction of the differentiated human BM-MSCs and from human tenocytes

The differentiated adipocytes, chondroblasts and osteoblasts obtained from the differentiated assays of human BM-MSCs p6 [Section 4.3.1.3] were subjected to RNA extraction using the RNeasy mini kit (Qiagen). The results are shown in the Table 4.7. The RNA from human tenocytes was also extracted to test the primer pairs for tenogenesis gene expressions (Scleraxis,

Tenascin-C, and Collagen III). The RNA was converted into their complementary DNA (cDNA) following the protocol described in Section 4.3.3.2 and gene expression specific to the lineages were identified using PCR. DNA products were visualised using gel electrophoresis as described in Section 4.3.3.2.4.

| Cell type | The means of RNA concentration (ng.uL$^{-1}$) ± 95 % Cl | |
|-----------|--------------------------------|--------------------------------|
|           | **Day 14** | **Day 21** |
| Osteoblasts | $7.63 \pm 1.75$ | $3.71 \pm 0.81$ |
| Chondroblasts | $4.52 \pm 4.63$ | $12.05 \pm 4.36$ |
| Adipocytes | $71.97 \pm 70.76$ | $84.62 \pm 157.50$ |

**Table 4.7 RNA levels extracted from the differentiated human BM-MSCs and quantified using Nanodrop-spectrophotometer.** Data are presented as mean (n=3) ± 95% Cl.

The quantity of RNA isolated in all lineages increased over the culture period, except for the osteogenesis cultures. The RNA isolated from human tenocytes (p7) was 842.89 (n=2) ± 2.88 ng.$\mu$L$^{-1}$.

### 4.4.2.6. Primer design and validation using RT-PCR

Primer pair sequences to identify the genes of interest and the reference genes were designed manually using NCBI and PRIMER Blast tools. The transcript genes were amplified using the protocol as described in Section 4.3.3.2, using the primer pairs presented in Table 4.3. The templates used were the Day 21 samples of the differentiated human BM-MSCs and from the human tenocytes. The PCR products were visualised using 3.5% (w/v) agarose gel, stained with SYBR®Safe DNA gel stain (Invitrogen™), separated by electrophoresis (110 V, 45 min), and imaged using UV light. The results are shown in Figure 4.16.
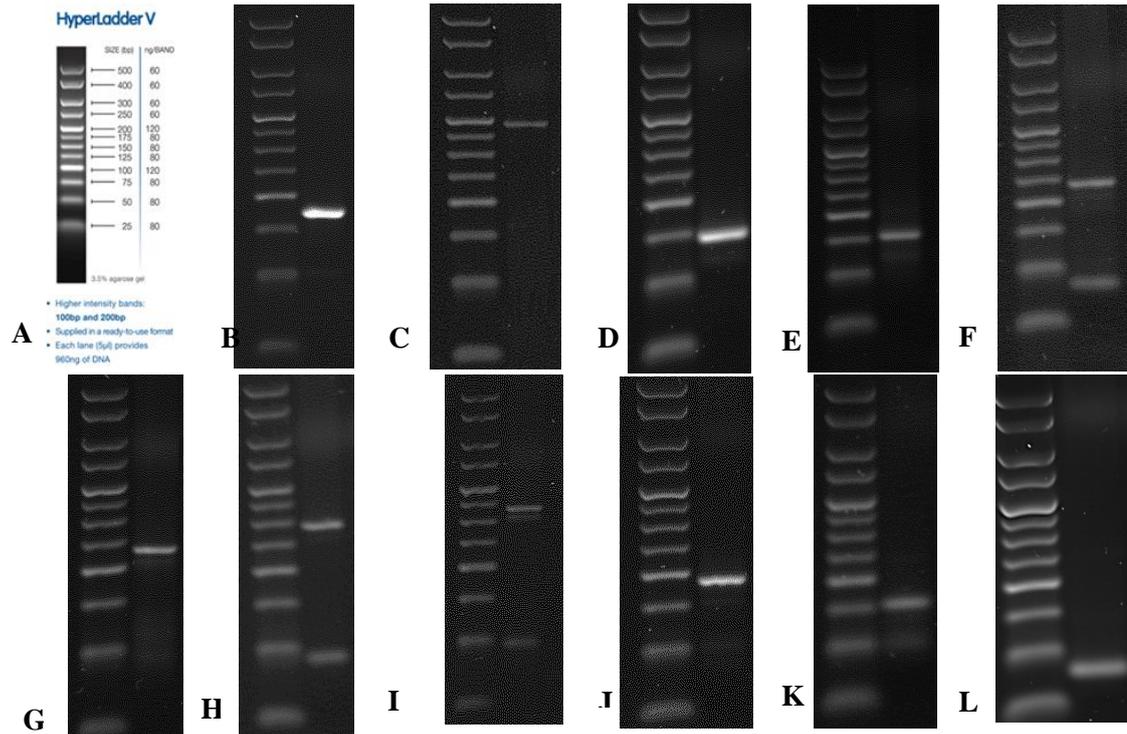
**Figure 4.16 Separation of the lineage specific gene transcripts of the differentiated human BM-MSCs and the tenocytes using gel electrophoresis at 110 V for 45 min**. (A) Hyperladder 25 bp, (B) β-actin; 85 bp (C) GADPH; 189 bp (D) Collagen I; 71 bp (E) Collagen II; 76 bp (F) Collagen III; 116 bp (G) Osteopontin; 116 bp (H) PPARγ; 140 bp (I) Runx2; 174 bp (J) Scleraxis; 91 bp (K) Sox9; 69 bp (L) Tenascin-C; 102 bp.

Using the gel electrophoresis, the PCR products for βactin, GADPH, collagen I, collagen II, osteopontin and scleraxis revealed as a single band with the DNA length matched to the expected size. These corresponded to the single amplified products as predicted by the PCR melting curve analysis [Figure 4.17 A]. The gel electrophoresis of PCR products for collagen III, PPARγ and Sox 9 all had two bands; one band at the expected product length and another at 45 bp, suspected to be primer dimers. The primer concentration was reduced from 1.0 mM to 0.5 mM and two bands were still found. The dissociation curves of the real time PCR amplification of these genes showed two peaks; one peak that had a higher melting temperature (collagen III, PPARγ and Sox 9 melted at 85, 81 and 87 $^{0}$C respectively) and another smaller peak, which melted at 72 $^{0}$C for all of the PCR products [Figure 4.17 B, C, D].
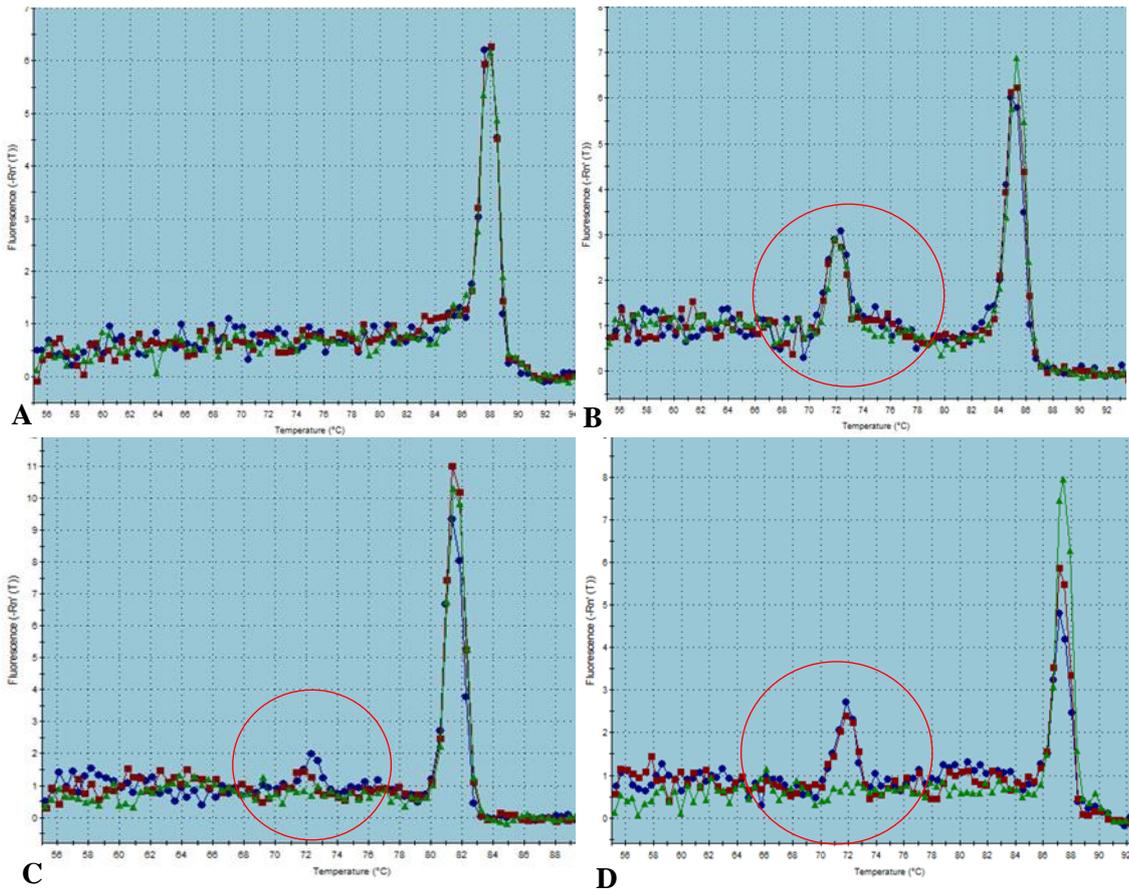
**Figure 4.17 Dissociation curves of (A) βactin, (B) Collagen III, (C) PPARγ and (D) Sox 9 during real time PCR.** The primer concentration was 0.5 mm

Gel electrophoresis of the Runx 2 gene showed 3 bands; one band was at the expected length (174 bp), one very dim band was found at around 160 bp and another one at 45 bp. The dissociation curve of the Runx 2 PCR products showed three peaks, one small peak which melted at 72 $^{0}$C and two peaks overlapping one another, which melted at 80 $^{0}$C and 82 $^{0}$C [Figure 4.18]. This had indicated that the amplified DNA's were not specifically to the expected DNA.
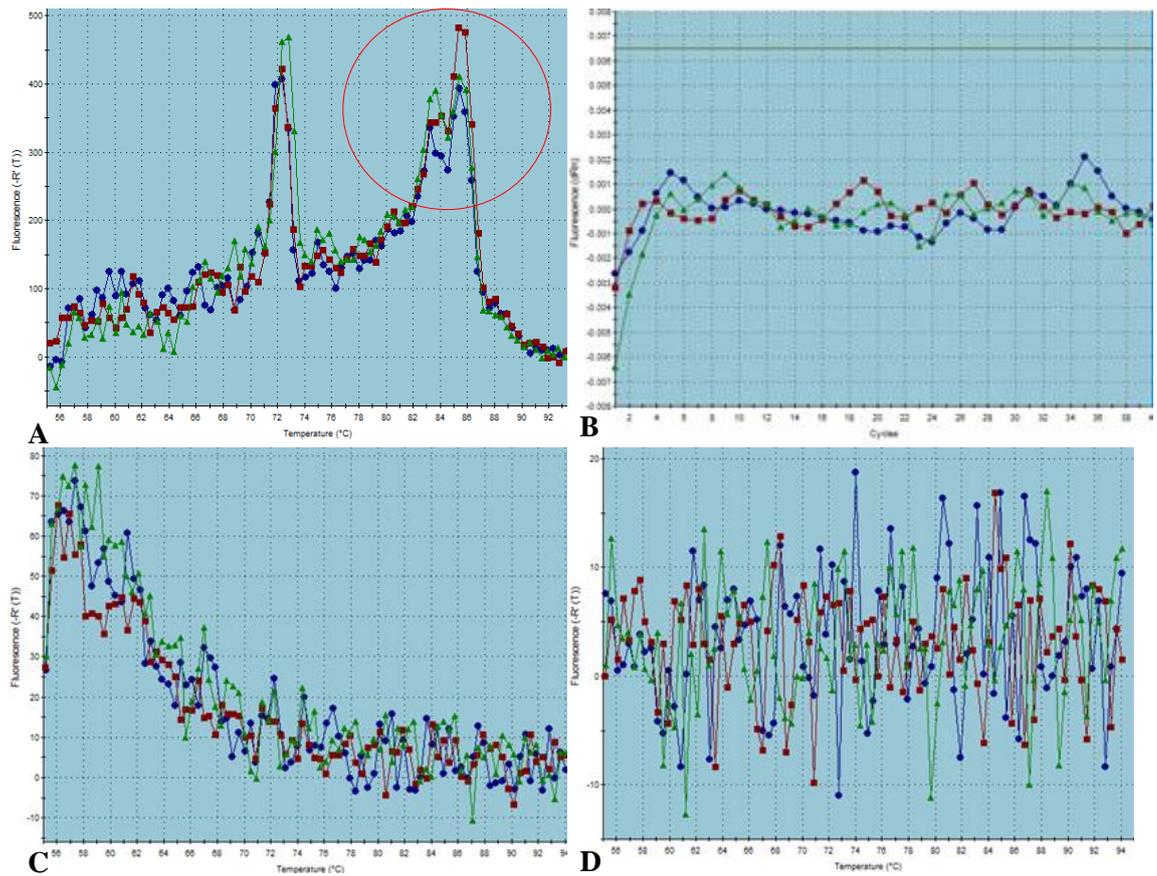
**Figure 4.18 Dissociation curve of the Runx 2 PCR products** (A) The sample; Runx 2 and osteoblasts Day 21, (B) the template only control, (C) the primer only control and (D) the water control.

The tenascin-C primer pairs had no DNA band detected on gel electrophoresis [Figure 4.16 L]. However, there was an amplification threshold detected at the 21st -23rd cycle [Figure 4.19 A]. The dissociation curve for this primer pair in the real time PCR amplification had showed with two peaks; one peak melted at 83 $^0$C and another peak at 72 $^0$C (circled in red in the Figure 4.19 B). No amplifications were found in the template only control [Figure 4.19 C], the primer only control [Figure 4.19 D] and the water control [Figure 4.19 E].

Three different primer pairs for the tenascin-C were designed and tested using the primary cell of human tenocytes, however the results were similar. The tenascin-C primer pair with results presented here was then chosen.
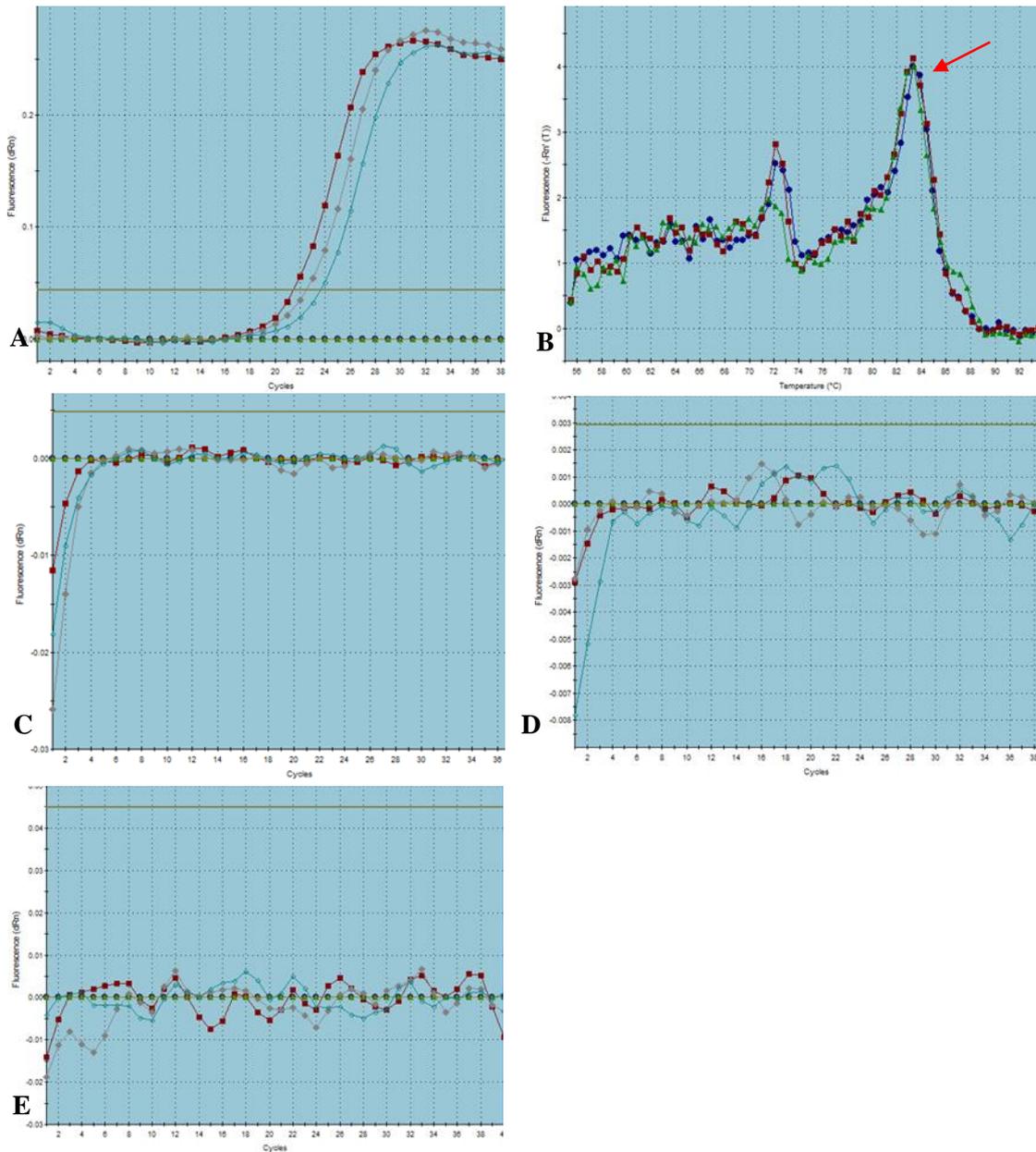
**Figure 4.19 Tenascin-C amplification using human tenocytes.** The (A)    amplification curve   of the sample and its (B) dissociation curve. The controls; (C) primer only, (D) template only and (E) water control. Red arrow indicates the melting peak of the suspected DNA product for tenascin-C.

## 4.5. Discussion

In this chapter, MSCs for studying the regeneration of the decellularised PPT scaffolds were validated and prepared. Porcine BM-MSCs were initially used to learn the techniques for cell handling and to develop different methods. Later on, the developed methods were deployed to human BM-MSC to investigate the effects of cyclic strains in the decellularised PPT scaffolds.

**Porcine MSC**

The porcine BM-MSCs used in this study were successfully isolated using Percoll gradient centrifugation. FACS analysis of the porcine MSC at p5 showed that the cells strongly expressed CD 44 (cell adhesion marker) and CD 29 (integrin β1 marker), were positive for CD 90 (a marker of stemness), and essentially failed to express MHC II; the protein expressed by antigen presenting cells to introduce antigen and to educate CD $4^+$ cells (8.39%), and CD 45 (hematopoietic marker; 6.03%). During expansion of the cells in culture, the cells were fibroblastic in shape and plastic adherent. The cells were also shown to be capable of differentiation into adipocytes, chondroblasts and osteoblasts. Adipogenesis was identified after seven days culture in adipogenic medium. Osteogenesis differentiation was carried out at two cell densities (6,000 $cells.cm^{-2}$ and 3,000 $cells.cm^{-2}$), and the cells were shown to develop aggregates and nodules at Day 7 at the higher cell density, faster than the lower density, which was identified after 14 days. The mineralisation of the bone matrix was also more apparent at the higher cell density compared to the lower cell density, shown by the Alizarin red staining of calcium accumulation in the osteogenesis cell layer. Thus, cell density affected the osteogenic capability of the porcine MSCs. Chondrogenesis was developed using 10 μL cell pellets ($10^7$ $cells.mL^{-1}$). Differentiation was shown by the 21-day time point, marked by the GAGs accumulation stained by Alcian blue dye. The chondrogenesis after 14-days incubation had been washed away as serum was present in the cell pellet and reduced the cell pellet attachment to the plastic surface, therefore it was unable to be presented.

This study aimed to investigate the responses of the human BM-MSCs in the decellularised PPT scaffolds incubated with and without cyclic strain for 7 days, and one of the analyses of those responses was to identify the level of transcript genes expressed by the human BM-MSCs. The transcript gene, which was the RNA, were quantified and the levels expressed in different populations were compared using RT-PCR. Porcine BM-MSCs were used in the initial studies to develop the technique to extract RNA and to investigate number of cells required to generate a sufficient RNA.

A series of porcine BM-MSCs in different cell numbers were extracted for their RNA using RNeasy mini kit to investigate the number of cells to obtain a sufficient level of RNA. The RNA concentration measured using the NanoDrop spectrophotometer ND-1000 showed that when RNA was extracted from cells at a density of 20,000 and 10,000, the RNA levels were proportional to the cell number, while the levels of RNA extracted from 1000 and 500 cells were highly variable. High deviations among repeated readings might have been due to sample inhomogeneity (Qiagen, 2012b), as the RNA samples were not rigorously mixed due to the sensitivity of RNA (Bustin et al., 2010). However, there were no problems with the extraction and quantification of RNA from 20000 and 10000 cells despite all samples being treated in the same way. Perhaps the RNA concentration isolated from 1000 and 500 cells was extremely low (less than 2 ng.$\mu L^{-1}$), beyond the lowest sensitivity limit of the NanoDrop spectrophotometer (2 – 3000 ng.$\mu L^{-1}$). The A260/280 ratios of the RNA extracted from 1000 and 500 cells were also not reliable, as repeated readings gave negative values. Samples with an extremely low RNA concentration can generate negative readings (Gallagher and Desjardins, 2008).

The A260/280 ratio of the RNA extracted from 20000 cells was just below the lower limit indicative of pure RNA. Low A260/280 ratios indicate a decrease of 260 nm absorbance such as nucleic acid, or an increase of 280 nm absorbance such as: phenol or buffer, EDTA at > 10 mM, different proteins, conjugates, metalloproteins and cell debris, or low pH solution (Qiagen, 2012b, Nolan et al., 2006). All possible contaminants had been eliminated throughout the

extraction. The RNA amount per cell found in the 20,000 cell extraction was about 15 pg per cell, which was within the range of total RNA found in each mammalian cell ( $10 - 30$ pg per-cell) (Davis et al., 1994). The RNA concentration of 20000 cells, however, was sufficient enough to generate a PCR (maximum volume of template for a PCR reaction using QuantiFast (Qiagen) is 2.5 µL). Therefore, the cell number to be used later when moving to the studies of cell-seeded decellularised PPT scaffolds was about 20000 cells.

**Human BM-MSC**

The human BM-MSCs used in this study expressed CD 73, CD 90, CD 105, HLA DR and lacked CD 14, CD 19, CD 34, CD 45 and HLA ABC expression (Aldridge., 2011). They were provided at p3, had a fibroblastic shape, were plastic adherent, capable of self-renewal, able to undergo trilineage differentiation (adipocytes, chondroblasts and osteoblasts). They also expressed lineage specific genes such as PPARγ (adipogenesis), SOX 9 and collagen II (chondrogenesis), and osteopontin (osteogenesis). Initial culture of these cells showed that the majority of the cells had a long spindle shape; however, the cells after p7 were found to be larger and flatter in morphology, grew slower and were more heterogeneous in shape and size. This indicated that after passage 7 the cells were probably becoming senescent. Senescent cells have been reported to be large spread cells with more podia and no spindle morphology (Dimri et al., 1995, Sethe et al., 2006). Human BM-MSC at p7 have also been reported to downregulate the PENK gene (cellular growth marker) compared to p3 (Bellayr et al., 2014). High passage (p21 and p16) human BM-MSC have been reported to stop dividing due to an upregulation of cyclin-dependent kinases expression (Coppé et al., 2010, Fridlyanskaya et al., 2015). Others have found that unhealthy BM-MSCs isolated from osteoarthritis donors started senescence as early as p5, marked by positive β-galactosidase staining that indicated an aging process (Mareddy et al., 2007). Besides passaging, donor age might affect cellular aging. BM-MSCs from young donors (up to 18 years old) have been reported to exhibit more spindle shape cells, express lower alkaline phosphatase and have better growth kinetics compared to BM-MSC from

older donors (59 to 75 years old) (Baxter et al., 2004). Since the human BM-MSCs used in this study potentially started to senescence after p7, the passage number of human BM-MSCs used throughout the study was not later than p6.

Human BM-MSCs (3,000 cells per cm$^2$) cultured in osteogenic medium produced more aggregates after 14 days of culture compared to 21 days of culture. This might have been due to the cells continuing to proliferate during osteogenic induction and the cell layers lifting off the culture substrate as they differentiated. The culture medium became very cloudy most likely due to the production of calcium phosphate deposition (mineralisation) as the cells differentiated towards the osteogeneic lineage. This behaviour was in agreement with the results of the previous researcher using these cells (Aldridge, 2011). Simann et al (2015) found that BM-MSCs isolated using heparin had increased calcium deposits due to upregulation of the bone morphogenic protein (BMP4) marker, and not alkaline phosphate (mRNA) expression. When the human BM-MSC were cultured in adipogenic medium there was extensive adipogenesis. This could have been an indication of cellular senescence, since it has been reported that senescent MSCs show adipocytic tendencies (adipogenic switch) and loose osteogenic potential (Ross et al., 2000). However, the human BM-MSCs in the control groups were fusiformic and growing. Morphologically, the cells showed no signs of senescence. Another study reported to detect the transcript genes for adipogenesis such as PPARɣ, lipoprotein lipase and FABP expressed by human BM-MSCs during the first three days of culture in induction medium containing dexamethasone, iso-butylmethylxanthine and insulin (Hung et al., 2004). Or perhaps the human BM-MSC colony expressed high levels of CD146, that were reported to have a tendency to differentiate into adipocytes (Rasini et al., 2013). The confluence of the cells cultured in the adipogeneic induction medium was apparently the same over the time, perhaps the cells stopped growing once the adipogeneic induction began (Aldridge., 2011). GAGs accumulation stained by Alcian blue was found in the 14 and 21 days inductions in the chondrogenesis medium. Human BM-MSCs which express high levels of CD 29 (more than

90%) have been reported to strongly express Col2A1, aggrecan and SOX 9 (Cicione et al., 2010).

In this chapter, the primer pairs to characterise the possibilities of the lineage fates of the human BM-MSCs were tested using RNA extracted from the tri-lineage differentiated cells. The lineage genes to be tested were PPARγ (adipogenesis), SOX 9 and collagen II (chondrogenesis), Runx 2 and osteopontin (osteogenesis). Tenascin-C, scleraxis, collagen I and collagen III were also tested for the tenogenesis lineage. The reference genes were β-actin, GADPH and S28R.

It was important for future experiments to establish a methodology for the reliable extraction of RNA, as the quality of RNA is very important for success of the downstream RT-qPCR (Bustin, 2000, Bustin et al., 2010). The RNA of the lineage cells differentiated from human BM-MSCs were extracted, and it was found that all samples had a pure RNA with an A260/280 ratio (2), except the samples from the chondrogeneic differentiation which were less than 2. This might have been due to the chondrogeneic pellets formed in culture developing into cartilage-like tissue, and the RNA extraction process not being as efficient as the extraction of RNA from cells.

The RT-qPCR followed the MIQE guidelines (minimum information for publication of quantitative Real-Time PCR experiment) (Bustin et al., 2009, Bustin et al., 2010). The primer-pair sequences for development of the molecular analyses were precisely selected to generate a specific PCR product (Sharrocks, 1994, Walters et al., 2011); PrimerBlast was used to reduce microsatellites (Ye et al., 2012). Primer stocks were aliquoted to avoid the repeated freeze-thaw that might have caused degradation of the single-stranded short nucleotides (Bartlett, 2003). A two-step PCR was used in this study to avoid mixing the reverse transcriptase and the DNA polymerase in one tube, as the reverse transcriptase may inhibit the PCR amplification (Huggett et al., 2013). Visualisation of the DNA products amplified using all of the primer pairs upon gel electrophoresis showed that all of the primer pairs were specific with the exception of Runx2. This might have been because of the nature of Runx2 sequences has diverse target products

(Vimalraj et al., 2015). The Runx2 transcript gene is very important in osteogenesis fate. The Runx2 transcipt gene products are upregulated in pre-osteoblasts, however they are downregulated in mature osteoblasts as Runx2 is not involved in calcification (Zhang et al., 2014). Osteopontin has been shown to be upregulated in BM MSC during mineralisation and after 20 days incubation in osteogenesis medium (Komori, 2009). Since calcification was demonstrated in the present study, the gene of interest selected as a marker for osteogenesis was osteopontin. When the samples from the chondrogenic differentiation were analysed, DNA bands for collagen II and SOX 9 were visible at 76 bp and 69 bp, respectively, indicating active chondrogenesis.

Amplification and separation of DNA for tenascin-C revealed with none of the expected DNA band, but only a short DNA band at 45 bp, which was suspected to be primer dimers. The dissociation curve of the real-time PCR reaction showed two amplifications; a peak which melted at 84 $^0$C, suspected the expected DNA - and a peak which melted at 72 $^0$C, suspected to be the primer dimers. Perhaps the primary cell of human tenocytes monolayer expressed low tenascin-C. Tenascin-C has been reported to be expressed in tendon due to a response to compression (Martin et al., 2003). It is also expressed in injured tissue, and in tendon during development and embryogenesis (Nishio et al., 2005). However, it was not possible to obtain an embryogenesis tendon or an injured human tendon to test the tenascin-C primer pair. Human pancreatic ductal adenocarcinoma (Esposito et al., 2006) or human testis and human fetal brain lysate (Abcam, 2014) are suggested to be used as the positive control for tenascin-C antibody labelling. Therefore, based on the data shown above, the primer pair for tenascin-C was determined.

The viability of human BM-MSCs was measured using ATPlite assay. The ATPlite assay of the different densities of human BM-MSCs (0.25, 0.5, 1, 2 and 4 x $10^5$) showed a linear relationship between the cell number and their luminescence counts per second ($r^2 = 0.9948$). This indicated that the method used to extract the ATP from the cells was consistent.

The standard culture media (DMEM) with low (1.0 g.L$^{-1}$) and high (4.5 g.L$^{-1}$) glucose concentrations to incubate the human BM-MSCs were compared with a commercial culture medium. When the human BM-MSC were incubated in the standard culture medium with high and low glucose concentrations supplemented with 10% (v/v) FBS, they produced comparable growth curves to a commercial culture medium (MesenCult®) after 11 and 17 days of incubation. FBS concentration was found to affect the growth of the human BM-MSC more than the glucose concentration. After 11 days of incubation, the ATP counts of the cells cultured in the high and low glucose culture medium with 10% (v/v) FBS and 5% (v/v) FBS, showed no differences in growth compared to the commercial medium with 10 % (v/v) commercial serum provided by the supplier (MesenCult®). Human BM-MSCs cultured with low FBS concentrations (1 and 2 % (v/v)) showed significantly slower cellular growth. These findings agreed with a previous study of human BM-MSCs study using five commercial serum-free media (SFM), which showed reduced population doubling rate, cell yield, colony fibroblastic unit forming (CFU-F) and less cells with spindle shape compared to the DMEM complete medium containing 10% (v/v) FBS and 2 ng.mL$^{-1}$ bFGF (Gottipamula et al., 2016). This finding has confirmed to use the DMEM low (1.0 g.L$^{-1}$) glucose culture medium to incubate the human BM-MSCs, supplemented with 10% (v/v) FBS.

As the human and porcine BM-MSCs had been verified for their mesenchymal properties, the cells were then prepared for the seeding studies presented in the Chapter 5.

## 4.6. Conclusion

1. Porcine BM-MSCs were successfully isolated, expanded and shown to exhibit multipotential mesenchymal stem cell properties following the criteria set down by the the ISCT.

2. It was shown that 20,000 cells porcine BM-MSCs gave a sufficient quantity of RNA for RT PCR analysis.

3. Human BM-MSCs were shown to have multipotential mesenchymal stem cell properties by cellular morphology, trilineage differentiation capacity and lineage gene expression.

4. Adequate concentrations of RNA of sufficient quality could be extracted from differentiated human BM-MSCs with the exception of the chondrogenic cells. The RNA extracted from BM-MSC differentiated into chondrocytes had a low A260/280 ratio.

5. Low glucose DMEM ($1.0$ g.L$^{-1}$) supplemented with 10% (v/v) FBS was a suitable culture medium for human BM-MSC.

6. The relationship between different densities of human BM-MSCs and ATP measurements was shown to be linear, indicating that the ATP assay was an acceptable assay to evaluate cell number in future experiments.

# CHAPTER 5

# SEEDING OF MSC ONTO DECELLULARISED TENDON SCAFFOLD

## 5.1. Introduction

In order to carry out the study of the human BM-MSC on decellularised PPT scaffolds in response to uniaxial tensile strains, the cells had to be seeded onto scaffolds. The decellularised tendon scaffolds referred in this chapter were produced as described in Chapter 3, and shown to have less than 50 ng DNA per mg dry weight, and no visible DNA using DAPI staining (Crapo et al., 2011). The BM-MSCs were isolated from porcine and human marrow tissue and characterised as described in Chapter 4. The cells met the criteria of mesenchymal cells (Horwitz et al., 2005, Rasini et al., 2013). They had a fibroblastic morphology, were plastic adherent, able to differentiate into adipocytes, osteoblasts and chondrocytes, and the porcine MSC were CD $29^+$, CD $40^+$, CD $90^+$ and CD $45^-$, HLA class II $^-$. The human MSC were CD $73^+$, CD $90^+$, CD $105^+$, HLA DR$^+$, CD $14^-$, CD $19^-$, CD $34^-$, CD $45^-$ and HLA ABC$^-$.

The aim in this chapter was to culture cell-seeded scaffolds in a bespoke research bioreactor, TenCell-1, in which the effects of the application of cyclic tensile strain could be investigated. It was therefore necessary to produce scaffolds of the correct size for use in TenCell-1, and investigate their mechanical properties in order to determine any changes due to cell behaviour in subsequent studies. A range of different approaches to seed sufficient cells onto scaffolds of a size compatible with use in TenCell-1 were investigated through studies of cell attachment, cell viability and isolation of adequate amounts of RNA for PCR analysis. Moreover, the protocol for the long-term use of TenCell-1 was also determined.

## 5.2. Aims and objectives

Aim: to develop a method for seeding MSC onto decellularised PPT scaffolds appropriate for studies of cellular differentiation in response to uniaxial tensile strain in the TenCell-1 bioreactor.

Objectives:

1. To develop methods for preparation of scaffolds of the appropriate size for studies in TenCell-1 bioreactor
2. To determine the mechanical properties of the appropriately sized scaffolds
3. To develop a method for cell-seeding of the appropriately sized scaffolds
4. To develop a protocol for the use of TenCell-1 bioreactor for long term culture

## 5.3. Materials and methods

### 5.3.1. Introduction of TenCell-1 bioreactor

The cell-seeded decellularised PPT scaffolds needed to be cultured in TenCell culture wells of the TenCell-1 bioreactor, to study the effects of uniaxial tensile strains. The TenCell-1 bioreactor provides an in-vitro culture environment for a 3D system, housing eight culture wells for delivering mechanical stimulation, and eight culture wells for the static controls [Figure 5.1 A].
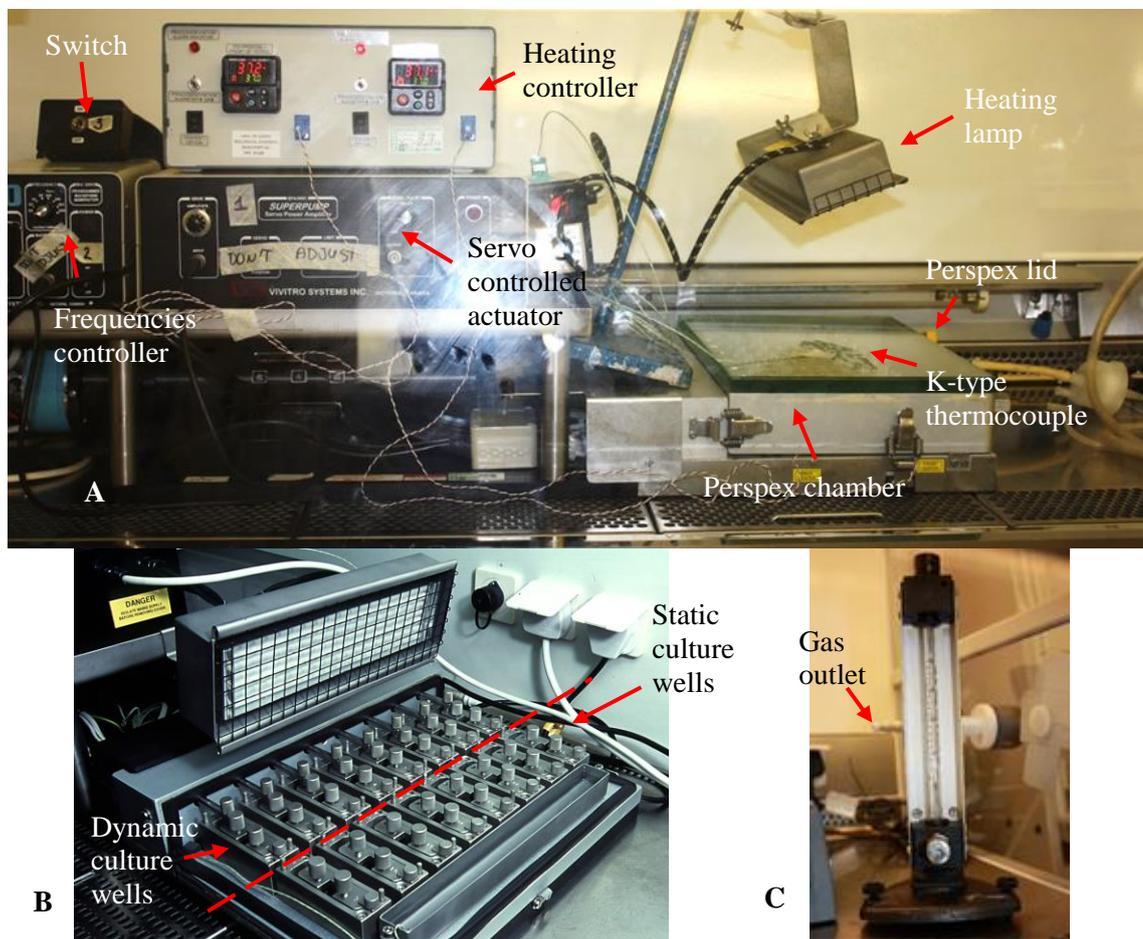


**Figure 5.1 All the compartments of the TenCell-1 bioreactor and components.** (A) TenCell-1 bioreactor, (B) layout of TenCell culture wells in situ the Perspex chamber, (C) the gas outlet and pressure meter.

The TenCell culture wells are labelled, and were placed in order on a heating plate, following the layout in the Perspex chamber [Figure 5.1 B]. The Perspex chamber for incubation has a manual gassing system controlled through a pressure meter [Figure 5.1 C]. Target temperature in this chamber can be controlled. The TenCell culture wells and inserts were manufactured from medical grade stainless steel that is reusable, autoclave-able and a good heat conductor. They were electro-polished before use to prevent releasing ions. Each TenCell culture well of the dynamic station is comprised of two clamping systems to hold the construct in place; one side is fixed to the well, the other attached to a controller arm. The dynamic arms are connected to the servo-controlled actuator to apply a linear displacement range from 1 – 10 mm with different cyclic amplitudes that can be set, while the clamp holders of the static are fixed to the well.

### 5.3.1.1. Characterisation of TenCell-1 bioreactor

In initial studies, it was found that the temperature controller in the TenCell-1 bioreactor was malfunctioning. There were also issues with the calibration of the displacement arms attached to the servo-controlled actuator. The TenCell-1 rig was repaired in the School of Mechanical Engineering, University of Leeds. The arms were calibrated, the TenCell culture wells and inserts were electropolished, and the heating rods, temperature controller, and the silicon rings of the Perspex lid and the chamber were replaced. Following this, the temperature profile of the TenCell-1 bioreactor was determined.

### 5.3.1.1.1. Temperature profile of the TenCell wells

The temperature profile of each TenCell culture well was observed. It was very important that all culture wells maintained the same conditions. All TenCell culture wells and their inserts were set in place, and each well was filled with 5 ml PBS solutions. The temperature of the PBS was measured using a T-type thermocouple (model: IT-21, Physitemp Instrument Inc, USA) connected to a digital thermometer (HI 92804C). The diameter of the probe is 0.41 mm and has

an accuracy of ± 0.1 $^0$C, with a time constant at 0.08 s. The thermal controller of the TenCell-1 rig was set at 37 $^0$C, and the temperature of the solutions was measured every 30 min for 6 h.

### 5.3.1.1.2. Determination of the volume of culture medium in TenCell-1 culture well

The depth of culture medium above the cell-seeded scaffolds was very important to provide an optimal oxygen exchange and to maintain cellular viability. For the dynamic cell culture wells, when the inserts of the clamps were fastened to the arm (connected to the servo-controlled linear actuator), the clamps were raised by 2 mm to prevent the wear of the bottom of the culture well during the application of cyclic strain [Figure 5.2]. This caused the cell-seeded scaffold to tilt upwards; if the culture medium had about 2-3 mm medium depth at the static position, this would expose the cell-seeded scaffold to the air. The culture medium depths using a series of medium volumes in the dynamic and static culture wells were therefore measured to determine the optimum culture medium volume for (a) the dynamic and (b) the static wells.
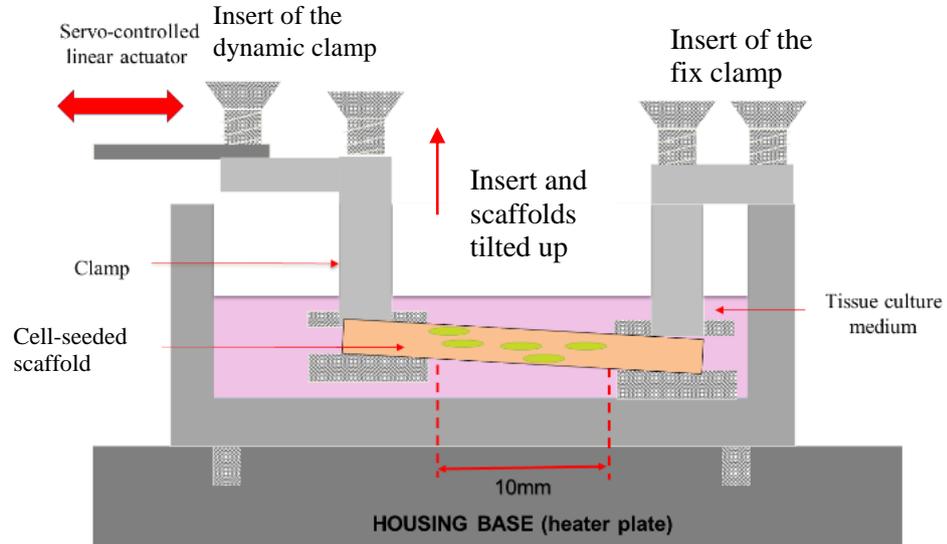


**Figure 5.2 A schematic of a single component of TenCell culture well** with a decellularised PPT scaffold mounted and the dynamic insert fastened to the servo-controlled linear actuator. Image was reproduced from Vassilis (2013) (Vassilis, 2013).

Decellularised PPT scaffolds were mounted in the TenCell culture wells and placed in the TenCell-1 bioreactor; the depth of the medium in the dynamic wells (n=3) was determined at

the tilted part, and the static wells (n=3) at the centre of the scaffold. A digital calliper (Mitutuyo) was used to measure the medium depth. Briefly, the calliper sat on the top of the well, the tip of the probe pointing to the centre between the grips. The tip of the probe was brought down to the air-medium phase and zeroed, then the tip was placed against the tissue surface. The differences were calculated as the medium depth. This was repeated three times, and a mean was taken.

### 5.3.1.1.3. Observation of evaporation rate of the TenCell-1 culture wells

The volume loss in the TenCell culture well during a standard incubation (37 $^0$C) in the TenCell-1 bioreactor for a certain period was estimated. This was carried out after the volume of culture medium had been determined and its thermal profile had settled.

All TenCell culture wells (n=12) were filled with 5 mL culture medium [Figure 5.3 A]. The reservoir wells (four stations; well no 1, 8, 9 and 16) and the waterbath were filled with sterile water (5 and 50 mL respectively) with Amphotericin (10 µg. mL$^{-1}$) to inhibit any mycotic growth. The inserts of all TenCell culture wells were placed in the wells, which were positioned according to the layout shown in the Figure 5.3 D. The set-up of the TenCell-1 bioreactor was as described in Section 5.3.1.2.2 below. The Perspex lid was sealed following the protocol from the Section 5.3.1.2.3. The TenCell-1 rig was switched on for 3 x 24 h at 37 $^0$C, and the total volume of medium left in the culture wells and solutions in the reservoir wells was measured using a 5 mL Stripette™ pipet.

The TenCell well surface area (1442.79 mm$^2$) and the TenCell insert (628.53 mm$^2$) are shown in Figure 5.3 B&C. The surface area of culture medium in the well that was exposed to air was 178.76 mm$^2$ (1.79 cm$^2$).

The evaporation rate was calculated using the following equations:

**Equation 11:**

$$\text{Percentage of medium loss per day} = \frac{average\ of\ medium\ left\ per\ day}{5\ mL} \ x\ 100\ \%$$

**Equation 12:**

$$\text{Estimation of evaporation rate} = \frac{average\ of\ medium\ left\ per\ day\ (mL)}{1.79\ cm^2}$$

Data was arcsine transformed and the mean (percentage medium loss) (n=3) ± 95% Cl determined and back transformed for presentation.
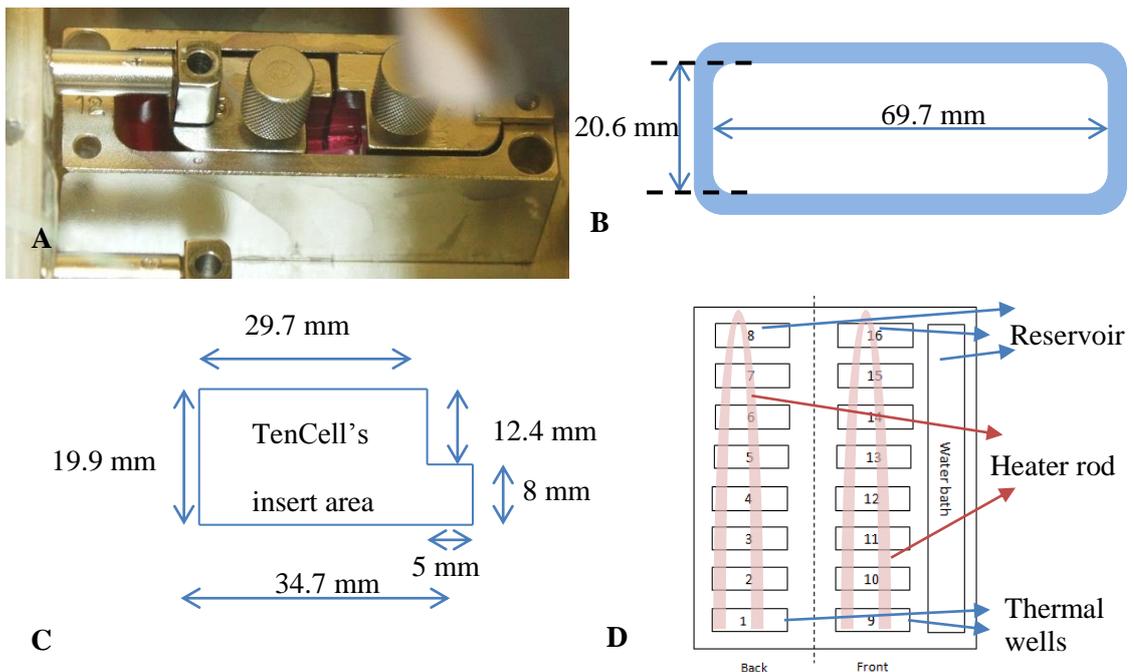


**Figure 5.3 Properties of the TenCell culture well and the inserts**. (A) A component of culture well; (B) the scale of a well and (C) the grip. (D) The layout of the in-house TenCell culture wells, seated on the Perspex chamber heating plate. Well no 1, 9, 8 and 16 were used as the reservoir wells. Wells no 1 and 9 were also used to measure the temperature (well no 1 indicates the temperature from the heater rod located at the back, and well no 9 at the front). Two T-type thermocouple probes were placed in wells no 1 and 9 to measure the temperature of the medium in the culture well. The red-shadow loops show the position of the heating rod underneath the Perspex chamber.

**5.3.1.2. Protocol for setting up the TenCell-1 bioreactor for culture of cell-seeded scaffolds**

TenCell-1 bioreactor was set up according to the protocol outline below in order to ensure consistent conditions. Maintaining an aseptic environment, stable temperature and pH were critical factors.

### 5.3.1.2.1. Preparation of materials and apparatus

All metal components (TenCell culture wells), an empty metal tray (to transfer TenCell culture wells from the class II hood to the TenCell-1 rig), and two sets of dissection equipment were sterilised by dry heat at 190 $^0$C for 4 h. The TenCell components were split into two storage metal tins. One set was used for the TenCell-1 set up (water well, 4 wells of the reservoir wells, all the associated keys, bolts, rods and screws, mounting plate and hook) – the other set was used for the TenCell culture wells. The culture wells in the storage tin were placed in order, following the layout of the wells in the TenCell-1 rig to create a smooth working flow during mounting the cell-seeded decellularised PPT scaffolds. A humidification flask was wrapped in aluminium foil, and the tubes sealed in an autoclave bag. All components were sterilised by humidified air at 121 $^0$C for 20 min, 15 psi and dried at 37 $^0$C overnight.

### 5.3.1.2.2. Setting up the TenCell-1 bioreactor before mounting the samples

In the Class II cabinet hood which housed the TenCell-1 rig, after UV sterilisation, the Perspex chamber (heating plate) and the lid were wiped thoroughly using Trigene 1 % (v/v), then sprayed with ethanol 70 % (v/v), followed by cleaning the hood. The tips of the T-wire thermocouple were soaked in ethanol 70 % (v/v). The reservoir wells, temperature regulator wells and the water well were installed in the Perspex chamber as described in Figure 5.3 D, using sterile gloves. The water bath was affixed to the Perspex chamber using an Allen bolt (M3 – 25 mm), and the reservoir wells using an Allen bolt (M4 – 30 mm). The humidification flask was filled with 150 mL sterile water and heated to 37 $^0$C. The sterile tubes were assembled to the flask, fitted with a sterile air filter (Midisart®) to filter the gas entering the TenCell-1 chamber. Two sterile decellularised PPT scaffolds (without cells) were mounted in the thermal wells (well no 1 and 9). The tips of the T-wire thermocouple, connected to a temperature controller, were inserted into the decellularised PPT scaffold to give a precise reading of the temperature. All reservoir and thermal wells were filled with sterile water with Amphotericin B

(10 µg.mL$^{-1}$). The Perspex chamber was sealed following the protocol described in Section 5.3.1.2.3.

### 5.3.1.2.3. Protocol to seal and lift the Perspex lid

The lid and the chamber had a silicon seal. The lid was lifted to make sure that the silicon layer was intact, thus ensuring proper sealing of the chamber to prevent contamination and overheating (caused by over-compensation of heat loss by the heater system) and consequent evaporation of the culture medium. Once all wells and bath were in place, the Perspex chamber was sealed tightly by pushing the lid down vertically and to the side, and then the latches were fastened in order from the back to the front. With both tabs open, the chamber was humidified for 15 min by connecting the tube from the humidification flask to the yellow tab. A K-wire thermocouple was affixed to the lid underneath the heating lamp to monitor the heating of the lid. The temperature of the heating lamp was set at 50 $^{0}$C to prevent medium evaporation. The heater was initially set at 34 $^{0}$C, followed by increments of one $^{0}$C until the target temperature had achieved (37 $^{0}$C) (usually in 90 min). Finally, the window of the hood was closed and the Class II cabinet switched off to allow the apparatus to settle.

### 5.3.1.2.4. Mounting of cell-seeded scaffolds in TenCell culture wells

This was carried out in a Class II safety cabinet. A sterile tray was placed in the centre of the hood and TenCell culture wells, apparatus and the dissection sets placed in order. Using sterile gloves, each culture well was filled with 5 mL of pre-warmed complete culture medium. Once the working station was set up, the cell-seeded decellularised PPT scaffolds were transferred to the hood. Each pair of cell-seeded scaffold holders was removed from the storage metal tin using a hook [Figure 5.4], placed on the mounting plate and the grips loosened. The cell-seeded decellularised PPT scaffold was transferred to the grips by holding both ends of the sample using two pairs of tweezers. The cell-seeded scaffold was mounted such that the fascicles were aligned symmetrically at the centre. The grips were then fastened firmly. The scaffold holder with the sample mounted was transferred immediately using the hook, and immersed into the

culture well. Once all samples were mounted, the metal tin housing the TenCell culture wells was transported to the Class II hood housing the TenCell-1 rig.



**Figure 5.4 A hook to move the inserts and a mounting plate to place the inserts.**

In the TenCell-1 rig, the TenCell culture wells loaded with cell-seeded scaffolds were placed in order following the layout described in Figure 5.3 D. The clamps were fastened to their wells using an 8.5 mm thumbscrew, and the dynamic clamp fixed to the arms connected to the servo-controlled actuator using an 18 mm thumbscrew. Both ends of the construct holder of the static wells were fixed with an 8.5 mm thumbscrew. Once the scaffold holders were fixed to their wells, the culture wells were fixed to the Perspex chamber using rods and an Allen bolt (M3 – 25 mm). The TenCell-1 bioreactor chamber was humidified by the warm steam as described in Section 5.3.1.2.3, followed by 5 % (v/v) $CO_2$ gassing through the black tab at 40 mmHg for one h. All tabs were then closed. During the humidification and the gassing, the temperature was monitored and kept stable at 37 $^0$C. Finally, the displacement and the frequency were set to the desired amount using the servo-controller, and strain was applied to the dynamic wells. The amount of displacement (mm) was calculated using the engineering strain formula [Section 5.3.3.3].

**5.3.1.2.5. Protocol to shut down and clean the apparatus**

After all the cell-seeded scaffolds had been removed, the heater was switched off and the tubes and thermocouples disconnected from the chamber. The TenCell culture wells were removed and all components rinsed under tap water, followed by immersing the components in Trigene solution 1% (v/v) for 2 h. The wells were cleaned using a toothbrush followed by sonication in

distilled water (Ultrasonic Well, Fisher Scientific) for 1 h at room temperature. After sonication, all the apparatus was rinsed in distilled water and dried at 37 $^0$C overnight with the wells face down. All components were sterilised when dry. After the apparatus had returned to room temperature, the Tencell-1 rig was gently wiped clean using Trigene 1% (v/v) and sprayed using ethanol 70% (v/v), followed by cleaning the surface of the Class II cabinet. The cabinet was switched off, the window closed, and the UV light switched on for 1 h sterilisation.

### 5.3.2. Scaffolds preparations for cell seeding

### 5.3.2.1. Introduction

The cell-seeded decellularised PPT scaffolds needed to be cultured in TenCell culture wells to study the effects of uniaxial tensile strain. The scale of a TenCell culture well and the grips are shown in Figure 5.5 A&B. Each decellularised PPT was trimmed to fit the culture well. The maximum thickness of the scaffold for 3D culture to allow optimal oxygenation and penetration of nutrients should be less than 1 mm (Ingram et al., 2004). The appropriate 3D size of decellularised PPT scaffolds was therefore 20 mm length, 10 mm width, with a thickness of between 0.6 – 0.8 mm. The decellularised PPT scaffold stated in this chapter referred to the decellularised PPT after being trimmed down to a 3-D working size scaffold (20 x 10 x 0.6 – 0.8 mm$^3$), unless otherwise stated.
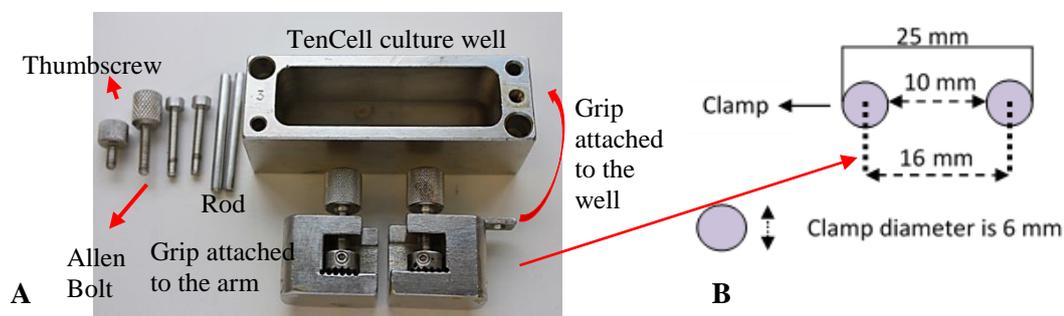


**Figure 5.5 (A) TenCell culture well and components,** (B) the scaffold holder (grip) dimension.

**5.3.2.2. Preparation of appropriately sized 3D decellularised PPT scaffolds for cell-seeding**

Prior to the scaffold preparation procedure, the dissection kits, dissection clamp [Figure 5.6] and tray were heat sterilised; filter papers, aluminium foil, autoclave tapes, microscope slides, cover slips and petri dishes were sealed in a double-layer autoclave bag and autoclaved. Sterile PBS was used throughout this procedure, prepared following Chapter 2, Section 2.1.5.1. The decellularised PPTs were thawed at 4 $^0$C overnight. Decellularised PPT scaffolds were prepared in the Class II safety cabinet unless otherwise stated.

To generate the decellularised PPT scaffolds with consistent size, a reusable and autoclave-able dissection clamp was designed and manufactured by School of Mechanical Engineering University of Leeds. The dissection clamp consists of a well with two grips (fixed and removable), and apparatus [Figure 5.6]. During the preparation, the well was filled with sterile PBS to wet the tendon and prevent fibre damage.
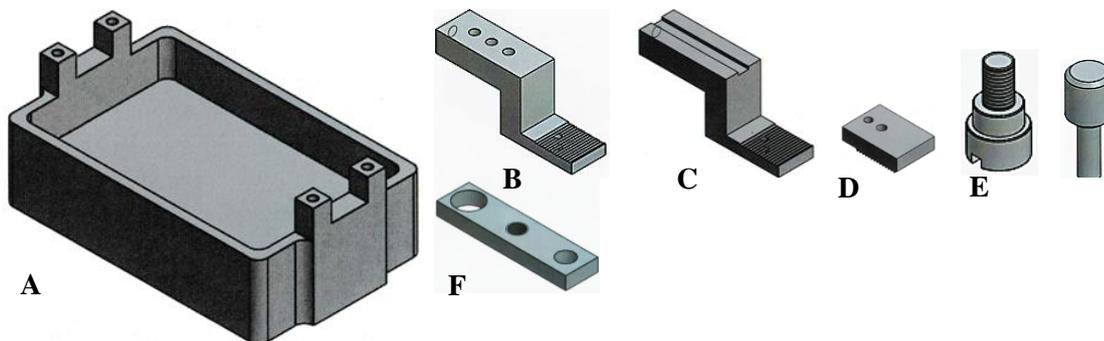


**Figure 5.6 Dissection clamp and its apparatus.** (A) The well and the inserts/ clamps (B) a fix grip and (C) a removeable grip, (D) the grip top, (E) a bolt and a pin, and (F) a removeable bar. The images were drawn by Rhys Moore, University of Leeds School of Mechanical Engineering technician, using SolidWork CSWP software. Used with permission.

Scaffold thickness is very important to maintain cellular viability across the scaffold; a thickness gauge (J-40-V Schmidt) [Figure 5.7] was therefore used to measure the scaffold thickness. However, the original upper anvil (resolution of 0.01 mm per 0.0005 inch and 0.5 kPa pressure) was found to squeeze the tendons, especially the decellularised tendons, as these scaffolds became swollen with fluid and hence softer. The original upper anvil was therefore

replaced by a smaller and ligther custom-made titanium anvil in order to accurately measure the scaffold thickness.

The original anvil was 38 mm in diameter, weight was 83.46 g; the replacement was 25 mm in diameter, weight 12.02 g.



Custom-made anvil

**Figure 5.7 The thickness gauge** (J-40-V Schmidt)

### 5.3.2.2.1. Setting up the working station

The working station was prepared as shown in Figure 5.8 A. A sterile tray was placed in the centre of the hood; the dissection clamps, blades, sterile gloves, filter paper, microscope slides and cover slips were removed from the first layer of the autoclave bag and placed on the tray. The thickness gauge was wrapped in sterile aluminium foil and placed on the tray. The wells of a 6-well plate were filled with 2 mL of completed culture medium, and the plates placed next to the dissection clamp, outside the tray. Using sterile gloves, the base of the lower anvil of the thickness gauge was covered with two sterile microscope slides affixed with sterile autoclave tape, and the upper anvil affixed with a sterile cover slip. A decellularised PPT was mounted to the dissection clamp and the dissection well filled with sterile PBS solutions up to the bottom level of the tendon [Figure 5.8 B].
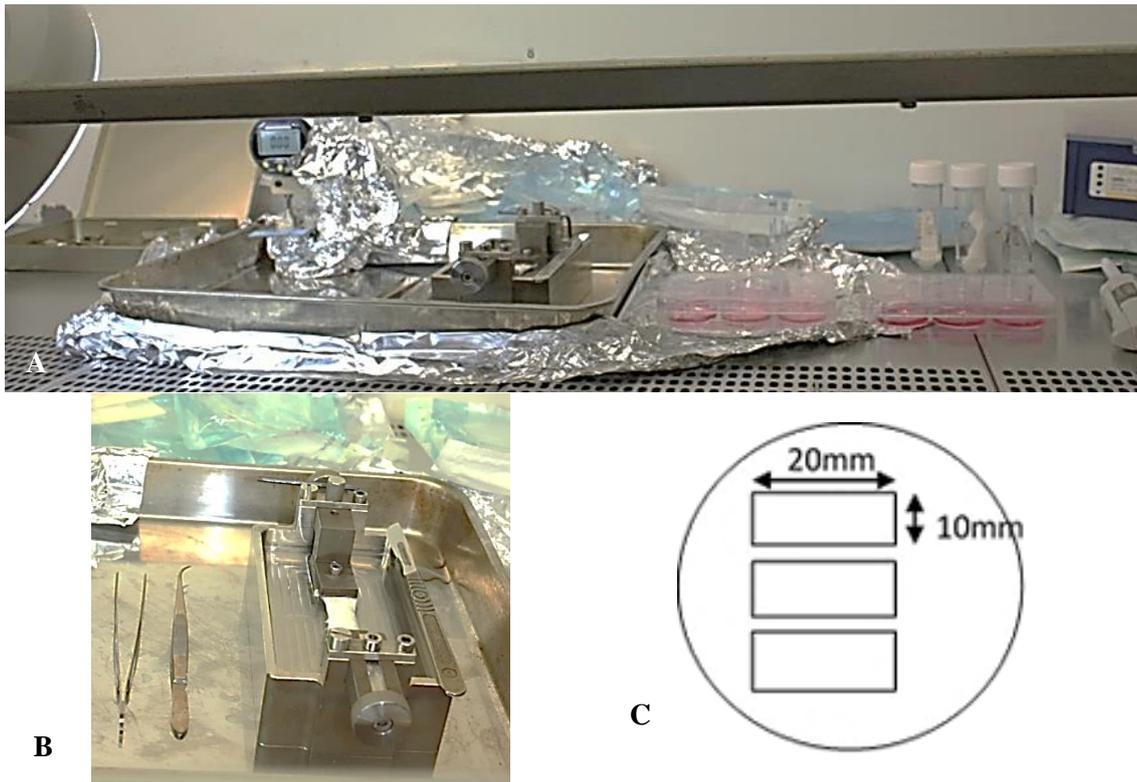
**Figure 5.8 The working station to prepare the decellularised PPT scaffolds.** (A) Inside the Class II safety cabinet. (B) A decellularised PPT mounted in a dissection clamp and the well filled with sterile PBS solutions. (C) An isolation plate with a template drawn beneath the plate to size the scaffold.

### 5.3.2.2.2. Technique to prepare the decellularised PPT scaffolds

The whole bulk of the decellularised PPTs were trimmed and shaped into the working size tendon scaffolds. The trimmed tendon scaffolds (decellularised PPT scaffolds) were preconditioned in a culture medium in order to replace PBS solution that might be trapped in between fibres with culture medium. This scaffold preconditioning aimed to prepare the tendon scaffold to be more cell-receptive before seeding.

Initially, connective tissue on the tendon surface was carefully removed without cutting the fibres. An initial incision was made at the top of the tendon, cut horizontally about 10 mm in width and 0.8 mm in depth. The fibres were carefully pulled downward, up to 20 mm length, and the end was cut with scissors. The thickness of the isolated fascicle was then measured three times. The protocol to measure the scaffold thickness is described in Section 5.3.2.2.3. Only

scaffolds with a thickness of 0.6 to 0.8 mm were collected. Each scaffold was then immediately immersed in a well of a 6-well plate containing 2 mL of DMEM low glucose complete medium, until all decellularised PPT scaffolds had been collected. Once the decellularised PPT had been harvested, each scaffold was shaped to obtain a size of 20 mm length and 10 mm width using the template drawn underneath the isolation plate [Figure 5.8 C].

The preconditioning plate was prepared by gluing the SteriStrip™ (3M) on the centre of the plate. The SteriStrip™ was required to prevent the scaffolds from floating or being inversed while loaded with culture medium, as the SteriStrip™ would hold the scaffolds in position. After all the decellularised PPT scaffolds were collected and shaped, three decellularised PPT scaffolds were aligned in each preconditioning plate [Figure 5.9 B]. Two mL of DMEM complete medium was added to the edge of the plate, not directly to the scaffolds, to maintain the humidity in the plate during the preconditioning. The plates were then transferred to an incubator 5% (v/v) $CO_2$ in air at 37 $^0$C and left overnight.
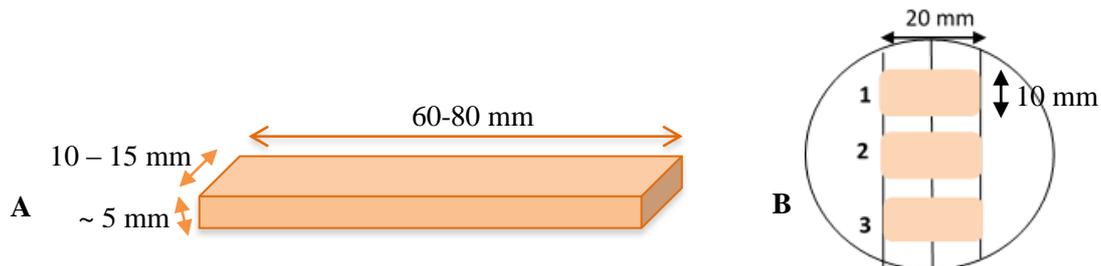


**Figure 5.9 Dimension of decellularised PPT** (A) a whole bulk of a decellularised PPT. (B) The decellularised PPT scaffolds at the appropriate 3D size, three scaffolds were aligned in each plate.

**5.3.2.2.3. Protocol to measure the thickness of the decellularised PPT scaffold**

Using a sterile autoclave tape, the upper anvil of the thickness gauge was affixed with a sterile cover slip and the bottom anvil was affixed to two microscope slides, then the thickness gauge was zeroed. The harvested decellularised PPT scaffold was positioned on a sterile microscope slide and the thickness measured. The scaffold was then returned to the well and measured two more times at 5 min intervals. An average was then taken.

**5.3.2.3. Characterisation of the decellularised PPT scaffold post conditioning**

**5.3.2.3.1. Sterility and contact biocompatibility of the decellularised PPT scaffold**

It was necessary to determine that the procedure used to prepare the scaffolds of appropriate size did not compromise the scaffolds sterility and biocompatibility. The sterility of the decellularised PPT scaffolds was determined as described in Chapter 3; Section 3.3.3.1. Porcine and human BM-MSCs were used for the contact biocompatibility assay following the protocol described in Chapter 3; Section 3.3.3.2. Tendon samples (n=3) were cut to 5 x 5 x 0.6 - 0.8 mm$^3$, affixed into wells of a 6-well plate using SteriStrip™. Each plate had a negative control (SteriStrip™) and a positive control (cyanoacrylate glue). Porcine and human BM-MSCs cell suspensions were prepared at 6000 cells.cm$^{-2}$ and added to each well. The samples and the controls were incubated for 48 h and stained using Giemsa to highlight cell morphology. Images were taken from stained and unstained samples.

**5.3.2.3.2. Investigation of capacity of decellularised PPT scaffolds to endure cyclic tensile strain**

Prior to undertaking studies of cell-seeded scaffolds under uniaxial tensile stain in TenCell-1, it was necessary to ensure that the scaffolds remained intact when subjected to cyclic strain. The decellularised PPT scaffolds were therefore subjected to the highest displacement in this study (8 %) at 1 Hz cyclic strain for 4 hours in the TenCell-1 bioreactor. The TenCell-1 bioreactor was prepared as described in Section 5.3.1.2. The decellularised PPT scaffolds (n=4) were mounted in wells no 2, 3, 4, and 5 (dynamic wells) [Figure 5.10]. The TenCell culture wells were filled with 5 mL of PBS and the chamber was sealed [Section 5.3.1.2.3]. The heater was switched on, set at 37 $^0$C, and the displacement programed at 8 % strain. Displacement for 8 % strain was calculated using the equation for engineering strain [Equation 14]. Initial sample length was 10 mm (gauge length or the distance between two inserts in the TenCell culture

well), therefore the displacement for 8 % strain was 0.87 mm. The decellularised PPT scaffolds were cyclically extended with 0.87 mm displacement for 4 hours, 1 Hz at 37 $^0$C.



Tendon scaffold clamped in the dynamic wells

Thumbscrew fastened the arm to the dynamic clamp

K-type thermocouple affixed on the lid

Culture well no 2
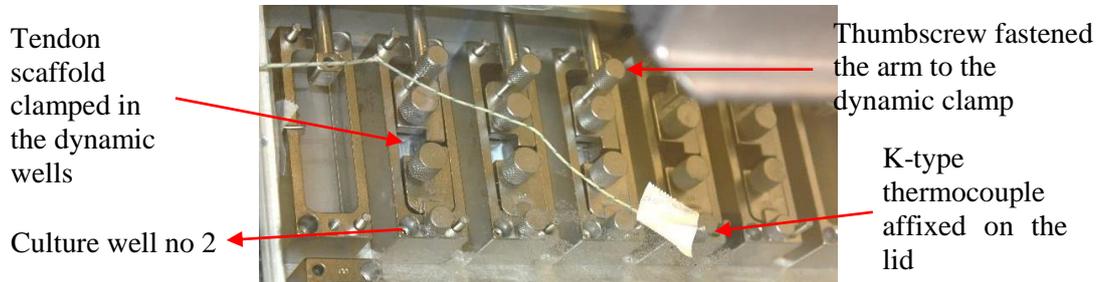
**Figure 5.10 Investigation of decellularised PPT scaffolds to endure a cyclic strain.**

### 5.3.3. Biomechanical testing of the decellularised PPT scaffold

The mechanical properties of the decellularised PPT (20 x 10 x 0.6 - 0.8 mm$^3$) were investigated using uniaxial tensile test on an Instron 3365. Tests were conducted in a BioWell (PBS at 37 $^0$C) chamber to create a physiological environment.

The sample was immersed into the BioBath chamber and stretched with a 500 N load-cell until mechanical failure at the low rate; 10 mm.min$^{-1}$. Low failure rate was used to allow enough time to recruit all tendon components and exhibit the viscoelastic behaviour. Before starting the failure test, the decellularised PPT scaffolds were not subjected to a biomechanical preconditioning as the specimen size was very thin and small. Also, the sample was immersed into a PBS solution at 37 $^0$C. A 500 N load cell was used, as the ultimate failure stress (UTStress) of the tendon scaffolds were found to exceed the capacity of 50 N load cell. Native decellularised PPT scaffolds were used as the control. BlueHill software was used to record the data.

## 5.3.3.1. Sample mounting on the mounting clamp

Before mounting, the thickness of the decellularised PPT scaffold was measured three times and a mean was taken. The Figure 5.11 A shows the thickness gauge, a custom-made titanium clamp, and the apparatus to fix the decellularised PPT scaffolds onto the clamp.
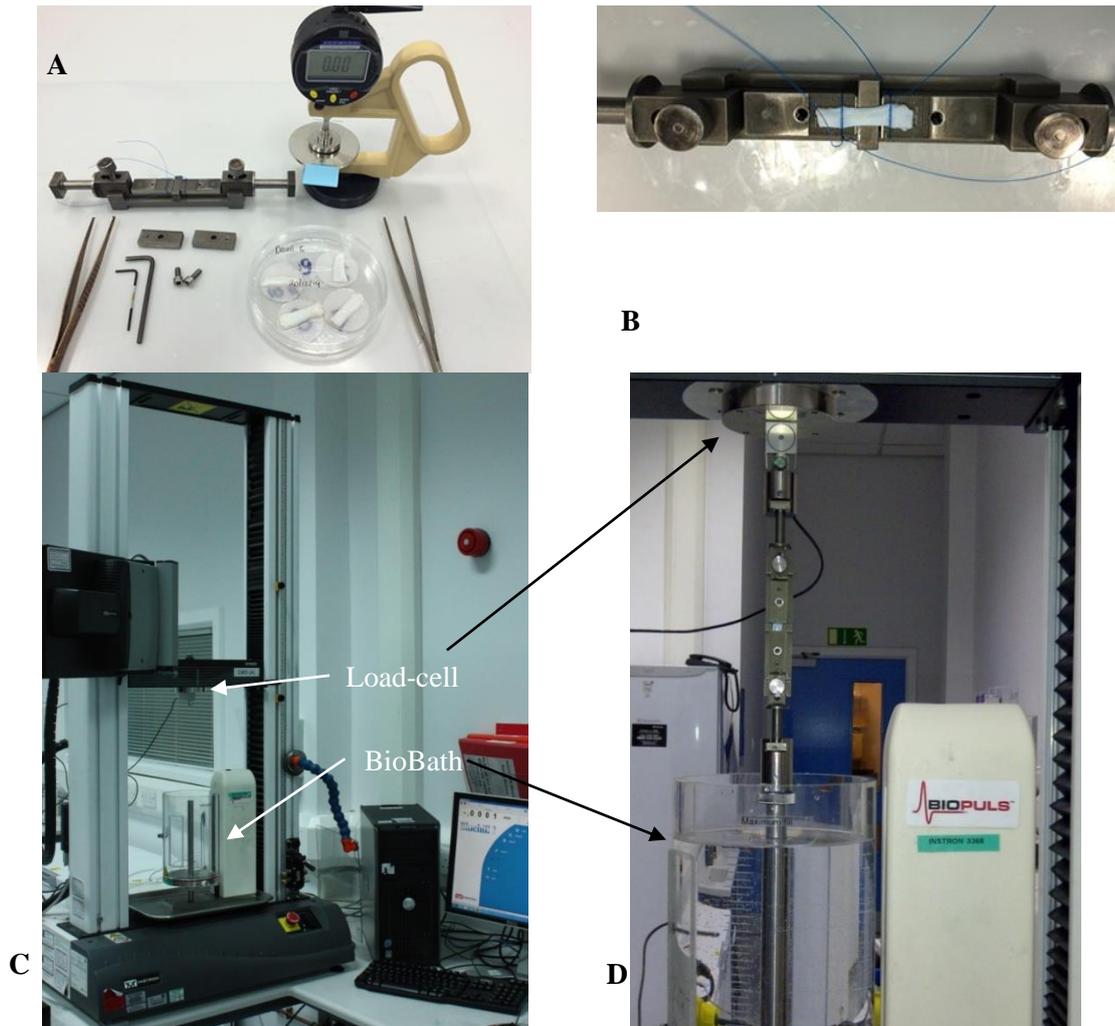


**Figure 5.11 Investigation of the decellularised PPT scaffold biomechanical properties.**
(A) The thickness gauge, a mounting clamp, a pair of fine serrated fix grips and moderate serrated grip-tops, and two tweezers to mount the decellularised PPT scaffold on the mounting plate. (B) A custom-made titanium clamp with a decellularised PPT scaffold looped with suture. (C) The Instron 3365 with BioBath and 500 N load-cell installed. (D) A decellularised PPT scaffold mounted in the mounting clamp and installed in the loading frame of the Instron 3365, with BioBath filled with PBS solutions.

The sample was mounted on the mounting clamp with fine serrated fixed grips and a 6 mm gauge length base plate. The decellularised PPT scaffold was positioned at the centre of the

clamp, with both ends looped using 6.0 Silk sutures (Ethicon) [Figure 5.11 B]. The sample was fixed with a moderate serrated grip-top, with a sandpaper placed in between to protect the tendon from being cut during the tensile test. The clamps were fastened and the width of the sample was measured using digital Vernier callipers (Mitutuyo). The sample was wet with PBS and then mounted in the Instron 3365 [Figure 5.11 C].

### 5.3.3.2. Mounting the sample grips into the Instron and the biomechanical testing

The distance between the load-frames of the Instron was reduced to close to the length of the titanium grips, after that, the sample grip was mounted into the machine [Figure 5.11 D]. The grip was then aligned vertically to the load-frames; the gaps between the grips and the load frame were approximately 2 mm. The baseplate was removed and the sample in the loading frame immersed in the BioBath. Using the Bluehill software, the force applied to the grips mounted in the Instron was zeroed and the testing was immediately started. The sample was extended without preloading and pre-conditioning. The extension rate was constant at 10 mm.min$^{-1}$ until failure, and the data recorded at a frequency of 10 Hz. All information about the sample dimensions and gauge length were entered in the software; during the testing, the displacement and force over the time were recorded. Only data generated from the samples that failed at the mid substance was collected [Figure 5.12 A and B].
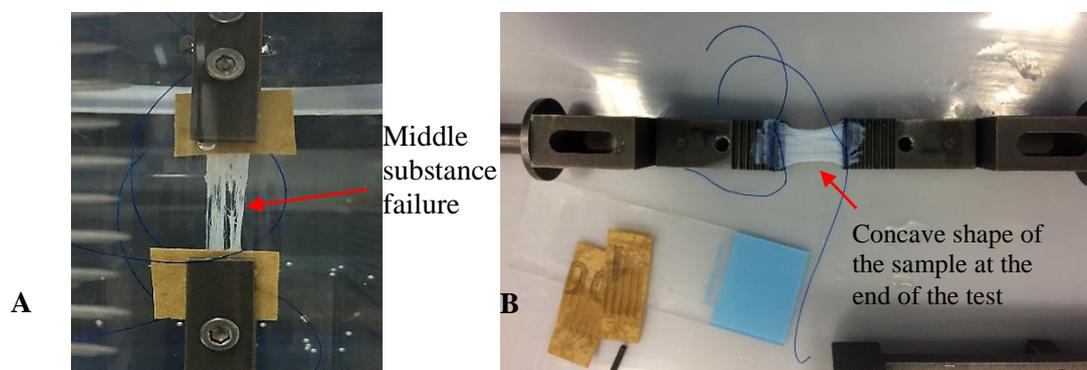


**Figure 5.12 Tendon specimens at the end of the failure test using Instron 3365.** (A) The torn fibres with the typical mid-substance failure. (B) Sample by the end of the test with a concave shape indicating an imminence of mid-substance tear.

**5.3.3.3 Data processing**

The raw data recorded the value of force (N), extension (mm) and time (s), and were exported to Microsoft Excel (version 2003 and 2007, Microsoft Corporation). The data were then converted to engineering stress ($\sigma$) and engineering strain ($\varepsilon$) responses of each sample by normalising the initial sample dimension. The calculation was performed manually following the sum of;

Equation 13;

$$Engineering\ stress\ (\sigma) = \frac{F\ (N)}{A\ (mm^2\ )}$$

The engineering stress ($\sigma$) is represented in MPa where the force (F) is in Newtons and the cross sectional area (A) is in mm$^2$. The cross sectional area of the sample is the width (mm) x thickness (mm).

The engineering stain ($\varepsilon$) is the percentage of the sample elongation ($\Delta$l) divided by the original sample (gauge) length (($l$) added with the elongation ($\Delta l$)). As showed in;

Equation 14:

$$Engineering\ strain\ (\mathcal{E}) = \frac{\Delta l\ (mm)}{l\ (mm) + \Delta l\ (mm)}$$

The stress-strain value was plotted as the stress-strain slope [Figure 5.13] and the behaviour of each specimen was characterised using five parameters; ultimate tensile strength (UTStress) ($\sigma_{fail}$), ultimate tensile strain (UTStrain) ($\varepsilon_{fail}$), elastin phase slope ($E_{elas}$), collagen phase slope ($E_{coll}$), and the relaxation modulus (Young modulus; $E(t)$).

The UTStress ($\sigma_{UTS}$) was determined as the initial point of the sample to reach the highest stress value, and the UTStrain ($\varepsilon_{UTS}$) was determined as the strain value at which the sample began to fail. The collagen phase slope ($E_{coll}$) was determined by fitting a linear trend-line between two points selected manually in the linear part of the curve between the initial toe of the curve and the yield point of the failure region. The elastin phase slope was determined by the area underneath the stress strain curve up to the strain limit of 0.05 due to the sample size being relatively small. This limit for fascicles was similar to the value cited by others (Yamamoto et

al., 1999), slightly lower than the suggested limit for an intact tendon, which is 0.07 (Allen et al., 1999). The strain limit at 0.05 was taken and the elastin slope was achieved by integrating the strain between zero and 0.05 to determine the area.

The young modulus $E(t)$ was calculated using:

Equation 15;

$$E(t) = \frac{Engineering\ Stress\ (\sigma)\ (MPa)}{Engineering\ Strain\ (\mathcal{E})}$$

Where the $\sigma$ was the engineering stress and the $\mathcal{E}$ was the engineering strain as stated above. The data for the decellularised and the native tendon specimens were analysed using unpaired Student's t-tests, to compare the two means of each biomechanical parameter (the variances of each group were assume homocedasticity, as heteroscedatic has not affected testing sensitivity when testing an equal sample size) (Sokal, 1995). Data is presented as the mean (n=6) ± 95% C.l.
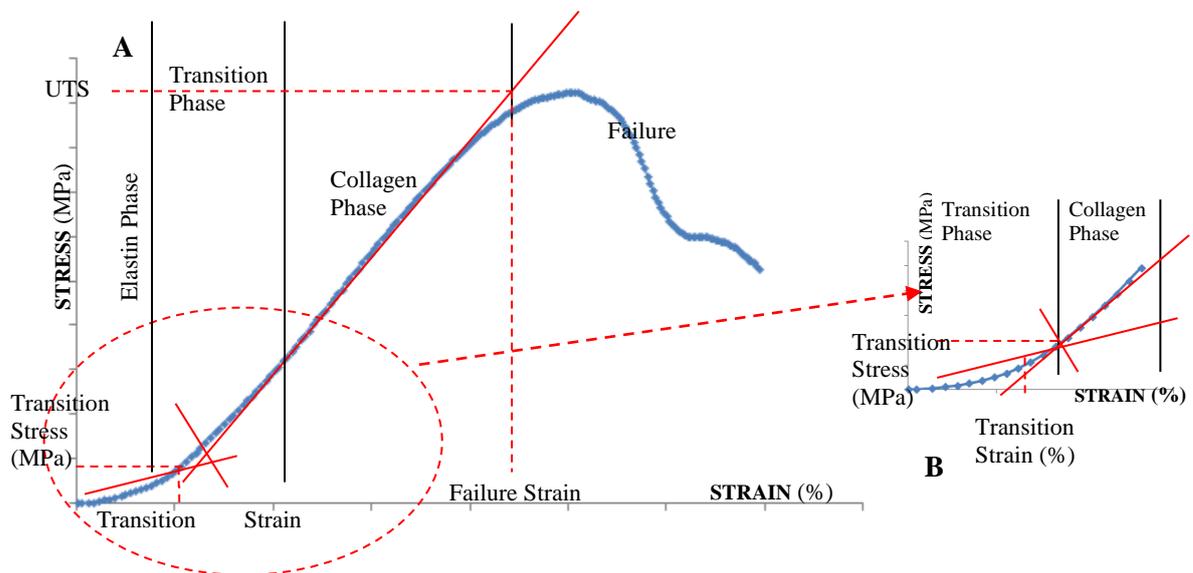


**Figure 5.13 Stress-strain curve of a native tendon**. (A) The stress strain slope with the biomechanical parameters. (B) The toe region highlighted from the whole stress-strain curve.

## 5.3.4. Development of seeding technique using porcine BM-MSCs

A method to seed the decellularised PPT scaffolds that gave the highest cell viability was initially developed using porcine BM-MSCs, for subsequent use with human BM-MSCs. Cell viability was determined using Live/Dead staining as described in Chapter 2; Section 2.2.5.1 and ATPlite™ assay as described in Chapter 2; Section 2.2.5.2. Tendon scaffolds were prepared as described in Section 5.3.2.2.2. Optimal seeding condition was determined by comparing the highest percentage of viable cells (calculated using the Equation 16) and the highest seeding efficiency (calculated using the Equation 17 below) among different methods.

### 5.3.4.1. Cell seeding using direct method and incubation for 4, 6 and 12 h

Seeding efficiency using a direct seeding method was investigated. The target seeding area was at the centre of the decellularised PPT scaffold ($1.0 \times 1.0 \ cm^{-2}$). The decellularised PPT scaffolds were obtained from decellularised PPT batch 3. Scaffolds were seeded using $4 \times 10$ µL of a suspension of $0.5 \times 10^5 \ cells.cm^{-2}$ porcine BM-MSCs at p4 seeding density. The cell suspensions were prepared at $6.25 \times 10^5 \ cells.mL^{-1}$ to achieve the $0.5 \times 10^5 \ cells.cm^{-2}$ seeding density. Cell-seeded scaffolds were incubated for 4, 6 and 12 h (n=3).

Decellularised PPT scaffolds were prepared as described above. On the seeding day, the excess culture medium at the edge of the preconditioning plate was discarded, and the decellularised PPT scaffolds were blotted dry using a sterile filter paper. The cells were prepared at the desired density and the decellularised PPT scaffolds were seeded [Figure 5.14 A].
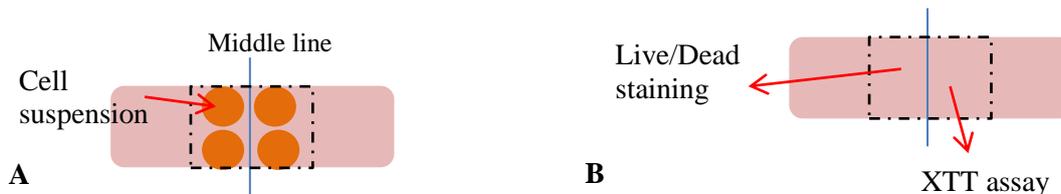


**Figure 5.14 Direct seeding method** (A) using a $4 \times 10$ µL cell suspension. The dashed square is the imaginary seeding area (about $0.5 \times 1.0 \ cm^2$). (B) The post-seeded samples were cut into two halves. One-half was investigated for cellular viability using Live/Dead assay;

the other was analysed using XTT assay. However, the XTT assay did not work and is therefore not presented.

One mL of culture medium was carefully added to the edge of the plate to maintain its humidity. The plates were incubated at 37 $^0$C, 5 % (v/v) $CO_2$ in air for 30 min to allow the cells to adhere to the scaffold. Culture medium (10 mL) was added to the plate drop-wise (not directly to the samples), and the plates transferred to a 5 % (v/v) $CO_2$ in air 37 $^0$C incubator for 4, 6 and 12 h. The viability of the samples was assessed using Live/Dead assay at each time point [Figure 5.14 B].

Quantification of cellular viability using XTT assay was found not to be suitable for this study, as the level of orange colour of the formazan products from the reduction of the tetrazolium ring in the reagent by the mitrochondrial dehydrogenases in the viable cells was affected by the phenol red in the culture medium, which was used to culture the cell-seeded tendon scaffolds. Following this finding, XTT assay was no longer used.

This experiment was repeated twice. The second direct seeding experiment aimed to determine which seeding condition (6 h and 12 h) was optimal. The 4 h experiment was excluded as this seeding duration was found to be impractical. In this repeated experiment, each sample was cut into two halves; one half was analysed using Live/Dead assay and another half was analysed for its RNA quantity.

### 5.3.4.2. Cell seeding using a cell suspension in a 6-well plate

The seeding efficiency using a cell suspension in the well of a 6-well plate was investigated. Scaffolds were prepared from decellularised PPTs batch 3 and after the preconditioning, the decellularised PPT scaffolds (n=3) were placed into each well of a 6-well plate.

A cell suspension (3.0 x 10$^5$ mL$^{-1}$, 3 mL) of porcine BM-MSCs at p3 was added into each well to achieve a seeding density of 3000 cells.cm$^{-2}$. The 6-well plates were placed in a humidified modular incubator and $CO_2$ 5 % (v/v) gas was pumped in for 15 min, and the tab was left

opened to keep replenished the $CO_2$. The chamber was transferred to an incubator $CO_2$ 5 % (v/v), 37 $^0$C for 4 days. Samples were analysed using Live/Dead assay [Chapter 2; Section 2.2.6.1].

### 5.3.4.3. Calculating cellular viability of Live/Dead assay

Cellular viability was calculated using the following equations:

Equation 16;

$$Percentage\ viable\ cells = \frac{\sum viable\ cells}{\sum counted\ cells}\ x\ 100$$

Equation 17;

$$Seeding\ efficiency = \frac{\sum viable\ cells}{\sum initially\ seeded\ cells}\ x\ 100\ \%$$

**Data analysis**

Data analysis for the percentage of viable cells and seeding efficiency were arcsine transformed and analysed using one-way ANOVA followed by calculation of the MSD ($p<0.05$) by the Tukey test. T method was also used to statistically determine the individual differences of the percentage of viable cells and the seeding efficiency between different time points. Data was back-transformed for presentation. Data for the total counted viable cells were analysed using one-way ANOVA and the (MSD) was determined by the p value $< 0.05$ using Tukey multiple comparisons tests. Data of the Live/Dead assay is presented as described in Chapter 2; Section 2.2.5.1.

### 5.3.4.4. RNA extraction of porcine BM-MSCs seeded scaffolds incubated for 6 and 12 h

The RNA was extracted from the porcine BM-MSCs seeded decellularised PPT scaffolds after 6 h and 12 h (n=3) incubation using a standard method. Native porcine PTs (n=3) were used as the positive control, and the concentration of RNA was presented as ng per mg tissue wet weight per mL (ng.mg$^{-1}$.mL$^{-1}$).

**Solutions**

Solutions such as the DNAse I (2.5 KU.$\mu$L$^{-1}$) and RLT buffer containing $\beta$-mercaptoethanol (10 $\mu$L.mL$^{-1}$) were prepared as described in Chapter 4; Section 4.3.1.4. The working solution for the Proteinase K (Qiagen) was prepared by adding 1 mL of stock solution (600 mAU.mL$^{-1}$) with 19 mL of RNase/DNase free water to make 30 mAU.mL$^{-1}$ working solution.

**Method**

The post-conditioned decellularised PPT scaffolds prepared from the decellularised PPTs batch (3) (n=3) were seeded with porcine BM-MSCs (p4) (0.5 x 10$^5$ cells.cm$^{-2}$) following the protocol described in Section 5.3.2.2.2 and incubated for 6 and 12 h at 37 $^0$C, 5% (v/v) CO$_2$. The method to extract RNA was using RNeasy mini kit (Qiagen), and the tissue lysis was carried out using Proteinase K 30 mAU.mL$^{-1}$.

Briefly, the cell-seeded decellularised PPT scaffolds - after 6 and 12 h incubation - and the native porcine PTs were cut in the middle to the size of 3 x 3 x 3 mm$^3$ with an approximate weight of 30 mg. The tissues were immediately immersed in RNAlater RNA stabilization reagent (Qiagen) (10 mL.mg$^{-1}$ weight tissue). Then were then finely macerated using a sterile blade and soaked into the 600 $\mu$L of RLT buffer (containing $\beta$ mercaptoethanol), followed by the addion of 600 $\mu$L of Proteinase K (30 mAU.mL$^{-1}$) into the lysate. The lysates were then enhanced mechanically by triturating three times followed by incubation in a heated Eppendorf shaker (Eppendorf) at 55 $^0$C for 10 min with 700 rpm agitation. After this, a homogenisation step was performed using a blunt needle (no 16) and a 1 mL syringe, to triturate the solution 10 times. Finally, the tissue was separated using centrifugation at 10,600 g for 3 min. The clear supernatant was then carefully harvested, transferred into a 2 mL Eppendorf, and 700 $\mu$L of 70 % (v/v) ethanol was added, followed by triturating three times. After this step, the RNA was isolated from the column following the protocol described in Chapter 4; Section 4.3.1.4.

**Data presentation**

The concentration of RNA extracted from each sample group is presented as ng per total scaffold (ng per scaffold), with the mean (n=3) ± 95 % Cl. This was calculated by multiplying the elution concentration (ng.µL$^{-1}$) to the total elution volume (30 µL), multiplied by 4 to calculate the amount of RNA from the whole scaffold (as each extraction was taken from a quarter of scaffold).

**5.3.4.5. Determination of a protocol to quantify ATP levels in cells seeded tendon onto decellularised PPT scaffolds**

The initial seeding study used the XTT assay to quantify cellular viability, however the XTT assay did not give the desired result, as explained in Section 5.3.4.1. Therefore, this section was aimed to investigate a protocol to quantify cellular viability using ATPlite™ assay; by quantifying the ATP level of viable cell.

Four decellularised PPT scaffolds (n=4) were produced from the decellularised PPTs batch (5), seeded with porcine BM-MSCs (p4) using the direct seeding method at a density of 0.5 x 10$^5$ cells.cm$^{-2}$, and incubated for 12 h. After 12 h incubation, the samples were analysed using 1.5 mL volumes of lysis buffer/ substrate solutions. This experiment had a negative control group (an acellular scaffold without cells; n=4), and a group of culture medium only (n=4) to eliminate the background signal. Each cell-seeded scaffold was cut into four quarters and one quarter of the sample was proceeded for the viability test. Only one quarter sample was used in this experiment because the amount of sample to be used in the final experiment (Chapter 6) was one quarter for each validation technique.

One quarter of each sample was placed in a dried empty Bijou, weighed three times, and a mean value was taken. The tissues were then finely macerated using a sterile blade (no 22) and immersed into each well of a 12-well plate containing 1.5 mL of lysis buffer. The plates were agitated at 700 rpm for 20 min. Substrate solution (1.5 mL) was added into each sample and the

plate was agitated (700 rpm, 20 min) in the dark. Finally, 100 µL of each sample with three replicates were transferred into the wells of an Optiplate™ (Perkin Elmer). The plate was covered using TopSeal (Perkin Elmer) and the luminescence was then counted per second (CPS) measured using a Chameleon plate reader after 10 min adaptation in the dark and the data was collected using MikroWin software.

**Data analysis**

Background counts (CPS medium only control) were subtracted from the test readings. The CPS was then multiplied by the ratio between the total reaction volumes to the volume of the measured sample. This was multiplied by 4, to estimate the luminescence of the seeded scaffolds (each sample was generated from a quarter of scaffold). The volume ratio was calculated as follows, the total volume was 3 mL (1.5 mL of lysis buffer added with 1.5 mL of lyophilised substrate solution), therefore the lumination (CPS) was multiplied by 30 (a ratio of 3 mL to 100 µL aliquots). The difference between the control (decellularised scaffold only) and the seeded scaffolds in all groups was analysed using one-way ANOVA with Tukey's multiple comparison test. The MSD was calculated at $p < 0.05$.

## 5.3.5. Cell seeding of human BM-MSCs on decellularised PPT scaffolds

The protocol for cell seeding onto the decellularised PPT scaffolds was the direct seeding method described in the Section 5.3.4.1. The Live/Dead assay was carried out as described in Chapter 2; Section 2.2.6.1, and the ATPlite assay was carried out as described in Chapter 2; Section 2.2.6.2, unless otherwise stated.

### 5.3.5.1. Determination of duration of cell-seeding

For practical purposes, the scaffolds could be seeded for 6 h (during the working day) or overnight (12 h). The effects of seeding for 6 h and 12 h on the viability of the seeded human BM-MSCs were therefore investigated.

Three groups were compared and there were three replicates of each; the cell-seeded scaffolds, the decellularised PPT scaffolds (negative control), and culture medium only (for the background). Human BM-MSCs at p5 were seeded on the scaffolds (decellularised PPTs batch (5)) at a seeding density of 1.0 x $10^5$ cells.cm$^{-2}$. Each sample was cut into two halves, one-half for Live/Dead assay and another half for ATPlite assay.

## 5.3.5.2. Determination of seeding density for human BM-MSCs on decellularised PPT scaffolds using viability assays

Three different cell densities were investigated 0.5 x $10^5$ cells.cm$^{-2}$, 1.0 x $10^5$ cells.cm$^{-2}$, and 2.0 x $10^5$ cells.cm$^{-2}$. The aim of this experiment was to determine the optimum seeding density of human BM-MSC to give sufficient amount of RNA for PCR analysis. Human BM-MSCs at p6 were seeded on the decellularised PPT scaffolds obtained from the decellularised PPTs batch (5). There were three groups of n=3; the cell-seeded scaffolds, the control scaffolds (the decellularised PPT scaffolds only) and the culture medium only. Cell viability and data analysis were described in Section 2.2.6.1 for the Live/Dead assay and the Section 5.3.5.2 for measuring the ATP levels from tissue.

## 5.3.5.3. RNA extraction of human BM-MSCs at $10^5$ cells.cm-2

A protocol to extract RNA from the human BM-MSCs seeded on decellularised PPT scaffolds was determined by optimising the protocol described for porcine MSC [Section 5.3.4.5]. Compared to Section 5.3.4.5, the protocol used here included (i) a lower concentration of Proteinase K (10 mAU.mL$^{-1}$) and (ii) no agitation during the tissue lysis step. The efficacy of DNA removal on the purification column was investigated by amplifying the eluted RNA a housekeeping gene, βactin.

Three groups of different templates were analysed in each PCR amplification; (i) the RNA elution to detect any remaining genomic DNA, (ii) the conversion of the mRNA to cDNA as the positive control, and (iii) the negative controls (template only, primer only and RNAase/DNase

water only). The protocol for PCR was as described in Chapter 4; Section 4.3.3.2, and the PCR products were visualised using gel electrophoresis.

**Solutions**

Solutions for RNA extraction were prepared as described in Chapter 4; Section 4.3.1.4. Proteinase K was prepared at 10 mAU.mL$^{-1}$, by adding 1 mL of stock solution (600 mAU.mL$^{-1}$) to 59 mL of RNase/DNase free water.

**Method**

Four decellularised PPT scaffolds (decellularised PPTs batch (5)) seeded with human BM-MSCs at p5 (1.0 x 10$^5$ cells.cm$^{-2}$) for 12 h, and cut at a size of 3 x 3 x 3 mm$^3$ (circa 30 mg). The tissues were immediately immersed in RNAlater RNA stabilization reagent (Qiagen) (10 mL per 1 mg tissue). After the RNA stabilisation, the tissues were finely macerated using a sterile blade and soaked in RLT buffer (containing β mercaptoethanol), then Proteinase K (10 mAU.mL$^{-1}$) was added. Tissue lysis was enhanced by triturating three times followed by incubation in a heated Eppendorf shaker (Eppendorf) at 55 $^0$C for 10 min without agitation. The lysate was homogenised using a blunt needle (no 16) and a 1 mL syringe to triturate 10 times. The lysate was separated from the tissue by a centrifugation at 10,600 g for 3 min, followed by transferring the clear supernatant carefully into a 2 mL Eppendorf. Next, 700 μL of 70 % (v/v) ethanol was added to the supernatant and mixed by triturating. The RNA was then isolated from the column as described in Section 5.3.4.5.

**Data presentation**

The quantity of RNA isolated is presented as ng.μL$^{-1}$ (mean (n=4) ± 95% Cl) and the A260/280 ratio to indicate the purity of the sample is presented as mean (n=4) ± 95% Cl. The DNA products were visualised using gel electrophoresis 3.5% (v/v) agarose gel.

### 5.3.5.4. Viability of human BM-MSC seeded on decellularised PPT scaffolds and incubated in TenCell-1 for 24 hours

In order to determine whether the conditions in the TenCell-1 bioreactor would support cell viability on decellularised PPT scaffolds, cell-seeded scaffolds were cultured in (i) TenCell culture wells in the TenCell-1 bioreactor, (ii) in TenCell culture wells in a standard incubator, and (iii) in a 6-well plate. Cell-seeded scaffolds were cultured with and without constraint in the TenCell culture wells in order to determine any effect of constraint on the viability of the cells.

**Preparation**

The TenCell-1 bioreactor was prepared as described in Section 5.3.1.2. Sterile Nalgene tubs with ports of gaseous exchange in the lid were used to house TenCell culture wells during incubation in the standard incubator to prevent contamination. The Nalgene tubs were soaked in Trigene 0.1 % (v/v) for 1 h and dried. The lids were fastened and tubing from the gas ports connected to a 0.2 μm pore sized air filter that was covered with aluminium foil and autoclaved.

**Method**

Six groups were compared with three replicates in each group. Two groups of cell-seeded scaffolds were cultured in TenCell culture wells in Nalgene culture tubs at 37 $^{0}$C, 5 % (v/v) $CO_2$; with one group clamped (constrained) and the second group unclamped. Two groups were placed in TenCell culture wells in the TenCell-1 bioreactor, again with one group unclamped, the second group clamped. One group of cell-seeded scaffolds was cultured in a 6-well plate in a standard incubator and used as the positive control. The negative control was unseeded decellularised PPT scaffolds placed in a standard incubator.

Decellularised PPT scaffolds were isolated from the decellularised PPTs batch (5) and seeded using human BM-MSCs (p5) at 1.0 x $10^5$ cells.cm$^{-2}$. The cell-seeded scaffolds were mounted in the TenCell culture wells as described in Section 5.3.1.2.4. TenCell-1 bioreactor was set as described in Section 5.3.1.2. The cell-seeded scaffolds incubated in the standard incubator

(constrained and unconstrained groups) were mounted in the TenCell culture wells which were then placed in the sterile Nalgene tubs with the lid loosened to allow air exchange [Figure 5.15 A] and in the TenCell-1 bioreactor [Figure 5.15 B]. After 24 h, the experiment was terminated and the samples harvested, was cut into two halves; for Live/Dead assay and for ATPlite assay.



**Figure 5.15 Static incubation in the TenCell culture wells.** Samples incubated for 24 h at $37^0$C, 5 % (v/v) $CO_2$ in air, transferred to: (A) a culture tub (Nalgene) and placed in a standard incubator, (B) TenCell culture wells and placed in the TenCell-1 bioreactor.

## 5.4. Results

### 5.4.1. Properties of TenCell-1 bioreactor

#### 5.4.1.1. Temperature profile of the TenCell-1 bioreactor

In initial studies, it was found that the temperature controller in the TenCell-1 bioreactor was malfunctioning. There were also issues with the calibration of the displacement arms attached to the servo-controlled actuator. The TenCell-1 rig was then repaired in School of Mechanical Engineering, University of Leeds. The arms were calibrated, the TenCell culture wells and inserts were electropolished and the heating rods, temperature controller and the silicon rings of the Perspex lid and the chamber were replaced. Following this, the temperature profile of the TenCell-1 bioreactor was determined, and found to be stable at 37 $^0$C after 90 min heating [Figure 5.16].
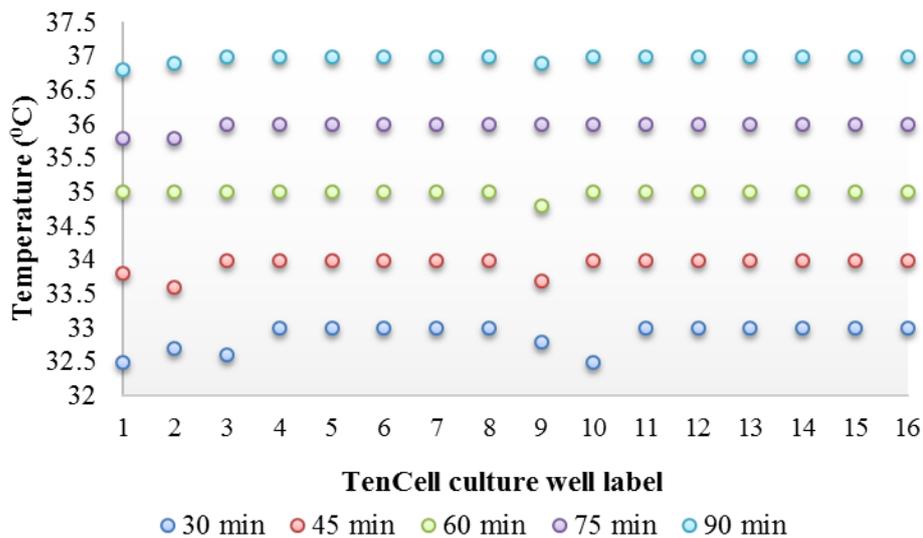


**Figure 5.16 Temperature profile of TenCell-1 rig.** All TenCell culture wells (16 culture wells) were all filled with PBS solution and the temperature was measured each 30 minutes until they reached a stable temperature for cell culture (37$^0$C).

The temperature of the PBS in each TenCell culture well increased gradually without exceeding the target temperature. The PBS temperature in all of the wells was 36.8 – 37 $^0$C.

**5.4.1.2. Determination of culture medium volume in the TenCell culture wells**

A series of culture medium volume: 4, 5, 6 and 7 mL were investigated for their medium depth in the TenCell culture wells. The results are presented in Figure 5.17.
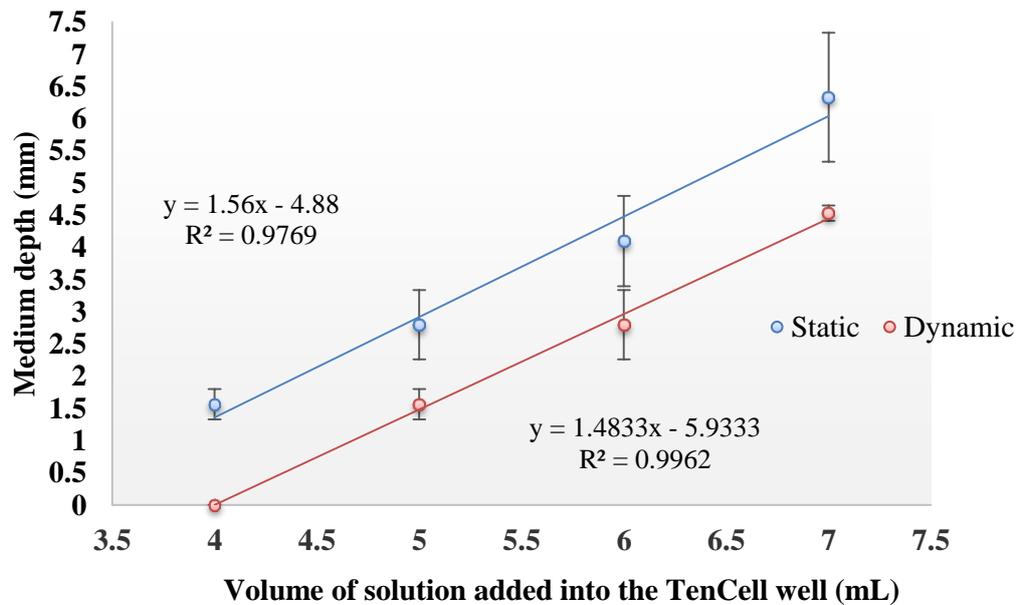


**Figure 5.17 Relationship between the culture medium volume to its depth in TenCell culture well with decellularised PPT scaffold mounted in each well**. Data was presented as mean (n=3) ± 95 % Cl.

The medium depth was found to be linear to its volume, in both static ($R^2$ = 0.977) and dynamic ($R^2$ = 0.996) wells. The differences of the medium depth found in all wells observed between the static and dynamic groups, were about 1.2 – 1.5 mm. Figure 5.17 shows that using 5 mL of culture medium in the TenCell culture wells had created an optimum medium depth in the static group, while in the dynamic group, the medium was relatively flooded over the scaffolds. In contrast, the 4 mL culture medium had the scaffolds of the dynamic group exposed to the air, while the 6 mL had the static scaffolds submerged. This results of this finding was to use 5 mL of culture medium to incubate cell-seeded decellularised PPT scaffolds in the TenCell culture wells.

**5.4.1.3. Determination of the evaporation rate of the TenCell culture wells**

All TenCell culture wells (n=12) were initially loaded with 5 mL of culture medium, and the reservoir wells (n=4) were loaded with 5 mL of PBS. The volume of culture medium remaining in each well was measured after 3 days of operation of the TenCell-1 bioreactor.

After 3 x 24 h of operation, the volume of culture medium remaining in the wells was $3.82 \pm 0.1$ mL (mean $\pm$ 95% Cl). The evaporation rate was estimated to be about 217.9 μL per $cm^2$ per day. This indicated that 0.39 mL of medium (7.8 %) was lost per day. The result of this finding was to change the culture medium in the TenCell culture well every two days.

## 5.4.2. Preparation of decellularised PPT scaffolds of the appropriate size for studies in TenCell

Each full sized decellularised PPT generated some 4 to 5 decellularised PPT scaffolds with a size of 20 x 10 x 0.6 -0.8 $mm^3$. This is illustrated in Figure 5.18.



**Figure 5.18 Preparation of decellularised PPT scaffolds at the appropriate size** (20 x 10 x 0.6 -0.8 $mm^3$) in the preconditioning plate.

**5.4.2.1. Characterisation of the prepared decellularised PPT scaffolds; sterility test**

All samples showed no growth in the nutrient broth medium and the Nutrient agar, fresh blood agar plates and Sabouraud dextrose agar plates after 7-days incubation at 37 $^0$C.

## 5.4.2.2. Contact biocompatibility of decellularised PPT scaffold

The contact biocompatibility assay using the post conditioned decellularised PPT scaffolds porcine and human BM-MSCs showed that the decellularised PPT scaffolds was nontoxic and biocompatible to the porcine and human BM-MSCs. Porcine BM-MSCs were seen to grow up to and into the sample [Figure 5. 19 A, B]. The cellular morphology of the porcine BM-MSC incubated with decellularised PPT scaffolds was similar to the negative control [Figure 5. 19 C, D] and to the cultures of porcine MSCs only [Figure 5. 19 E, F]. In the positive control of cyanoacrylate, cells were dead [Figure 5. 19 G] and were washed away after the Giemsa staining [Figure 5. 19 H].
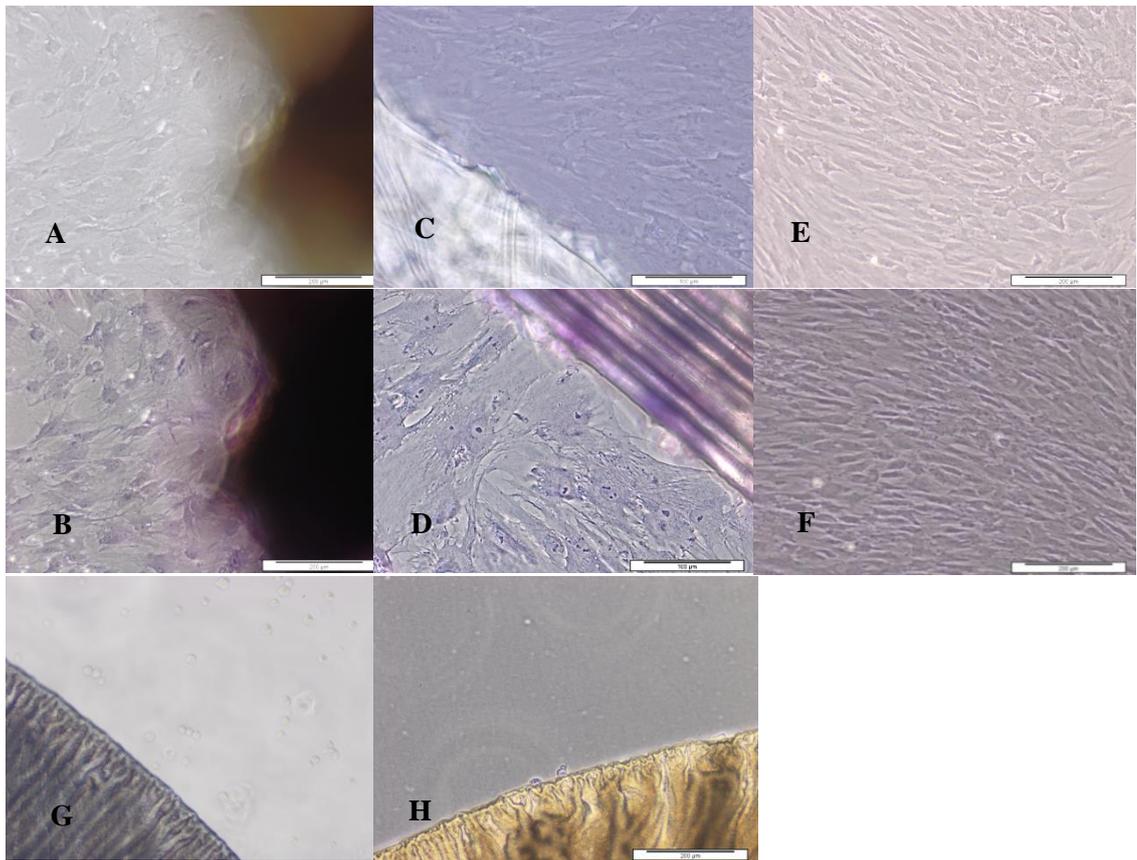


**Figure 5.19 Contact biocompatibility assay of decellularised PPT scaffold with porcine BM-MSC**. (A, B) Conditioned tendon, (C, D) negative control, (E, F) cells only, (G, H) positive control. A, C, E, G images were captured prior to staining and B, D, F, H were captured after Giemsa staining. Images were taken at 200x magnification. Scale bars represent 200 μm.

Human BM-MSCs grew up to and into the decellularised PPT scaffolds [Figure 5.20 A, B], and showed no difference in cellular morphology to the negative control [Figure 5.20 C, D]; before and after Giemsa staining. In contrast, in the positive control, most cells were dead and floating [Figure 5.20 G], and no cells remained on the plate after Giemsa staining [Figure 5.20 H].
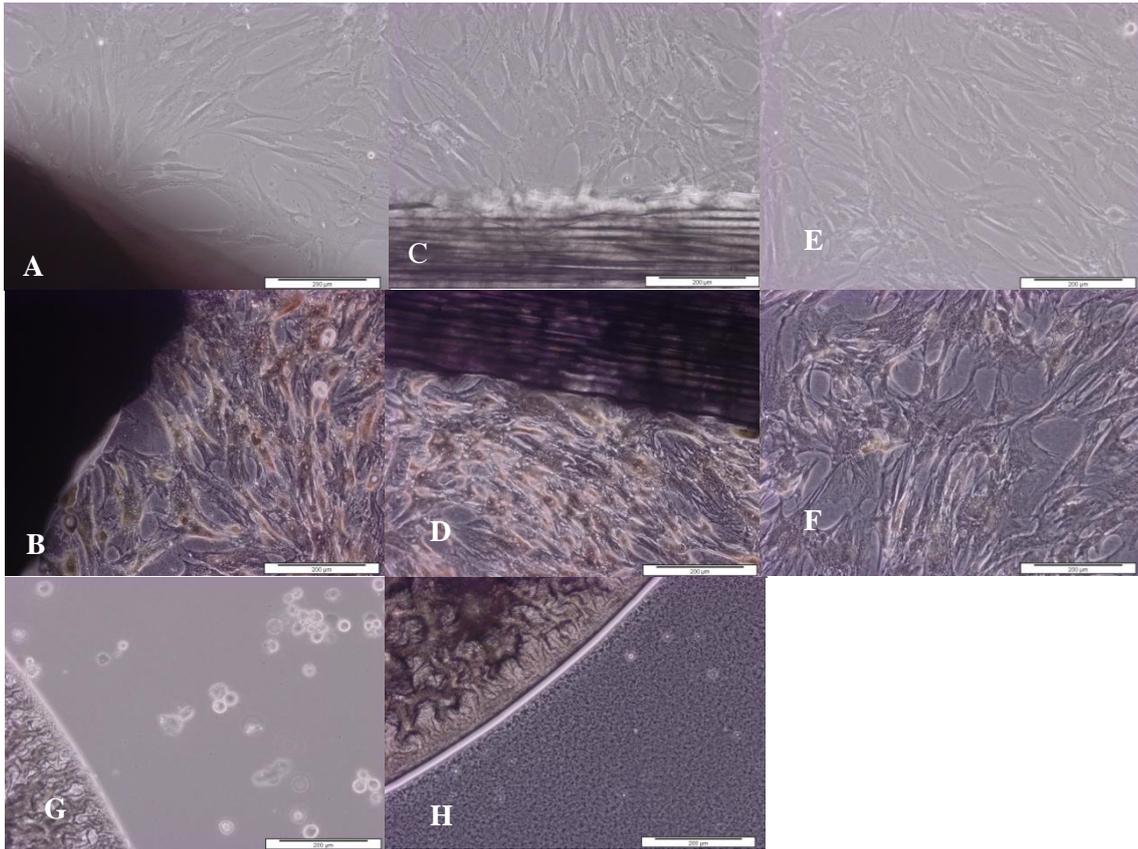


**Figure 5.20 Contact biocompatibility assay of decellularised PPT scaffolds with human BM-MSCs**. (A, B) Conditioned samples, (C, D) negative control, (E, F) cells only, and (G, H) positive control. A, C, E, G were imaged prior to staining and B, D, F, H were imaged after Giemsa staining. Images were captured at 200x magnification. Scale bars represent 200 µm.

### 5.4.2.3. Decellularised PPT scaffold resistance to cyclic uniaxial tensile strain of 8 % at 1 Hz for 4 hours

All decellularised PPT scaffolds (n=4) were found to be resistant to the cyclic strains at 8 % displacement (0.87 mm), 1 Hz for 4 h at 37 $^0$C. This finding had confirmed the feasibility of studying cell-seeded scaffolds using TenCell-1 bioreactor.

### 5.4.3. Biomechanical testing of the decellularised PPT scaffolds

Six samples of decellularised PPT scaffolds (20 x 10 x 0.6 – 0.8 mm$^3$) prepared from decellularised PPTs batch (5) were analysed for their biomechanical properties by uniaxial tensile testing. The stress-strain curves are presented in Figure 5.21.
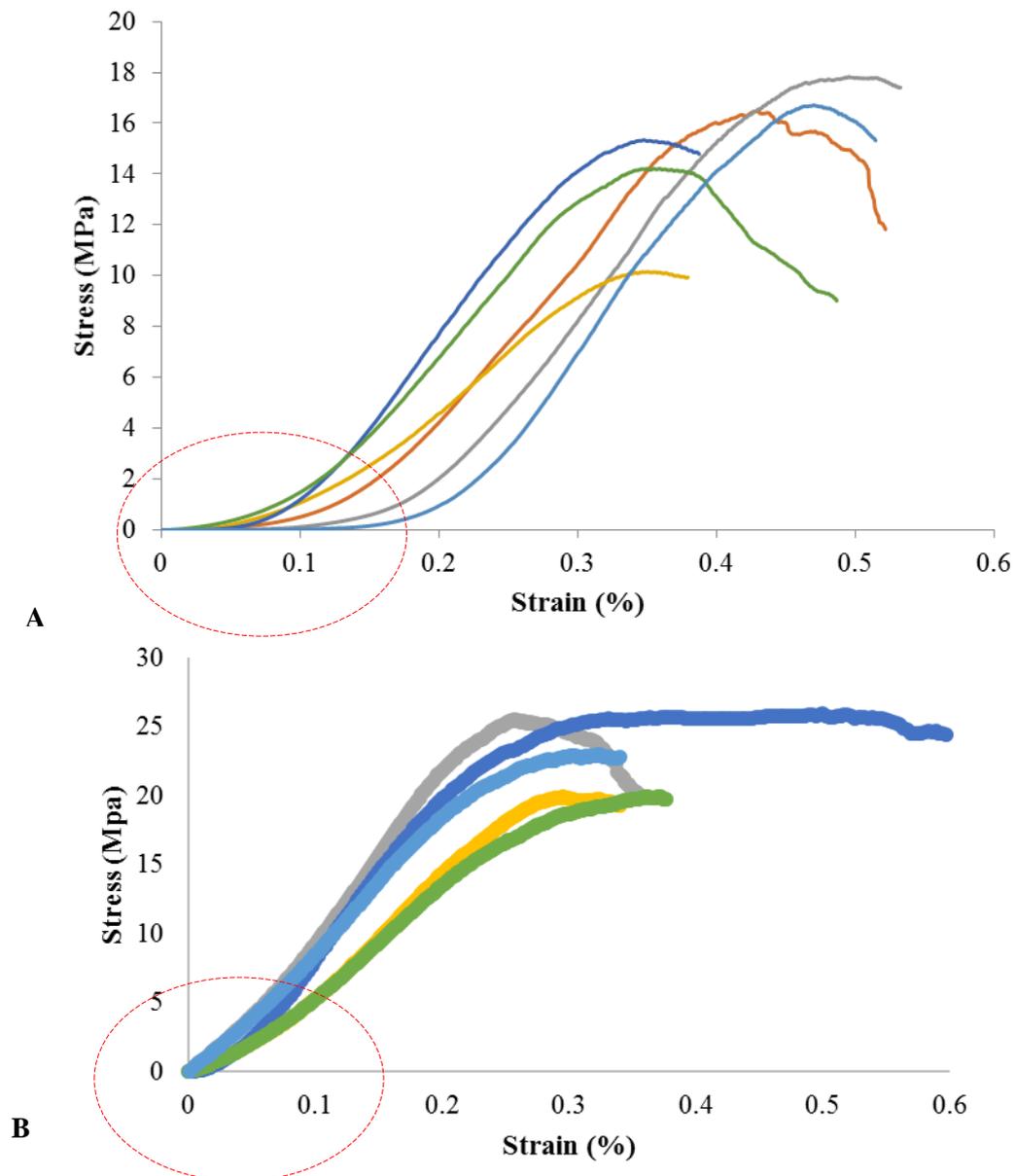


**Figure 5.21 Stress-strain curves of decellularised PPT scaffolds and native porcine PTs subject to uniaxial tensile testing,** (A) decellularised and (B) the native porcine PT scaffolds. The dashed-red circles are to highlight the toe region.

The majority of the biomechanical parameters derived from the stress-strain curves were not significantly different when the decellularised and native porcine PTs were compared using the Student's t-test [Figure 5.22]. However, the elastin phase slope for the decellularised PPT scaffolds (1.86 ± 2.13 MPa) was significantly lower compared to the native tendons (26.76 ± 16.82 MPa; p=0.017) [Figure 5.22 D].
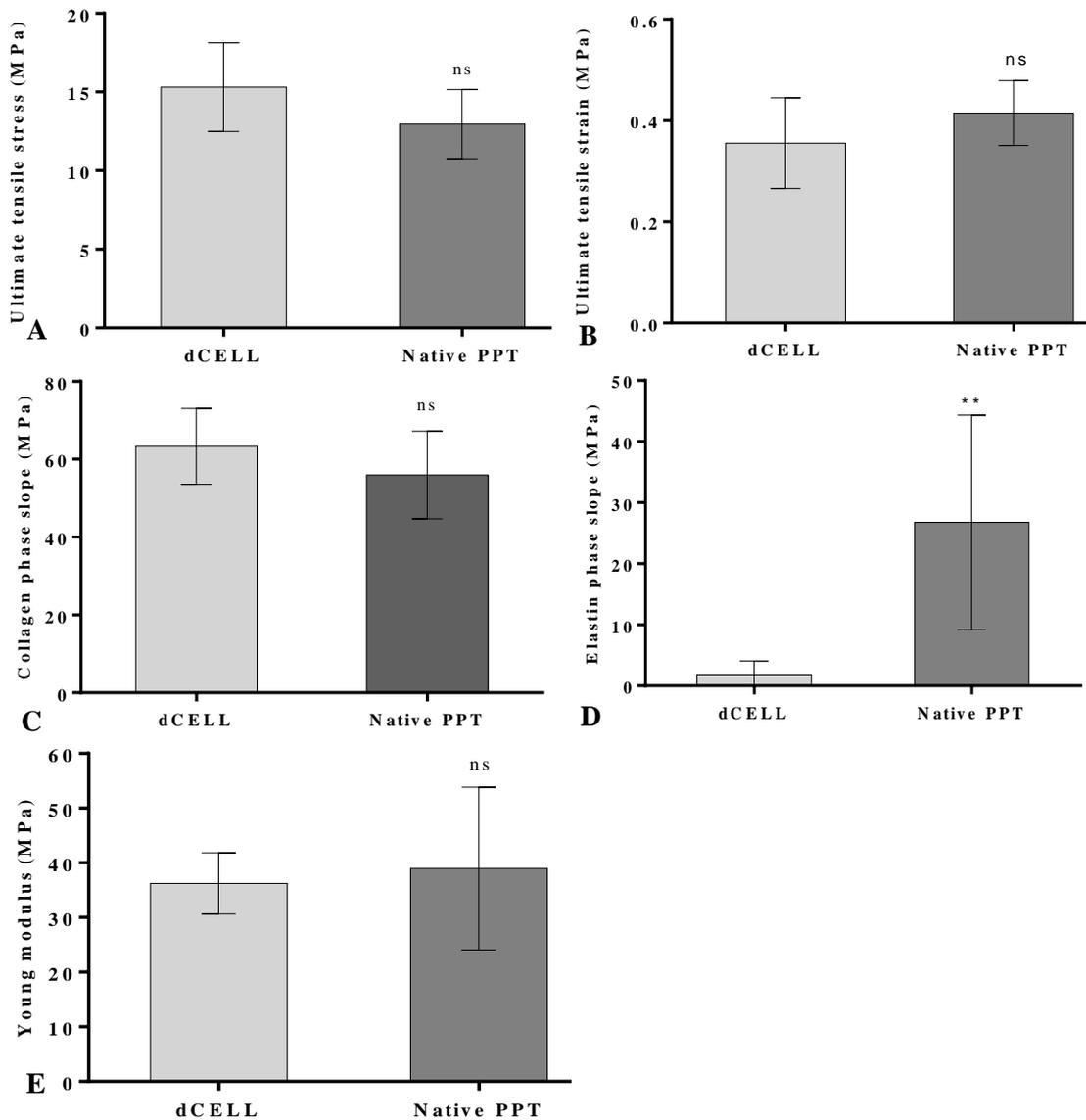


**Figure 5.22 Biomechanical parameters of the decellularised PPT scaffolds compared to the native tendons.** (A) UTStress, (B) UTStrain, (C) collagen slope slope, (D) elastin slope and (D) Young's modulus. Data is presented as the mean (n=6) ± 95% Cl. ** indicates significantly different (p<0.05).

## 5.4.4. Determination of method for seeding porcine BM-MSCs onto decellularised PPT scaffolds

### 5.4.4.1. Viability of cells on the decelularised porcine PT scaffolds seeded using direct seeding method

The images of Live/Dead assay of the porcine BM-MSCs ($0.5 \times 10^5$ cells.cm$^{-2}$) seeded onto decellularised PPT scaffolds using direct seeding method had showed that the cells were successfully attached to the scaffolds after 4 h [Figure 5.23 A], 6 h [Figure 5.23 B] and 12 h [Figure 5.23 C] seeding incubations. The viable porcine BM-MSCs seeded onto decellularised PPT scaffolds were quantified using ImageJ software and presented in Figure 5.24, Figure 5.25 and Figure 5.26.
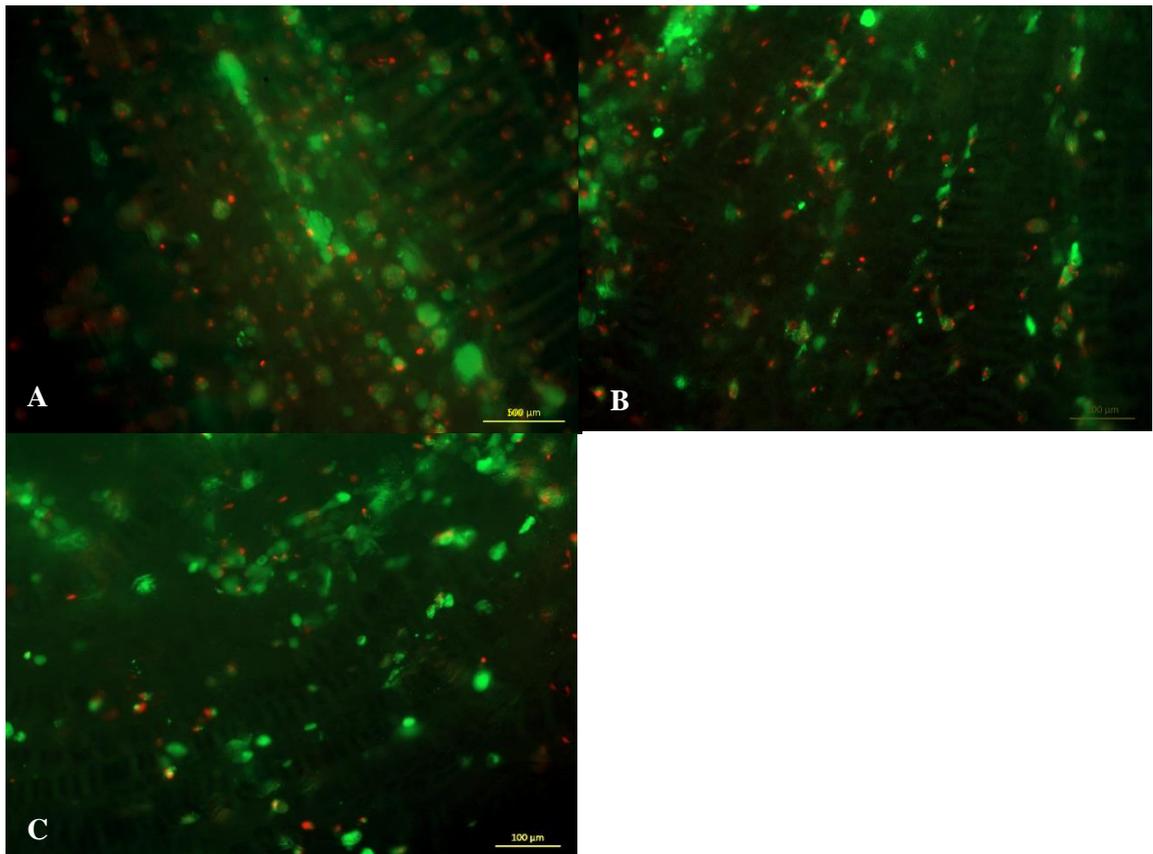


**Figure 5.23 Live/Dead assay of porcine BM-MSCs (p5) seeded onto the decellularised PPT scaffolds using direct seeding methods,** and incubated for (A) 4 h, (B) 6 h and (C) 12 h. Images were captured using fluorescence microscope at 50x magnification. Scale bars represent 200 µm.
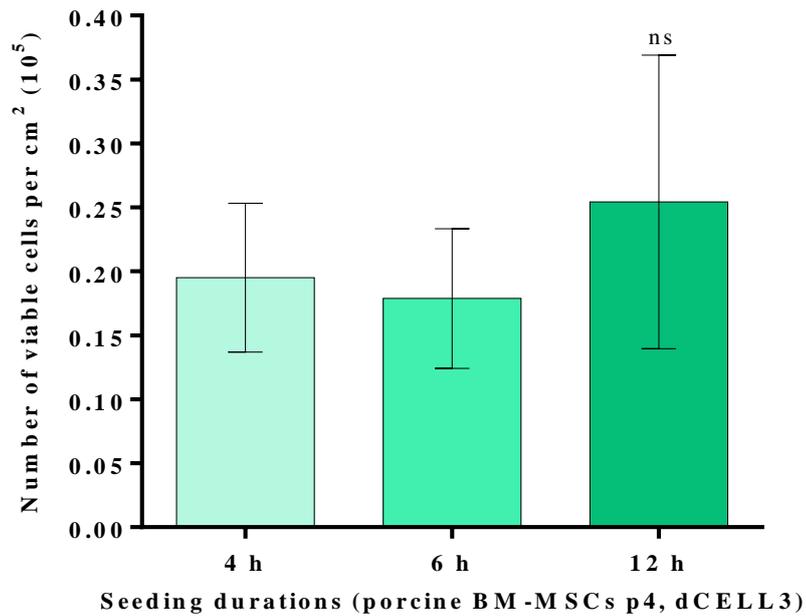
**Figure 5.24 Number of viable porcine BM-MSCs (1 x 10$^5$) per cm$^{-2}$ per scaffold of the cell-seeded decellularised PPT scaffolds using direct seeding methods**. Data was analysed using one-way ANOVA, followed by Tukey's multiple comparisons test. Data is presented as the mean of viable cells (10$^5$) (n=3) ± 95 % Cl.
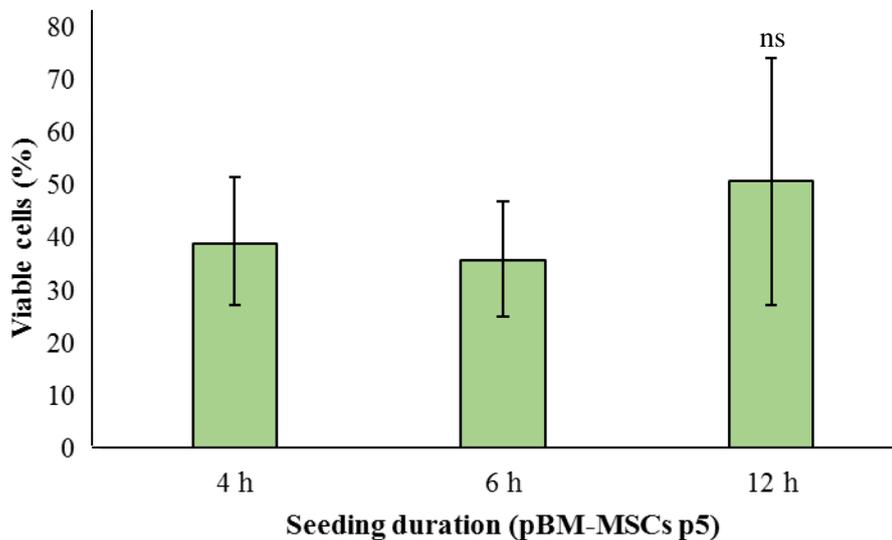


**Figure 5.25 Percentage of viable porcine BM-MSCs (1 x 10$^5$) per cm$^{-2}$ per scaffold of the cell-seeded decellularised PPT scaffolds using direct seeding methods.** Data was arcsine transformed and analysed using one-way ANOVA, followed by Tukey's test to determine the MSD (p<0.05) and presented as the mean (n=3) with 95 % Cl upper and lower limits.
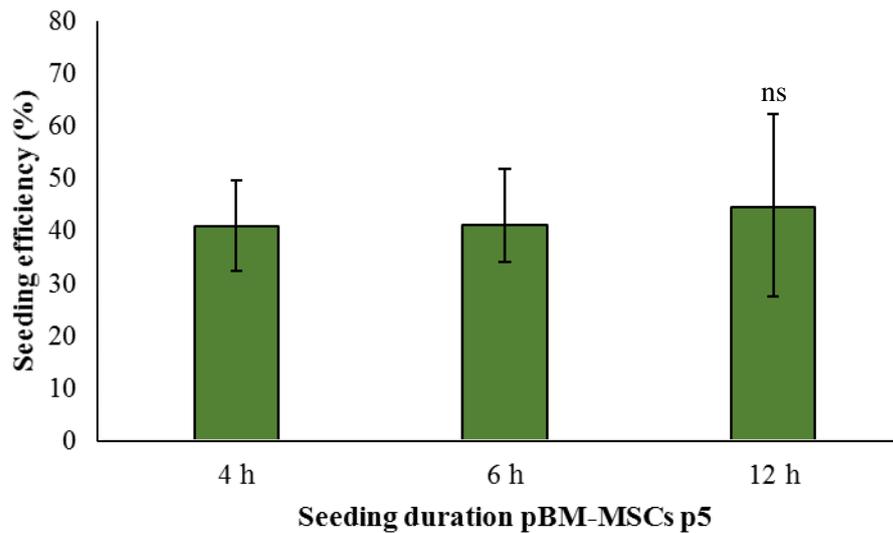
**Figure 5.26 Seeding efficiency of viable porcine BM-MSCs (1 x 10⁵) per cm⁻² per scaffold of the cell-seeded decellularised PPT scaffolds using direct seeding methods.** Data was arcsine-transformed and analysed using one-way ANOVA followed by Tukey's test to determine the MSD ($p<0.05$). T-test analysis was used to determine the differences between groups. Data was back-transformed for presentation with the mean (n=3) with 95 % Cl of upper and lower limits.

The seeding duration to incubate the porcine BM-MSCs-seeded onto the decellularised PPT had showed to have no effects to the number of viable cells ($p>0.05$), to the percentage of viable cells ($p>0.05$), and to the seeding efficiency ($p>0.05$).

**5.4.4.2. Viability of cells on the decellularised porcine PT scaffolds incubated in the cell suspension in a 6-well plate**

Images of the Live/Dead assay of the cells on the decellularised PPT scaffolds (n=3) after seeding using 3 mL of porcine BM-MSCs p3 ($3.0 \times 10^5$ cells per well) and 4-days incubation showed that few cells were present [Figure 5.27 A]. The number of viable cells found per scaffold was approximately $0.43 \pm 0.35 \times 10^5$ cells (mean (n=3) $\pm$ 95% Cl) [Figure 5.27 B], and the percentage of viable cells was 47 % (mean (n=3) $\pm$ 95% Cl) [Figure 5.27 C]. However, the seeding efficiency using this method was extremely low [Figure 5.27 D].

The seeding method using cell suspension had indicated that this technique was not efficient.
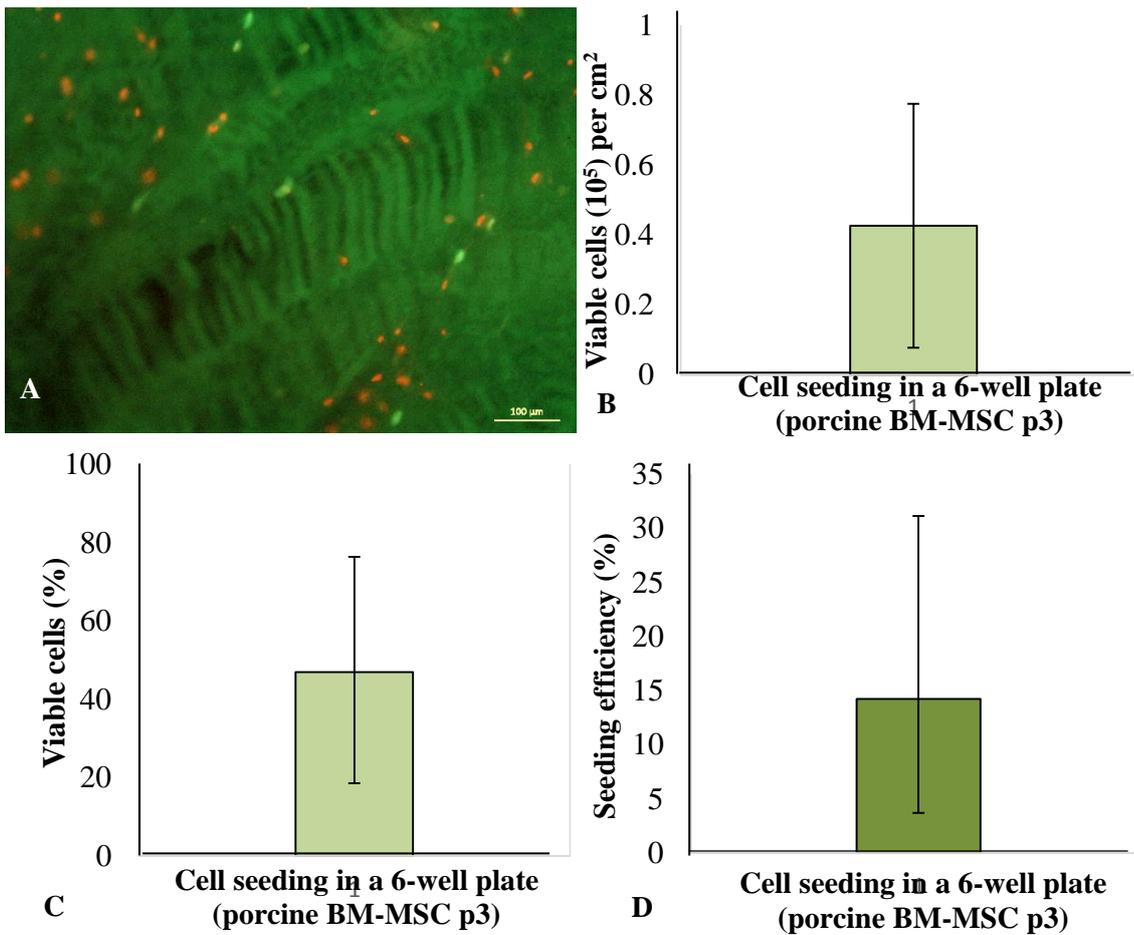
**Figure 5.27 Live/Dead assay of porcine BM-MSCs seeded onto decellularised PPT scaffolds in a cell suspension.** (A) Live/Dead image was captured at 100x magnification. Scale bar represent 200 μm. (B) The number of viable cells counted per $cm^{-2}$ per scaffold. (C) Percentage of viable cells per $cm^{-2}$ per scaffold and (D) the seeding efficiency per $cm^{-2}$ per scaffold. Data is presented as the mean (n=3) ± 95% Cl limits. Percentage data was arcsine transformed prior to calculation of the error bars and back transformed for presentation.

### 5.4.4.3. Viability of cells on the decelularised porcine PT scaffolds seeded for 6 h and 12 h using direct method; Live/Dead assay

This experiment was a repeated experiment from 5.4.4.2 to emphasis which seeding duration that optimum. Two time points of seeding duration were compared; 6 h [Figure 5.28 A] and 12 h [Figure 5.28 B]. Figure 5.28 shows that the viable cells had dominated in both groups.
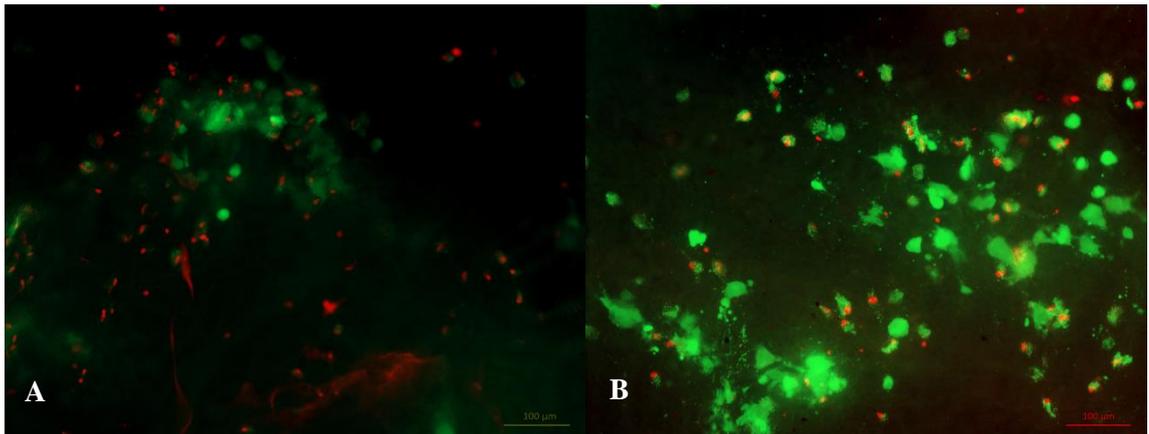
**Figure 5.28 Live/Dead assay of porcine BM-MSCs (p4) (0.5 x 10$^5$ cells.cm$^{-2}$) seeded onto decellularised PPT scaffolds for 6 and 12 h;** (A) 6 h and (B) 12 h seeding incubations. Images were taken at 50x magnification. Scale bars represent 200 µm.

The number of viable cells were quantified from the Live/Dead assay and presented in Figure 5.29, Figure 5.30 and Figure 5.31.
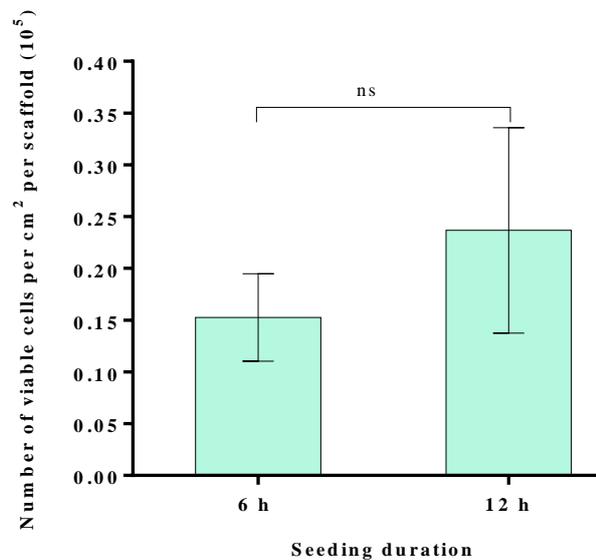


**Figure 5.29 Number of viable porcine BM-MSCs seeded onto decellularised PPT scaffolds for 6 and 12 h**. Data was analysed using Student-t test, presented as the mean (n=3) ± 95% Cl.
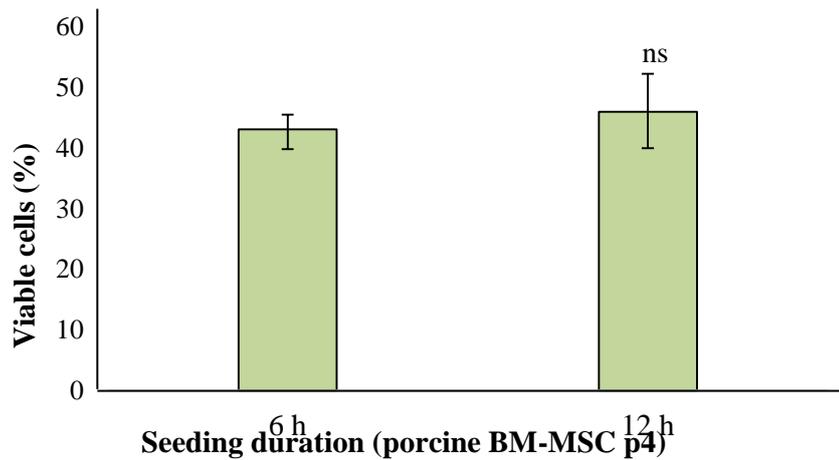
**Figure 5.30 Percentage of viable porcine BM-MSCs seeded onto decellularised PPT scaffolds for 6 and 12 h.** Data was arcsine-transformed for analysis using Student's t-test and back transformed for presentation with the mean (n=3) ± 95 % Cl upper and lower limits.
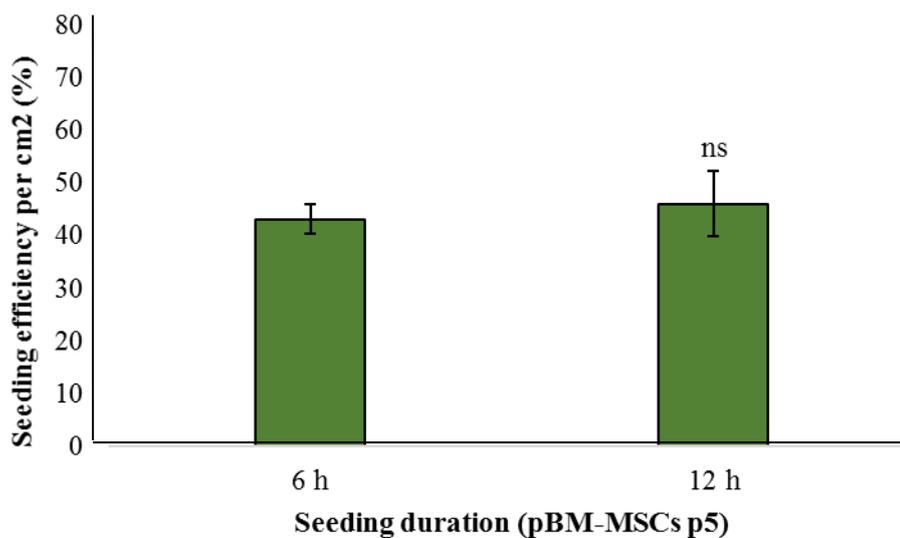


**Figure 5.31 Seeding efficiency (%) of porcine BM-MSCs seeded onto decellularised PPT scaffolds for 6 and 12 h.** Data was arcsine-transformed and analysed using Student t-test, then back transformed for presentation with the mean (n=3) ± 95 % Cl upper and lower limits.

There were no significantly differences of the number of viable cells [Figure 5.34], percentage of viable cells [Figure 5.35], and the seeding efficiency [Figure 5.36] when the porcine BM-MSCs were seeded onto the decellularised PPT scaffolds for 6 or 12 h.

### 5.4.4.4. RNA levels of porcine BM-MSCs seeded on decellularised PPT scaffolds for 6 and 12 h using direct method

The RNA analysis presented in this section was determined from the other half of the cell-seeded sample for which Live Dead analysis is presented in Section 5.4.4.3. Total RNA extracted from porcine BM-MSCs after seeded ($0.5 \times 10^5$ cells.cm$^{-2}$) on the decellularised PPT scaffolds for 6 h was $42 \pm 0.72$ ng.100 $\mu$L$^{-1}$ and 12 h was $126.3 \pm 0.4$ ng.100 $\mu$L$^{-1}$. Data is presented as the mean (n=3) $\pm$ 95 % Cl. The A260/280 ratio of the 6 h seeding incubation was $0.83 \pm 2.41$ and the 12 h was $1.86 \pm 0.07$. Data is presented as the mean (n=3) $\pm$ 95 % Cl. Total RNA extracted per scaffold analysed from both groups showed that the 12 h seeding incubation had higher total RNA compared to the 6 h incubation. Due to this finding, the subsequent experiments to incubate the decellularised porcine PT scaffolds after seeding were 12 h.

### 5.4.4.5. Viability of cells on the decelularised porcine PT scaffolds seeded for 12 h using direct method; ATPlite™ assay

The ATP levels of the porcine BM-MSCs ($0.5 \times 10^5$ cells.cm$^{-2}$) seeded for 12 h on the decellularised PPT scaffolds was $2.37 \pm 1.75 \times 10^6$ CPS (the mean (n=4) $\pm$ 95 % Cl) [Figure 5.37]. The ATP level of the cell-seeded scaffolds was significantly higher compared to the negative control (p=0.001).
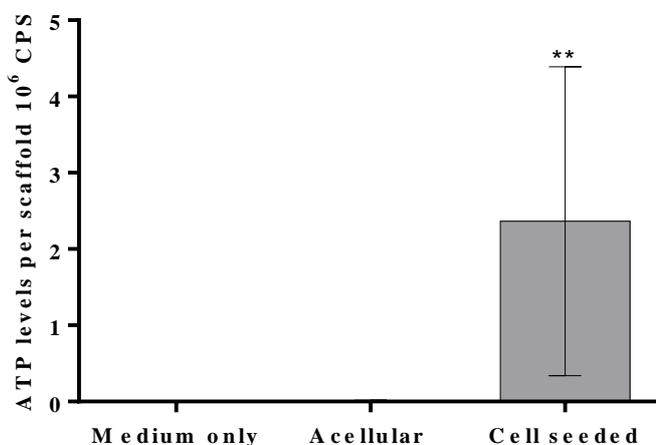


**Figure 5.32 ATP levels of porcine BM-MSCs seeded on decellularised PPT scaffolds after 12 h seeding incubation.** Data was analysed using one-way ANOVA, followed by Banferroni's multiple comparison test. Data is presented as the mean (n=4) $\pm$ 95 % Cl.

## 5.4.5. Seeding of human BM-MSCs on decellularised PPT scaffolds

Scaffolds were seeded for 12 h using direct method with $0.5 \times 10^5$, $1.0 \times 10^5$, and $2.0 \times 10^5$ cells.cm$^{-2}$ human BM-MSCs. The samples were cut into four quarters; one quarter for cell viability analysis using Live/Dead assay [Section 5.4.5.1], one quarter for ATPlite assay [Section 5.4.5.2] and one quarter for RNA extraction [Section 5.4.5.3].

## 5.4.5.1. Determination of appropriate number of human BM-MSC to seed onto the decellularised PPT scaffolds; Live/Dead assay

Scaffolds were seeded with $5 \times 10^4$, $1 \times 10^5$ and $2 \times 10^5$ cells.cm$^{-2}$ human BM MSC and incubated for 12 h. The cells on the scaffolds were assessed using Live/Dead staining. The results are shown in Figure 5.33.
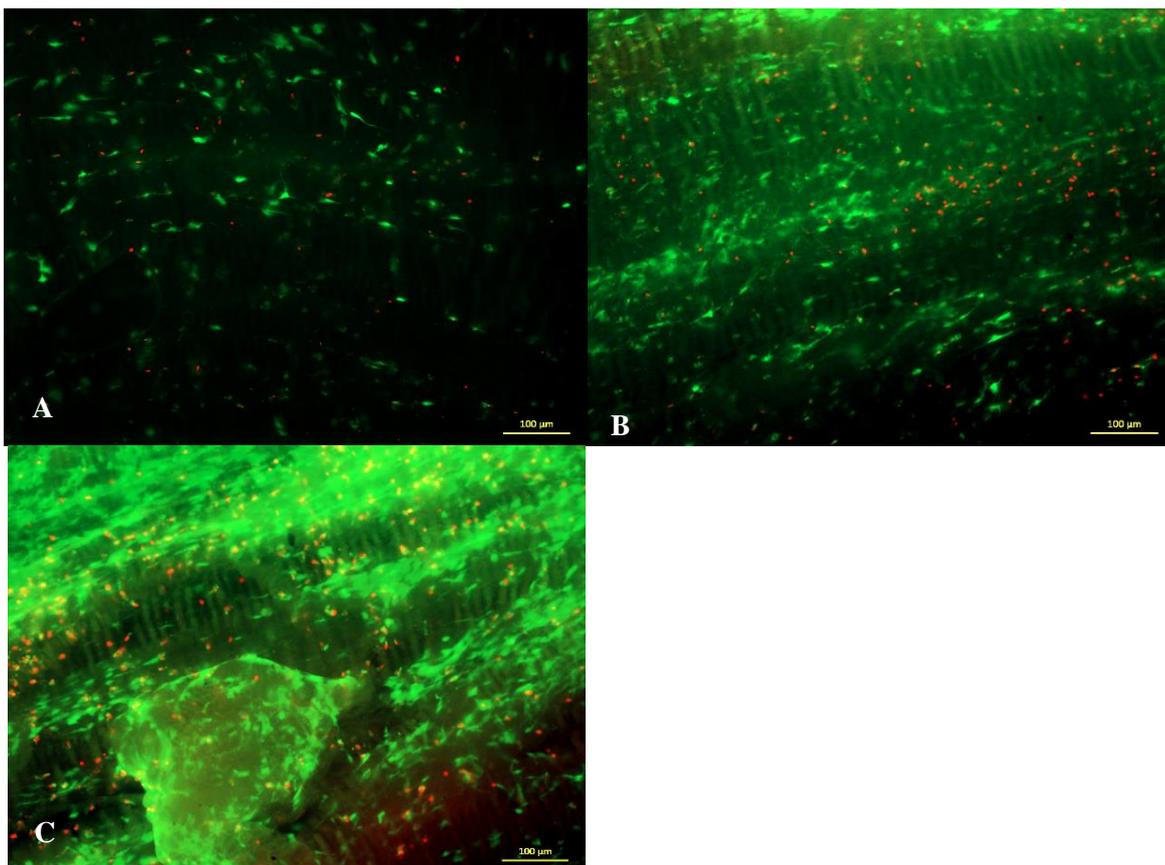


**Figure 5.33 Live/Dead staining of human BM-MSCs seeded on decellularised decellularised PPT scaffold in different seeding densities**. The images of the (A) $0.5 \times 10^5$ cells.cm$^{-2}$, (B) $1.0 \times 10^5$ cells.cm$^{-2}$, (C) $2.0 \times 10^5$ cells.cm$^{-2}$ taken at 50 x magnification. Scale bars represent 200 μm.

When seeded at the highest cell density ($2.0 \times 10^5$ cells.cm$^{-2}$), the cells covered the scaffolds and aggregated [Figure 5.33 C]. When seeded at $0.5 \times 10^5$ cells.cm$^{-2}$, however, the cells were evenly dispersed across the scaffold [Figure 5.33 A]. The cells seeded at $1.0 \times 10^5$ cells.cm$^{-2}$ were not only evenly dispersed, however also had higher density [Figure 5.33 B]. The number of viable cells present was determined by cell counting.

The percentage of viable cells and the seeding efficiency were presented to determine the optimal cell density to seed human BM-MSCs onto decellularised PPT scaffolds. In this experiment, the percentage of viable cells was significantly higher when cells were seeded at $0.5 \times 10^5$ cells.cm$^{-2}$ ($p<0.05$) compared to cell-seeded at $1.0 \times 10^5$ cells.cm$^{-2}$ or $2.0 \times 10^5$ cells.cm$^{-2}$ [Figure 5.34].
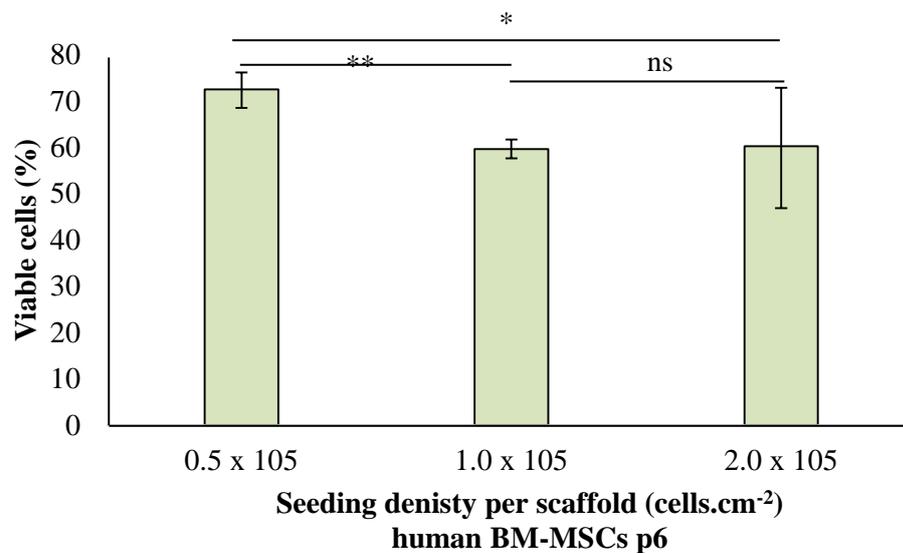


**Figure 5.34 Percentage of viable human BM-MSCs present when seeded for 12 h at different cell densities on decellularised PPT scaffolds.** Data is presented as the mean (n=3) ± 95 % Cl limit. Data was arcsine transformed prior to calculation and then back transformed for presentation. Data was analysed using one-way ANOVA followed by Tukey's test. (*) indicates p<0.05, (**) p<0.01.
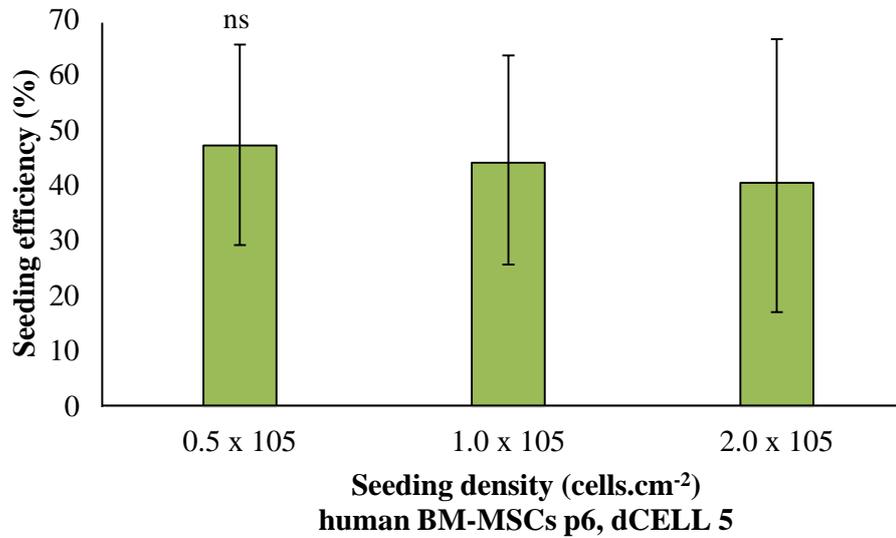
**Figure 5.35 Seeding efficiency of human BM-MSC seeded onto decellularised PPT scaffolds at different seeding densities.** Data was arcsine transformed and analysed by one-way ANOVA with Tukey's test. Data is presented as the mean (n=3) ± 95% Cl limit. Data was back-transformed for presentation.

There were no difference in seeding efficiency in all the seeding densities (p>0.05) [Figure 5.35].

**5.4.5.2. Determination of appropriate number of human BM-MSC to seed onto the decellularised PPT scaffolds; ATPlite™ assay**

The ATP levels of the human BM-MSCs seeded on decellularised PPT scaffolds were analysed and presented in Figure 5.36.

All groups were found to be significantly different to each other (p<0.001). This linearity had showed that the technique to isolate ATP from the cell-seeded decellularised PPT scaffolds was consistent.
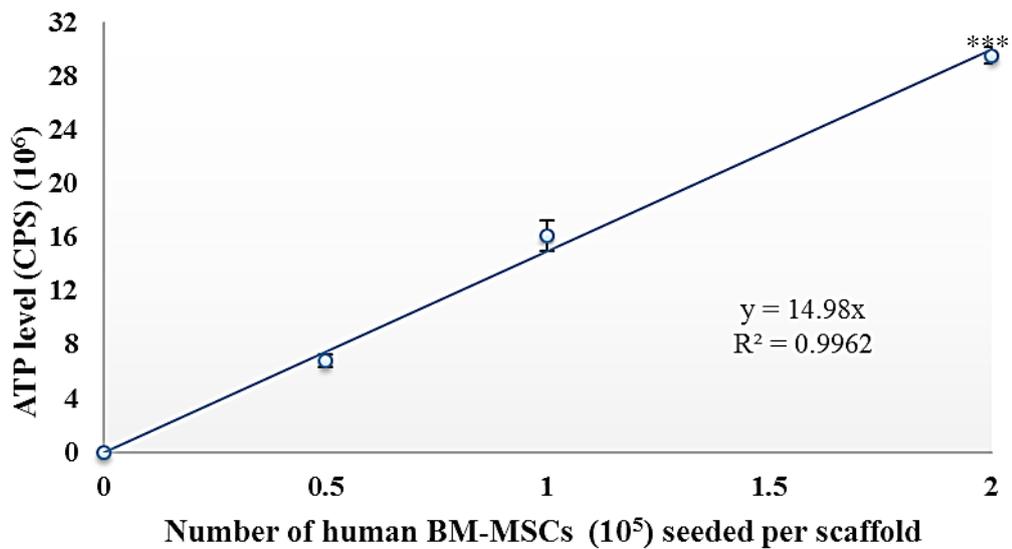
**Figure 5.36 ATP levels (CPS ($10^6$)) of human BM-MSC seeded on the decellularised PPT scaffolds at different seeding densities**. Data is presented as the mean (n=3) ± 95% Cl. Data was analysed using one-way ANOVA and Tukey's test. *** indicates p<0.001.

In the experiment to determine the optimum seeding density for human BM-MSCs, the cell viability assay had showed that different seeding densities had no effect to the seeding efficiency, although the percentage of viable cells was higher in the $0.5 \times 10^5$ cells.cm$^{-2}$, however the slide image of the Live/Dead assay of the $1.0 \times 10^5$ cells.cm$^{-2}$ showed a well dispersed cells sufficient and not too dense. Therefore, the following studies after this section used $1.0 \times 10^5$ cells.cm$^{-2}$ seeding density.

## 5.4.5.3. RNA levels extracted from human BM-MSCs seeded on decellularised PPT scaffolds for 12 h using direct method

RNA was extracted from human BM-MSCs seeded at $1.0 \times 10^5$ cells.cm$^{-2}$ on decellularised PPT scaffolds (n=4) in order to determine that sufficient RNA could be isolated for subsequent PCR analysis. The results indicated that RNA concentration of 30 µL total volume of elution was $6.27 \pm 1.67$ ng.µl$^{-1}$ (mean (n=4) ± 95 % Cl). The A260/280 ratio, the purity indicator of the RNA was $1.87 \pm 0.35$ (mean (n=4) ± 95% Cl). This had indicated that the protocol to extract RNA from human BM-MSCs with $1.0 \times 10^5$ cells.cm$^{-2}$ seeding density had generated sufficient RNA.

The elution of the RNA was amplified for the βactin transcript gene by real time PCR to investigate the efficacy of DNA digestion on column. Data was presented in Figure 5.37.
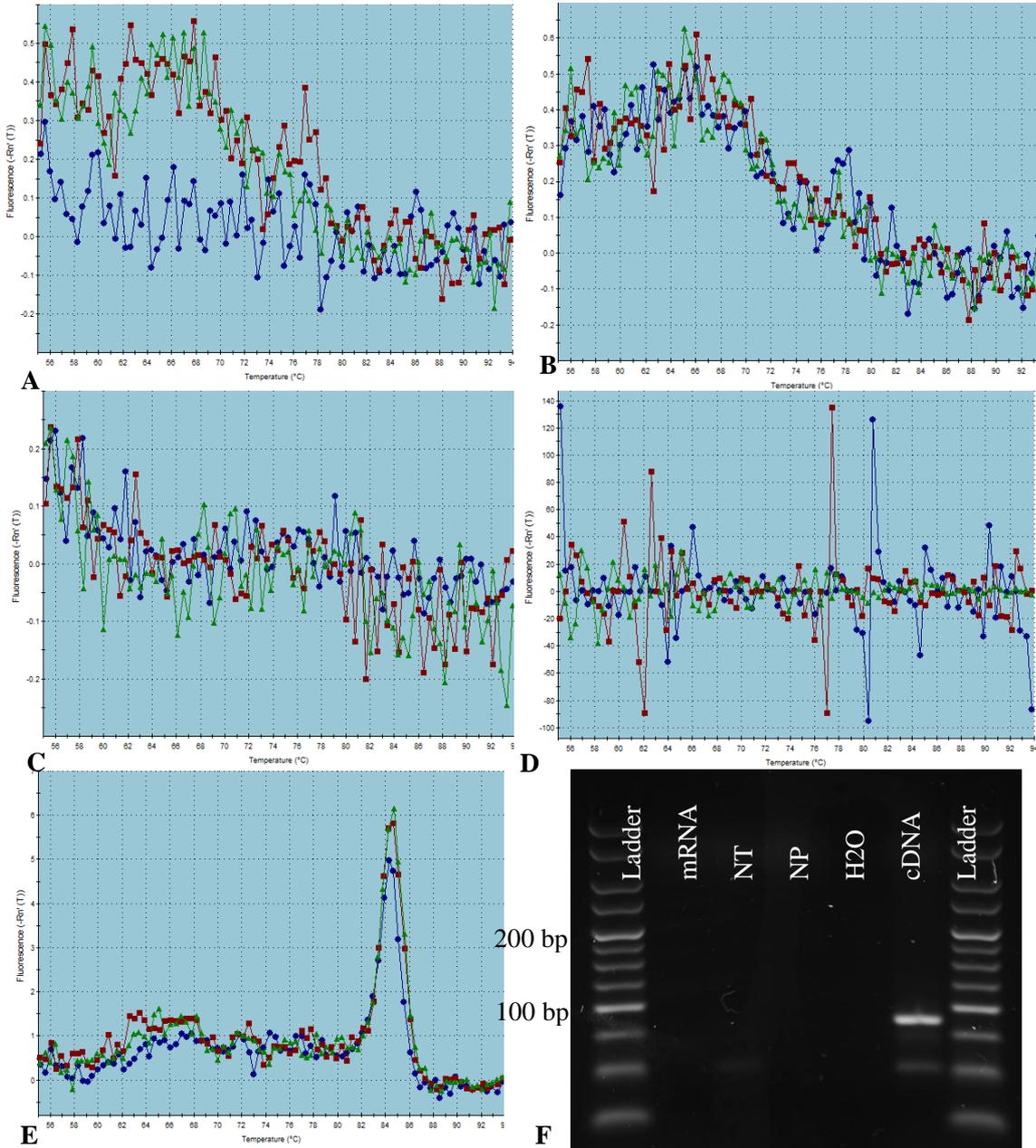


**Figure 5.37 Dissociation curve of the RT-PCR amplification of βactin gene** using template (A) RNA (B) primer only (C) template only (D) water control (E) the positive control; the cDNA of the tested RNA. (F) The DNA products of the βactin identified at 85 bp. No product was found in the amplification using RNA as the template, compared to the positive control (cDNA) and the negative controls.

The dissociation curves of the RT-PCR using βactin gene showed no product after amplification of RNA [Figure 5.37 A], however a product peak which melted at 84 $^0$C was found in the positive control (cDNA from the test RNA) [Figure 5.37 E]. No peaks were found in the sample without template [Figure 5.37 B], RNA template without primer [Figure 5.37 C] and water control [Figure 5.37 D]. A DNA band at 85 bp suspected to be the βactin gene was present upon gel electrophoresis of the amplified cDNA. No bands were present in the RNA sample or in all negative controls [Figure 5.42 F]. This had indicated that the RNA purification had successfully eliminated the genomic DNA using on column system.

## 5.4.6. Incubation of human BM-MSCs seeded on decellularised PPT scaffolds in a TenCell culture wells and TenCell-1 bioreactor

Human BM-MSCs were seeded onto decellularised PPT scaffolds and cultured in TenCell culture wells in the standard incubator, in TenCell wells in TenCell-1 bioreactor; with and without constraint or in a 6-well plate in order to determine whether the cells retained viability after 24 h of culture under different conditions.

Human BM-MSCs were analysed using the Live/Dead assay. The resulting images are presented images in Figure 5.43. The Live/Dead images showed that the human BM-MSC seeded onto decellularised PPT scaffolds and incubated in the standard incubator for 24 h had a greater density [Figure 5.43 B] compared to the other groups. There were no significant differences in the Live/Dead assay of the human BM-MSCs cultured under all conditions in the TenCell culture wells; with constraint [Figure 5.43 C, D] and without constraint [Figure 5.43 E, F], in the standard incubator or in the TenCell-1 bioreactor, respectively.
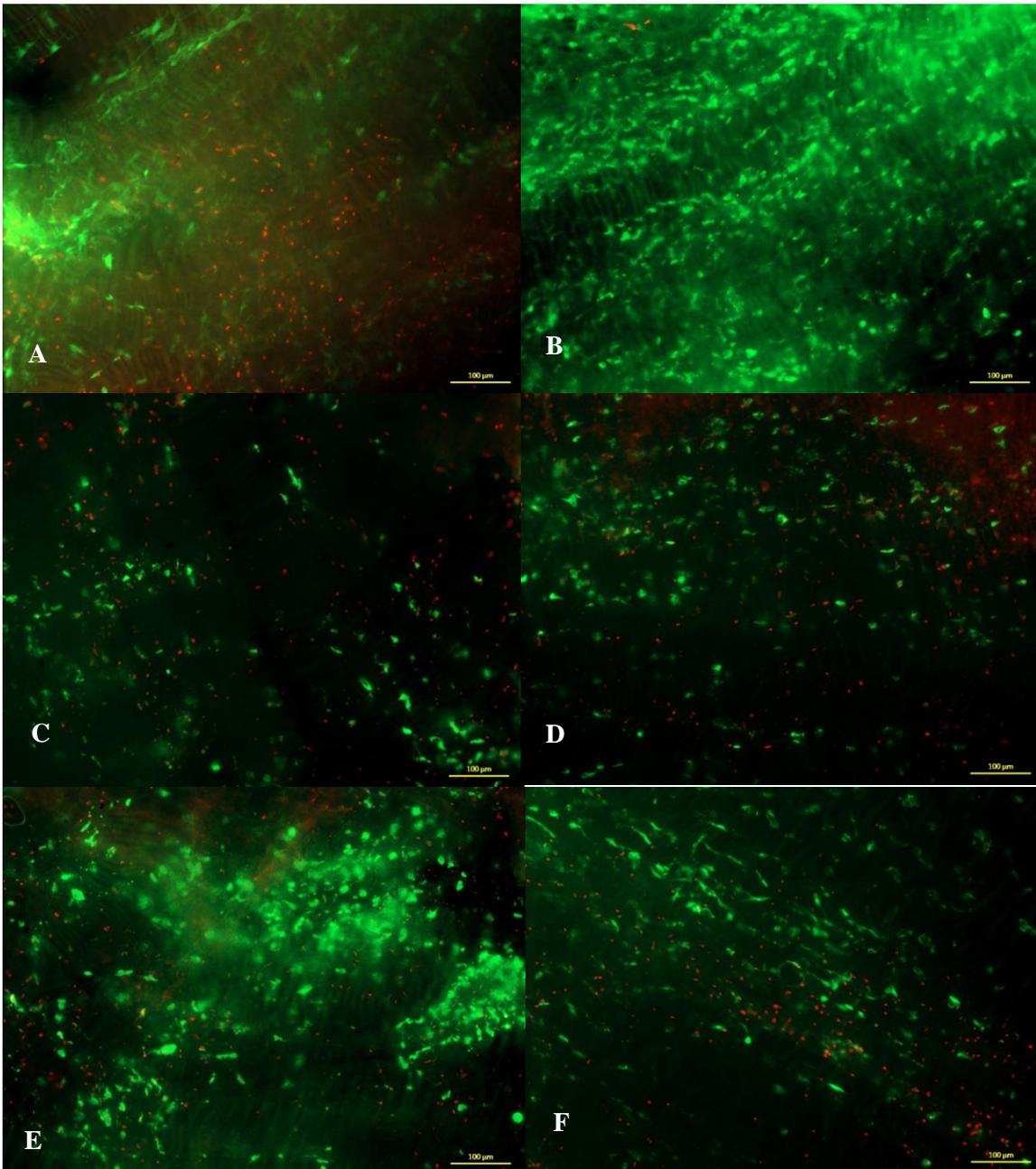
**Figure 5.38 Live/Dead staining of the human BM-MSCs (p4) seeded onto decellularised PPT scaffolds after 24 h static incubation in different conditions.** The images of the (A) Time zero, (B) 6-well plate, (C) TenCell well with constraint in the standard incubator, (D) TenCell well without constraint in the standard incubator, (E) TenCell well in the TenCell-1 with constraint, and (F) TenCell well in the TenCell-1 without constraint. Images were capatured at 50x magnification. Scale bars represent 200 μm.

There were significantly more viable cells present on the scaffolds incubated in the standard incubator without constraint in 6-well plates than in any of the other conditions [Figure 5.39].
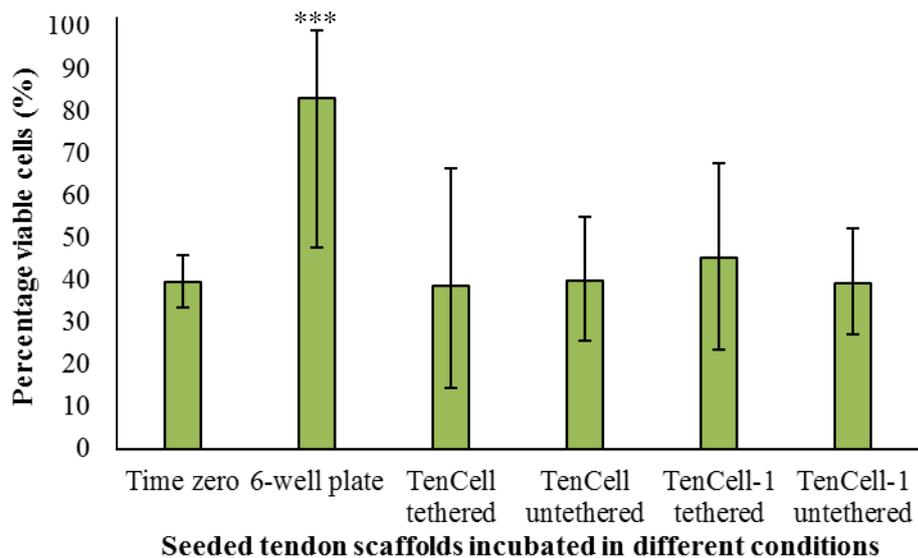
**Figure 5.39 Number of viable human BM-MSCs present on the decellularised PPT scaffolds after 24 h incubation under different conditions.** Data is presented as the mean (n=3) ± 95% Cl. Data was analysed using one-way ANOVA, followed by Tukey's test. *** indicates p <0.01.

The number of viable cells found among all samples incubated in TenCell wells with both constraint or without constraint culture conditions showed no differences (p>0.05). Samples incubated in the TenCell culture wells in both conditions also had no significantly difference to the T-0 group (p>0.05). However, samples incubated in the 6-well plate incubated in the standard incubator without constraint had the percentage of viable cells significantly higher compared to all other conditions (p<0.01) [Figure 5.39].

The ATP levels were also determined and it was found that the ATP levels of the samples incubated in the 6-well plate was $17.43 \pm 4.74 \ 10^6$ CPS (mean (n=3) (± 95 %) Cl) were significantly higher compared to the other groups (p<0.0001). The ATP levels among all samples cultured in the TenCell wells with and without constraint, incubated in the TenCell-1 or standard incubator had no differences (p>0.999) [Figure 5.40].
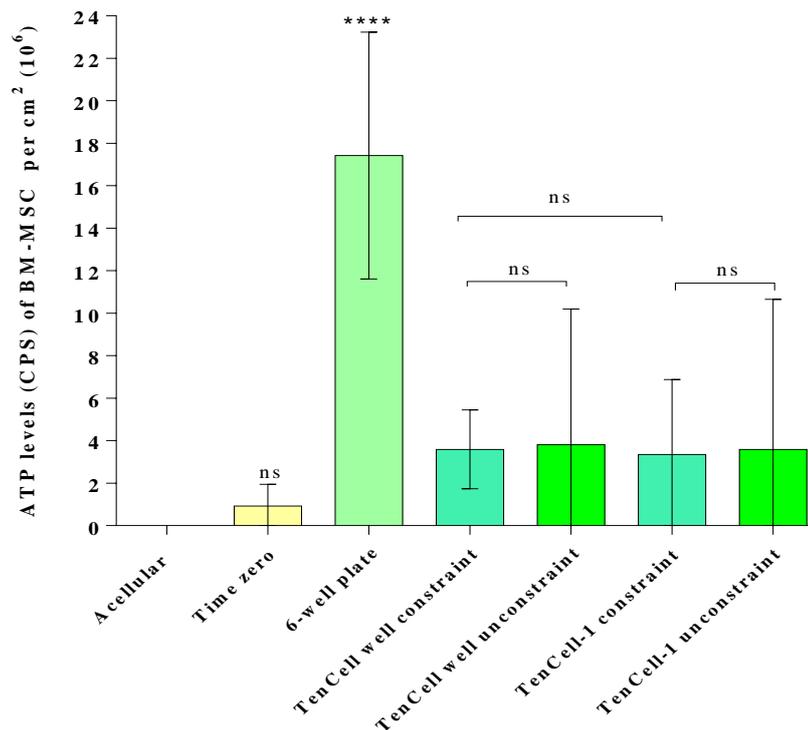
**Figure 5.40 ATP levels (CPS) of human BM-MSC present on the decellularised PPT scaffolds after 24 h incubation under different conditions.** Data is presented as the mean (n=3) ± 95% Cl. Data was analysed using one-way ANOVA, followed by Tukey's test.

This experiment showed that all samples of human BM-MSCs seeded on decellularised PPT scaffolds incubated in the TenCell wells and cultured for 24 h in static, with or without constraint, in the standard incubator or in the TenCell-1 bioreactor, had no significant differences in the percentage of viable cells and ATP levels. This indicated that the constraint incubation of the human BM-MSCs on the decellularised PPT scaffolds has no effects on cellular viability. All samples incubated in the TenCell culture wells showed that the performance of the TenCell-1 bioreactor was comparable to the standard incubator in terms of providing appropriate culture conditions. The exception was the culture wells; when a 6 well plate was used to culture the sample placed in a standard incubator, the cellular viability was significantly higher than all other groups.

This experiment confirmed that the constrained incubation conditions of human BM-MSCs seeded on decellularised PPT scaffolds in the TenCell culture well has no effect on cellular viability.

## 5.5. Discussion

Initial investigation of the performance of TenCell-1 bioreactor, which was used for culture of the BM-MSC seeded scaffolds, following maintenance of the bioreactor, showed the temperature control to be stable after 90 min. The rate of evaporation of water from the culture medium in the TenCell wells was determined to be about 0.39 mL per day. The information was needed to determine how often to replace the culture medium in the wells during longer-term incubations. It was concluded that the medium should be replaced every other day.

The planned use of the TenCell-1 bioreactor to study the differentiation of human BM MSC in response to cyclic tensile strain meant that the decellularised PPT scaffolds needed to be prepared in dimensions suitable for use in the rig (20 x 10 x 0.6 – 0.8 mm$^3$). The decellularised PPT scaffolds were successfully prepared using a robust protocol that produced scaffolds which fitted consistently in the TenCell culture wells, whist remaining sterile and biocompatible with porcine and human BM-MSCs. The scaffolds were also shown to resist 1 Hz cyclic strain at 8 % displacement for 4 h.

The decellularised PPT scaffolds were also shown to retain essential biomechanical properties when compared to the native tendon - the exception was the elastin phase slope, which was significantly reduced.  A strain limit of 5 % was used to determine the elastin phase slope of the stress strain curve (Yamamoto et al., 1999), a method which has been adopted for native fascicles. The decellularised PPT scaffolds showed a prolonged toe region above 0.05 strain. It is possible that the decellularised PPT scaffolds became swollen with fluid and that this increased the cross-sectional area and led to a reduction in viscous resistance (Glover, 2010). Also, it is possible that the swollen decellularised PPT scaffolds were slack during mounting on the clamps for the failure test, while this condition was not found in the native tendons. The major purpose of determining the biomechanical properties of the decellularised PPT was to enable any changes to the scaffold biomechanical properties resulting from cellular activity to be determined in subsequent studies, and this was achieved.

There were several approaches to precondition the scaffolds prior to cell seeding in order to prepare a cell-friendly microenvironment in the scaffold. Synthetic scaffolds need preconditioning step due to their lack of attachment factors, for example using RGD, fibronectin and super fibronectin to coat a poly(carbonate-urea)urethane for artery replacement (Rashid et al., 2004). Biological scaffolds such as tendons underwent simpler steps prior to seeding, such as hydrating the scaffolds using PBS solutions (Omae et al., 2009), or with culture medium for 3 h (Yazdani et al., 2009). In this chapter, tendon scaffolds were hydrated using complete culture medium (FBS 10% (v/v)) for 12 h, placed at 37 $^0$C and 5% (v/v) $CO_2$ in air.

All Live/Dead assays of the cell-seeded PPT scaffolds presented in this chapter showed cellular attachment to the decellularised PPT scaffold (porcine or human BM-MSC). An ATPlite™ assay was used to estimate cellular survival and proliferation by quantifying the ATP extracted from the metabolically active cells. This indicated that the production and preparation of the decellularised tendon scaffolds generated a cell receptive microenvironment. Tendon sheets (epitenon) were also removed during the scaffolds preparation, as they were reported to inhibit cellular infiltration during the seeding process (Chang, 2012).

In this study, there were no Live/Dead assay and no ATPlite assays of the native porcine PTs as the positive control. That was because the protocol developed to isolate the decellularised PPT scaffolds could not be applied to isolate a tissue with viable cells (native-viable PPTs), as this protocol needed 3 h in total to isolate the working size scaffolds, while the PPT had to be immersed in unheated PBS solution. This procedure will kill the cells in a native-viable PPT. However, if developing a new protocol to isolate a fresh porcine PTs, then comparing results from two different protocols would be difficult.

Porcine BM-MSCs were used to develop the seeding technique. Seeding rings were initially used to study the seeding method onto the decellularised PPT scaffolds. However, this technique had an efficiency of less than 40 % in all seeding durations, where the proportion of viable cells was found to be less than 30%, and no significant differences were detected between

any seeding durations. This technique resulted in low numbers of viable cells per cm$^{-2}$ per scaffold. The number of viable cells found in the 4 h, 6 h and 12 h samples, post seeding, using seeding rings, were $0.139 \pm 0.032$ x $10^5$ cells.cm$^{-2}$, $0.137 \pm 0.02$ x $10^5$ cells.cm$^{-2}$, $0.135 \pm 0.08$ x $10^5$ cells.cm$^{-2}$ (mean (n=3) $\pm$ 95 % C.l.) respectively. Leaking of the cell suspension during seeding was suspected of being the major cause of cell loss or cell death, due to dehydration. Seeding of the cells by incubating the tendon scaffolds individually with a cell suspension was also not favourable. The seeding was inefficient, as it needed 900,000 cells per construct, however only 14.24 % of viable cells were found per cm$^{-2}$ per scaffold. Hence it was concluded that the direct seeding method was the most practical and efficient, with a 12-h incubation. This approach generated the highest seeding efficiency and the largest number of viable cells on the scaffolds.

Cells respond to different microenvironment conditions by expressing transcript genes however, the expression might be transient. These expressions can be preserved and identified by immediately soaking the samples once isolated with RNA stabilisation solution (Bustin, 2002). RT-PCR is a sensitive method used to identify changes at the molecular level, by amplifying the expressions of a sparse amount of RNA to a detectable level. It is important to generate good quality mRNA for analysis (Bustin, 2002). The quantity of RNA (ng per total volume elution) isolated from the porcine BM-MSC ($0.5$ x $10^5$ cells.cm$^{-2}$) seeded on the decellularised PPT scaffolds was therefore investigated after 6 h and 12 h incubations, in order to determine if adequate levels of RNA were recoverable for molecular studies. The levels of RNA recovered were however extremely low and not consistent with either the number of cells seeded or the data from the Live/Dead assays. This indicated that the protocol used to extract RNA was inadequate to extract RNA from the cell-seeded decellularised PPT scaffolds. It could also have been due to the limitation of the NanoDrop ND-1000 spectrophotometer that had exceeded its lowest limit capability (2-3000 ng.$\mu$l$^{-1}$), as both RNA quantification and the A260/280 ratio had a broad deviation.

The protocol used followed the technical guidance of RNA handling for qPCR analysis (Bustin, 2000, Nolan et al., 2006). This included; (i) immersing the tissue sample in the RNAlater RNA stabilisation reagent to prevent RNA degradation, (ii) storing eluted RNA at -80 $^{0}$C, as mRNA is a very unstable molecule, and (iii) eliminating DNA on the column for 15 min, at room temperature. Prolonged DNase treatment can cause further RNA degradation during storage. The protocol, however, had a step to lyse the samples with rigorous agitation. This might had damage the RNA (Bustin et al., 2009, Huggett et al., 2013).

Therefore, an optimal method was used to extract RNA from human BM-MSC ($10^5$ cells.cm$^{-2}$) seeded onto decellularised PPT scaffolds; a lower proteinase K concentration (10 mAU.mL$^{-1}$) was used, and the protocol did not use rigorous agitation. In addition, to confirm the efficacy of DNA elimination on column, RT-qPCR was used to identify any genomic DNA contaminating the extracted RNA, and βactin was used as the transcript gene for amplification of the RNA template. Any DNA products were then visualised on agarose gel. Using these modifications to the process, it was shown that sufficient RNA (186 ± 50.1 ng in 30 μL$^{-1}$ RNA elution) (mean (n=4) ± 95 % Cl) was isolated from each cell-seeded scaffold, and the process successfully eliminated genomic DNA.

The optimal seeding density of human BM-MSCs was then determined by investigating three seeding densities (0.5 x $10^{-5}$, 1.0 x $10^{-5}$ and 2.0 x $10^{-5}$ cells.cm$^{-2}$). There were no differences in the seeding efficiency among different seeding densities however, the percentage of viable cells was significantly higher when cells were seeded at 0.5 x $10^{-5}$ cells.cm$^{-2}$ compared to other groups. It was decided to use a seeding density of 1.0 x $10^{-5}$ cells.cm$^{-2}$ for the human BM-MSCs in subsequent experiments because: (i) the cells were evenly dispersed across the scaffold, indicating that if they were incubated for 7 days would not become overcrowded, (ii) the amount of RNA extracted from scaffolds seeded at 0.5 x $10^{-5}$ cells.cm$^{-2}$ density would be insufficient for molecular analysis.

Before moving on to study the effects of cyclic tensile strain on the differentiation of the human BM-MSC seeded onto decellularised PPT scaffolds, it was necessary to determine if the culture medium conditions in TenCell retained cell viability when the scaffolds were constrained. The viability analysis of the human BM-MSCs seeded on the decellularised PPT scaffolds and incubated for 24 h in TenCell culture well, with or without constraint, in the TenCell-1 bioreactor or the standard incubator, showed no differences. However, the samples incubated in the 6-well plate were significantly higher in the percentage of viable cells and the ATP levels compared than the others. This may be because the 6-well plate is coated, while the TenCell culture well is reusable, being made from medical-grade stainless steel without coating. As the aim of this experiment was to see the effect of 24 h static-constraint incubation in the TenCell culture well to the cellular viability of the cell-seeded decellularised PPT scaffold and no correlation was found, therefore, this finding had fulfil the Null hypothesis; which is the viability of cells in the tendon scaffolds showed no significant differences when cultured with or without constraint after 24 h in TenCell culture well.

This chapter has established all the technical elements needed to study the effects of cyclic strain to human BM-MSCs when incubated in decellularised PPT scaffolds. The techniques are the preparation of the decellularised PPT scaffolds, seeding techniques and duration, seeding density, techniques to analyse the viability assays and to extract RNA, preparation and techniques for RT-qPCR, and the protocol to use the TenCell-1 bioreactor for long term culture. Therefore, the next chapter sets out to achieve the aim of the whole study.

## 5.6. Conclusions

1. The procedure to prepare decellularised PPT scaffolds for incubation in the TenCell-1 bioreactor maintained the scaffolds' sterility, biocompatibility, and the majority of their biomechanical properties.

2. Seeding technique using a direct method followed by 12 h seeding incubation was shown to be the most practical, and yielded the highest cellular viability.

3. Rigorous agitation during the tissue lysis of the cell-seeded scaffolds for RNA extraction impaired RNA quality and quantity.

4. The optimal cell density to seed human BM-MSCs onto decellularised PPT scaffolds was $1.0 \times 10^5$ cells.cm$^{-2}$ which generated a sufficient quantity of RNA for molecular analysis.

5. The viability of human BM-MSCs seeded onto decellularised PPT scaffolds was not affected by a static strain/ constraint incubation conditions in the TenCell culture well for 24 h.

6. Cell viability of the human BM-MSCs seeded onto decellularised PPT scaffolds and incubated in TenCell culture wells showed no difference from those incubated in the TenCell-1 bioreactor or the standard incubator.

# Chapter 6

# The effects of uniaxial tensile strain and the differentiation of human MSC seeded onto acellular porcine patella tendon scaffolds

## 6.1. Introduction

In the previous chapters, the production and characterisation of a decellularised PPT scaffold was described, human MSCs were characterised and methods for seeding human MSC onto the scaffold were developed. Methods were developed to enable extraction of sufficient quantities of RNA for molecular analysis, target genes were identified for determination using PCR and the methodology validated. It was also shown that MSCs seeded onto the scaffolds remained viable when loaded into the culture wells of TenCell-1.

All of the elements required to test the hypothesis that MSC would differentiate in response to cyclic tensile strain were in place. In this chapter, the response of human BM-MSCs to 4, 6 and 8 % cyclic tensile strain at a frequency of 1 Hz over 7-days was investigated. The effects of cyclic strain on cellular infiltration into the scaffold, cell proliferation, cell differentiation, ECM production and mechanical properties of the scaffolds were assessed.

## 6.2. Aim and objectives

The aim of this chapter was to investigate the effect of uniaxial cyclic tensile strain on the differentiation of human BM-MSCs seeded onto decellularised PPT scaffolds.

Objectives:

1. To culture human BM-MSC seeded decellularised PPT scaffolds in the TenCell-1 bioreactor under static conditions and under conditions of applied 4 %, 6 % or 8 % cyclic tensile strain at 1 Hz for 7 days.

2. To determine the effects of applying uniaxial tensile strain at 4, 6 and 8% at 1 Hz to human BM-MSC seeded onto decellularised PPT in culture on the infiltration of the cells into the scaffold, cell proliferation, gene expression, ECM production and biomechanical properties of the scaffolds in comparison to human BM-MSC seeded onto decellularised PPT in static culture.

## 6.3. Materials and methods

### 6.3.1. Materials

Decellularised PPT scaffolds were batch (6) (Chapter 3). Human BM-MSCs were at passage 4 (Chapter 4). The cell-seeded scaffolds were incubated in DMEM low glucose (1.0 g.L$^{-1}$) culture medium (Chapter 2; Section 2.2.3.1). The TenCell-1 bioreactor (Chapter 5; Section 5.3.2.1), fluorescence/ confocal microscopes (Chapter 6; Section 6.3.2.4), and Instron 3365 (Chapter 5; Section 5.3.3) have been described.

### 6.3.2. Method

The protocol for preparation of the decellularised PPT scaffolds is described in Chapter 5; Section 5.3.2. Preparation and set-up of the TenCell-1 bioreactor is described in Chapter 5; Section 5.3.1.2. The method used to seed the human BM-MSC onto the decellularised PPT scaffolds is described in Chapter 5; Section 5.3.4.2 or otherwise stated.

#### 6.3.2.1. Culture of human BM-MSC seeded decellularised PPT scaffolds in TenCell-1 bioreactor

For each cyclic tensile strain regimen to be tested (4%, 6% or 8%), there were three different groups of human BM-MSC seeded scaffolds: (i) one group at time zero (T-0; n=3); (ii) one group (n=6) incubated in the TenCell-1 bioreactor for 7 days with mechanical stimulation, and (iii) one group (n=6) incubated in the TenCell-1 bioreactor for 7 days without mechanical stimulation (static control). The biological and biomechanical properties of the cell-seeded scaffolds were immediately analysed after seeding (T-0) and after 7 days culture in TenCell-1 (dynamic and static). Thirty-three of the decellularised PPT scaffolds were prepared for each of the three experiments to be conducted at 4 %, 6% and 8% uniaxial tensile strain. Of these, 15 were seeded for 12 h with human BM-MSCs (p4) using 4 x 10 μL cell suspension (2.5 x 10$^6$ cells.mL$^{-1}$ ) using the direct method. The other half (15) were left unseeded (acellular) for use as

negative controls. The negative controls were allocated for the various assays as shown in Figure 6.1.
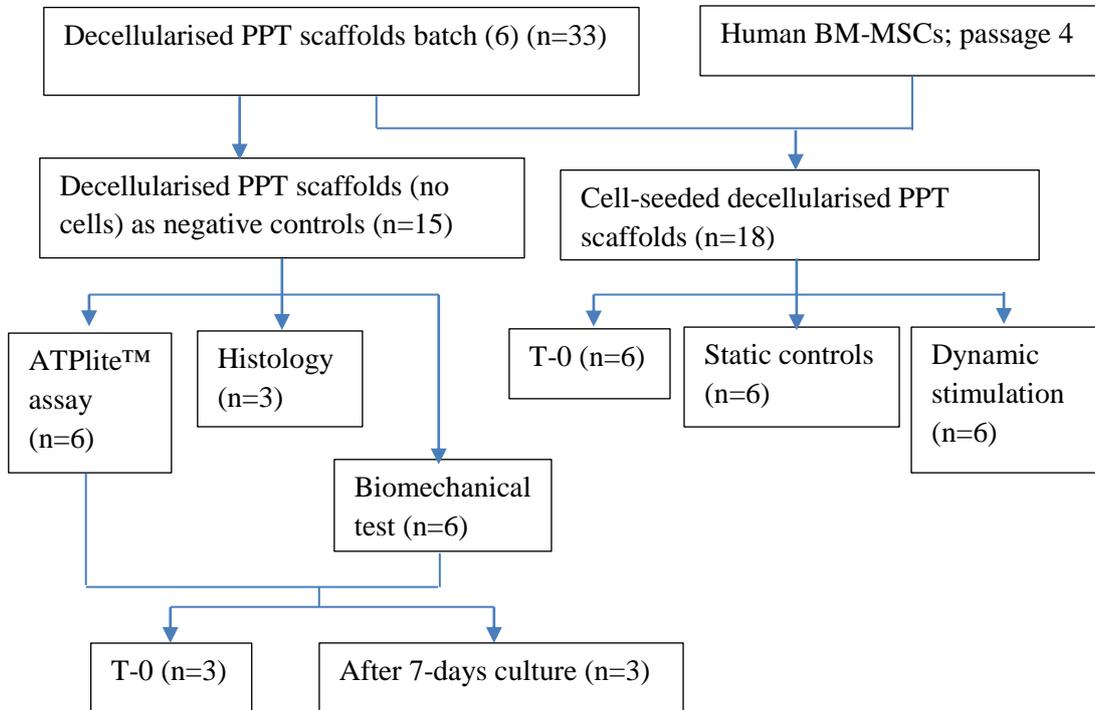


**Figure 6.1 Sample grouping for studies the incubation of human BM-MSCs seeded onto decellularised PPT scaffolds subject to uniaxial cyclic strain**.

The cell-seeded decellularised PPT scaffolds were mounted into the TenCell culture wells and placed in order in the Perspex chamber of the TenCell-1 bioreactor. The arms of the dynamic clamps of each well were fastened to the controlled-servo actuator. The day the samples were loaded into the TenCell-1 bioreactor was designed as Day 0. The amount of the displacement applied to the dynamic wells in TenCell-1 was calculated by using the engineering strain formula [Equation 2]. Sample length (distance between clamps) was constant at 10 mm, therefore 4 % strain was achieved by 0.42 mm displacement, 6 % strain by 0.64 mm displacement, and 8 % strain by 0.86 mm displacement. The cell-seeded decellularised PPT scaffolds were subject to mechanical stimulation each day; 14,400 cycles per day (4 h, 1 Hz; from 8 am to 12 pm), for 7 days (100,800 cycles in total). The culture medium was replaced every 48 h following the protocol described in the Section 6.3.2.2. A summary of the experimental approach is presented in Table 6.1.

| Day | Time | Working day | Activities |
|-----|------|-------------|------------|
| 1 | | Day -2 | Scaffold preconditioning |
| 2 | 08.00 | Day -1 | Cells seeded onto scaffolds; TenCell-1 preparations |
| 3 | 08.00 | Day 0 | Cells seeded scaffolds loaded into TenCell-1; 4 h mechanical stimulation (10.00). <br><br> Cell-seeded T-0 sample collection and analysis; <br><br>     a) culture medium for sterility test, <br><br>     b) samples for ATPlite™ assay <br><br>     c) samples for Live/Dead assay <br><br>     d) samples for RNA extraction <br><br>     e) samples for fixation for histology analysis |
| 4 | 10.00 | Day 1 | 4 h mechanical stimulation |
| 5 | 09.00 | Day 2 | Medium changed; 4 h mechanical stimulation (10.00) |
| 6 | 10.00 | Day 3 | 4 h mechanical stimulation |
| 7 | 09.00 | Day 4 | Medium changed; 4 h mechanical stimulation (10.00) |
| 8 | 10.00 | Day 5 | 4 h mechanical stimulation |
| 9 | 09.00 | Day 6 | Medium changed; 4 h mechanical stimulation (10.00) |
| 10 | 10.00 | Day 7 | 4 h mechanical stimulation |
| 11 | 10.00 | Tissue harvest | Sample collection and analysis; <br><br>     a) culture medium for sterility test, <br><br>     b) samples for ATPlite™ assay <br><br>     c) samples for Live/Dead assay <br><br>     d) samples for RNA extraction <br><br>     e) samples for fixation for histology analysis |
| 12 | Mechanical testing | | Samples analysed for biomechanical properties. |

**Table 6.1 Experimental timetable for studies of the effect of uniaxial tensile strain on human BM-MSC seeded decellularised PPT scaffolds**

## 6.3.2.2. Protocol for harvesting and processing of the T-0 samples

The T-0 samples (n=6) were prepared for analysis on Day 0. This required that each sample was divided into four portions as shown in Figure 6.2.
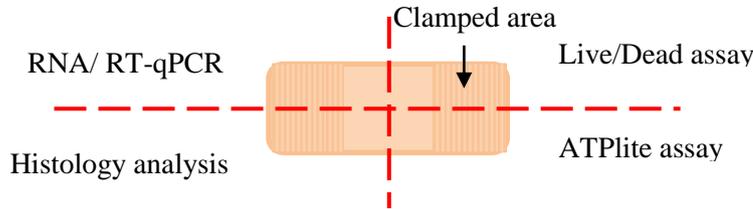


**Figure 6.2 Sampling of each cell-seeded decellularised PTT for analysis.** In order to perform all of the analyses, it was necessary to dvidie the scaffolds into four sections as shown. The shaded area is the dead/ clamped area and was not included in the analysis.

The sample was cut into four quarters and each quarter was proceeded for each analysis. Details of the techniques to collect the sample for analysis are described in Section 6.3.2.4 (Analysis method). It was necessary to carefully aliquot the samples into wells of pre-prepared plates in order to preserve the integrity of RNA, and perform the Live/dead and ATP assays immediately. The plates were prepared and samples aliquoted as shown in Figure 6.3.
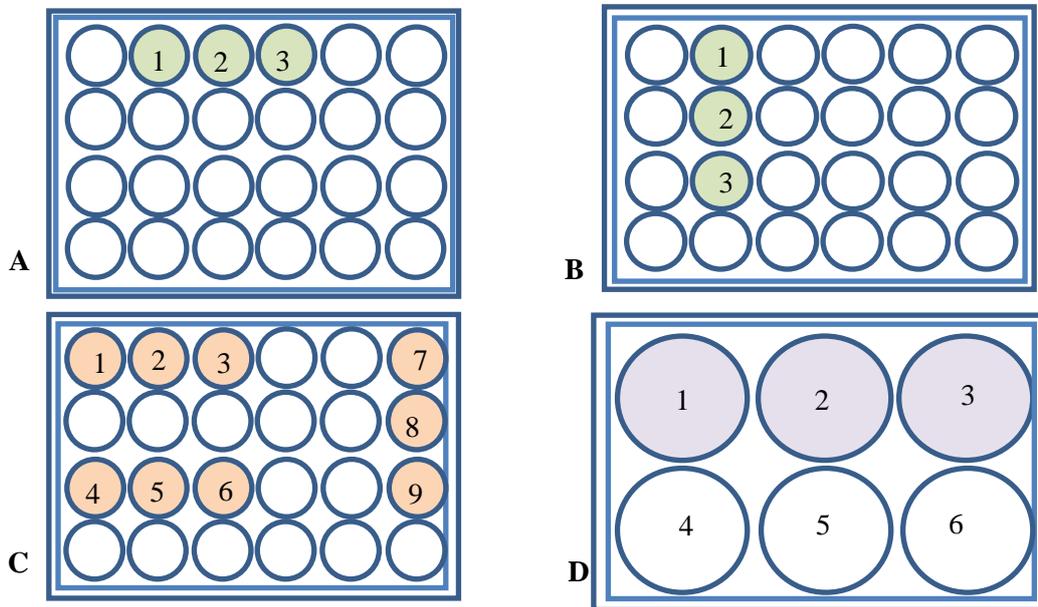


**Figure 6.3 Plate preparation and labelling for the analysis of the T-0 samples.** Plate for (A) Live/Dead assay, (B) RNAlater RNA stabilisation solutions, (C) ATPlite™ assay, and (D) biomechanical testing. The well numbers 1, 2 and 3 were for the T-0 group, well numbers 4, 5, 6 were for the unseeded decellularised PPT control and well numbers 7 – 9 for the culture medium only. The agarose plates (FBA, nutrient agar, Sabouraud agar) for sterility tests and histology cassettes and a pot of 10 % (v/v) NBF were also prepared (not shown).

**6.3.2.3. Protocol to replace culture medium**

The Perspex lid was removed (Chapter 5; Section 5.3.1.2.3) and the culture medium was carefully aspirated using a sterile blunt needle (18G x 1½'') and 10 mL syringe without any contact with the actuator arms, as they were not sterile. Then 5 mL of fresh complete culture medium (37 $^0$C) was added using the same approach. A new sterile syringe/ needle was used to to aspirate or to refill each well.

**6.3.2.4. Protocol for harvesting the day 7 samples from the TenCell-1 bioreactor**

**Preparation**

Before terminating the experiment in the TenCell-1 bioreactor, the plates of reagents were prepared and labelled as described in Figure 6.4, in the Class II cabinet hood.
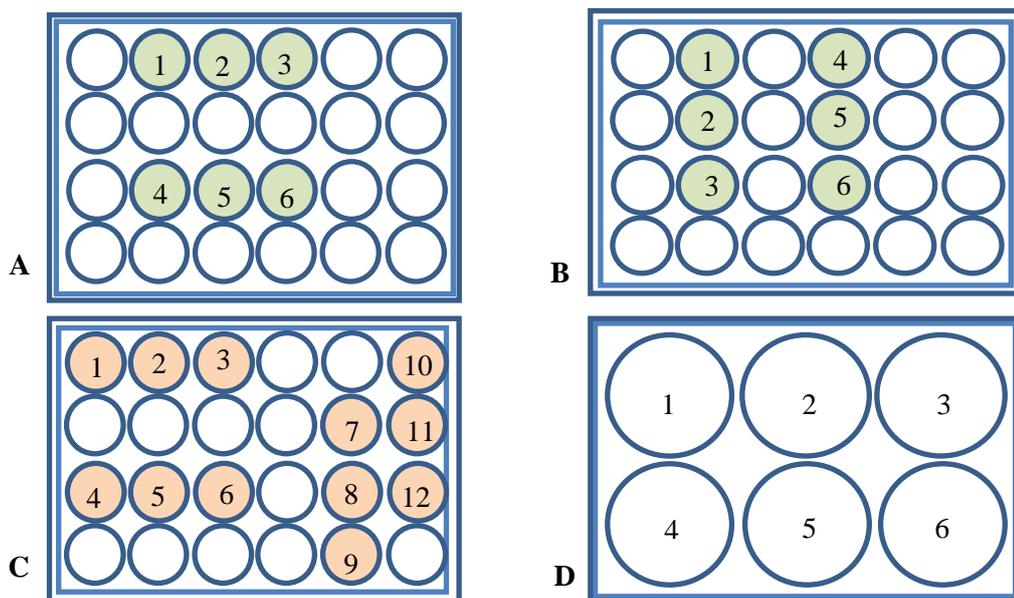


**Figure 6.4 Plates preparation and labelling for analysis of the samples after 7-days incubation in the Tencell-1 bioreactor:** (A) Live/Dead assay; Calcein AM and Ethidium homodimer (3 μM) in 2 mL PBS, (B) RNAlater RNA stabilisation solutions (10 μL.mg$^{-1}$), (C) ATPlite™ assay; lysis buffer (500 μL), and (D) biomechanical testing; sterile filter paper with PBS. The wells numbers 1, 2, 3 denote the dynamic group, well numbers 4, 5, 6 for the statics, well numbers 7 – 9 were for the unseeded decellularised PPT scaffolds, and well numbers 10 – 12 for the culture medium only. The agarose plates (FBA, nutrient agar, Sabouraud agar) for sterility test and histology cassettes and a pot of 10 % (v/v) NBF were also prepared (not shown).

The biological analyses (n=3) of the dynamically cultured cell-seeded scaffolds were harvested from TenCell culture wells number 2, 3 and 4, and from the static wells number 11, 12, and 13. The biomechanical properties were analysed using cell-seeded scaffolds from culture wells number 5, 6 and 7 (dynamic group) and 13, 14 and 15 (static group).

**Analysis Methods**

On the termination day, 250 μL of culture medium from each TenCell culture well was collected immediately after the Perspex lid was removed, and placed into each well of a 96-well plate for sterility testing. The cell-seeded scaffolds were then harvested and cut into four quarters as shown in Figure 6.2.

Briefly, each pair of culture well-clamps with a cell-seeded decellularised PPT scaffold fitted was transferred from its well using a hook and placed on the mounting plate. The sample was cut through the centre between the clamps using a sterile blade. The left grip with half of the sample attached, replaced in the culture well. The right grip with half the sample was placed on a sterile plate and the sample removed. The squeezed/ clamped area was discarded and the remaining sample was cut into two halves. One half was cut into two quarters; the upper quarter was used for the Live/Dead assay, while the lower quarter was for the ATPlite assay. The other half of the sample was then placed on a sterile plate. The sample was cut into two quarters; the upper quarter was immersed into RNAlater RNA stabilisation solution, and the lower half was positioned into a histology cassette and immersed into 10 % (v/v) NBF (Figure 6.2).

After all samples had been harvested, the plate with samples for Live/Dead assay was immediately transferred into a 37 $^0$C incubator, and the assay conducted as described in Chapter 2; Section 2.2.5.1. The ATPlite™ plate was processed as described in the Chapter 5; Section 5.3.6. The plates with samples in the RNA later were stored at 4 $^0$C and the RNA was extracted on the same day (Chapter 5; Section 5.3.9.3). Samples for biomechanical testing was stored at 4 $^0$C and analysed the following day as described in Chapter 5; Section 5.3.3.2.

Gene expression analysis using RT-qPCR was conducted when samples from all experiments (4 %, 6 % and 8 %) had been collected. The PCR procedure was carried out as described in Chapter 4; Section 4.3.3.2. The layout of the 96-well plate for each reaction was as shown in Figure 6.5. Each PCR reaction comprised: (i) reference gene (S28 R), (ii) gene of interest (GOI), (iii) no template control for each strain experiment, (iv) water control, and (v) no primer controls (GOI and reference gene). The expression of eight genes was analysed (Tenascin-C, Scleraxis, collagen III, collagen I, collagen II, Sox 9, PPARγ and osteopontin).

| Strain | 4 % | | | 6 % | | | 8 % | | | No template | | |
|---|---|---|---|---|---|---|---|---|---|---|---|---|
| Group | T-0 | Stat | Dyn | T-0 | Stat | Dyn | T-0 | Stat | Dyn | 4 % | 6 % | 8 % |



**Figure 6.5 Plate lay out for analysis of transcript gene expression using RT-qPCR in a 96-well plate**. NP refers to no primer, Stat refers to static and Dyn refers to dynamic group.

**6.3.2.5. Protocol for use of confocal microscopy**

Samples subjected to the Live/Dead assay were visualised using confocal microscopy following visualisation by fluorescence microscopy. The confocal microscope (LSM510, Zeiss) was used with Zen 2009 software to visualise the samples, with 405 diodes (He: Ne) and an Argon laser

at 50 % strength output. The experimental program was set for Z-stack with 10 images for the time series (10 μm each). The 3-D image size was 142.58 μm (x), 142.58 μm (y) and 100 μm (z). Samples were initially visualised using a low-magnification objective (100 x) to view the whole sample, then once the area of interest was determined, this was visualised at 630 x magnification with immersion oil applied to the objective lens. At this point, the pinhole was set at 1 AU. The scan speed was set at 6 to 7, averaging was 4 and the bit depth was set at 8-bit. The channel filters were FITC (488 nm) and Rhodamine (543 nm). Using the Z stack acquisition, the 3-D image was initially live-scanned, the top and the bottom-end section planes of the focused area were determined. Information such as the number of slices (10) and the intervals were input into the system. Each scan produced a 4-D dataset and the files were saved as a single LSM file for further analysis.

### 6.3.3. Statistical analysis

All numeric data was initially visualised for distribution using a Q-Q plot to determine normality. Data was transformed when not normal. The numerical data was then calculated using Microsoft excel (2007), analysed and presented using GraphPad Prism 6.

## 6.4. Results

## 6.4.1. Viability of human BM-MSC seeded onto decellularised PPT and harvested after 12 hours (T0) or following 7 days of culture in TenCell-1 subject to dynamic strain (4%, 6% or 8%) or cultured statically

### 6.4.1.1. Analysis by Live/Dead cell staining by flourescence microscopy

The Live/Dead images of the Day 0 (T-0) and Day 7 samples showed that the cell number in the dynamically and statically cultured scaffolds had increased over the time, compared to the time zero (T-0) (Figure 6.6).

The human BM-MSC seeded decellularised PPTs that had been cultured statically in each of the three experiments showed predominalty dead cells, while the human BM-MSC seeded decellularised PPTs that had been cultured dynamically, had more viable cells. There was no apparent difference between the viable and dead cells present in human BM-MSC seeded decellularised PPTs, which had been cultured under different conditions of dynamic strain (4, 6 or 8%).
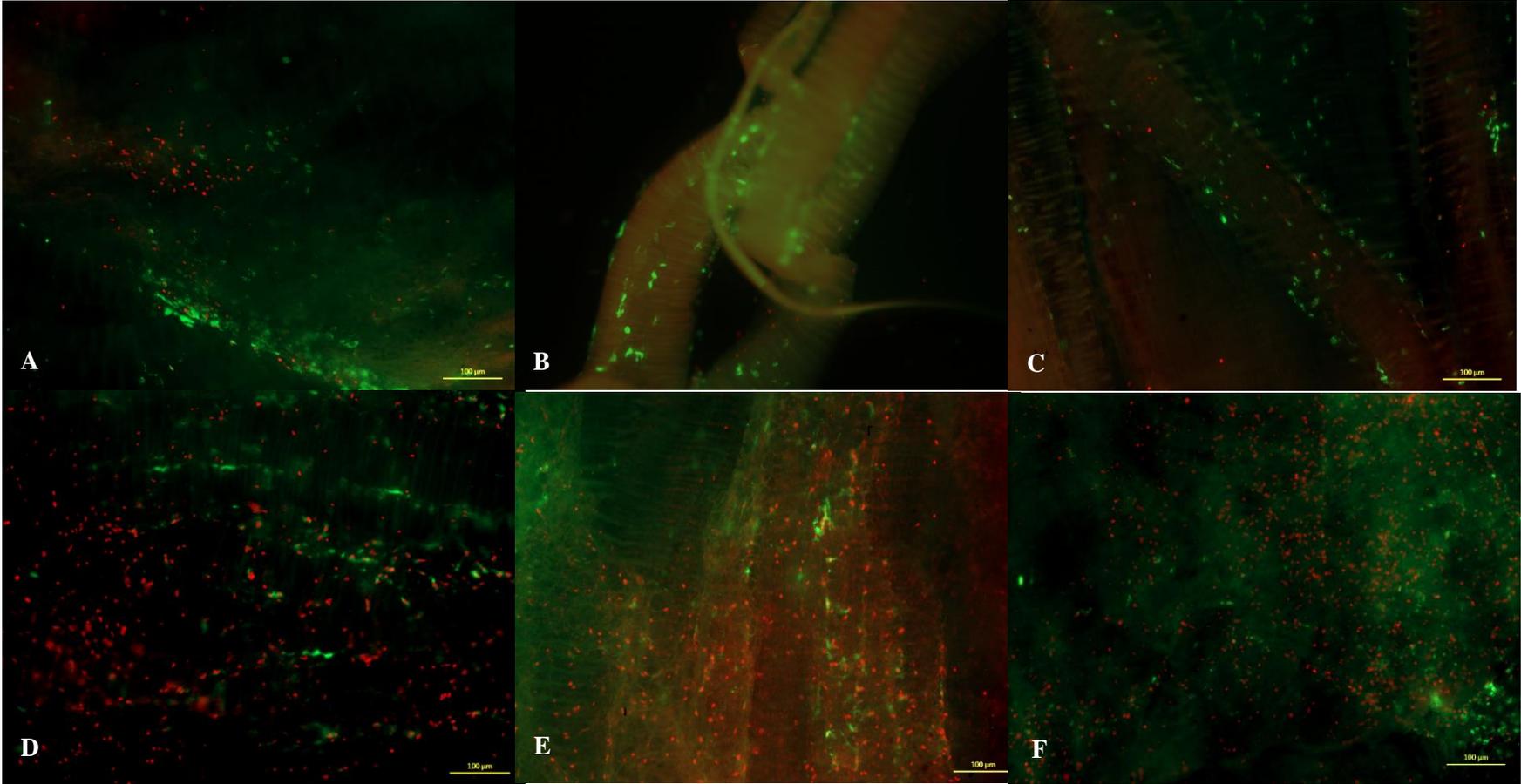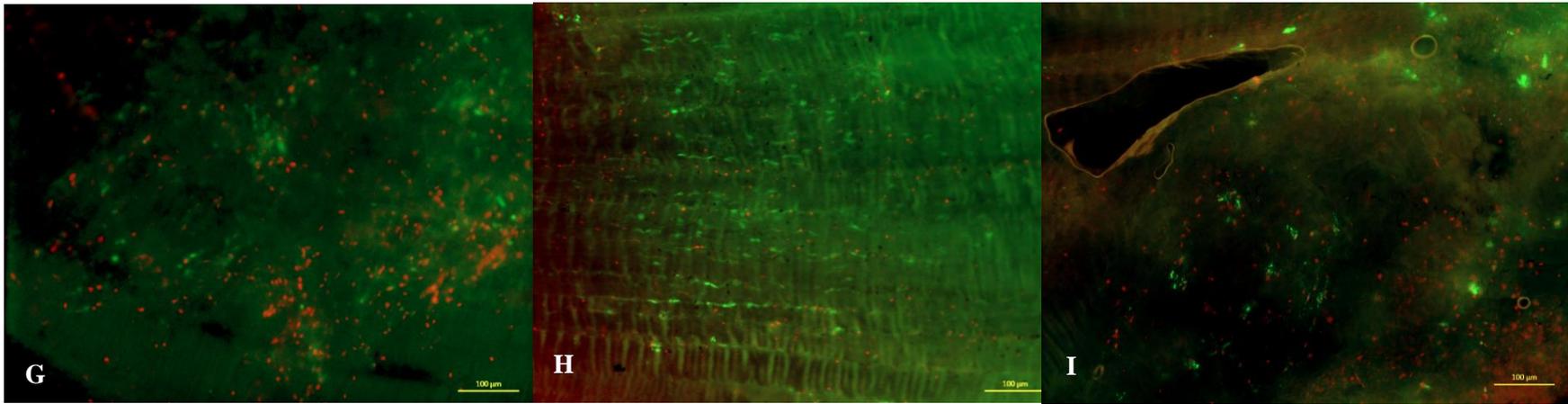
**Figure 6.6 Live/Dead images of the Day 0 (T-0) and Day 7 samples incubated with and without tensile strain.** A, B, C show representative images of the T0 samples from each experiment. D, E, F show representative images of the cell-seeded scaffolds cultured in TenCell-1 under static conditions, and (G, H, I) show representative images of the cell-seeded scaffolds cultured in TenCell-1 under dynamic conditions. A, D, G the 4 % displacement experiment; B, E, H the 6 % displacement experiment, and C, F, I are the 8 % displacement experiment. Images were captured at 50 x magification using fluoresecence microscopy. Scale bars represent 100 μm.

**6.4.1.2. Analysis by Live/Dead cell staining by confocal microscopy.**

Confocal microscopy enabled determination of the infiltration of viable cells into the scaffolds. The samples were imaged from the surface using a 10 slice image-series up to 100 μM depth with 10 μM thickness for each plane.

The following legends for each slice plane of the confocal images are refered to the depth of the slices as follow: (A) 0.0 μm, (B) 1.1 μm, (C) 2.2 μm, (D) 3.3 μm, (E) 4.4 μm, (F) 5.5 μm, (G) 6.6 μm, (H) 7.7 μm, (I) 8.8 μm (J) 9.9 μm, unless otherwise stated.
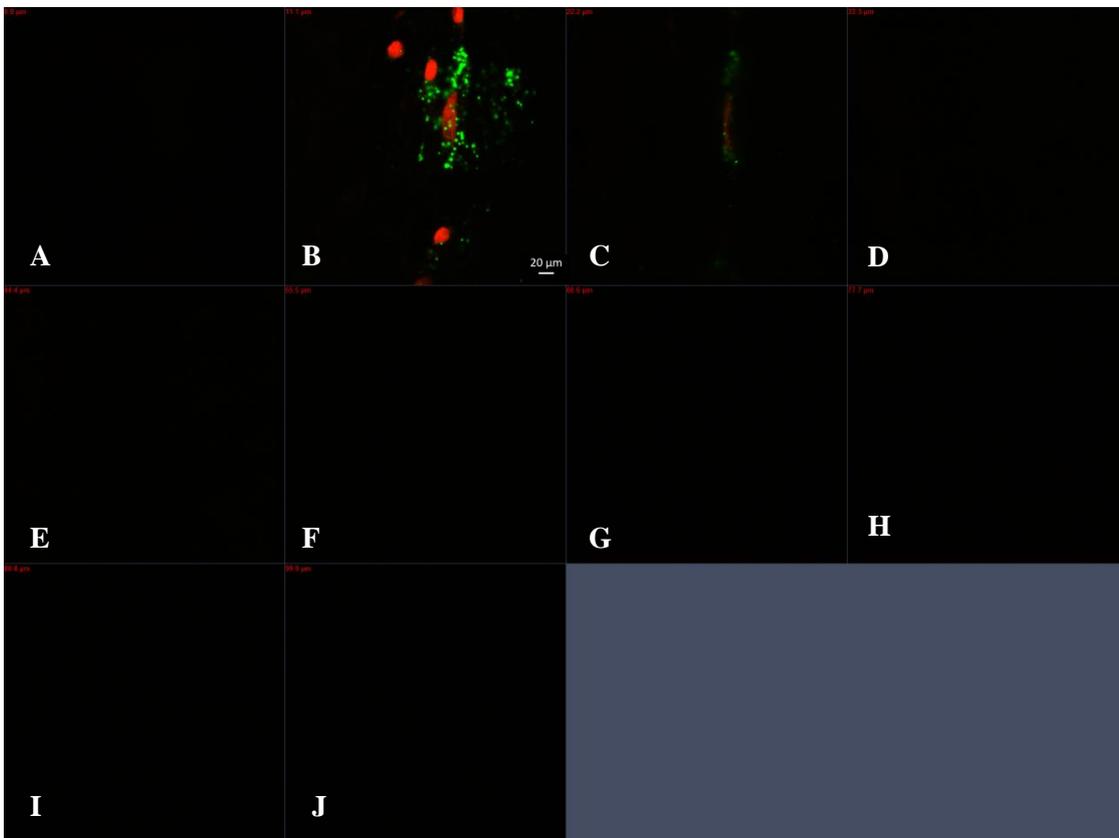


**Figure 6.7 Confocal imaging of the T-0 sample captured at 630 x magnification**. Scale bar indicates 20 μm.

The human BM-MSCs seeded on decellularised PPT scaffolds for 12 h (Day 0/ T-0) were found aggregated in the same plane not deeper than 30 – 40 μm, at the surface [Figure 6.7 B]. This indicated that the cells had not migrated into the scaffold during the initial 12 h of culture.

All static controls; the static 4 %, the 6 % and the 8 % showed similar trends. The cells were found at a deeper depth compared to the T-0 samples, with apparently more viable cells. The confocal images of human BM-MSC seeded decellularised PPTs that had been cultured statically, also showed some cells that appeared to be stained with Calcein-AM and Ethidium homodimer at the same time (pointed by white arrow), with a cell shape and size that was spherical and enlarged [Figure 6.8 B, C, D]. This trend was not found in the T-0 or in the cells from the scaffolds that had been cultured dynamically. An example is shown in Figure 6.8 repreenting the z-stack of the human BM-MSC seeded decellularised PPT cultured statically in the 4 % strain experiment.
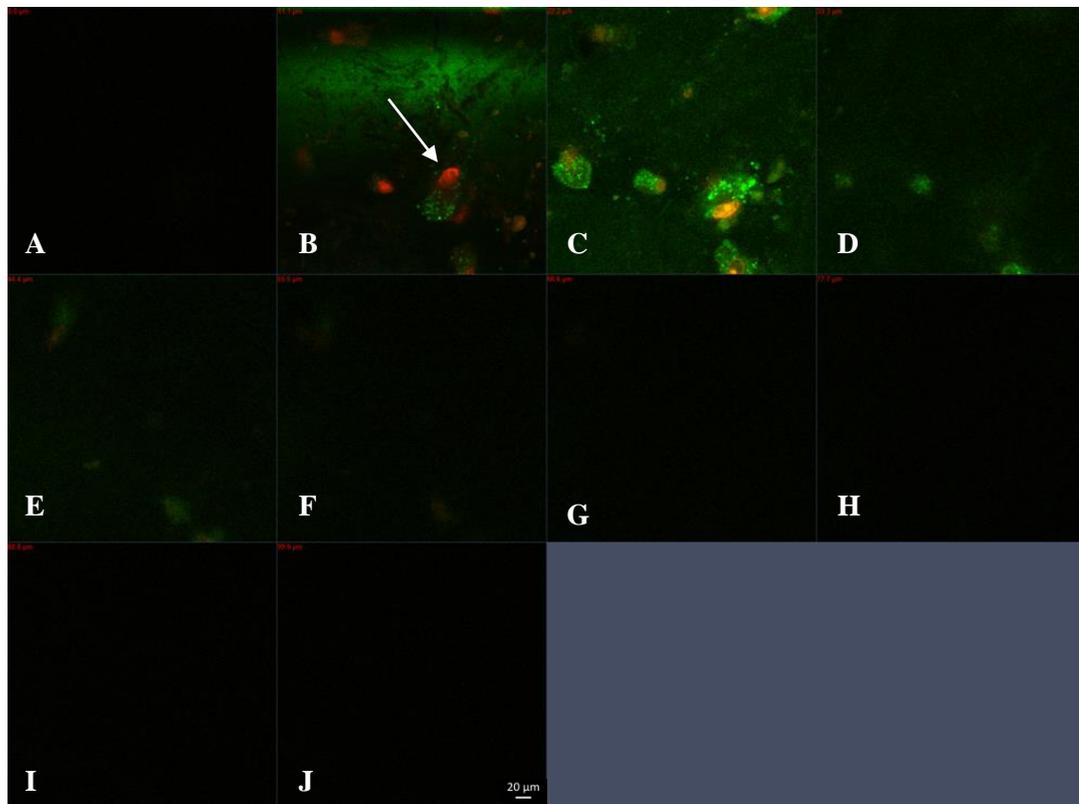


**Figure 6.8 Confocal imaging of the human BM-MSC seeded decellularised PPT cultured in static at 630 x magnification.** White arrow points at the cell with both Ethidium homodimer and Calcein stained at the same time. Scale bar indicates 20 μm.

Confocal images of the human BM-MSC seeded decellularised PPT scaffold cultured at 4 % strain revealed an absence of any live or dead cells throughout a 100 μM depth. A single image (not Z stack) was captured separately at a depth of 100.72 μM which revealed some fusiform viable cells in a lattice formation [Figure 6.9]. This trend was also observed in the confocal

images of the human BM-MSC seeded decellularised PPT scaffold cultured at 6 % strain [Figure 6.10]. Several viable cells were found in the confocal images of the human BM-MSC seeded decellularised PPT scaffold cultured at 8 % strain [Figure 6.11] arranged in lattice in the centre of the sections. The confocal images of Live/Dead stained human BM-MSC seeded decellularised PPT scaffold cultured at all cyclic strains (4, 6 and 8 %) revealed no dead cells.
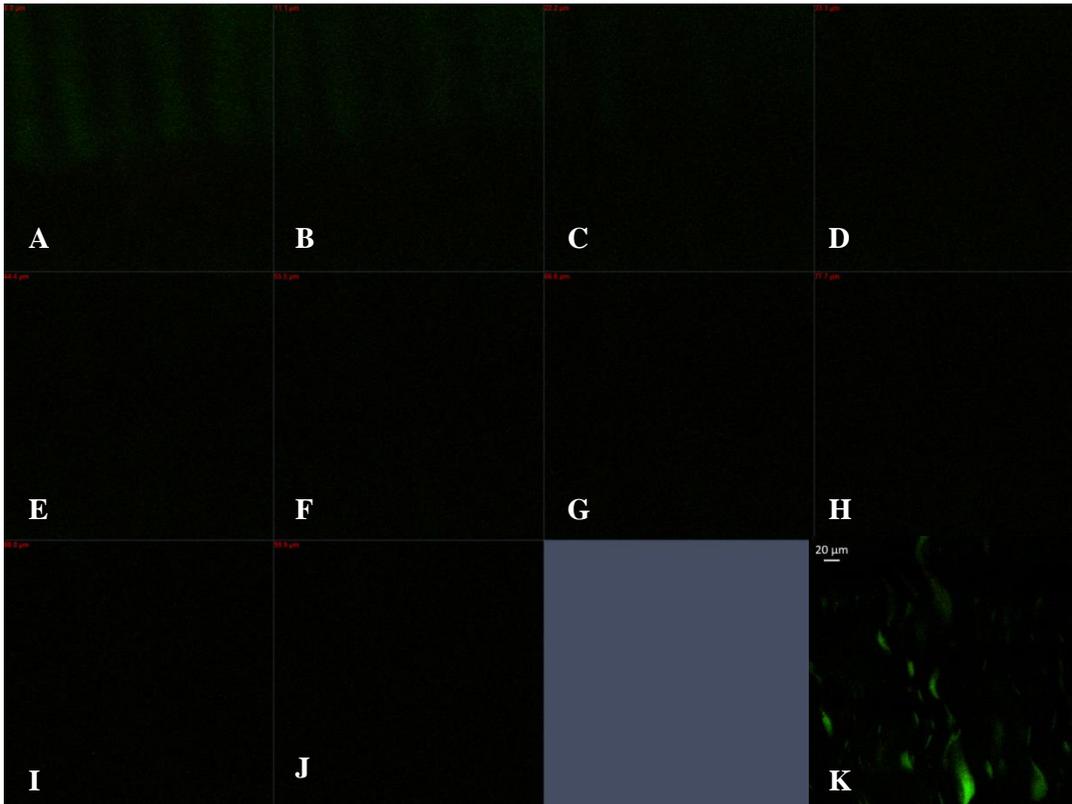


**Figure 6.9 Confocal imaging of the human BM-MSC seeded decellularised PPT cultured dynamically at 4 % strain at 630 x magnification**. (K) An image was captured separately at 100.72 µM depth showed viable cells. Scale bar indicates 20 µm.
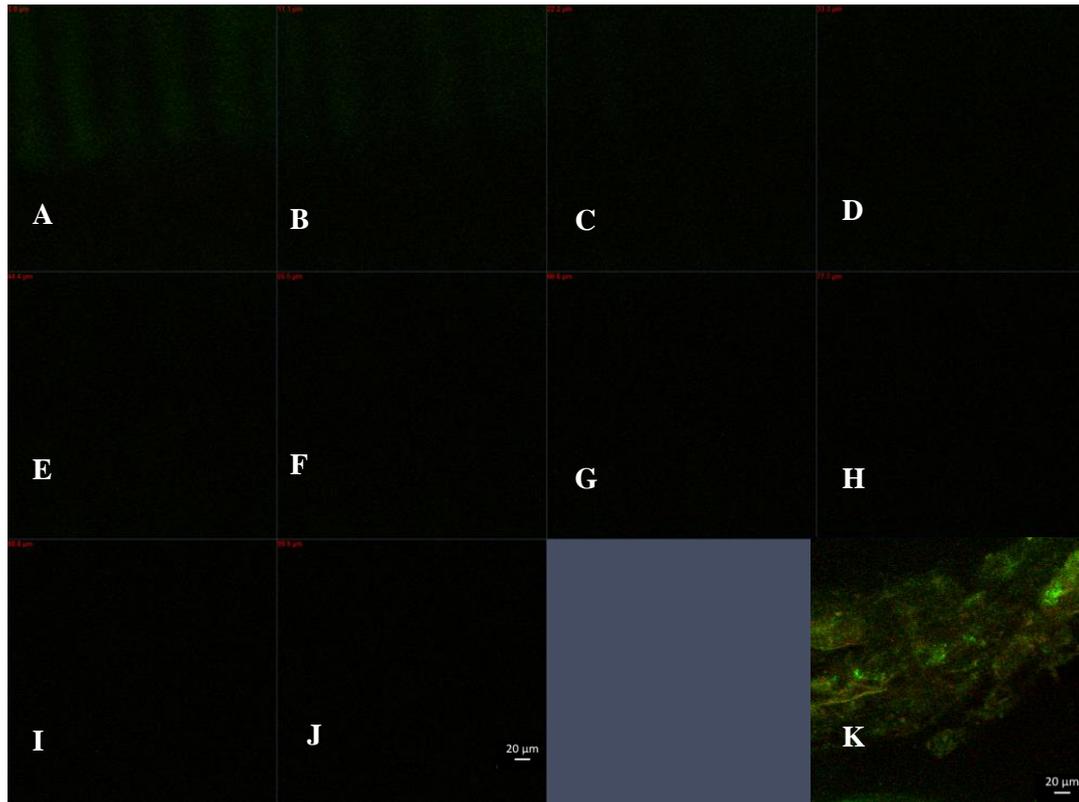
**Figure 6.10 Confocal imaging of the human BM-MSC seeded decellularised PPT cultured dynamically at 6 % strain at 630 x magnification**. (K) Imaged with viable cells was captured separately at 103.45 µM depth. Scale bar indicates 20 µm.
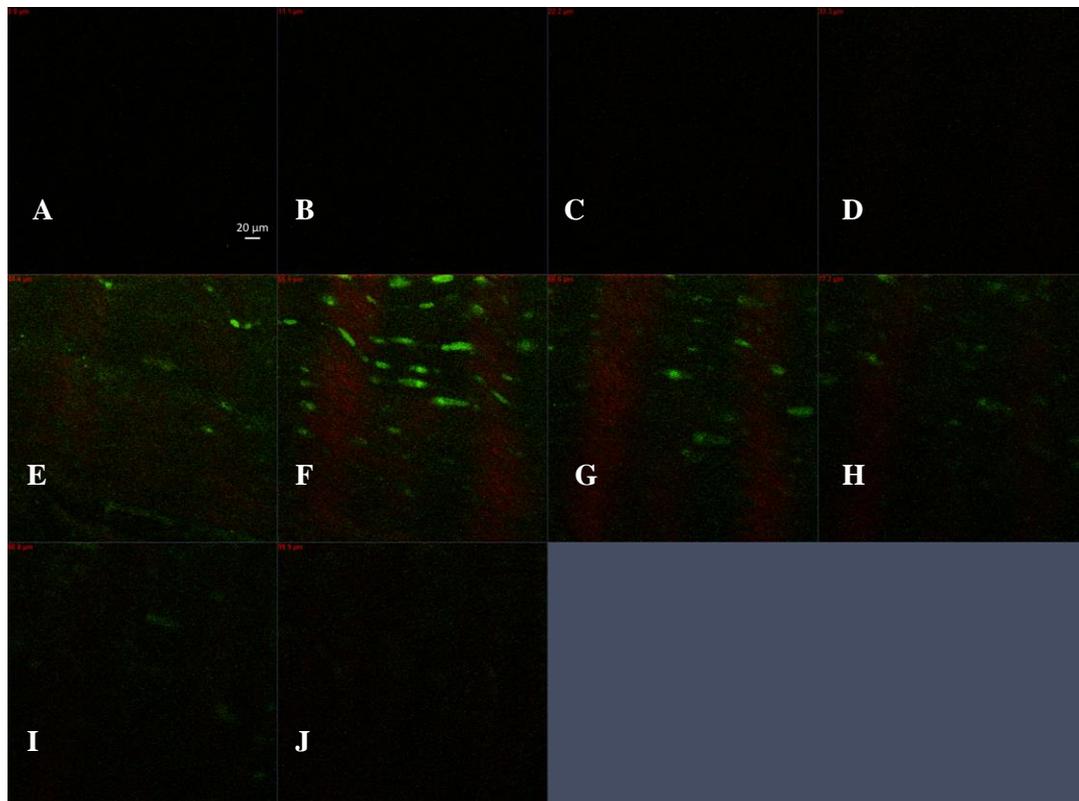


**Figure 6.11 Confocal imaging of human BM-MSC seeded decellularised PPT cultured dynamically at 8 % strain captured at 630 x magnification**. Scale bar indicates 20 µm.

### 6.4.1.3. Viable cell counting using Live/Dead assay

The percentage viable human BM-MSCs seeded onto decellularised PPT scaffolds was quantified using ImageJ software. The percentage of viable cells was calculated and the Live/Dead data had indicated a decrease in viability of cells in the decellularised scaffolds after 7-days incubation under static conditions, in all three experiments - compared to the Day 0 (T-0) - although this was not significant.

The proportion of viable cells in the cell-seeded scaffolds cultured with 6 % cyclic tensile strain was significantly higher compared to the statically cultured 6 % strain control and statically cultured 8 % strain control ($p<0.05$). There were no differrences found between the percentage viable cells in the human BM-MSC seeded decellularised PPT cultured dynamically at 4 %, 6 % of 8% strain after 7 days of culture, while the others groups showed no differences among them ($p>0.05$) [Figure 6.12].
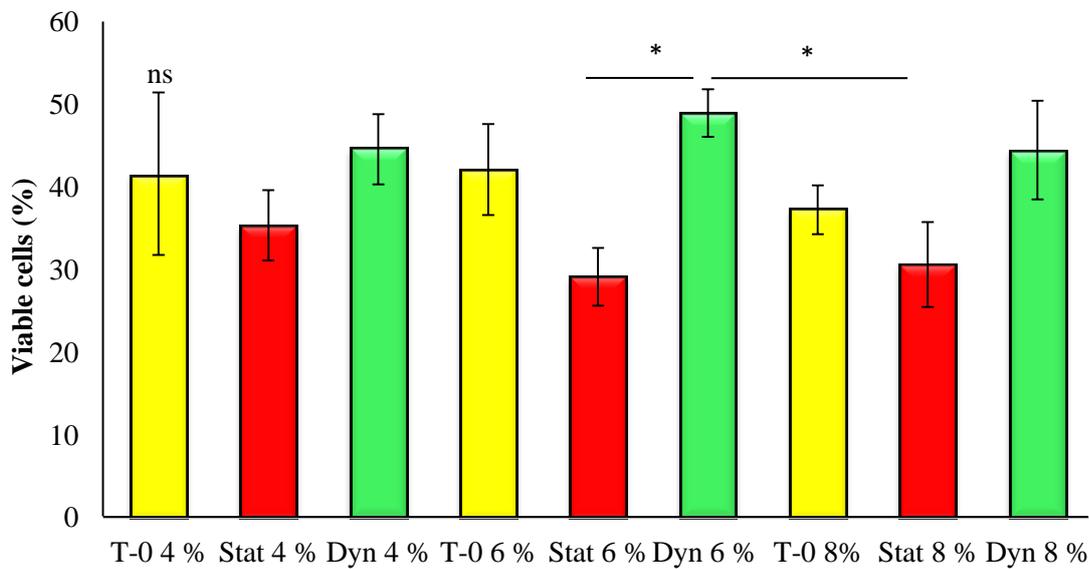


**Figure 6.12 Percentage of viable cells per human BM-MSC seeded decellularised PPT cultured statically or dynamically at 4, 6 and 8% strain.** Data is presented as the mean of percentage of viable cells (n=3) ± 95 % Cl limits. Data was arcsin transformed and analysed using one-way ANOVA, followed by the T method, and back transformed for the presentation. (*) represents $p<0.05$. T-0 was the day zero group, Stat and Dyn were the 7 day cultures in Tencell-1 bioreactor; with and without mechanical strain, respectively.

**6.4.1.4. Viability assay; ATPlite™ assay to quantify the ATP levels**

The ATP levels of all samples [Figure 6.13] incubated in the TenCell-1 bioreactor after 7 days were significantly higher compared to the T-0 groups. The ATP levels of the human BM-MSC seeded decellularised PPT cultured statically in the 4 % and 6 % strain experiments had increased significantly ($p<0.05$) by 2.35 fold and 2.88 fold respectively from the Day 0 samples for each experiment, while ATP levels of the human BM-MSC seeded decellularised PPT cultured statically in the 8 % strain experiment had increased by 1.9 fold, which was not significantly increased compared to the T-0 samples for the 8 % strain experiment. The ATP levels of the human BM-MSC seeded decellularised PPT cultured dynamically at 4, 6 and 8% strain had increased significantly compared to their static controls, by 4.7 fold, 9.15 fold and 3.79 fold respectively. The ATP levels of the human BM-MSC seeded decellularised PPT cultured dynamically at 6 % strain were the highest and significantly greater than the 4% and 8% strain groups ($p<0.0001$). There was no difference found between the ATP levels of the human BM-MSC seeded decellularised PPT cultured dynamically at 4 % and 8 % strain ($p=0.131$).
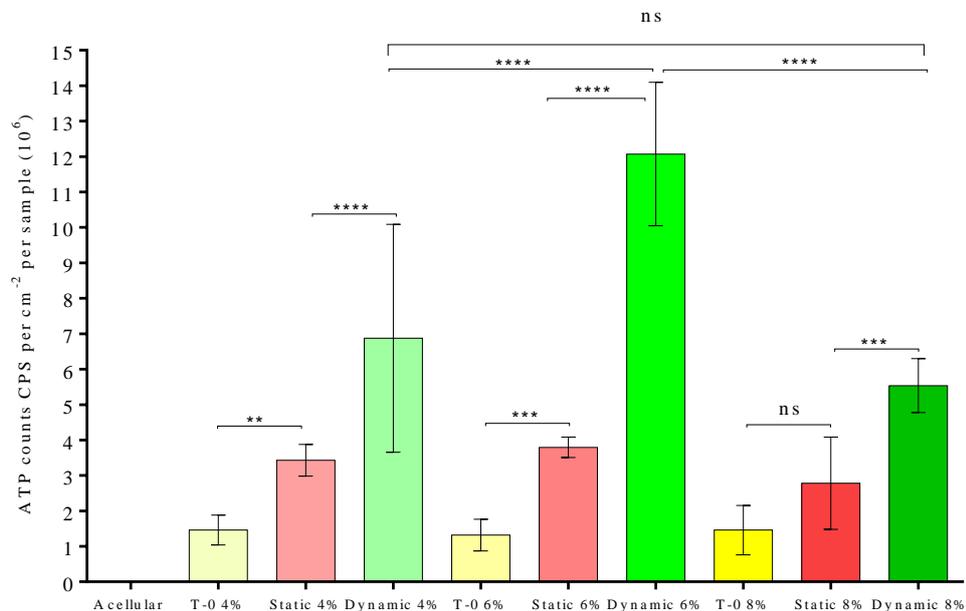


**Figure 6.13 ATP levels (CPS 10⁶) per cm⁻² per human BM-MSC seeded decellularised PPT cultured scaffold.** Data is presented as the mean of CPS ($10^6$) (n=3) ± 95 % Cl. Data was analysed using one-way ANOVA followed by T-method. **** indicates $p<0.0001$, *** indicates $p<0.001$, ** indicates $p<0.01$. T-0 was the day zero group, Stat and Dyn were the 7 day cultures in Tencell-1 bioreactor; with and without mechanical strain, respectively.

**6.4.2 Biomechanical properties of the human BM-MSC seeded decellularised PPT cultured under dynamic strain or statically**

Samples of the human BM-MSC seeded decellularised PPT cultured for 12 hours (T0) and for 7 days in the TenCell-1 bioreactor under 4, 6 or 8% cyclic strain or statically were analysed for their material properties using unixial tensile tests. The force (N) and elongation (mm) slopes generated from each sample were converted to the stress strain curves which are presented in Figure 6.14.
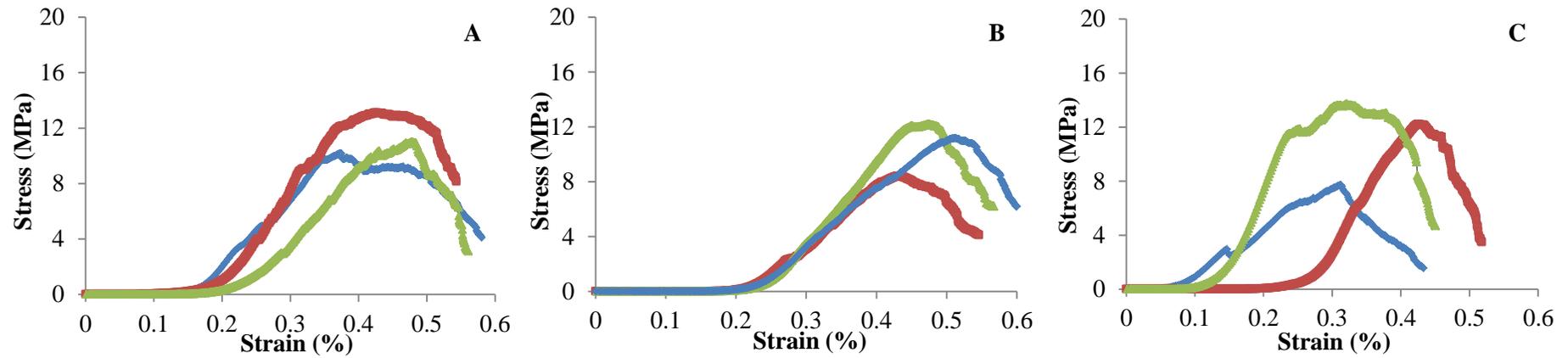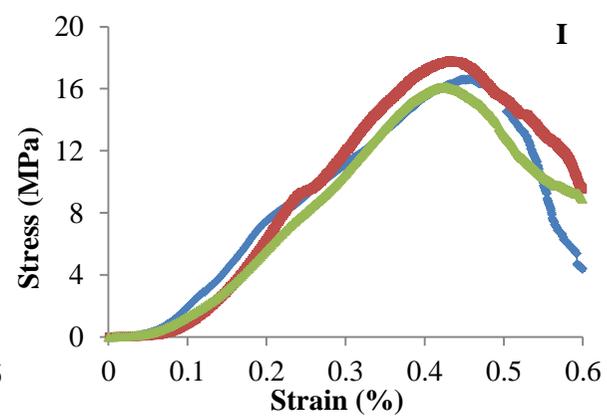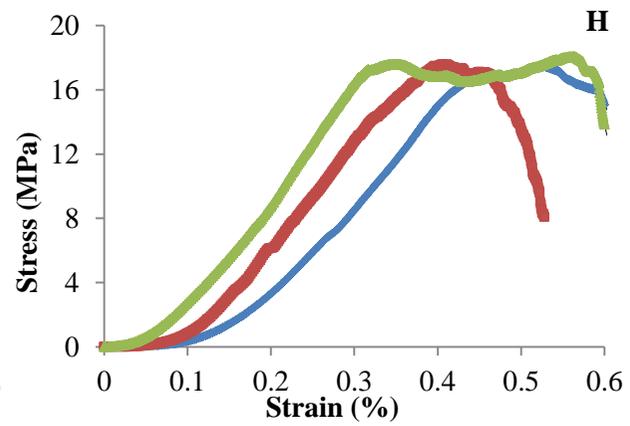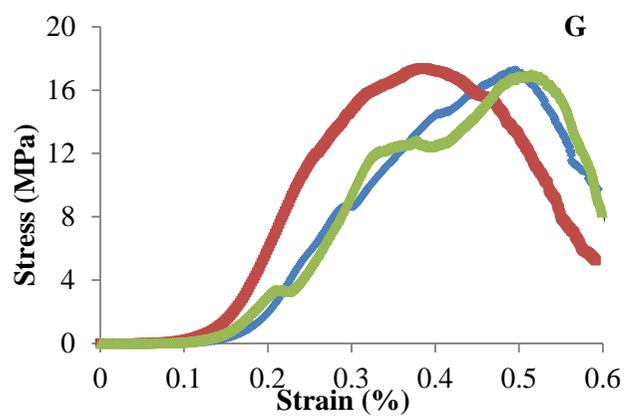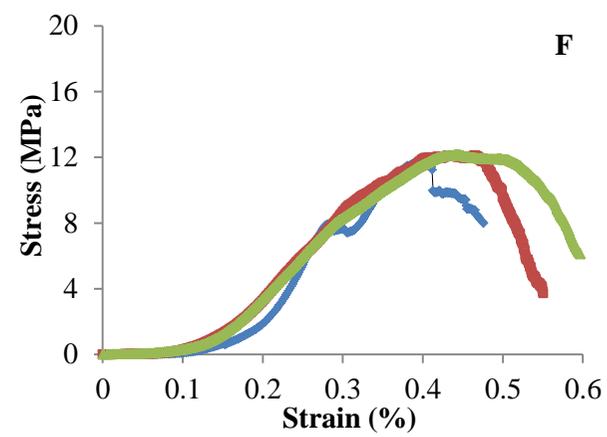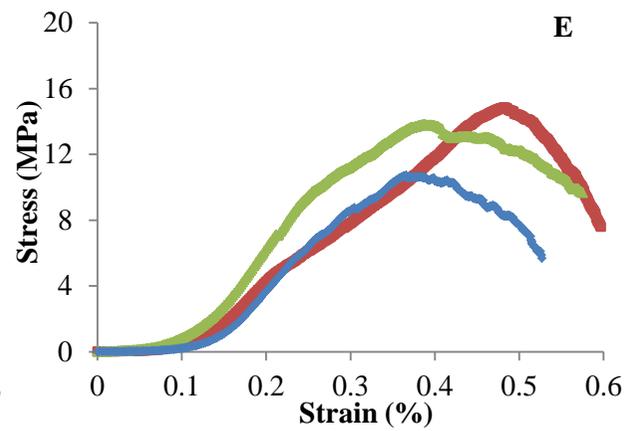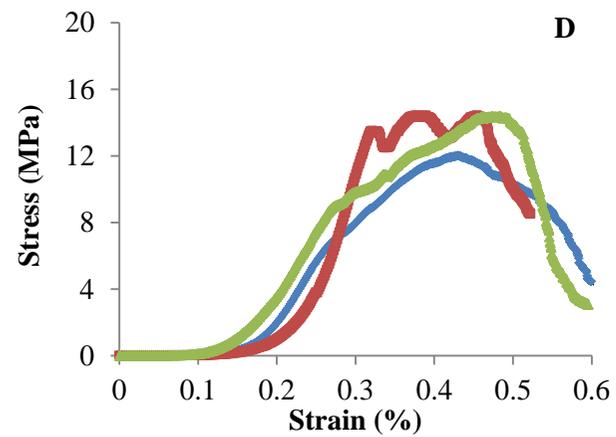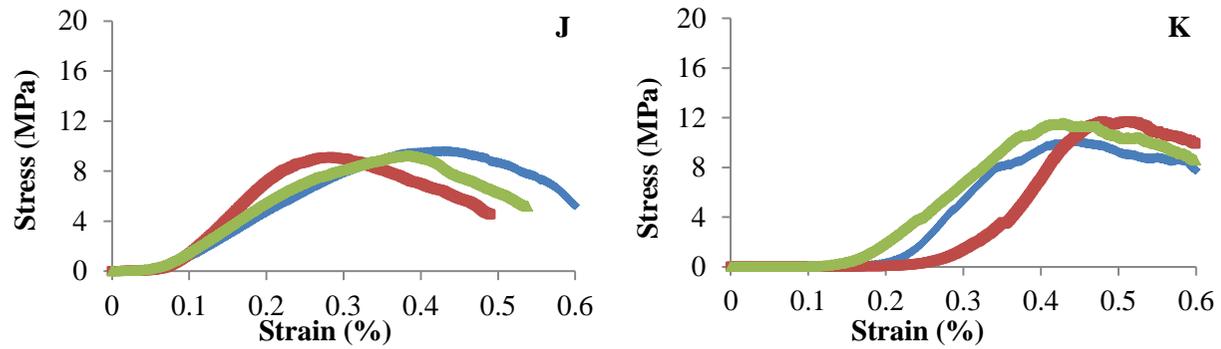
**Figure 6.14 Stress strain slope of the human BM-MSCs seeded decellularised PPT scaffolds**; A, B, C the Day 0 (T-0) samples. D, E, F and after 7 days incubation in TenCell-1 statically, and G, H, I under dynamic tensile strain. A, D, G are the 4 % strain group; B, E, H are the 6 % strain group and C, F, I are the 8 % strain groups. The native tendon (J) and the non-seeded decellularised tendon (K) are presented as the controls. Each slope represents one specimen, and each graph represents each group (n=3).

The strain-stress slope of the the human BM-MSC seeded decellularised PPT cultured under 6 % dynamic strain [Figure 6.14 H] showed a plateau peak that was not seen in any other groups. The toe regions of all T-0 samples were prolonged [Figure 6.14 A-C] as seen as in the decellularised PPT scaffolds (without cells) [Figure 6.14 K]. The toe region of the dynamically cultured cell-seeded scaffolds, especially the human BM-MSC seeded decellularised PPT cultured under 6 % [Figure 6.14 H] and 8 % dynamic strain [Figure 6.14 I], had less than 0.1 strain limit that was also demonstrated in the native PPT scaffolds [Figure 6.14 J]. While the toe region of the static controls seemed to reduce compared to the T-0 samples, it was not comparable to native tissue. This indicated that the human BM-MSCs after initial seeding (12 h) had little effect on the stress strain curves, while after 7-days static incubation the elastic phase slope had improved, although not to the same extent as in the human BM-MSC seeded decellularised PPT cultured under cyclic strain, which were similar to native tissue.

The force and elongation data were analysed and presented as five biomechanical parameters to indicate the mechanical properties of the human BM-MSCs seeded decellularised PPT scaffolds after being subjected to 4 %, 6 % and 8 % cyclic strain for 7 days in TenCell-1 bioreactor. The results are presented in Figures 6.15- 6.19.
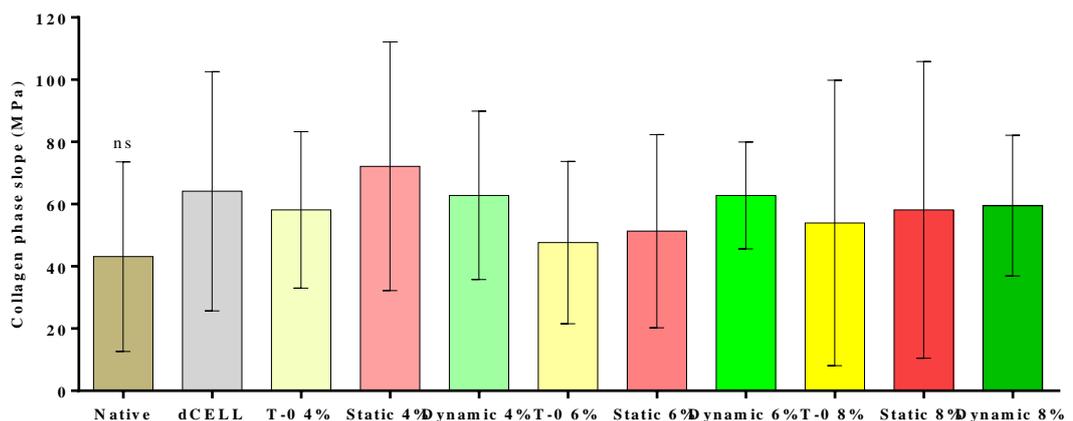


**Figure 6.15 Collagen phase slope of the human BM-MSC seeded decellularised PPT cultured after 7 days incubation with cyclic strain**. The static (after 7 days culture), T-0, native PPT scaffolds were compared. Data is presented as the mean (n=3) ± 95 % Cl. Data was analysed using one-way ANOVA followed by Tukey's multiple comparisons test. ns indicates not significantly different. T-0 was the day zero group, Stat and Dyn were the 7 day cultures in Tencell-1 bioreactor; with and without mechanical strain, respectively.

There were no differences in the collagen phase slopes among all sample groups [Figure 6.15].
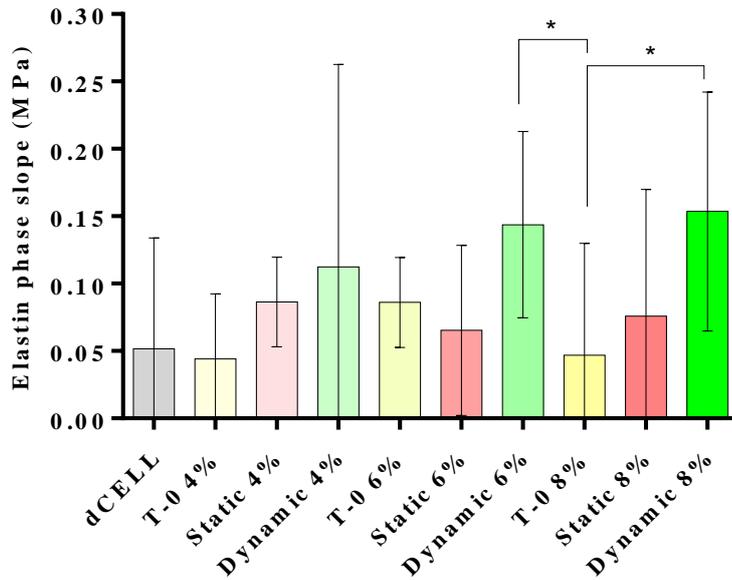


**Figure 6.16 Elastin phase slope of the human BM-MSC seeded decellularised PPT cultured for 7 days incubation with cyclic strain**. The static (after 7 days culture) and the T-0 groups were compared. Data is presented as the mean MPa (n=3) ± 95 % Cl. Data was analysed using one-way ANOVA followed by Tukey's test. (*) represents $p < 0.05$. T-0 was the day zero group, Stat and Dyn were the 7 day cultures in Tencell-1 bioreactor; with and without mechanical strain, respectively.

The elastin phase slope of the native scaffolds is not presented because the cut off strain limit of 0.07 used to analyse all sample groups was far too long for the the native scaffolds. The elastin phase slope of the native scaffolds was 0.98 ± 0.69 MPa (the mean (n=3) ± 95 % Cl). The difference of the elastin phase slope between the T-0 8 % to the Dynamic 8 % and Dynamic 6% was significant ($p < 0.05$), no differences were found among other groups.
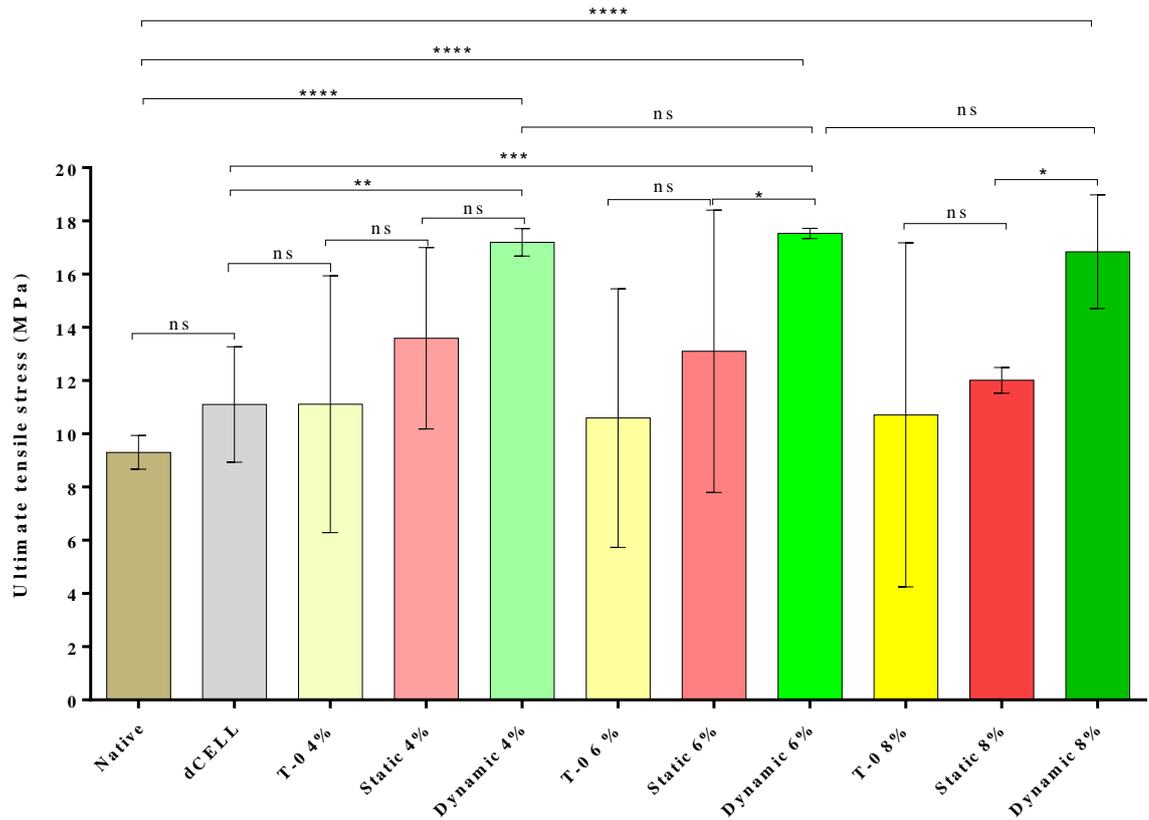
**Figure 6.17 Ultimate tensile stress (UTStress) of the human BM-MSC seeded decellularised PPT cultured for 7 days incubation with cyclic strain**. The static (7 days culture), T-0, native PPT scaffolds were compared. Data was analysed using one-way ANOVA, followed by T method post-test to determine the differences between two means. Error bars denote mean MPa (n=3) ± 95 % Cl. * indicates p<0.05, ** indicates p<0.01, *** indicates p<0.001, **** indicates p<0.0001. T-0 was the day zero group, Stat and Dyn were the 7 day cultures in Tencell-1 bioreactor; with and without mechanical strain, respectively.

All groups of the cell-seeded scaffolds incubated with cyclic strain for 7 days showed a significantly increases of their UTStress compared to their static controls. This indicated that the cyclic strain had improved the stiffness of the cell-seeded matrix scaffold significantly higher than the native (p<0.0001), and also was significantly higher than the decellularised PPT scaffolds (p<0.05) [Figure 6.17].

There were no differences in the UTStress among samples incubated with 4 %, 6 % and 8 % cyclic strain (p>0.05). The stiffness of the seeded scaffolds incubated under static condition was not different to the native tendons and the decellularised scaffolds (p>0.05).
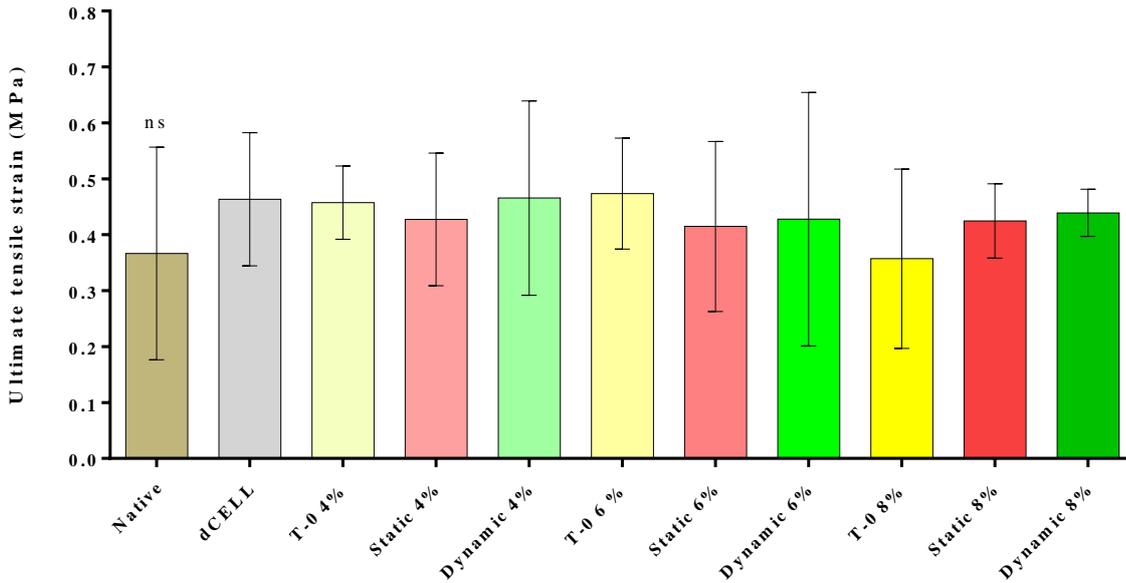
**Figure 6.18 Ultimate tensile strain (UTStrain) of the human BM-MSC seeded decellularised PPT cultured for 7 days incubation with cyclic strain**. The static, T-0, native PPT scaffolds were compared. Data is presented as the mean (n=3) ± 95 % Cl. Data was analysed using one-way ANOVA followed by Tukey's multiple comparisons test. ns denotes not significantly different. T-0 was the day zero group, Stat and Dyn were the 7 day cultures in Tencell-1 bioreactor; with and without mechanical strain, respectively.

There were no differences in the UTStrain among all sample groups (p>0.05).
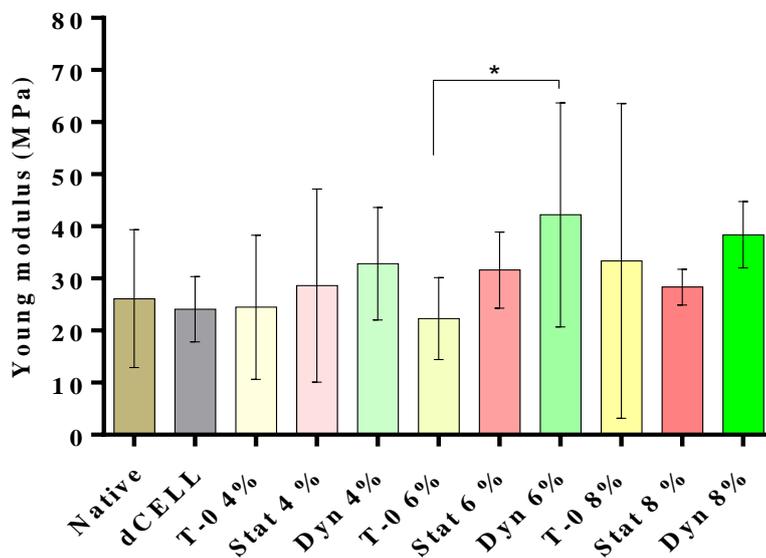


**Figure 6.19 Young`s modulus of the human BM-MSC seeded decellularised PPT after 7 days incubation with cyclic strains.** The static, T-0, native PPT scaffolds were compared. Data is presented as the mean (n=3) ± 95 % Cl. Data was analysed using one-way ANOVA followed by Tukey's test. (*) indicates p<0.05. T-0 was the day zero group, Stat and Dyn were the 7 day cultures in Tencell-1 bioreactor; with and without mechanical strain, respectively.

The modulus elasticity of the samples incubated with 6 % strain was significantly higher compared to the day (0) of the 6 % group (p<0.05), while no differences were found among other groups (p>0.05).

## 6.4.3. Histology analysis

### 6.4.3.1. H&E staining

The sections of the human BM-MSC seeded decellularised PPT scaffolds incubated under 4, 6 and 8 % strain were stained with H&E to highlight the nuclei and the tissue histoarchitecture.
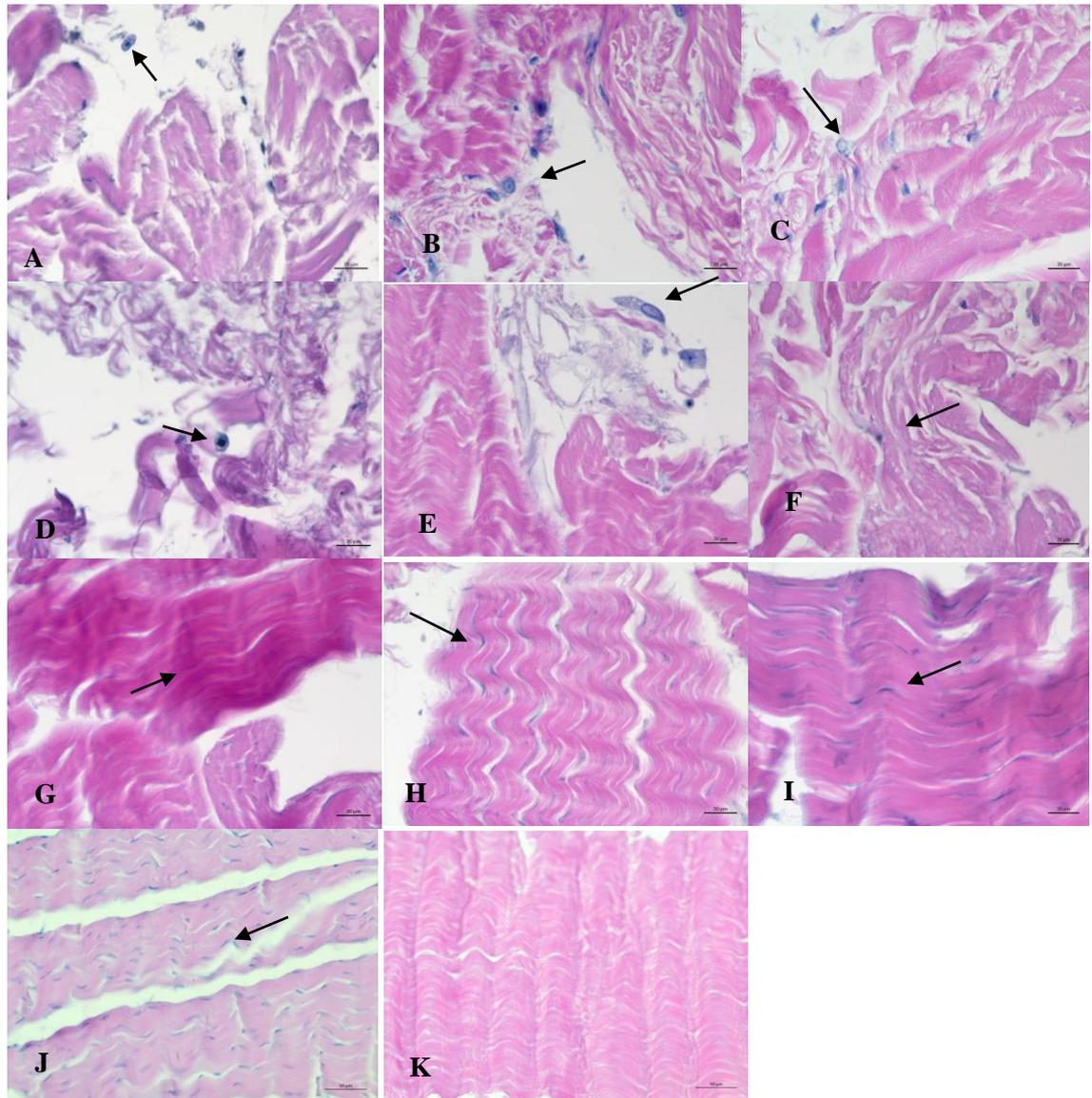


**Figure 6.20 H&E staining of the human BM-MSCs seeded decellularised PPT scaffolds.** A, B, C are sections of the T-0 samples. D, E, F are sections of samples cultured statically for 7 days and G, H , I are sections of the samples cultured under dynamic strain for 7 days. A, D G are the 4% strain group. B, E & H are the 6 % strain groups and C, F, I are the 8 % strain group. Sections of the controls, (J) native and (K) are also presented. The red arrows point to the nucleus shape. Images were captured at 200 x magnification. Scale bars represent 50 μm.

The fibres of samples incubated with cyclic strain were shown to be rearranged and the crimp formation was recovered [Figure 6.20 G, H, I]. In contrast, the T-0 samples [Figure 6.20 A, B, C] and the static controls [Figure 6.20 D, E, F] had the fibre structures broken down. The nuclei of the cells in all samples cultured under 4, 6 and 8 % mechanical strain [Figure 6.20 G, H, I] were found to be flattened and elongated, arranged in a lattice position in between the fibres. This trend was similar to the native tissue sections. The nuclei of the cells in sections of the T-0 samples and sections of the samples that had been cultured under static conditions for 7 days were located mainly at the surface of the tissue or in loosened areas. They were irregular in size and shape.

## 6.4.3.2. DAPI staining

The nuclei were stained using DAPI staining to ensure that the nuclei visualised by H&E staining were not artefacts.

DNA in the nucleus was stained using DAPI and were found to be present in all sections of the cell-seeded scaffolds. The nuclei of the T-0 samples were found mostly at the outer surface of the tissue [Figure 6.21 A]. In the samples when incubated under static condition for 7 days, the nuclei were found to be more dispersed compared to the T-0 samples. The nuclei were found mostly in the loosened tissue, however were solitary [Figure 6.21 B]. Interestingly, the human BM-MSCs seeded on the decellularised PPTs incubated under 6 % cyclic strain for 7 days were aggregated and arranged deep in the fibres [Figure 6.21 C]. DAPI images of the samples incubated under 4 and 8 % strain also showed similar results to the samples incubated under 6 % strain. The nuclei in the native PPT were well organised [Figure 6.21 E] and the sections of the decellularised PPT showed no evidence of DNA throughout the slide [Figure 6.21 D]. Accordingly, the results found in all sample groups stained with DAPI had similar trend with the same samples stained with H&E analysis.
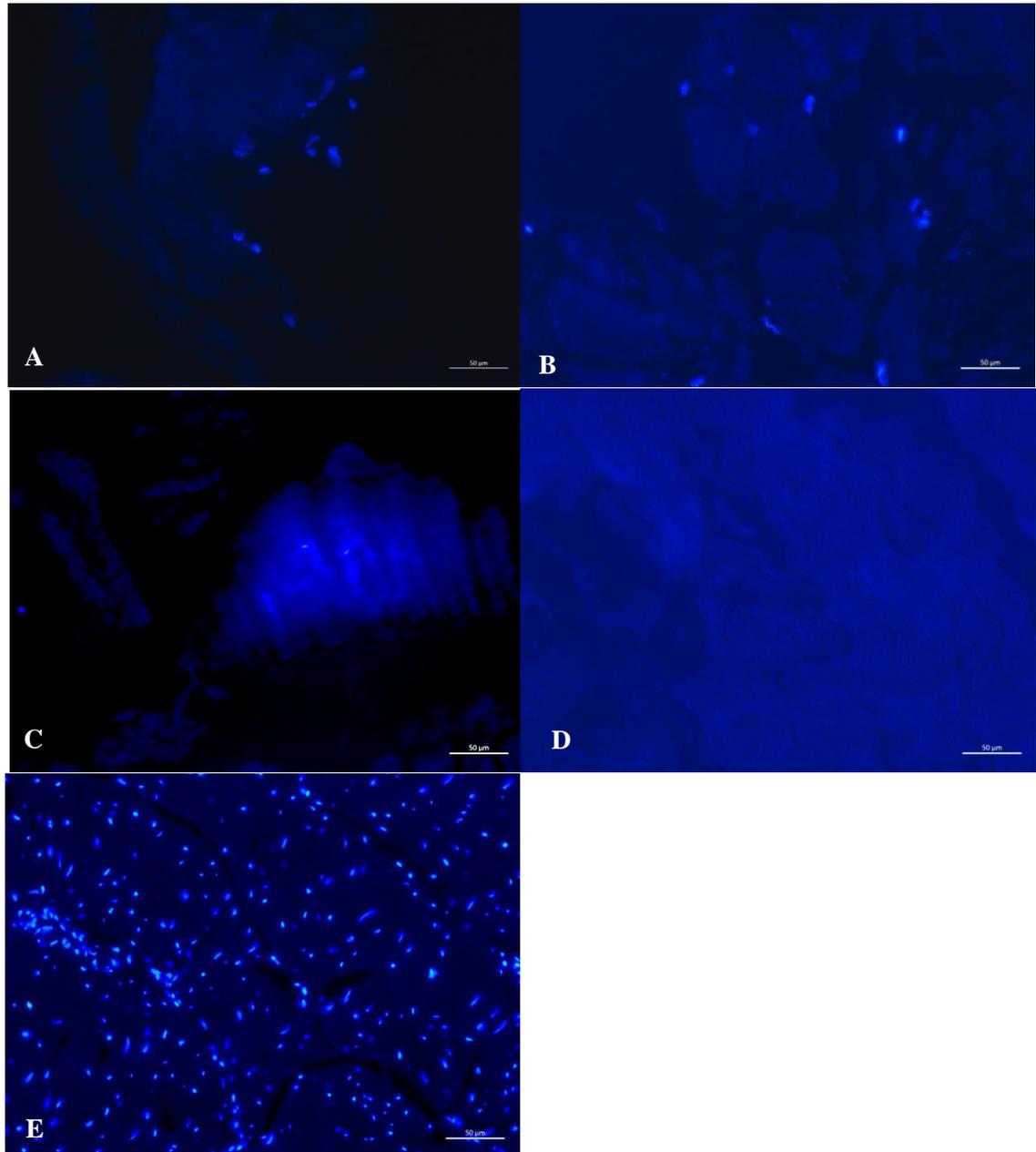
**Figure 6.21 DAPI staining of the human BM-MSCs seeded on the decellularised PPT scaffolds**. (A) Section of the T-0 samples, (B) section of the samples cultured statically for 7 days, and (C) section of the samples cultured under dynamic strain for 7 days. The controls; (D) section of the decellularised PPT scaffolds and (E) the native PPT. Images were captured using 200 x magnifications. Scale bars represent 50 µm.

## 6.4.4. Immunohistochemical analysis of Collagen I, III and Tenascin-C

Sections of the human BM-MSCs seeded decellularised PPT scaffolds from the dynamic strain experiments were labelled using antibodies to tenascin-C [Figure 6.22] with IgG2b as the isotype control antibody for tenascin-C [Figure 6.23], to collagen I [Figure 6.24] with IgG1 as

the isotype control antibody for collagen I [Figure 6.25] and collagen III [Figure 6.26] with

IgG1 as the isotype control antibody for collagen III [Figure 6.27].
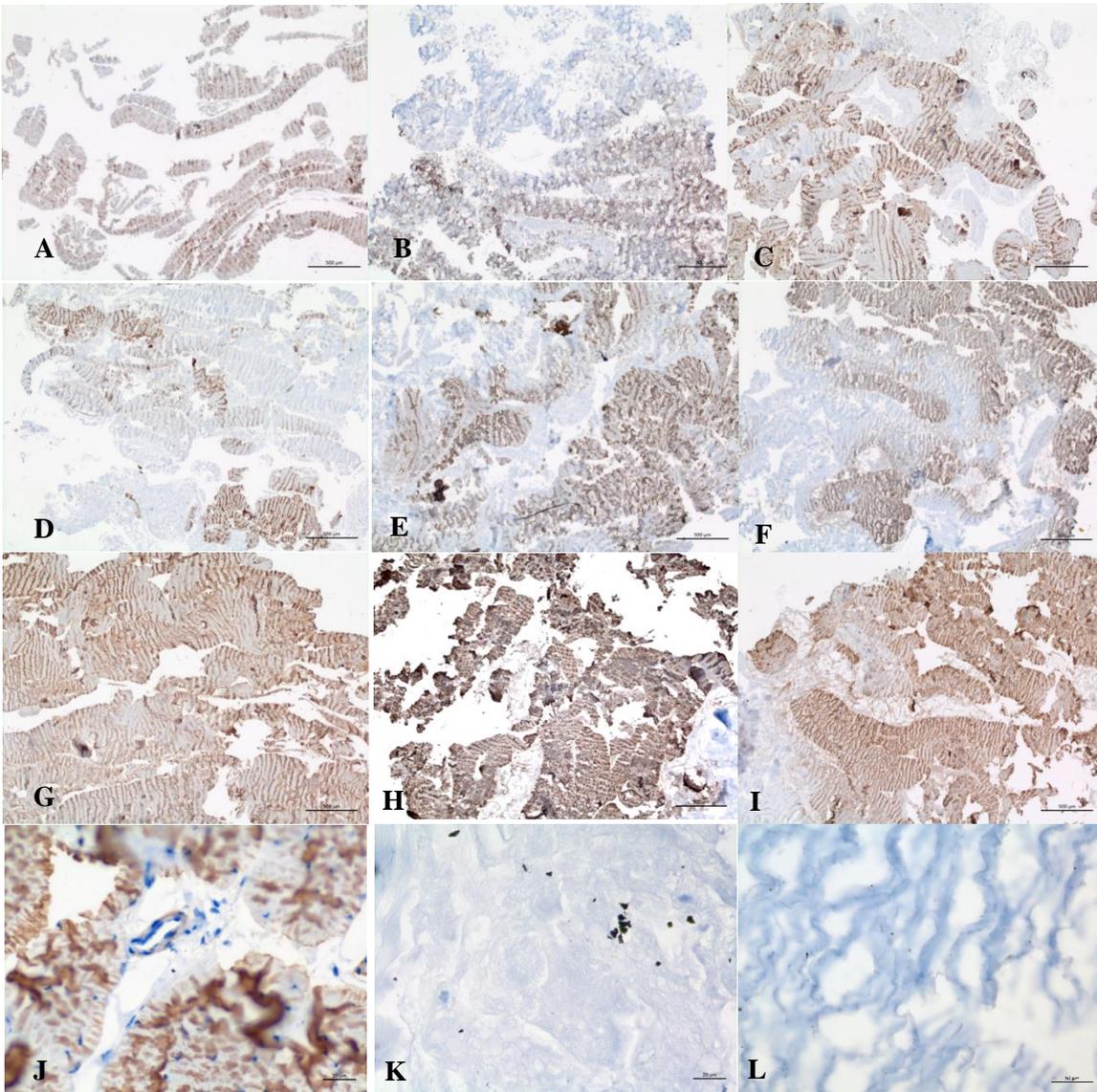


**Figure 6.22 Tenascin-C protein expression in sections of human BM-MSC seeded decellularised PPT cultured under static and dynamic conditions.** A, B, C are sections of T-0 samples, D, E, F are sections of 7-day statically cultured samples. G, H , I are sections of 7-day dynamically cultured sample. A, D, G are the 4 % strain group. B, E, H are the 6 % strain group, and C, F, I are the 8 % strain group. (J) is the positive control (native scaffolds), (K) is the negative control, and (L) is the decellularised PPT scaffold. The A - I sections were imaged at 20 x magnification (scale bars represent 500 µm).to demonstrate the whole section. The J - L sections were captured at 200 x magnification (scale bars represent 50 µm). Tenascin-C labelling was 1 in 100 dilutions.

All sections for tenascin-C labelling and the controls were proceed with trypsin antigen

unmasking that subjected the sections to high temperatures. Sections of the non-seeded

decellularised tendon [Figure 6.22 K] had shown that tenascin-C was washed away during the decellularisation process. In contrast, tenascin-C was expressed in the human BM-MSC seeded decellularised PPT after just 12 h of culture (T-0) [Figure 6.22 A, B, C], although it was not well distributed across the sections. This trend was also seen in the samples incubated for 7 days under static conditions in TenCell-1 [Figure 6.22 D, E, F].

Samples of the human BM-MSC seeded decellularised PPT scaffold that had been cultured under dynamic tensile strain at 4, 6 and 8 % showed increased tenascin-C expression which was distributed evenly across the sections [Figure 6.22 G, H, I], There were no apparent differences between the samples cultured under different strains.
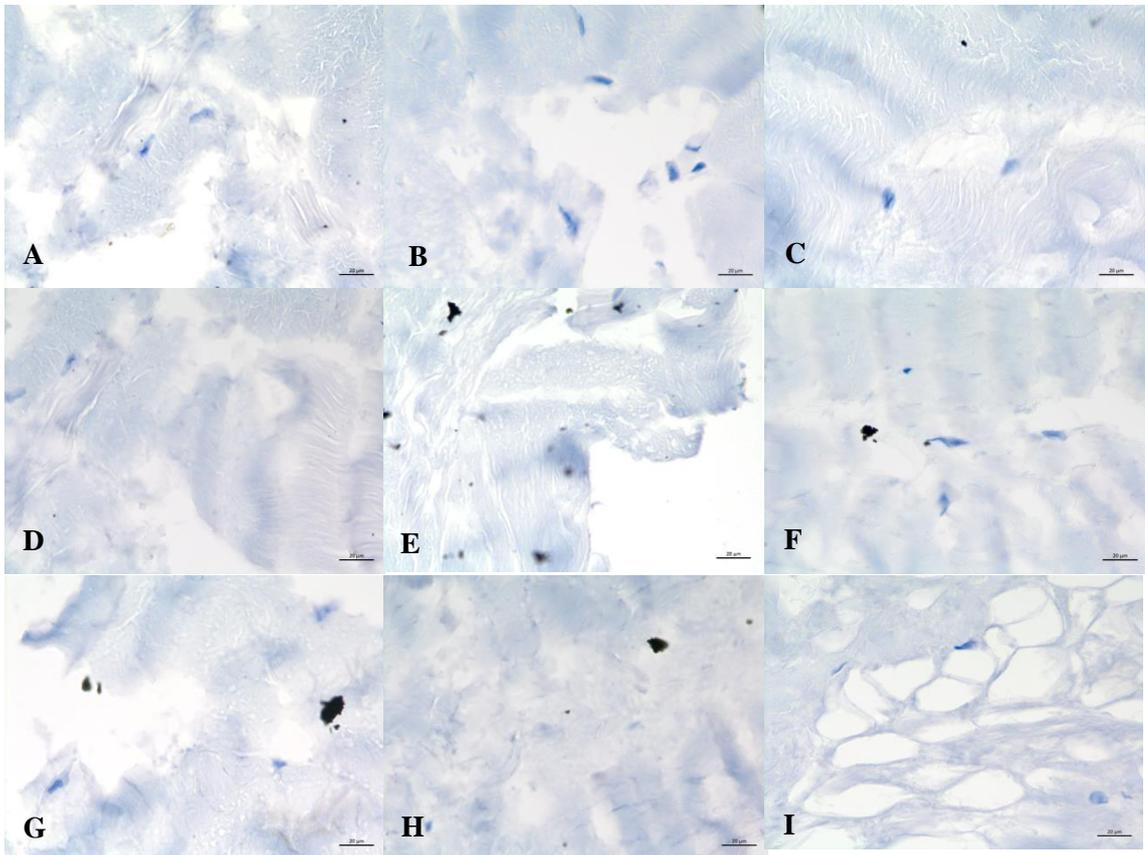


**Figure 6.23 Isotype control antibody stained sections of human BM-MSC seeded decellularised PPT cultured under static and dynamic conditions.** A, B, C are sections of T-0 samples, D, E, F are sections of 7-day statically cultured samples. G, H , I are sections of 7-day dynamically cultured sample. A, D, G are the 4 % strain group. B, E, H are the 6 % strain group, and C, F, I are the 8 % strain group. Images were captured at 200x magnification. Scale bars represent 50 μm.

All groups incubated with Tenascin-C isotype control antibody (IgG2b) showed no positive

staining [Figure 6.23].
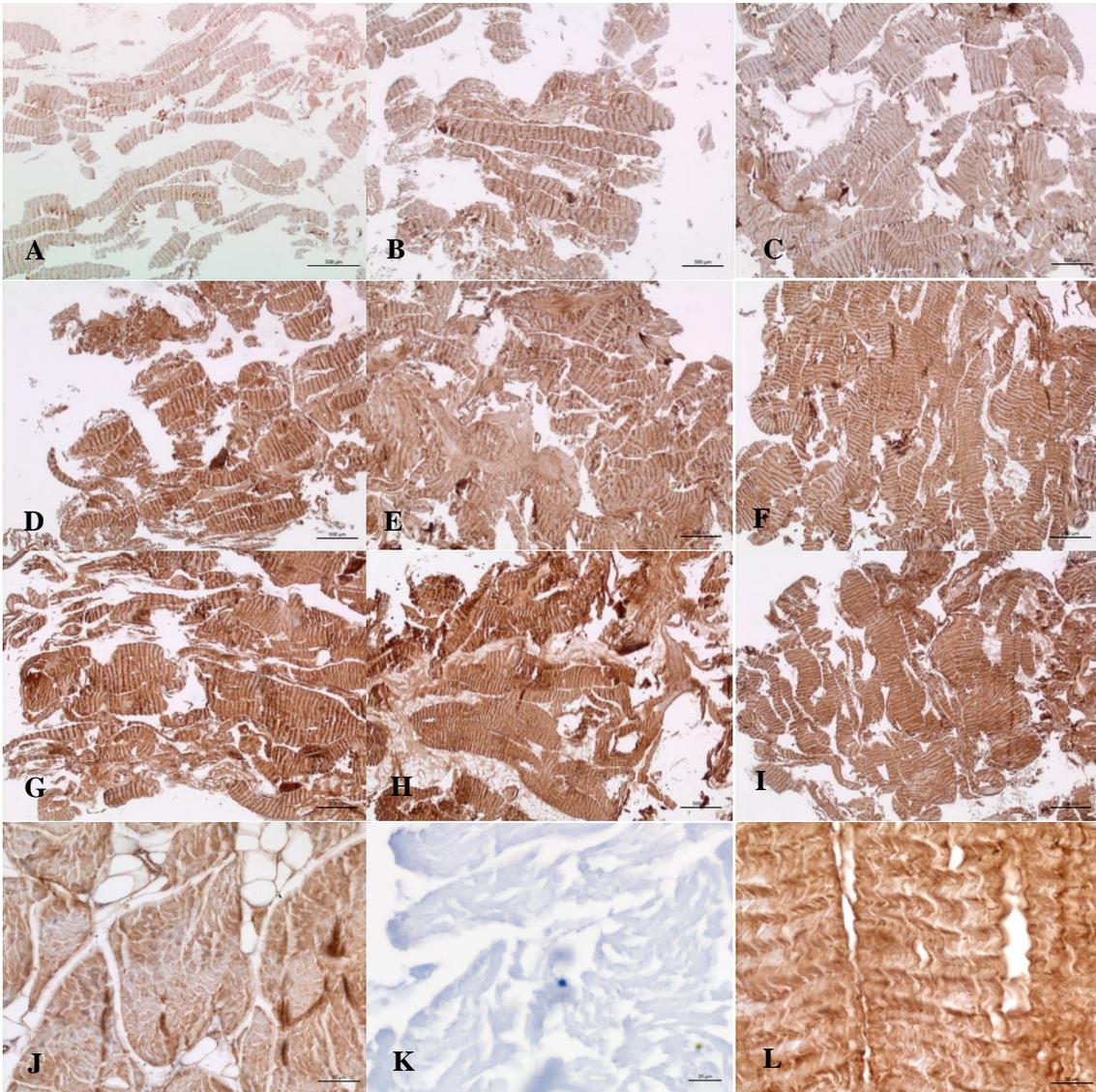


**Figure 6.24 Collagen I protein expression in sections of human BM-MSC seeded decellularised PPT cultured under static and dynamic conditions.** A, B, C are sections of T-0 samples, D, E, F are sections of 7-day statically cultured samples. G, H , I are sections of 7-day dynamically cultured sample. A, D, G are the 4 % strain group. B, E, H are the 6 % strain group, and C, F, I are the 8 % strain group. (J) is the positive control (native scaffolds), (K) is the negative control, and (L) is the decellularised PPT scaffold. The A - I sections were imaged at 20 x magnification (scale bars represent 500 µm) to demonstrate the whole section. The J - L sections were captured at 200 x magnification (scale bars represent 50 µm). Collagen I antibody was 1 in 100 dilutions.

All samples expressed collagen I across the sections [Figure 6.24 A-J, L]. There were no differences seen between the native [Figure 6.24 J], the decellularised tissue sections [Figure 6.24 L], and the cell-seeded on decellularised PPT scaffolds [Figure 6.24 A-I].
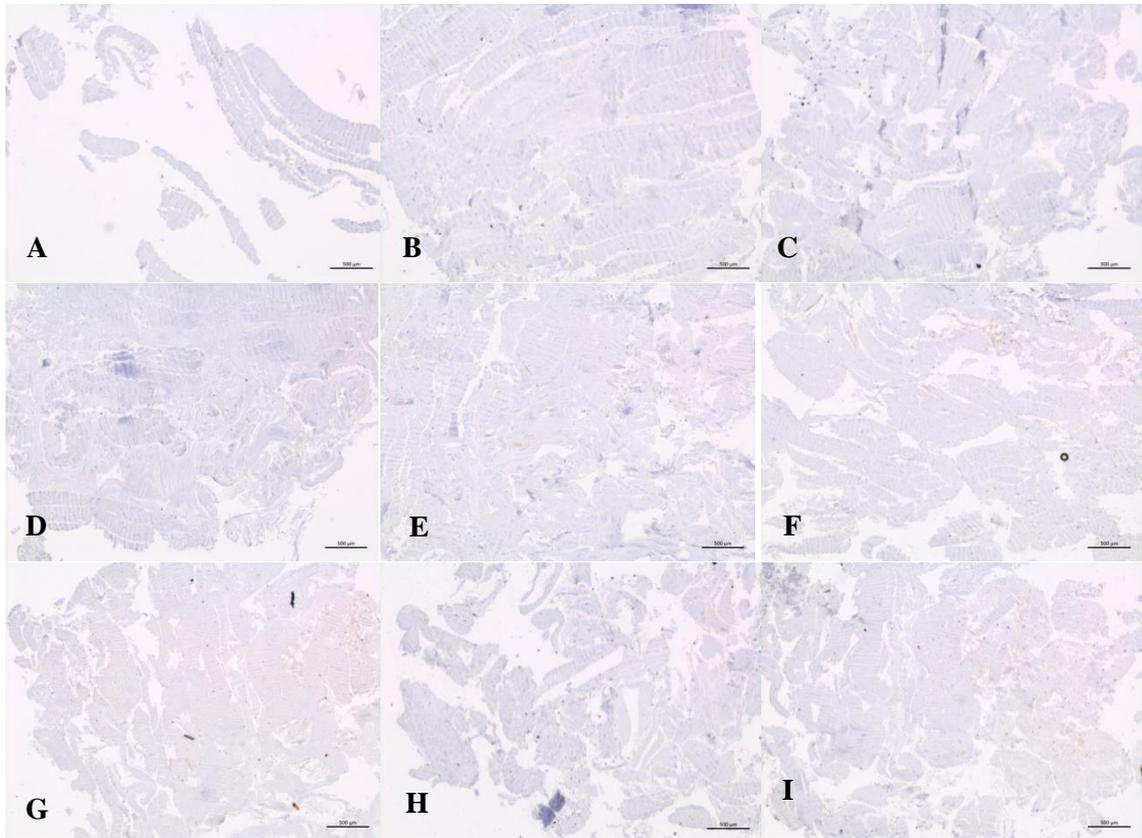


**Figure 6.25 Isotype control antibody for the Collagen I stained sections of human BM-MSC seeded decellularised PPT cultured under static and dynamic conditions.** A, B, C are sections of T-0 samples, D, E, F are sections of 7-day statically cultured samples. G, H , I are sections of 7-day dynamically cultured sample. A, D, G are the 4 % strain group. B, E, H are the 6 % strain group, and C, F, I are the 8 % strain group. Images were captured at 20x magnification. Scale bars represent 50 μm.

All groups incubated with Collagen I isotype (IgG1) [Figure 6.25] had showed no staining.
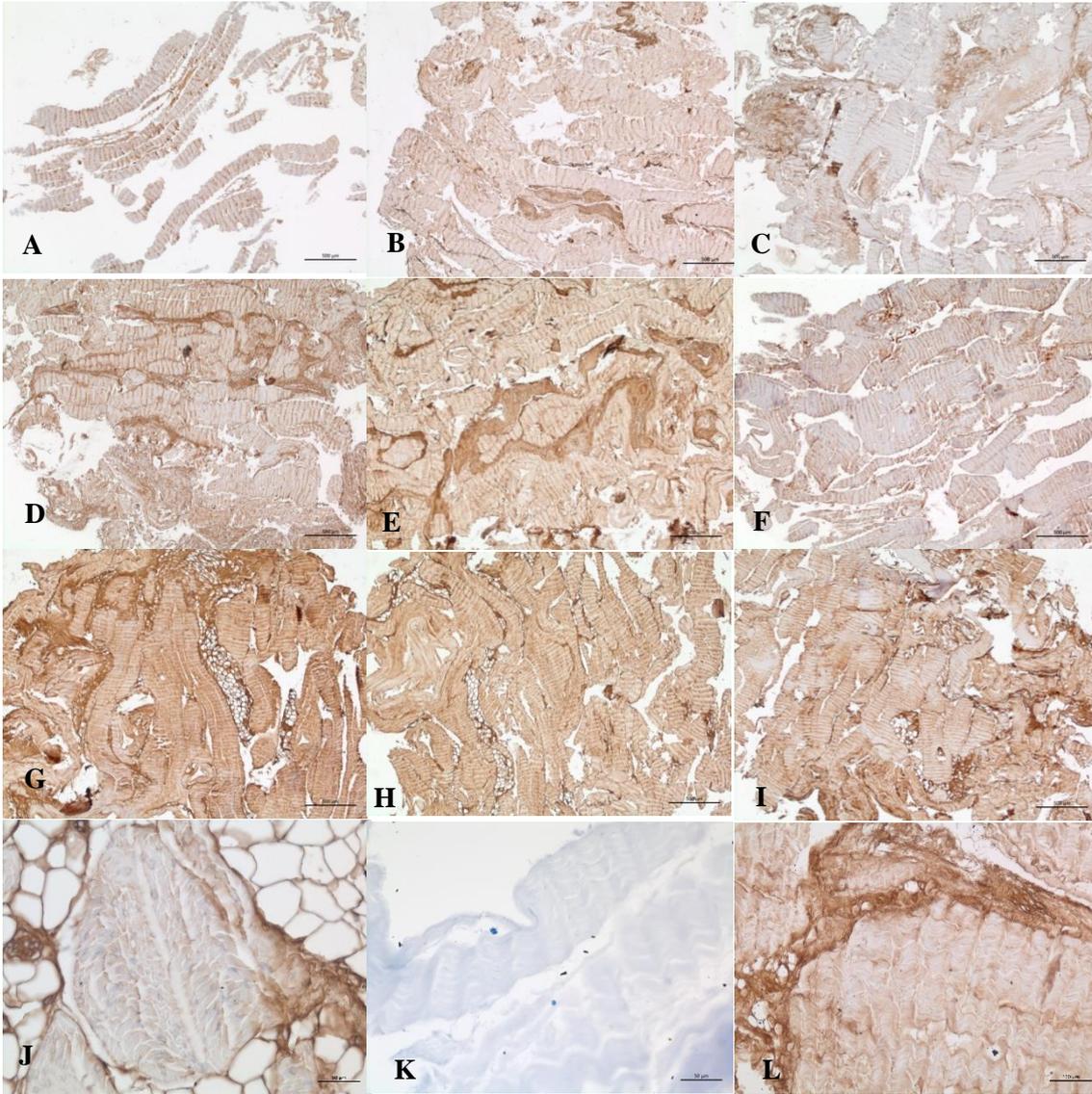
**Figure 6.26 Collagen III protein expressions identified using immunohistochemistry**. The A, B, C are the T-0, the D, E, F are the Static, the G, H , I are the Dynamic, the A, D, G are the 4 %, the B, E, H are the 6 %, and the C, F, I are the 8 %. (J) is the positive control (native scaffolds), (K) is the negative control, and (L) is the decellularised PPT scaffold. The A - I sections were imaged at 20 x magnification (scale bars represent 500 µm) to demonstrate the whole section. The J - L was captured at 200x magnification (scale bars represent 50 µm).

All sections of the cell-seeded samples were stained brown using antibodies to collagen III (1 in 50 dilutions) across the sections, while roughly no differences were seen among the groups [Figure 6.26].
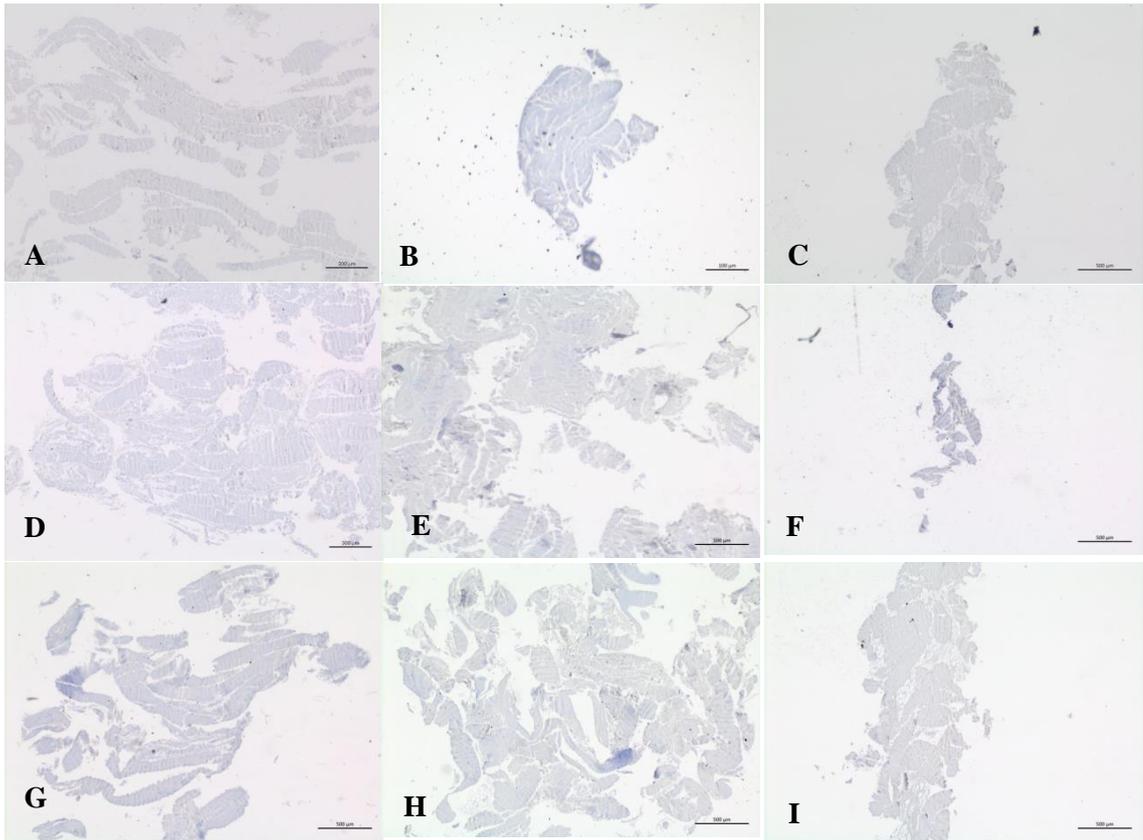
**Figure 6.27 Isotype control antibody for the Collagen III stained sections of human BM-MSC seeded decellularised PPT cultured under static and dynamic conditions.** A, B, C are sections of T-0 samples, D, E, F are sections of 7-day statically cultured samples. G, H , I are sections of 7-day dynamically cultured sample. A, D, G are the 4 % strain group. B, E, H are the 6 % strain group, and C, F, I are the 8 % strain group. Images were captured at 20x magnification. Scale bars represent 50 µm.

All groups incubated with collagen III antibody isotype control (IgG1 1 in 50 dilution) had showed no positive staining [Figure 6.27].

### 6.4.5. Determination of transcript gene expressions

The RNA extracted from the human BM-MSC seeded decellularised PPT scaffolds samples after 12 h incubation (T-0) and 7-days incubation in TenCell-1; with and without cyclic tensile strain at 4, 6 and 8 % was quantified, and the data is presented in Table 6.2.

The isolated RNA was reverse transcribed to complimentary DNA (cDNA) then amplified to the detected level to define transcript gene expression towards the tenogenic (tenascin-C,

collagen I, collagen III and scleraxis), the chondrogenic (collagen II and Sox9), the osteogenic

(osteopontin), and the adipogenic (PPARγ) lineages using two step RT-qPCR.

| Group | RNA concentration (ng.μl⁻¹) (mean (n=3) ± 95 % Cl) | Total RNA (ng in 30 μl) |
|---|---|---|
| T-0 4 % | $1.54 \pm 3.02$ | 46.2 |
| Static 4% | $2.56 \pm 0.49$ | 76.8 |
| Dynamic 4% | $6.30 \pm 1.82$ | 188.9 |
| T-0 6 % | $2.05 \pm 4.94$ | 61.5 |
| Static 6% | $3.37 \pm 2.75$ | 101.2 |
| Dynamic 6% | $7.77 \pm 6.56$ | 233.1 |
| T-0 8 % | $2.17 \pm 2.46$ | 65.1 |
| Static 8% | $2.88 \pm 1.38$ | 86.5 |
| Dynamic 8% | $8.52 \pm 1.72$ | 255.6 |

**Table 6.2 RNA quantification of human BM-MSC seeded decellularised PPT scaffolds samples after incubation for 12 h (T-0) or 7 days in the TenCell-1 bioreactor** under static or dynamic conditions.

Examples of representative dissociation curves obtained using each set of primer pairs are presented in Figures 6.28 - 6.30.
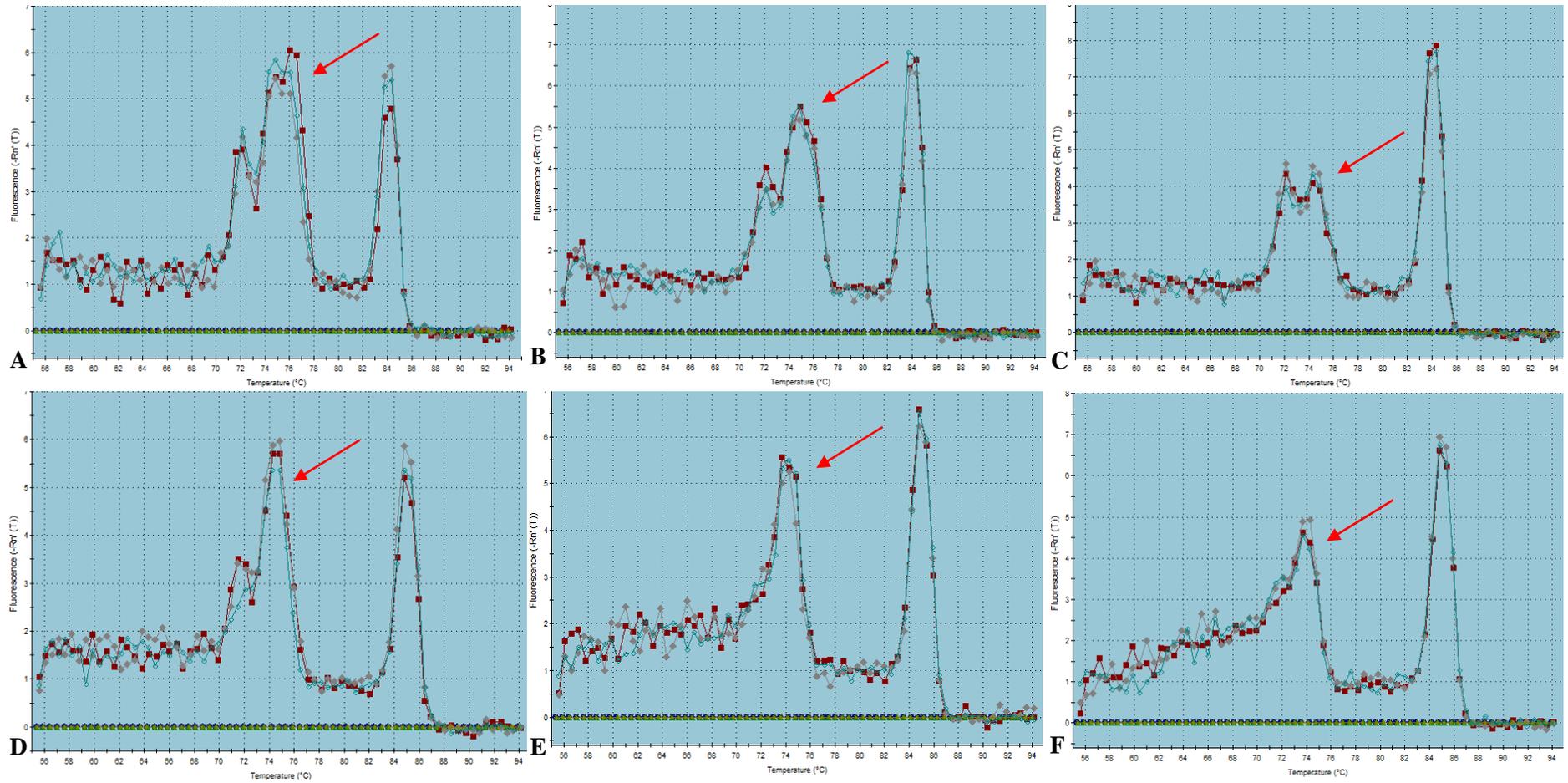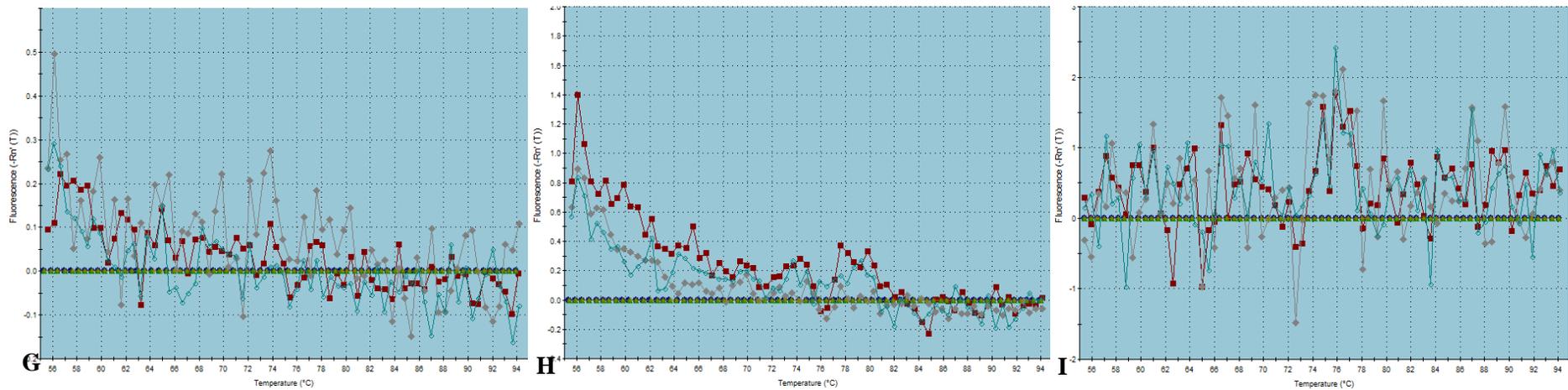
**Figure 6.28 Dissociation curves from RT-qPCR using primers for Tenascin-C and S28 R  (4% dynamic strain experiment).**
A, B, C show the dissociation curves for Tenascin-C, and D, E, F the dissociation curves for S28 R. A and D are T0 (12 hour seeded samples) from the 4% dynamic strain experiment. B and E are samples following 7 days culture in TenCell-1 from  the 4% strain experiment and C and F are samples following 7 days incubation in TenCell-1 with 4% dynamic strain. G is template alone, H is primer alone, and I is water alone controls. The red arrows point to an extra peak which melted at 74 – 75 $^0$C in all of the test samples, and (I) water control. The red arrows point to the melting curves found in all products melted at 74 – 75 $^0$C and had almost similar peak shape.

Amplification of the cDNA generated from the RNA isolated from the human BM-MSCs in the decellularised PPT scaffolds for each of the three experiments

at T-0 and after 7 days incubation under dynamic strain or statically in TenCell-1 was carried out using the established qPCR protocol.

The dissociation curves obtained following amplification of the cDNA using primers for Tenascin-C using samples from the 4% dynamic strain experiment

are shown in Figure 6.28 A, B, C. It was found that all of the samples (T-0; 7 day statically cultured and 7 day dynamically cultured) demonstrated multiple

peaks which melted at 72, 74 and 84 $^0$C. The dissociation curves obtained following amplification of the cDNA using primers for S28 R using samples from the 4% dynamic strain experiment are shown in Figure 6. 28 D, E, F.

It was found that all of the samples (T-0, 7-day statically cultured and 7-day dynamically cultured) also demonstrated multiple peaks which melted at 74 and 85 $^0$C. There were no peaks present in any of the control samples (Figure 6. 28 G, H, I). Similar data was obtained when samples of the cDNA from the 6% and 8% strain experiments were amplified using primers to Tenascin-C and S28 R. These results indicated that the PCR reactions were generating an additional product which melted at 74-75$^o$C which was not present in any of the controls. This meant that the data could not be reliably used to obtain a quantitative measure of the expression of the genes for Tenascin-C or S28R.
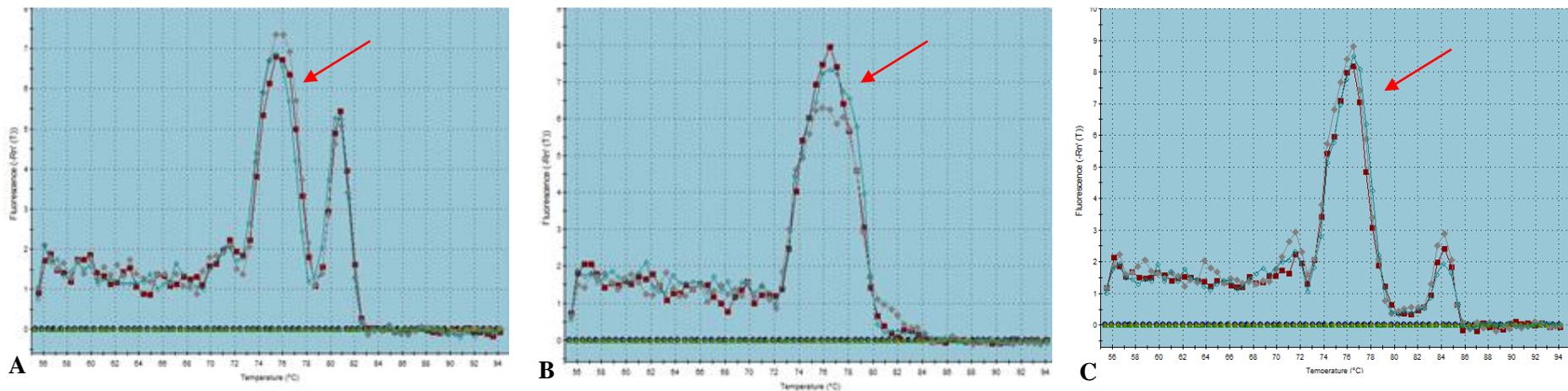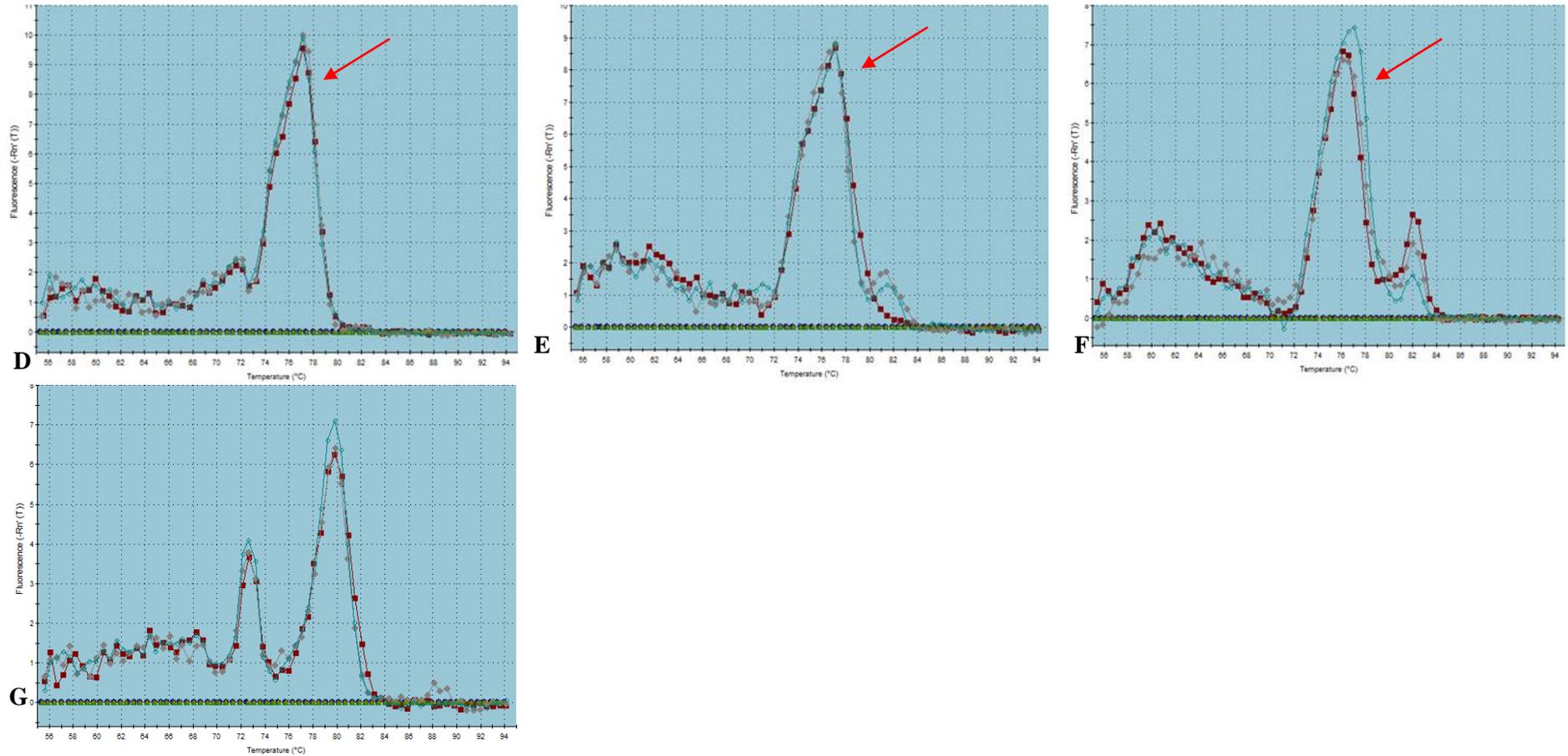
**Figure 6.29 Dissociation curves using primers for collagen I, collagen II, collagen III, SOX 9, PPARγ, osteopontin and scleraxis.** (A) Collagen I, (B) Collagen II, (C) Collagen III (D) SOX9, (E) PPARγ, (F) Osteopontin, and (G) Scleraxis from samples cultured for 7 days under 6% dynamic strain in TenCell-1. The red arrows points to an extra peak that melted at $76 - 77\ {}^{0}C$ in all of the samples.

Examples of the dissociation curves obtained when the cDNA obtained from samples that had been cultured for days under 6% dynamic strain was amplified using primers to collagen I, collagen II, collagen III, Sox 9, PPARγ, osteopontin and Scleraxis are shown in Figure 6.29.

For collagen I, collagen III and Scleraxis there were two peaks detected, but only one peak at 76-77$^{o}$C for the other genes of interest, and this appeared to a contaminating peak. All of the curves demonstrated an additional peak which melted at 76-77$^{0}$C as had been found above. Similar results were obtained when these genes of interest were analysed in samples of the T-0 and 7-day static cultures from the 6% dynamic strain experiment and the samples from the 4% and 8% strain experiments. These results indicated that the PCR reactions were again generating an additional product which melted at 74-75$^{o}$C which was not present in any of the controls. This meant that the data could not be reliably used to obtain a quantitative measure of the expression of the genes of interest.

As a result of the presence of the contaminating peak identified in all cDNA sample amplifications; experiments were conducted in an attempt to determine the source of the contamination. A series of different template concentrations were amplified using primers to GAPDH. The dissociation curve data obtained from the RT-qPCR is presented in Figure 6.30 and the DNA products were visualised using gel electrophoresis 3.5 % (w/v) agarose and presented in Figure 6.31.

The results showed the presence of a melting peak that melted at 88 – 89 $^{0}$C, which decreased with increasing dilution of the template and was suspected to be the GADPH peak. However, the contaminating peak at 78 – 79 $^{0}$C was present in each reaction and was not affected by the concentration of the template, indicating that whatever was being amplified was not dependent upon the concentration of the template used [Figure 6.30].
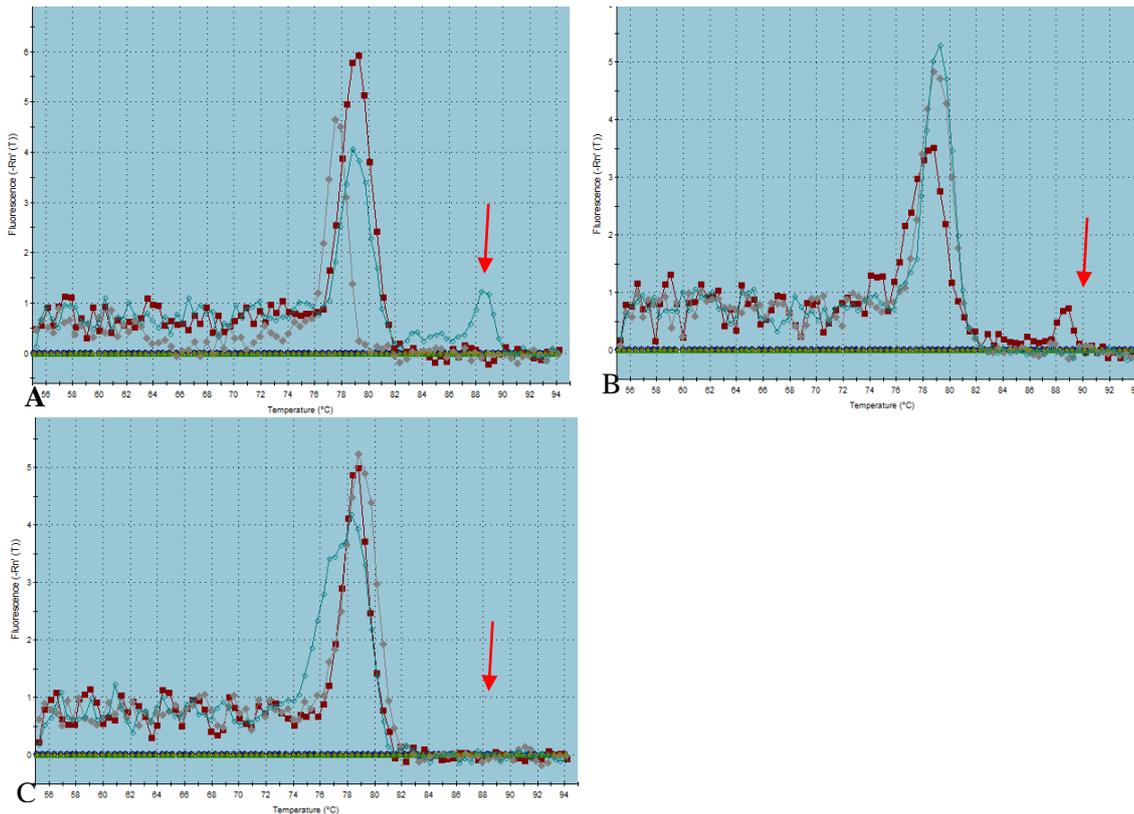
**Figure 6.30 Dissociation curves obtained following amplification of cDNA using primers for GADPH using a serial dilution of the template from the dynamically cultured at 4% strain sample.** (A) 1 in 2 dilution (B) 1 in 4 dilution, and (C) 1 in 8 dilution. The red arrows point to the peaks that melted above 80°C, that are suspected as the expected products.

The amplified DNA samples from this experiment (using primers to GAPDH) were visualised using 3.5 % agarose gel electrophoresis. Only the DNA amplified using the 1:2 dilution of the template generated a single band at 189 bp, suspected the GADPH - DNA product [Figure 6.31 A]. The DNA amplified using the 1:4 [Figure 6.31 B] and 1:8 dilutions [Figure 6.31 C] of the template failed to produce bands that could be visualised by gel electrophoresis. This indicated that there migh be not enough GADPH - DNA products generated from samples with templates were diluted upto 1:4 and 1:8 dilutions.

There were a similar peaks appeared in all amplifications and not been affected by the template concentrations. It is possible that the contaminating peak identified in the PCR reactions was not identified as DNA upon gel electrophoresis [Figure 6.31].
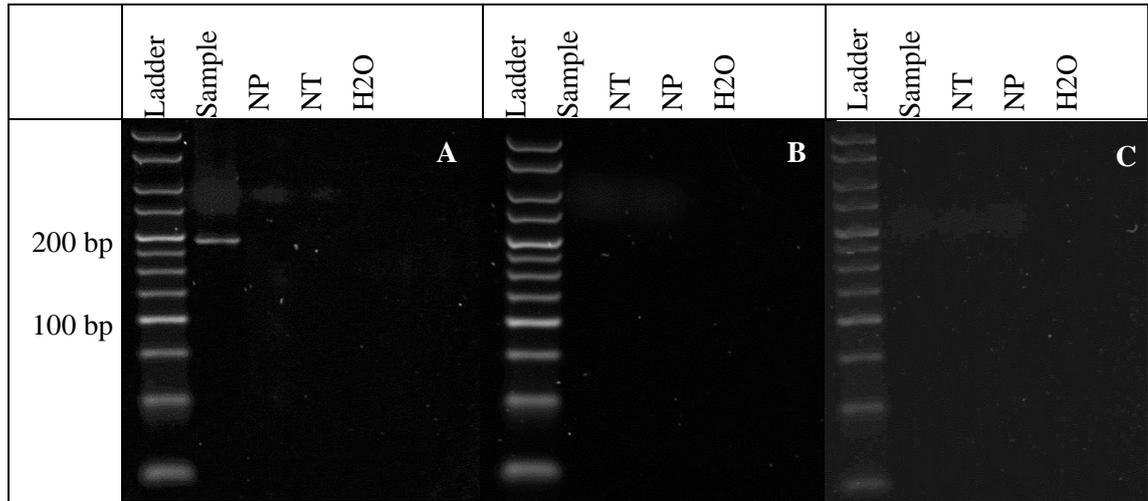
**Figure 6.31 Agarose gel electrophoresis of the PCR products from the amplification of cDNA using primers for GAPDH.** One single band was found in (A) with 1 in 2 dilution of the template, while (B) 1 in 4 dilution of the template and (C) 1 in 8 dilution of the template showed no band. NP is no primer control, and NT is no template control.

Since the RT-PCR data could not be quantified due to the problem of the contaminating peak in all samples, and given that the contaminating peak did not appear as a DNA band on agarose gel electrophoresis, it was decided to visualise the amplified DNA from the three experiments separated according to the length of the DNA produced using gel electrophoresis 3.5 % (110 V, 45 min).
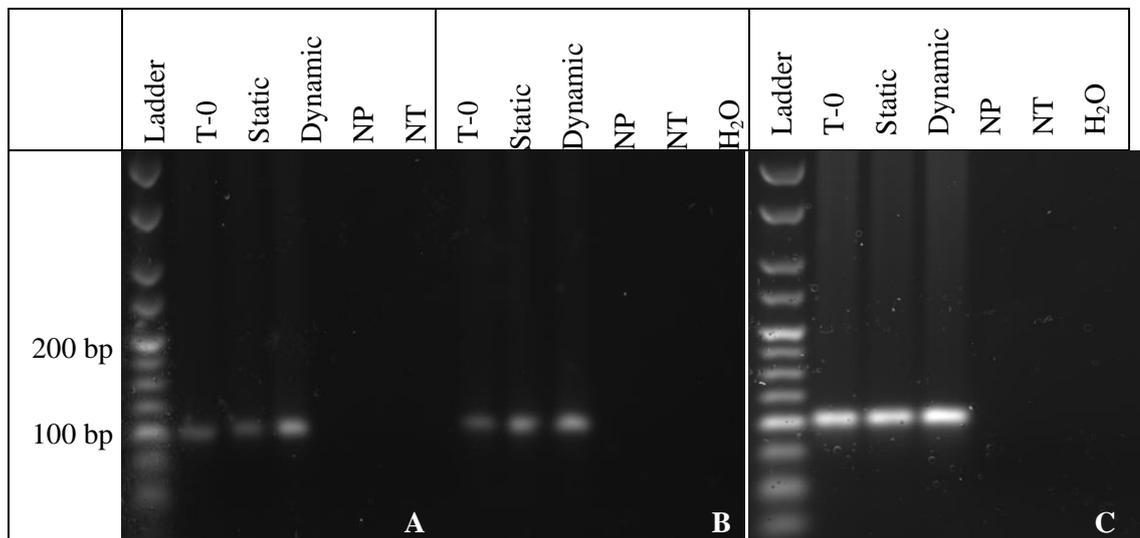


**Figure 6.32 Agarose gel electrophoresis of the PCR products using primers for S28R from the amplification of cDNA** of; (A) 4 %, (B) 6 %, and 8 % cyclic strength.

Analysis of the PCR products for the genes of interest showed that all human BM-MSCs seeded decellularised PPT scaffold samples after 12 h (T-0) or 7-days incubation, with and without cyclic tensile strain at 4, 6 or 8% had a single DNA band of the S28 R (100 bp) [Figure 6.32], collagen I (71 bp) [Figure 6.33 A, B, C], collagen III (116 bp) [Figure 6.33 G, H, I], and tenascin-C (102 bp) [Figure 6.34 A, B, C].
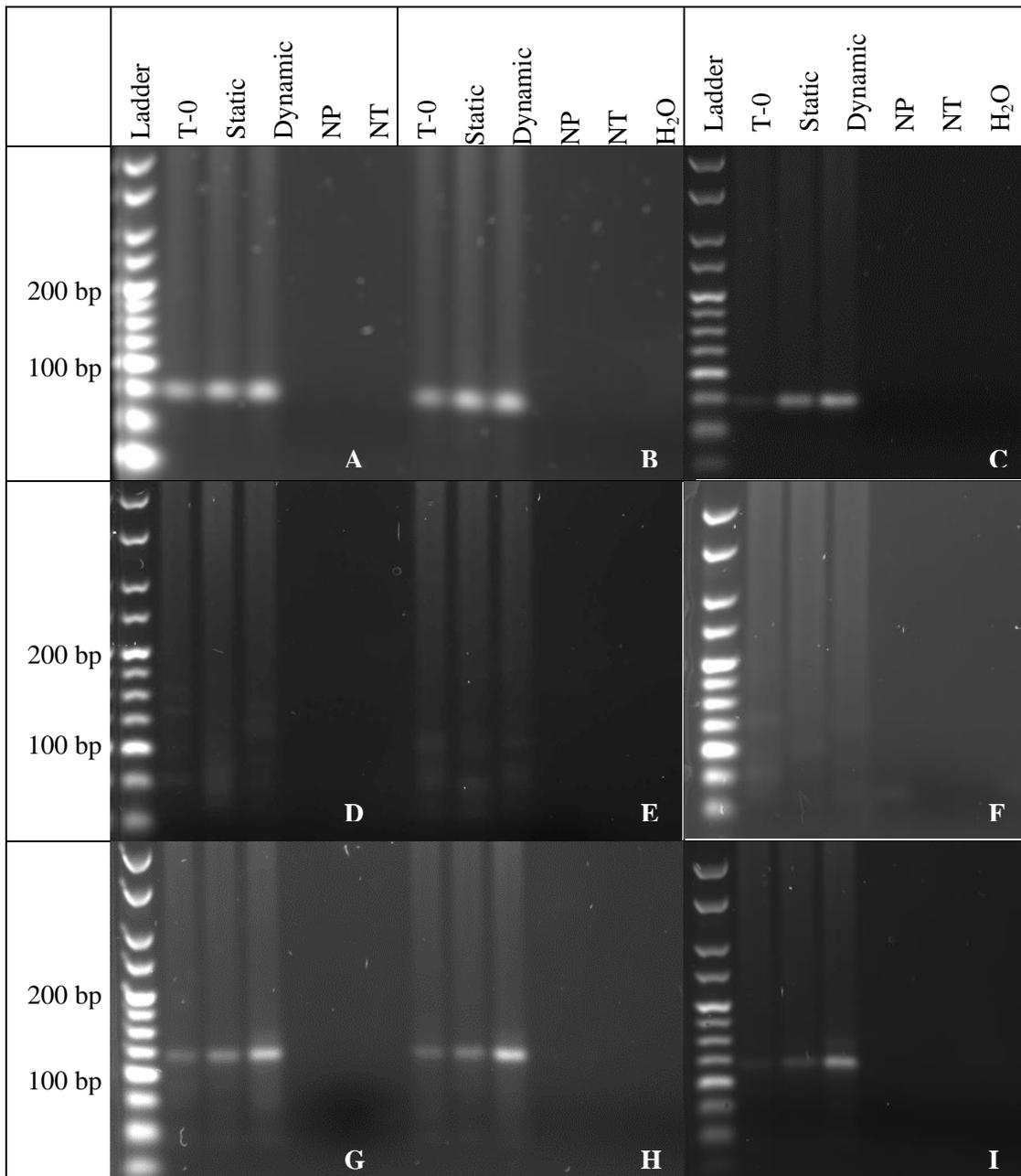


**Figure 6.33 Agarose gel electrophoresis of the PCR products**, using primers for (A, B, C) collagen I, (D, E, F) collagen II, (G, H, I) collagen III. And the amplification of cDNA from (A, D, G) the 4 % cyclic strain, (B, D, H) 6 % cyclic strain, (C, F, I) 8 % cyclic strain.
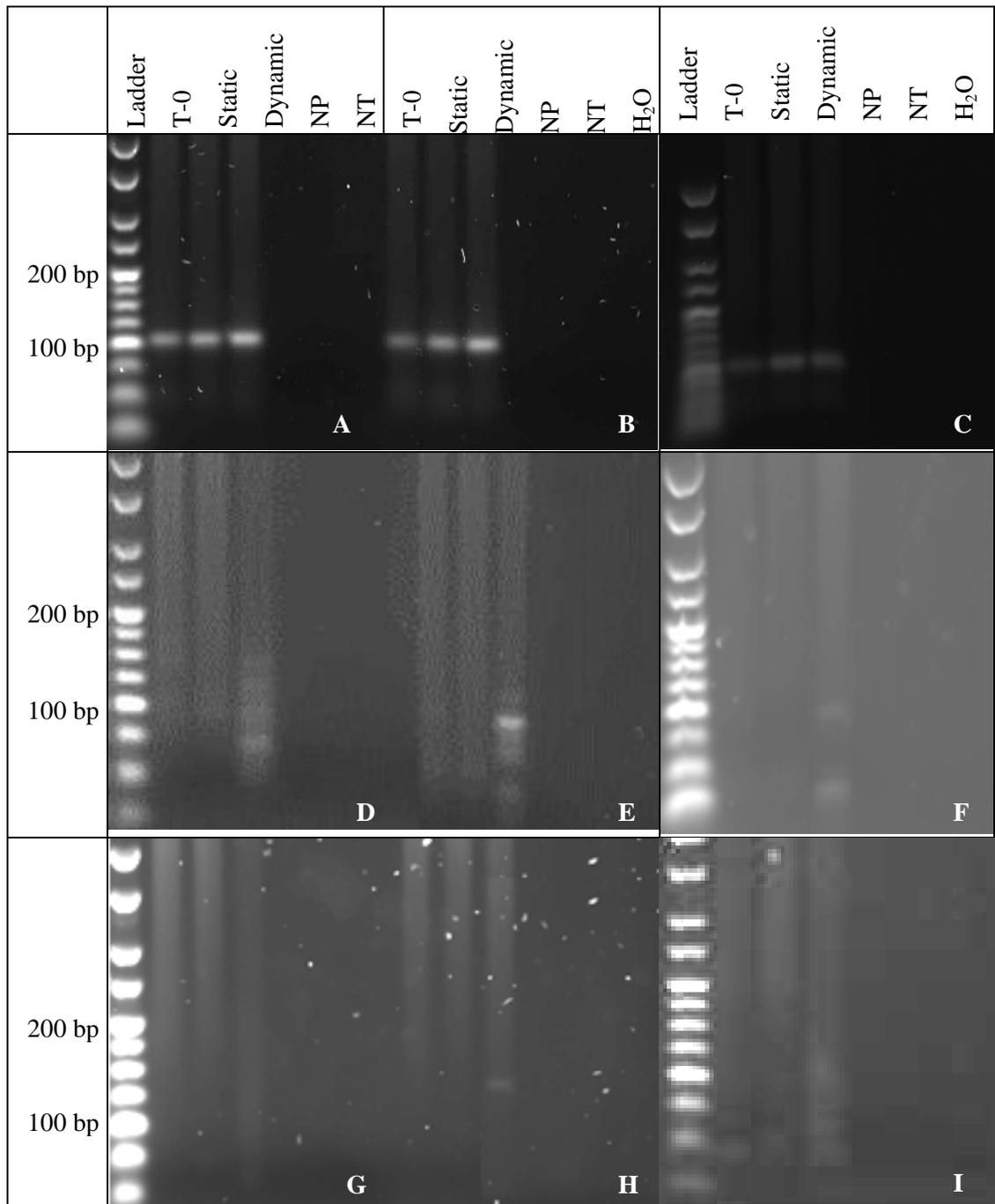
**Figure 6.34 Agarose gel electrophoresis of the PCR products, using primers for (A, B, C) tenascin-C, (D, E, F) scleraxis, (G, H, I) osteopontin**. And the amplification of cDNA from (A, D, G) the 4 % cyclic strain, (B, D, H) 6 % cyclic strain, (C, F, I) 8 % cyclic strain.

Only samples amplified from the cDNA of human BM-MSCs seeded decellularised PPT scaffolds cultured under dynamic strain at 6 % [Figure 6.34 E] and 8 % [Figure 6.34 F] gave a single band of the Scleraxis gene (91 bp). Osteopontin expression (116 bp) was present in the

human BM-MSCs in decellularised PPT scaffolds cultured under 6% dynamic strain [Figure 6.34 H].

No DNA bands representative of the genes for collagen II (76 bp) [Figure 6.33 D, E, F], PPARγ (140 bp) [Figure 6.35 A, B, C] or SOX9 (69 bp) [Figure 6.35 D, E, F] were visible in any samples. None of the controls showed any evidence of DNA bands.
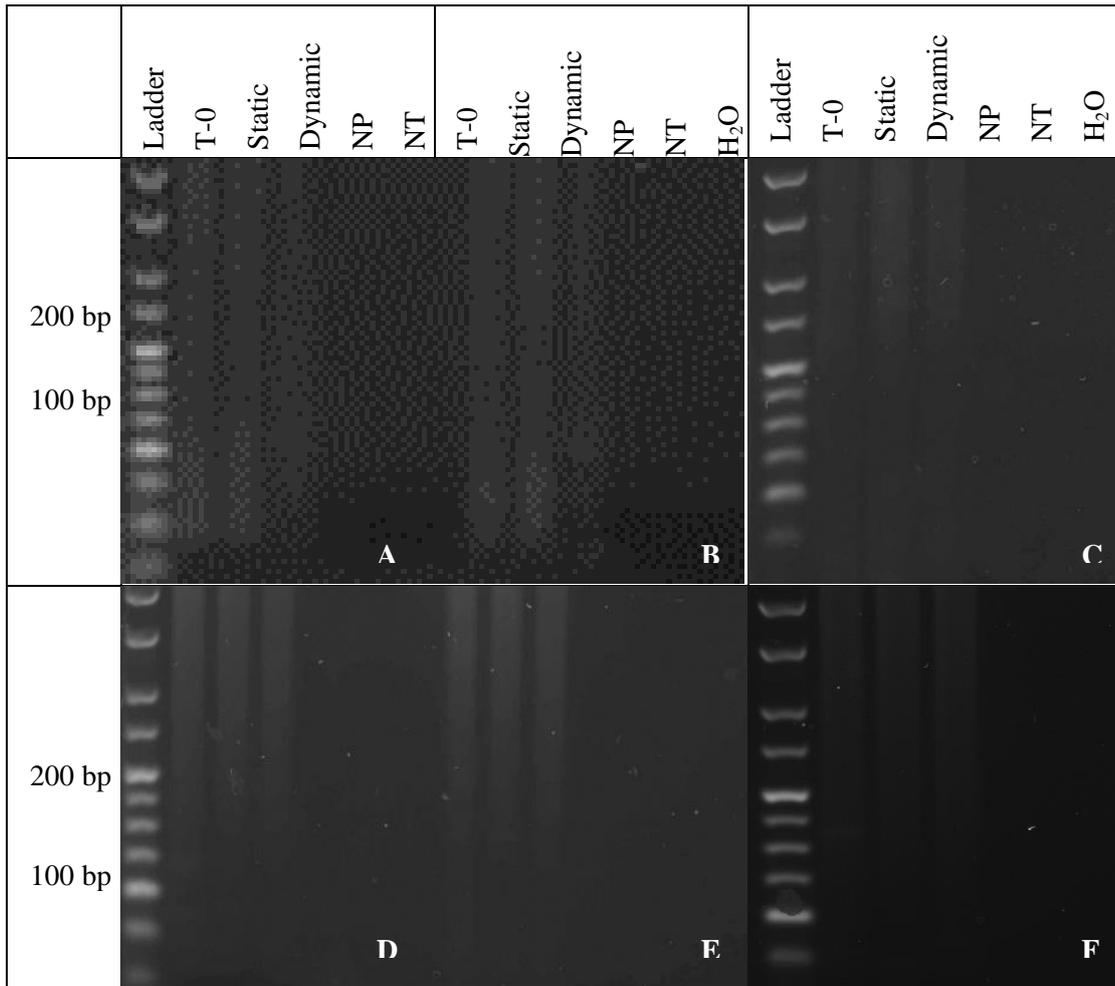


**Figure 6.35 Agarose gel electrophoresis of the PCR products, using primers for (A, B, C) PPARγ and (D, E, F) Sox9**. And the amplification of cDNA from (A, D) the 4 % cyclic strain, (B, E) 6 % cyclic strain, (C, F) 8 % cyclic strain.

Overall, the analysis of the gel electrophoresis presented above [Figure 6.31 – 6.35] showed that there was a consistent trend of no DNA band visible in the gel, while in the qPCR analysis, the dissociation curve (melted at 76 – 79 $^0$C) was found. Perhaps the extra peak appeared in the qPCR analysis was not a DNA, however a product that had emission at 280 – 502 nm (that similar with SyberGreen).

## 6.5. Discussion

The capability of the human BM-MSCs to attach to decellularised PPT scaffolds after seeding was presented in Chapter 5. The purpose of this chapter is to present further study of human BM-MSCs in decellularised tendon scaffolds in response to incubation with mechanical strain.

The Live/Dead assay indicated that the human BM-MSCs seeded onto decellularised PPT scaffolds and cultured under 6 % cyclic tensile strain had the highest percentage of viable cells. The viability of the cells seeded on the PPT scaffolds incubated under 4, 6 and 8 % cyclic tensile strain was significantly higher than samples incubated under static conditions, and application of 6 % strain resulted in the highest ATP levels compared to the other groups. The confocal imaging of the cell-seeded scaffolds of the samples incubated under static conditions clearly showed the cells were mostly stained with both Calcein and Ethidium homodimer. Perhaps those cells stained with both dyes and had enlarge shape were dying (Dimri et al., 1995, Sethe et al., 2006).

H&E staining of tissue sections showed that the human BM-MSCs-seeded in decellularised PPT scaffolds and cultured under 4, 6, and 8 % cyclic tensile strain for 7 days had collagen fibres that were aligned and the fibres demonstrated normal crimp. This was in contrast to the fibres of the decellularised PPT, which were loosened as a result of the decellularisation process. Moreover, the cells in the BM-MSC seeded decellularised PPT scaffolds incubated with 4, 6, and 8 % mechanical strain were found to have a spindle-fusiformic shape, arranged in a lattice formation in-between the fibres. This configuration is needed for cell-to-cell communication throughout the matrix (McNeilly et al., 1996). No differences were apparent due to the application of strains of different magnitudes. In the cell-seeded scaffolds incubated under static conditions for 7 days, the cells had an irregular shape and size, were found mostly in loosened or at the surface, and the collagen fibres appeared as a disorganised matrix. Immunohistochemical labelling using the tenascin-C antibody of the human BM-MSCs seeded onto decellularised PPT scaffolds following incubation under 4, 6 and 8 % cyclic strain showed that the sections had been stained positively, and the staining was widely dispersed. Sections of

the cell-seeded scaffolds incubated under static conditions for 7 days and the Day 0 samples were partially stained positive for tenascin-C. The non-seeded control decellularised PPT scaffolds showed no positive staining for tenascin-C, indicating that tenascin-C had been removed by the decellularisation process. Thus, it was demonstrated that tenascin-C was produced by the human BM-MSCs when they were seeded onto the decellularised PPT scaffolds, and that tenascin-C production was dispersed across the scaffolds in response to 4, 6 and 8 % cyclic tensile strain, however was not when cultured under static conditions for the same duration.

Unfortunately, it was not possible to quantify the levels of expression of genes of interest by the human BM-MSC seeded onto the scaffolds before and after 7-days incubation in the presence and absence of cyclic tensile strain. The dissociation curves obtained during real time PCR amplifications of the cDNA from the cell-seeded decellularised PPT scaffolds of all samples (T-0, static and dynamic groups) had several dissociation peaks, suggesting that each of the PCR amplifications generated more than one DNA product. Agarose gel electrophoresis was used to visualise the DNA, showed that samples which produced two peaks during the real time PCR amplifications, such as in the qPCR for tenascin-C and S28R, had only one DNA band that migrated at the expected DNA base pair length for tenascin-C and S28R. Samples which showed three peaks in the real time PCR amplifications, such as for scleraxis, revealed two DNA bands upon agarose gel electrophoresis, one at the expected DNA base pair length for scleraxis, and another with a length of 45 – 50 bp, suspected to be primer dimers. Samples with a single peak during the real time PCR amplification, such as for collagen II and Sox 9, failed to show a DNA band after agarose gel electrophoresis.

The same peak corresponding to a contaminating substance was found in the real time PCR amplifications of all of the samples. The contaminating substance had a melting point of approximately 74 -76 $^0$C, and the peak shape was similar between samples. Serial dilutions of the cDNA template were used to amplify GADPH, and this produced a peak with a melting point at 89 $^0$C (indicating the DNA), which decreased in proportion to the amount of template

used. A second contaminating peak was unaffected by the template concentration. This might indicate that the contaminating peak found in all real time PCR reactions at 74 - 76 $^{0}$C was not DNA.

It is possible that the contaminant was due to a substance with an absorbance wavelength similar to SyberGreen (280 – 502 nm), such as SDS at 497 – 520 nm. SDS is the detergent used to dissolve cells in the matrix, and was introduced during the early steps of the decellularisation protocol. This was followed by subsequent of thoroughly washing steps. SDS contamination in the sample can be detected using a colorimetric method, based on a methylene blue dye-binding assay that enables detection of the presence of SDS up to 0.00005 % or 150 ng per 300 µL (Arand et al., 1992a). Due to the time limits in this study, it was impossible to investigate the existence of the contaminant substance extracted from the decellularised PPT scaffold, as there were no sterile decellularised PPT scaffold remains and there was not enough time to generate a new batch of the decellularised PPTs.

Another point to highlight is the RNAs extracted from the cell-seeded scaffolds were also shown to be of low integrity. The A260/280 ratio was below the limit required to demonstrate RNA purity. The A260/280 ratio is believed to provide enough information for the RNA integrity (Nolan et al., 2006). Another method used to detect RNA integrity is by denaturing the elution in a polyacrylamide gel to visualise the proportion of the S28 and S18 band, that should be 2: 1 (Loening, 1967), however it was not applicable in this study as the total RNA elution volume was only 30 µL. Above all, the quantity of RNA extracted throughout the study using cell-seeded scaffolds were all below 10 ng.µL$^{-1}$. The method used to extract the RNA may require further optimisation to work with samples from tissue and samples with low RNA concentration.

Nevertheless, agarose gel electrophoresis revealed some qualitative data on the expression of the genes of interest in the human BM-MSC seeded decellularised PPT scaffolds. All of the samples (T-0, static and dynamic groups under 4, 6 or 8 % cyclic tensile strain) produced DNA

bands for collagen I, collagen III and tenascin-C. None of the conditions used to incubate the human BM-MSCs seeded decellularised PPT scaffolds promoted differentiation of the cells into cells expressing genes representative of adipogenesis (PPARγ), chondrogenesis (Sox 9; collagen II) or osteogenesis, with the exception the samples incubated under 6 % cyclic tensile strain for 7 days, which stimulated the BM-MSCs to express the gene for osteopontin. Interestingly, the incubation of the human BM-MSC seeded decellularised PPT for 7 days under 6 % and 8 % cyclic tensile strain induced the expression of scleraxis; the tenogenesis gene expressed by human BM-MSCs under tenogeneic condition (Schweitzer et al., 2001, Chen et al., 2012).

When the cell-seeded scaffolds were analysed for their biomechanical properties, it was found that the elastin phase slope and the UTStress were significantly higher in the BM-MSC seeded decellularised PPT scaffolds that had been cultured for 7 days under 6 % and 8 % cyclic tensile strain compared to the statically cultured controls. The Young`s modulus of the samples cultured under 6% cyclic tensile strain was also increased significantly compared to the Day 0 samples. The UTStress of the samples cultured under 6 % cyclic tensile strain for 7 days was significantly greater than the UTStress of the native PPT, the decellularised PPT scaffolds and the Day 0 control samples.

These data led to the conclusion that culture of human BM-MSCs seeded decellularised PPT scaffolds under 6 % cyclic tensile strain increased the matrix stiffness significantly. It was not possible to determine whether this increase in stiffness was due to matrix production as the production of ECM proteins (collagen I and III) was not quantified in these studies. Histological analysis had however shown that all cell-seeded scaffolds incubated under cyclic tensile strain had recovered the collagen crimp pattern, similar to native tissues. Collagen crimping is a phenomenon that has been suggested to provide stiffness in low loading conditions, where the tendon absorbs more energy (Jarvinen et al., 1999, Hansen et al., 2002). Moreover, cells aligned in the reorganised matrix, and this was reported to increase matrix elastic modulus and ultimate tensile strength compared to cells in a randon alignment (Grenier et al., 2005).

These experiments had sterility test of all samples at the end of each experiment with no growth of colonies, this ensured that there was no contamination with bacteria or yeast in these experiments. The ATP levels of the cells incubated with 6 % cyclic strain were the highest; had increased by 9 fold compared to the static control. The ATP levels of the cells in the samples incubated under 4 % strain had increased by 5 x fold, and the samples incubated with 8 % stain had increased by 4 x fold compared to the cells incubated under static conditions. According to the literature, extracellular and intracellular forces affect cellular fate and viability through the control of the nuclear activity (Rodriguez et al., 2013). In tendon, mechanical stress induces anabolic and catabolic processes to constantly maintain tendon ultrastructure and function through tendon remodelling (Jaalouk and Lammerding, 2009). Continuous application of small amounts of cyclic tensile strain has been shown to increase cellular viability through the downregulation of apoptosis markers (MMP 3 and MMP 13) (Maeda et al., 2009). Application of 2 % strain for 24 h downregulated catabolic gene expression indicating cellular death (caspase 12, MMP 9 - 13 - 14, ADAMTS 5), upregulated matrix proteins (decorin and fibronectin) and cytokines and signalling factors (TGF β1, VEGF and BMP 2) (Maeda et al., 2010b).

Tenascin-C has been suggested to affect cellular viability by acting as an apoptosis inhibitor (through αVβ3) and has also been reported to be an early marker for cellular proliferation (through binding with α9β1 and αVβ3) (Chiquet et al., 2004, Tucker and Chiquet-Ehrismann, 2015). Tenascin-C has also been shown to be a cellular adhesion marker in tendon healing and tissue remodelling, as well as in pathological conditions such as cancer and inflammation (Chiquet-Ehrismann et al., 2014). Tenascin-C has been reported to be rapidly assembled (less than 5 min) (Redick and Schwarzbauer, 1995) and rapidly transported out of the cell (although slower than assembly) (Jones and Jones, 2000). This might explain why tenascin-C labelling was positively stained in the cell-seeded scaffolds after 12 h of seeding. The cell-seeded samples that were incubated under static conditions also expressed Tenascin-C. This might also have been because of the cell-seeded scaffolds were incubated under constraint in the TenCell-1 culture wells and this had exerted tension on the cellular cytoskeleton, potentially inducing the

RhoA/ROCK pathway to release tenascin-C (Sarasa-Renedo et al., 2006). Therefore, it is not surprise as the cell-seeded scaffolds incubated in the static (as the control) had expressed tenascin-C transcript gene and the sections against the tenascin-C antibody were positively stained.

Scleraxis expression is a specific cellular response to mechanical strain and has been reported to be a specific marker for early tenogenesis during tissue formation (Schweitzer et al., 2001). Scleraxis has also been reported to induce the expression of tenascin-C (Edom-Vovard et al., 2002), in tendon stem/progenitor cells (TSPC) (Bi et al., 2007). Another specific tenogenesis transcript marker is Mohawk that has been reported to regulate MSCs through TGF β during tendon development and repair (Liu et al., 2015).

Osteopontin was expressed by the human BM-MSCs in the decellularised PPT scaffolds after incubation with 6 % cyclic tensile strains for 7 days. Osteopontin is the main marker for osteogenesis, however, osteopontin is also upregulated during inflammation, tissue remodelling and cells in a harsh environment (Denhardt et al., 2001, Chen and Jacobs, 2013). Osteopontin is believed to attract MSCs to the injury sites through integrin β1 channel (Zou et al., 2011), to promote the healing process in the skin of diabetic mice (Meng et al., 2014), and also to indicate cellular proliferation, migration and survival in neural stem cells (Rabenstein et al., 2015). It has also been reported to be expressed by cells during incubation, increased alkaline phosphatase activity and calcium aggregation when being expressed by high strength cyclic strain (10 %, 0.5 Hz) (Lohberger et al., 2014). Perhaps the 6 % cyclic uniaxial strain had recruited all actin-myosin components in the cell-seeded PPT scaffolds to engage. Extracellular-mechanical stimulation activates the AT1R channels to open the L type voltage-gated calcium channels and to mediate the $Ca^{2+}$ influx. This regulates the cytoskeletal contractility and affects the cell–matrix and cell–cell adhesion turnover. The more actin-myosin components recruited, the more $Ca^{2+}$ are needed (Yang et al., 2015). In addition, it may be that the expression of osteopontin by the human BM-MSCs in the tendon scaffolds after incubation under 6 % strain, was the response of the human BM-MSCs to acquire more calcium, or was a marker of the activities of osteopontin as stated above.

## 6.6. Conclusions

1. Mechanical cyclic strain in the physiological range was showed to improve cellular migration and infiltration, rearrange and recover the crimp of the collagen fibres in the cell-seeded scaffolds to be histologically tendon-like tissue.

2. The human BM-MSCs seeded onto the decellularised PPT scaffold incubated with 6 % and 8 % cyclic tensile strain for 4 h, 1 Hz per day (100,800 cycles) had directed the human BM-MSCs into the tenocyte-like cells that expressed scleraxis, tenascin-C, collagen I and collagen III after 7-days of incubation.

3. Human BM-MSCs in the decellularised PPT scaffolds incubated with 6 % cyclic strains (100,800 cycles, 4 Hz, 7 days) yielded the highest cellular viability compared to 4 % and 8 % strains.

4. The porcine source-decellularised tendon scaffold had successfully being remodelled by the human BM-MSCs into tendon-like tissue under the physiological circumstances of tendon.

5. This experiment had demonstrated that the physiological mechanobiology influenced cellular viability, proliferation, cellular migration and infiltration, and MSCs differentiation; however the ECM production was not quantified.

# Chapter 7 General Discussion

A torn ACL needs replacement, and biological grafts, in particular autograft is the gold standard due to its ability to integrate and remodel (Amiel et al., 1986, Legnani et al., 2010, Ghalayini et al., 2010b). However, neither of the biological grafts; autograft or allograft are ideal. Recently, tissue engineering has emerged as a solution to develop, design and construct material which not only functions anatomically and physiologically upon implantation, but is also long lasting. Xenograft, an inexhaustible source, has become an option for tissue replacement through the application of decellularisation technology. Several xenograft products are already available on the market, for example porcine submucosal intestine; Oasis® Matrix (Smith & Nephew, Andover, MA), or porcine dermis; Permacol™ (Mansfield, MA) for wound repair (Beers et al., 2016, Filisetti et al., 2016).

There are four elements in tissue engineering; scaffold, cells, growth factor and bioreactor. The University of Leeds has for decades prioneered methods to generate biological scaffolds from different tissues; such as aorta, ligament, bone, cartilage, meniscus, heart valve and dermis. In the present study, porcine patellar tendons were decellularised to generate acellular tendon scaffolds, applying the University of Leeds decellularisation protocol for tendon. The matrices of the decellularised PPTs were shown to be consistently acellular, had retained their major ECM components, were sterile, biocompatible, and receptive to different types of cells. Even so, the fibres of the matrices were slightly loosened, as shown in histology sections stained by H&E and Sirius-Red dyes. Two chemical agents used in this protocol might have caused collagen fibres to be disengaged; SDS to solubilize cells, and PAA to sterilise the matrix. This adverse effect on tendon fibres was reported by Huang et al. (2013), using the same PAA concentration as the University of Leeds protocol; 0.1 % (v/v) (Huang et al., 2013b). On the other hand, reports of matrix loosened caused by SDS to decellularise tendons came mostly from higher concentration than those used by the University of Leeds. SDS 1 % (w/v) caused decellularised porcine ACLs to become less receptive to porcine ACL fibroblasts (Harrison and Gratzer, 2005), and the fibre matrices became looser but was not cytotoxic (Gratzer et al.,

2006). The application of SDS 0.1 % (w/v) to decellularise porcine PPTs in the present study was shown to generate a biocompatible matrix, that was not toxic to different cell types - including BHK, 3T3 and L929 cells - and to progenitor cells, porcine and human BM-MSCs. The porcine and human BM-MSCs were attached to the scaffolds after 12 h seeding. The human BM-MSCs were also shown to infiltrate, migrate and proliferate throughout the matrix after 7-day incubation, with or without the application of cyclic uniaxial tensile strain (Chapter 6).

The tendon decellularisation protocol of the University of Leeds used SDS 0.1% (w/v) and PAA 0.1% (v/v), and although the fibre matrices were slightly altered, however, this condition had no effects on the biomechanical properties of the matrix. The UT Stress, UT strain, collagen phase slope and the Young`s modulus of the decellularised porcine PPT scaffold were no different compared to the native tendon, with the exception of the elastic phase slope, that was significantly reduced (Chapter 5). Interestingly, the depletion of the elastic phase slope was improved two or three fold from the acellular PPT matrix when the decellularised PPT scaffolds were seeded with human BM-MSCs and incubated with 100,800 cycles of 4, 6 and 8 % uniaxial strain for 7 days (Chapter 6). Although the elastic phase slope did not recover to reach the level of the native PPT scaffolds, however the 7-days incubation showed a promising result. It may therefore be concluded that the loosened matrix of the decellularised porcine PPT using the University of Leeds decellularisation protocol had minimal effects on the matrix biomechanical properties.

Other biomechanical studies of whole decellularised human patellar tendons produced using a similar decellularisation protocol focused on the elastic phase slope using a bi-linear analysis model, and it was reported that all of the biomechanical parameters of the toe region of the matrix were no different to native tendons (Herbert et al., 2016). The present study showed a reduction in the elastic phase slope, perhaps due to the size of the specimens of the decellularised porcine PPT scaffolds (fascicles), which was much smaller (20 x 10 x 0.6 – 0.8 mm$^3$) compared the specimen size used in Herbert et al (2016) study, which was a whole bulk of

human bone-patellar tendon bone. It is possible that a smaller specimen had less viscous resistance as liquid can rapidly infiltrate and fill the whole matrix, causing the matrix to become swollen and increase the cross-sectional area (Glover, 2010). Specimen size is one of the factors to calculate the engineering value, as shown in the equations to analyse the engineering parameters [Equation 13 & 15]. It is also possible that the differences between the human and porcine scaffolds were related to the different relative ages of the tissue donors. Porcine tissues are obtained from farming, harvested from pigs at 6-8 months, while human tissues are dependent on the availability of donors. Tendons of older people are less stiff (refer to Table 1.2).

It is also possible that the fibre matrix became looser as the result of the decellularisation process, but made it easier for cells to repopulate the matrix when matrices became microscopically more porous. Cells in the decellularised PPT scaffolds infiltrated deeper than the resolution of the laser confocal microscope (100 µM), after an incubation of 7 days in TenCell-1 bioreactor with exposure to cyclic strain (Chapter 6; Section 6.4.2.1). Cellular infiltration can be improved by an augmentation of the matrix porosity of the decellularised PPT scaffold. Porcine patellar tendon was decellularised using the same protocol followed by ultrasonification treatment, 360 W, 1 s pulse time for 1 min, achieving a penetration of human primary tenocytes up to 4 mm (to the centre of the scaffold) after 3 weeks of static incubation (Ingram et al., 2007).

It is important to obtain an acellular matrix that is free from cell remnants and DNA fragments, because the present study investigated the gene expression of human BM-MSCs in decellularised PPT scaffolds in response to mechanical strain. It was necessary to ensure that the gene evaluated was due to the seeded cells and not residual DNA. Chapter 3 demonstrated that the decellularised PPT had an absence of cell nuclei, shown by the H&E staining and also no double stranded DNA, as no staining was visible in the decellularised tendon matrix demonstrated by DAPI. The DNA content of all parts of the decellularised porcine PPTs was reduced by up to 99 % compared to native porcine PPTs. The quantity of DNA was found to be

consistently below 7 ng.mg$^{-1}$ dry weight among different batches, and these met the threshold criteria for an acellular matrix (50 ng.mg$^{-1}$ dry weight) (Crapo et al., 2011). Chapter 5; Section 5.4.5.3 demonstrated that there was no amplification after the RNA extracted from human BM-MSCs seeded for 12 h on decellularised PPT scaffolds. This indicated that there was no residual genomic DNA in the scaffolds, as PCR will not amplify RNA. This experiment also had a group of cDNA amplification converted from the RNA from the same source, which generated the DNA product of interest.

Cell populations in a scaffold are essential to the process of scaffold morphogenesis, tissue matrix turn-over and the wound healing process (Badylak et al., 2009, Cheng et al., 2014b). In this study, human BM-MSCs were used. These cells have been reported to contribute to the tendon repair and healing process (Gobbi et al., 2009). Rat BM-MSCs had similar tenogenesis capacity with day-14 rat embryogenic tenocytes (TPC) when cultured in collagen I matrix (Flexcell, USA), supplemented with 1 ng.mL$^{-1}$ TGF-β2, and incubated under cyclic tensile 1 %, 0.5 Hz, 1 h per day for 3 days. Both cell types expressed the same level of scleraxis, tenomodulin, and collagen I (Brown et al., 2015).

For the in-vitro study of cell responses to cyclic strain, human BM-MSCs were seeded onto the decellularised scaffolds and incubated in the TenCell-1 bioreactor. Decellularised PPTs were initially sized to 10 x 20 x 0.6 – 0.8 mm$^3$ in order to fit into the TenCell culture well of the TenCell-1 bioreactor, and the thickness of the scaffold had to be within the range that would allow the penetration of nutrients and oxygen in an in-vitro setting, which is less than 1 mm thickness (Ingram et al., 2007). In tissue engineering studies, various of biomaterials were used as a scaffold and seeded with different cell types using varied of seeding techniques. Basically, the seeding method depended on the type of scaffold. In the present study, the aim was to achieve cellular adhesion on the scaffold, followed by cell infiltration into the scaffold, such that the effects of tensile cyclic strain could be studied with the cells in a more physiological three-dimensional environment. Therefore, the number of seeded cells was a major consideration, as it was also necessary to seed sufficient cells to enable the extraction of sufficient RNA for

molecular analysis. To achieve this, a seeding ring was used at first. However, seeding tendon scaffolds using seeding rings produced a majority of dead cells (60 - 70 %) and a seeding efficiency of less than 30 %. The cell suspension had disappeared after 4, 6 or 12 h seeding. Leaking of culture medium was thought to have caused the cell loss, and was suspected of causing low cellular viability due to dehydration. Throughout the seeding ring experiment, a drop of culture medium was mostly found underneath the plate of the seeding ring [refer to Figure 5.14 B] and this had caused the seeding wells to dry. Cell viability was not affected by the duration of incubation post-seeding (4, 6 or 12 h).

The efficiency of seeding the decellularised porcine PPT scaffolds by immersion in porcine BM-MSCs suspension (3 mL of $3.0 \times 10^5$ cells.mL$^{-2}$) for 4 days was extremely low; 0.8 %. It was found to be ineffective, as the number of cells needed and the duration to seed were problematic (Chapter 5; Section 5.3.4.2). Other studies reported that rabbit tenocytes and BM-MSCs expressed the same level of collagen I and collagen III after being seeded on decellularised rabbit tendon using cell suspension ($2 \times 10^6$ cells.cm$^{-2}$) for 6 weeks (Kryger et al., 2007). In this study, the seeding technique using direct method with $4 \times 10$ μL and incubated for 12 h to allow the cells to adhere was found to be the most efficient and practical method, and was therefore used throughout the remainder of the study.

In tendon, mechanical stress induces anabolic and catabolic processes to constantly maintain tendon ultrastructure and function through tendon remodelling. High strain strength is believed to cause mechanical overuse that leads to acute or chronic tendinopathy mostly found during sports activitiy (Riley, 2004, Nourissat et al., 2015). Immobilisation of injured tendon during the repair stage was reported to upregulate the mRNA of collagen II and XII and to downregulate the mRNA of collagen III (Thomopoulos et al., 2008).

There are many mechanotransduction studies in the literature that use different cell types, different scaffolds and different culture conditions, with variety of reported results. The present study demonstrated that physiological mechanical strain (4 %, 6% and 8 % cyclic strain, 1 Hz, 4

h) incubated with standard culture medium (DMEM 1.0 g.L-1 glucose, supplemented with 10 % (v/v) FBS)) in the TenCell-1 bioreactor, led to a significantly increased viability of the human BM-MSCs in the tendon scaffolds compared to incubation without mechanical strain. There was evidence that culture of the human BM-MSCs in decellularised PPT scaffolds under 6 % cyclic tensile strain, 1 Hz, 4 h, 7 days had stimulated the human BM-MSCs towards tenogenic differentiation. These were shown by the expressions of mRNA for scleraxis, tenascin-C, collagen I and collagen III. The 6 % cyclic strain culture condition was also superior, as the ATP levels were significantly higher than other groups.

Many studies reported molecular responses as a result of mechano-transduction effects on cellular fates and viability. MMP was reported to play an important role in tissue remodelling though its catabolic effect and macrophage recruitment during the inflammation and wound healing processes. Lack of MMP 2 - 13 expression had been reported to cause significant delayed in MCL healing due to an absence of macrophage migration factor (Kitayama et al., 2011). A study reported that human tenocytes seeded on collagen I gels incubated with 3.5 % strain, 1 Hz 1 h per day upregulated the apoptosis markers; MMP 27 and ADAMTS 5 (Qi et al., 2008). Rat BM-MSCs seeded onto silicon membranes, incubated with 2.5%, 5%, 7.5% and 10% cyclic tensile strain, 0.17 Hz for 3 d had DNA fragmentation of 20.33% after exposure to 7.5% strain (11.51 % in the static control), and the fragmentation was increased by 47.09 % when exposed to 10 % strain (12.66 % in static) (Kearney et al., 2008). IL-1β was reported to improve human tenocytes survival when exposed to mechanical strain. Human tenocytes incubated in a collagen I hydrogel (Flexcell, USA) and subjected to 3.5 % strain, 1 Hz, 1 h per day had 10 % apoptosis cells after 3 days culture, and after 5 days, more than 95 % of cells had apoptosed, and an increase of MMP27 and ADAMTS5 expression by 100 %. Adding 100 pM of IL-1β into culture medium reduced ADAMTS5 expression by 55 % and promoted cellular viability through the upregulation of Connexin 43 expression (Qi et al., 2011).

ROS species has been reported to correlate with cellular viability when exposed to excessive non-physiological cyclic strain. Human BM-MSCs (taken from donors under ten years old)

seeded on elastic silicone wells (Flexcell) and stimulated with cyclic tensile strains 1 Hz for 24 h indicated that applying 12 % strain inhibited superoxide dehydrogenase activities and increased malondialdehyde (MDA) level, significantly higher compared to the 3 and 6 % strain groups (Li et al., 2011).

Low strain strength was found to increase the cellular viability through the downregulation of apoptosis markers. Fresh rat tails preconditioned with 3 % amplitude superimposed 2 % static strain for 10 min, then incubated with 2 % continuous cyclic strain for 6 h, had collagen III mRNA upregulated, while collagen I and biglican were constantly expressed. MMP3 and MMP 13 were upregulated when exposed to 10 min cyclic strain, however were downregulated when the exposure was extended (Maeda et al., 2009). Further study of cellular mechanobiology using microarrays had found anabolic effects after 24 h continuously exposed to 2 % cyclic strain, 3% amplitude, by downregulating the catabolic gene expressions indicating cellular death (capascase 12, MMP 9 - 13 - 14, ADAMTS 5), upregulating matrix proteins (decorin and fibronectin) and cytokines and signalling factors (TGF $\beta1$, VEGF and BMP 2) (Maeda et al., 2010a).

Anabolic activities in response to mechanical strain are also widely reported. Fibroblasts of chick embryo incubated on silicon membrane had doubled the increase of tenascin-C expressions after 6 h continuous exposure to 10 % cyclic strain, 0.3 Hz, compared to samples incubated without strain. The tenascin C expression was reduced by a substitute of TGF-$\beta1$ (5 ng.mL$^{-1}$) (Chiquet et al., 2004). Other studies also reported that 10 %, 0.3 Hz induced mouse fibroblasts in fibronectin coated silicone membrane to express tenascin-C. The RhoA/ROCK pathway is believed to increase the activates of actin contraction, which is mediated by integrin-linked kinase (ILK) (Maier et al., 2008). Rat BM-MSCs seeded in a 1 % (w/v) gelatine matrix incubated with 10 % cyclic strains, 1 Hz - for 12 h upregulated collagen I, collagen III and tenascin C expression. The expression of collagen I and collagen III were downregulated when the exposure was prolonged up to 24 h, leading to cells death, but tenascin-C expression was significantly increased (Zhang et al., 2008).

Another very important point to address was the failure to quantify gene expression in the cell-seeded porcine PPTs using RT-qPCR. This was due to an additional melting peak present in each dissociation curve obtained during gene amplifications (Chapter 6). SDS residue were suspected to be the contaminating substance responsible for the contaminant peak. Multiple washes following SDS treatment were reported to effectively eliminate SDS residue in decellularised tendon matrices. SDS treatment used at 0.5 % (w/v) concentration was eliminated by 10 PBS washes (Cebotari et al., 2010). Unfortunately, by the stage of the study that this problem was encountered, it was not possible to quantify the SDS remaining in the porcine PPT matrix due to time constraints. It had been shown earlier in this study that the decellularised porcine PPT matrix was biocompatible and non-toxic to cells (Chapter 3, Chapter 4, Chapter 5 and Chapter 6).

Perhaps there was residual SDS in the decellularised PPT matrix at a concentration, below the toxic level, however, RT-qPCR is a very powerful and very sensitive tool. It is possible that if extremely low levels of SDS were retained in the matrix, they might have been responsible for the emissions during excitation throughout the PCR amplification (Arand et al., 1992). These appeared consistently in all dissociation curves; with a similar peak shape and a similar melting temperature, despite different genes which were amplified, while all the controls showed no contaminating peak. Unfortunately, in the present study, it was not possible to amplify the DNA extracted from the non-cell seeded decellularised porcine PPT scaffold to ascertain whether the matrix had caused the problem, as there were no sterile scaffolds remaining by the time the problem was identified. SDS can be quantified using a colorimetric assessment using a methylene blue technique (Arand et al., 1992b).

It is also possible that most of the RNA extracted from the cell-seeded scaffolds was quantitatively and qualitatively below the satisfactory level, and this was the reason for the failure to obtain reliable qPCR amplification from the RNA extracted from the cell-seeded scaffolds (Chapter 6; Section 6.4.5). The development of a protocol to extract RNA was initially developed using different cell numbers (porcine BM-MSCs) (Chapter 4; Section 4.4.1.4). This

protocol found that approximately 20,000 cells were considered be sufficient to quantitatively and qualitatively recover RNA. Later, the RNA extracted from the tri-lineage differentiation of cells derived from human BM-MSC was also found to be qualitatively and quantitatively sufficient (Chapter 4; Section 4.4.2.5). In an exception to this, the RNA extracted from the chondroblasts was low in quantity and less pure. Perhaps the pellets of the chondroblasts obtained after 21-days incubation had formed a cartilage-like matrix, and the column system used to extract the RNA was not optimal for samples taken from cartilage-like tissue.

The development of a protocol to extract RNA was then applied to extract RNA from porcine BM-MSC seeded scaffolds (Chapter 5; Section 5.4.4.4), seeded with $0.5 \times 10^5$ cells.cm$^{-2}$ and incubated for 6 and 12 h. It was found that both seeding durations only allowed recovered of very low amounts and low quality RNA. Subsequently, the technique to extract RNA from human BM-MSCs seeded onto tendon scaffolds was improved by avoiding rigorous mixing, decreasing the Proteinase K concentration (10 mAU.mL$^{-1}$), increasing the number of cells seeded (to $1.0 \times 10^5$ cells.cm$^{-2}$), and allowing 12 h for cells to adhere after seeding (Chapter 5; Section 5.4.5.3). This method was found to give a sufficient amount of RNA (although the A260/280 ratio was just below the indication of good quality RNA), and was used throughout the study.

Nevertheless, the RT-qPCR amplifications of the RNA extracted from the differentiated human BM-MSCs and converted into cDNA generated single-sharp dissociation curves, which produced a single DNA product (Chapter 4; Section 4.4.2.6). On the other hand, the quality of the RNA extracted from the cell-seeded scaffolds incubated for 7 days in TenCell-1, was below the pure range. The A260/280 ratio is considered sufficient to indicate the purity of RNA (Nolan et al., 2006). Perhaps this study should have used a protocol to extract RNA that had been optimised for a sample from tissue that contains low amounts of RNA.

Since it was not possible to quantify the level of the expressions of genes of interest in this study, it was also not possible to determine whether the human BM-MSCs seeded onto the

decellularised PPT scaffolds produced ECM proteins when they were subjected to cyclic tensile strain. The only available data to indicate that this might have occurred was the qualitative PCR analysis of the gene expression for collagen I and III and tenascin-C. The immunohistochemical staining for collagen I and III was similar among all the native and decellularised porcine PPT and the cell-seeded porcine PPT scaffolds (Chapter 3 and Chapter 6). The decellularised PPT matrices retained the major components of the ECM, such as collagen I and III. However, tenascin-C was washed out of the porcine PPT scaffold following decellularisation. Interesting, it was shown that when the human BM-MSCs were seeded onto the decellularised porcine PPT scaffolds under any conditions (T-0 group, incubated statically or with cyclic tensile strain), there was tenascin-C present in the matrix as shown by immunocytochemical staining of the samples using anti- tenascin-C antibodies. As tenascin-C is an important macromolecule for the regulation of cellular proliferation, differentiation, migration and apoptosis (Tucker and Chiquet-Ehrismann, 2015), and the studies in Chapter 6 demonstrated that tenascin C was expressed in all conditions of decellularised PPT scaffolds when seeded with human BM-MSC. Perhaps, the key to accommodate graft remodelling and scaffold matrix turnover is graft repopulation.

## Significance of the work

The biological scaffolds studied in this thesis were taken from porcine patellar tendon, and generated throughout a decellularisation process, which was proprietary to the University of Leeds. In this in-vitro study, the incubation of human BM-MSCs in the decellularised tendon scaffold allowed successful derivation into the tenogeneic lineage within 7 days. BM-MSC are reported to play a role during the ligament/tendon healing process, when they are recruited from the adjacent marrow tissue to the injured site (Kader et al., 2002). While in tissue replacement, cellular repopulation of a graft is very important to conduct tissue regeneration and transform the graft into a native like tissue. In this study, the decellularised tendon scaffold has been shown to accommodate cellular repopulation and provided a cell-supportive microenvironment. If the decellularised tendon scaffold is subsequently implanted, then as a graft, the tendon

scaffold should be able to replace the tissue. Therefore, the findings of this study contribute to the body of knowledge which may have a significant bearing on the translation of biological scaffolds in the future. In addition, this study supports the possibility of utilising biological acellular scaffolds generated using this technology for clinical applications.

Morover, as far as the author understands, none of the previous mechanobiological studies on tendon or ligament have used a natural 3-D culture system, which mimicks the tendon or ligament histo-architecture and its matrix components exactly. This decellularised tendon is the most appropriate in-vitro model to investigate the 3-D mechanobiology of tendons or ligaments.

The magnitude and mechano-stimulation pattern of 6 % cyclic uniaxial tensile strain has been shown to support tenogenesis lineage differentiation within 7 days. This information might be useful for tendon/ ligament rehabilitation (physiotherapy) post tendon/ligament injury or graft replacement. Further investigation based on this finding for physiotherapy to support tendon/ligament healing process is still needed.

## Future studies

The present study was unable to quantify gene expression, as a contaminant melting peak appeared during the amplification of the RT-qPCR, and SDS residue was the suspected contaminant. Traces of SDS in a matrix can be quantified using colorimetric method to measure the methylene blue-SDS complex. This method has a sensitivity to trace SDS up to 0.00005% or 0.0056 $\mu$M. $\mu$L$^{-1}$ (Arand et al., 1992b). RT-qPCR amplification of decellularised PPT scaffold can also show if the contaminant peak appears. It is also necessary to develop an RNA extraction technique for cell-seeded tendon scaffolds. TRIzol extraction is an effective and superior way to obtain reliable RNA for subsequent RT-qPCR reaction, and has been reported tobe more consistent in generating a pure and sufficient quantity of RNA (Chadderton et al., 1997).

It would be interesting to investigate whether the mechanically exposed cell-seeded tendon scaffolds have intact or fragmented DNA. Besides the interest of mechanotransduction studies, it might be advantageous for the application of cell-seeded scaffolds in future use, as fragmented DNA leads to cell death (Kearney et al., 2008) or mutation. Fragmented DNA can be visualised by labelling the free 3'-OH termini of the terminal deoxynucleotidyl transferase mediated UTP-end with biotinylated nucleotide using the enzyme terminal deoxynucleotidyl transferase (TdT) (O'Brien et al., 1998).

It would be of interest to culture the human BM-MSCs-seeded on the decellularised PPT scaffolds in the TenCell-1 bioreactor, in a higher seeding density and for a longer period of time in order to investigate whether the cells synthesise new extracellular matrix proteins such as collagen I and collagen III. Radioisotope labelling of the collagen using [$^{3}$H]-proline and the precipitation was determined using 1 % Sirius red staining can highlight collagen synthesis (Lee et al., 1998). Higher seeding density might generate more RNA for gene expression analysis.

Also, the expression of osteopontin transcript gene by the human BM-MSCs in decellularised PPT scaffolds after 7-days incubation under 6 % cyclic tensile strain, raises a question of whether the osteopontin expressed at 7 days was (i) indicative of osteogeneic differentiation, or (ii) only a transient process. Osteopontin has been reported to be expressed transiently during the initial tendon healing process (Mori et al., 2007). Longer periods of study could be used to answer the question as to whether or not osteopontin expression is associated with matrix calcification. If not, then this finding might indicate the superiority of 6 % cyclic tensile strain in the pathway towards a tendon remodelling mode. Investigations with different time-points would be an advantage as they can reveal fluctuations in the expression of genes of interest over time.

This study investigated the behaviour of human BM-MSCs taken from a young donor. While the ligament injuries occur mostly in the young adult and in older people (20 – 70 y) (Winter, 2016), therefore it will be an advantage to study the behaviour of BM-MSCs taken from this group of people in a biological scaffold.

# Final Conclusions

Incubation of cell-seeded tendon scaffold increases the cell viability significantly compared to the incubation without mechanical strain. The culture of the human BM-MSC-seeded acellular porcine tendon scaffolds under cyclic tensile strain at a magnitude of 6 %, at a frequency of 1 Hz for 4 out of every 24 hours for 7 days, was shown to induce the human BM-MSCs towards tenogenesis. This study has increased knowledge of the effects of cyclic tensile strain on human BM-MSC, and will be of interest to those investigating aspects of tendon and ligament tissue engineering.

# References

ABCAM 2014. Immunohistochemistry Formalin/PFA-fixed paraffin-embedded sections, abreview for anti-tenascin C antibody (EPR 4219). Jan 23 2014 ed.: Abcam

ABOUSLEIMAN, R. I., REYES, Y., MCFETRIDGE, P. & SIKAVITSAS, V. 2008. The Human Umbilical Vein: A Novel Scaffold for Musculoskeletal Soft Tissue Regeneration. *Artificial Organs,* 32**,** 735-741.

AGLIETTI, P., BUZZI, R., GIRON, F., SIMEONE, A. J. & ZACCHEROTTI, G. 1997. Arthroscopic-assisted anterior cruciate ligament reconstruction with the central third patellar tendon. A 5-8-year follow-up. *Knee Surgery, Sports Traumatology, Arthroscopy,* 5**,** 138-44.

AHLFELD, S., LARSON, R. & COLLINS, H. 1987. Anterior cruciate reconstruction in the chronically unstable knee using an expanded polytetrafluoroethylene (PTFE) prosthetic ligament. *Am J Sports Med,* Jul-Aug 15**,** 326-30.

AINSWORTH, B. J. & CHAUDHURI, J. B. 2005. Bioreactors for Ligament Engineering. *In:* CHAUDHURI, J. & AL-RUBEAI, M. (eds.) *Bioreactors for tissue engineering, principles, design and operation.* The Netherland: Springer.

AKESON, W. 2003. Arthrofibrosis; the mechanicsm of proliferative scar production and potential therapeutic remedies to modulate the healing response. *In:* PEDOWITZ, R. A., O'CONNOR, J. J. & AKESON, W. (eds.) *Daniel's Knee Injuries, ligament and cartilage structure, function, injury and repair.* second ed. Philadelphia: Lippincott Williams&Wilkins.

AL-TURAIKI, M. 1986. *The human knee, functional anatomy, biomechanics and instabilities & assessment techniques,* Saudi Arabia, Al-Farazdak printing press.

AL-ZARAHINI, S., FRANCESCHI, J. P., COSTE, J., ZERROUG, B. & AL-SEBAI, W. 1997. Anterior cruciate ligament reconstruction by mini-arthrotomy. *International Orthopaedics,* 21**,** 161-3.

ALDRIDGE, A. R. 2011. *Development of methods for the in-vitro assessment of the adipogenesis and immunogenicity of human multipotent mesenchymal stromal cells.* PhD, University of Leeds.

ALDRIDGE., A. R. 2011. *Development of methods for the in-vitro assessment of the adipogenesis and immunogenicity of human multipotent mesenchymal stromal cells.* PhD, Leeds.

ALLEN, C. R., LIVESAY, G. A., WONG, E. K. & WOO, S. L. Y. 1999. Injury and reconstruction of the anterior cruciate ligament and knee osteoarthritis. *Osteoarthritis and Cartilage,* 7**,** 110-121.

ALTMAN, G. H., HORAN, R. L., LU, H. H., MOREAU, J., MARTIN, I., RICHMOND, J. C. & KAPLAN, D. L. 2002a. Silk matrix for tissue engineered anterior cruciate ligaments. *Biomaterials,* 23**,** 4131-4141.

ALTMAN, G. H., LU, H. H., HORAN, R. L., CALABRO, T., RYDER, D., KAPLAN, D. L., STARK, P., MARTIN, I., RICHMOND, J. C. & VUNJAK-NOVAKOVIC, G. 2002b. Advanced bioreactor with controlled application of multi-dimensional strain for tissue engineering. *Journal of Biomechanical Engineering,* 124**,** 742-9.

AMIEL, D., BILLINGS, E. & AKESON, W. H. 1990. Knee Ligaments; structure, function, injury and repair. *In:* DANIEL, D. D., AKESON, W. H. & O'CONNOR, J. J. (eds.) *Ligament structure, chemistry and physiology* New York: Raven Press.

AMIEL, D., FRANK, C., HARWOOD, F., FRONEK, J. & AKESON, W. 1983. Tendons and ligaments: a morphological and biochemical comparison. *Journal of Orthopaedic Research,* 1**,** 257-265.

AMIEL, D., KLEINER, J. B., ROUX, R. D., HARWOOD, F. L. & AKESON, W. H. 1986. The phenomenon of "ligamentization": anterior cruciate ligament reconstruction with autogenous patellar tendon. *Journal of orthopaedic research,* 4**,** 162-172.

AMIS, A., KEMPSON, S. & MILLER, J. 1988. Anterior cruciate ligament replacement. Biocompatibility and biomechanics of polyester and carbon fibre in rabbits. *Journal of Bone & Joint Surgery, British Volume,* 70**,** 628-634.

ANDERSON, A. W. & SMITH, J. J. 2009. Proximal tibial fracture after patellar tendon autograft for ipsilateral ACL reconstruction. *The Journal of Knee Surgery,* 22**,** 142-4.

ARAND, M., FRIEDBERG, T. & OESCH, F. 1992a. Colorimetric quantitation of trace amounts of sodium lauryl sulfate in the presence of nucleic acids and proteins. *Analytical biochemistry,* 207**,** 73-75.

ARAND, M., FRIEDBERG, T. & OESCH, F. 1992b. Colorimetric quantitation of trace amounts of sodium lauryl sulfate in the presence of nucleic acids and proteins. *Analytical Biochemistry,* 207**,** 73-5.

ARECHABALA, B., COIFFARD, C., RIVALLAND, P., COIFFARD, L. J. & DE ROECK-HOLTZHAUER, Y. 1999. Comparison of cytotoxicity of various surfactants tested on normal human fibroblast cultures using the neutral red test, MTT assay and LDH release. *Journal of Applied Toxicology,* 19**,** 163-5.

ARENDT, E. & DICK, R. 1995. Knee injury patterns among men and women in collegiate basketball and soccer. NCAA data and review of literature. *American Journal of Sports Medicine,* 23**,** 694-701.

ARNOCZKY, S. P., RUBIN, R. M. & MARSHALL, J. L. 1979. Microvasculature of the cruciate ligaments and its response to injury. An experimental study in dogs. *Journal of Bone & Joint Surgery - American Volume,* 61**,** 1221-9.

ASAI, S., OTSURU, S., CANDELA, M. E., CANTLEY, L., UCHIBE, K., HOFMANN, T. J., ZHANG, K., WAPNER, K. L., SOSLOWSKY, L. J. & HORWITZ, E. M. 2014. Tendon Progenitor Cells in Injured Tendons Have Strong Chondrogenic Potential: The CD105- Negative Subpopulation Induces Chondrogenic Degeneration. *Stem Cells,* 32**,** 3266-3277.

BADYLAK, S. F. 2002a. The extracellular matrix as a scaffold for tissue reconstruction. *Seminars in Cell & Developmental Biology,* 13**,** 377-83.

BADYLAK, S. F. The extracellular matrix as a scaffold for tissue reconstruction. Seminars in cell & developmental biology, 2002b. Elsevier, 377-383.

BADYLAK, S. F., FREYTES, D. O. & GILBERT, T. W. 2009. Extracellular matrix as a biological scaffold material: structure and function. *Acta biomaterialia,* 5**,** 1-13.

BARBER, F. A., HERBERT, M. A. & COONS, D. A. 2006. Tendon augmentation grafts: Biomechanical failure loads and failure patterns. *Arthroscopy-the Journal of Arthroscopic and Related Surgery,* 22**,** 534-538.

BARRETT, D. S. 1991. Proprioception and function after anterior cruciate reconstruction. *Journal of Bone & Joint Surgery - British Volume,* 73**,** 833-7.

BARRETT, G. R., LINE, L. L., JR., SHELTON, W. R., MANNING, J. O. & PHELPS, R. 1993. The Dacron ligament prosthesis in anterior cruciate ligament reconstruction. A four-year review. *American Journal of Sports Medicine,* 21**,** 367-73.

BARTLETT, J. A. S., D 2003. A short history of the polymerase chain reaction. *In:* BARTLETT, J. A. S., D (ed.) *PCR protocols.* 2nd ed. New Jersey: Humana Press.

BARTSCH, U. 1996. The extracellular matrix molecule tenascin-C: Expression in vivo and functional characterization in vitro. *Progress in Neurobiology,* 49**,** 145-168.

BATTULA, V. L., BAREISS, P. M., TREML, S., CONRAD, S., ALBERT, I., HOJAK, S., ABELE, H., SCHEWE, B., JUST, L., SKUTELLA, T. & BÜHRING, H.-J. 2007. Human placenta and bone marrow derived MSC cultured in serum-free, b-FGF-containing medium express cell surface frizzled-9 and SSEA-4 and give rise to multilineage differentiation. *Differentiation,* 75**,** 279-291.

BAXTER, M. A., WYNN, R. F., JOWITT, S. N., WRAITH, J. E., FAIRBAIRN, L. J. & BELLANTUONO, I. 2004. Study of Telomere Length Reveals Rapid Aging of Human Marrow Stromal Cells following In Vitro Expansion. *Stem cells,* 22**,** 675-682.

BEARD, D. J., KYBERD, P. J., FERGUSSON, C. M. & DODD, C. 1993. Proprioception after rupture of the anterior cruciate ligament. An objective indication of the need for surgery? *Journal of Bone & Joint Surgery, British Volume,* 75**,** 311-315.

BEERS, P. J., ADGERSON, C. N. & MILLAN, S. B. 2016. Porcine tri-layer wound matrix for the treatment of stage IV pressure ulcers. *JAAD Case Reports, 2***,** 122-124.

BELLAYR, I. H., CATALANO, J. G., LABABIDI, S., YANG, A. X., LO SURDO, J. L., BAUER, S. R. & PURI, R. K. 2014. Gene markers of cellular aging in human multipotent stromal cells in culture. *Stem Cell Res Ther, 5***,** 59.

BHAIRI, S. M. & MOHAN, C. 1997. *Detergents*, Calbiochem-Novabiochem.

BI, Y., EHIRCHIOU, D., KILTS, T. M., INKSON, C. A., EMBREE, M. C., SONOYAMA, W., LI, L., LEET, A. I., SEO, B.-M. & ZHANG, L. 2007. Identification of tendon stem/progenitor cells and the role of the extracellular matrix in their niche. *Nature medicine, 13***,** 1219-1227.

BIANCHI, M. E. 2007. DAMPs, PAMPs and alarmins: all we need to know about danger. *Journal of leukocyte biology, 81***,** 1-5.

BIANCO, P., RIMINUCCI, M., GRONTHOS, S. & ROBEY, P. G. 2001. Bone Marrow Stromal Stem Cells: Nature, Biology, and Potential Applications. *STEM CELLS, 19***,** 180-192.

BIRK, D. E. & MAYNE, R. 1997. Localization of collagen types I, III and V during tendon development. Changes in collagen types I and III are correlated with changes in fibril diameter. *European Journal of Cell Biology, 72***,** 352-61.

BISSELL, M. J. & AGGELER, J. 1986. Dynamic reciprocity: how do extracellular matrix and hormones direct gene expression? *Progress in clinical and biological research, 249***,** 251-262.

BOLTON, C. W. & BRUCHMAN, W. C. 1985. The GORE-TEX expanded polytetrafluoroethylene prosthetic ligament. An in vitro and in vivo evaluation. *Clinical orthopaedics and related research***,** 202-213.

BOOTH, C., FISHER., J. & INGHAM, E. 2001. *Low concentration SDS & Protease inhibitors for decellularisation*. UK patent application UK 0112586.3,EPO 02735577.5, PCT/GB02/02341,Australia 2002310589,.

BOOTH, C., KOROSSIS, S., WILCOX, H., WATTERSON, K., KEARNEY, J., FISHER, J. & INGHAM, E. 2002. Tissue engineering of cardiac valve prostheses I: development and histological characterization of an acellular porcine scaffold. *The Journal of heart valve disease, 11***,** 457-462.

BOSCH, P., PRATT, S. L. & STICE, S. L. 2006. Isolation, characterization, gene modification, and nuclear reprogramming of porcine mesenchymal stem cells. *Biology of Reproduction, 74***,** 46-57.

BOURZAC, C., SMITH, L., VINCENT, P., BEAUCHAMP, G., LAVOIE, J. P. & LAVERTY, S. 2010. Isolation of equine bone marrow- derived mesenchymal stem cells: a comparison between three protocols. *Equine veterinary journal, 42***,** 519-527.

BROWN, J. P., GALASSI, T. V., STOPPATO, M., SCHIELE, N. R. & KUO, C. K. 2015. Comparative analysis of mesenchymal stem cell and embryonic tendon progenitor cell response to embryonic tendon biochemical and mechanical factors. *Stem Cell Research & Therapy, 6***,** 89.

BURNETT, Q. M., 2ND & FOWLER, P. J. 1985. Reconstruction of the anterior cruciate ligament: historical overview. *Orthopedic Clinics of North America, 16***,** 143-57.

BURRIDGE, K. & CHRZANOWSKA-WODNICKA, M. 1996. Focal adhesions, contractility, and signaling. *Annual review of cell and developmental biology, 12***,** 463-519.

BUSTIN, S. 2002. Quantification of mRNA using real-time reverse transcription PCR (RT-PCR): trends and problems. *Journal of molecular endocrinology, 29***,** 23-39.

BUSTIN, S. A. 2000. Absolute quantification of mRNA using real-time reverse transcription polymerase chain reaction assays. *Journal of molecular endocrinology, 25***,** 169-193.

BUSTIN, S. A., BEAULIEU, J.-F., HUGGETT, J., JAGGI, R., KIBENGE, F. S., OLSVIK, P. A., PENNING, L. C. & TOEGEL, S. 2010. MIQE precis: Practical implementation of minimum standard guidelines for fluorescence-based quantitative real-time PCR experiments. *BMC molecular biology, 11***,** 74.

BUSTIN, S. A., BENES, V., GARSON, J. A., HELLEMANS, J., HUGGETT, J., KUBISTA, M., MUELLER, R., NOLAN, T., PFAFFL, M. W. & SHIPLEY, G. L. 2009. The MIQE

guidelines: minimum information for publication of quantitative real-time PCR experiments. *Clinical chemistry,* 55**,** 611-622.

BUTLER, D. L., DRESSLER, M. R. & AWAD, H. A. 2003. Functional tissue engineering assessment of function in tendon and ligament repair *In:* GUILAK, F., BUTLER, D. L., GOLDSTAIN, S. A. & MOONEY, D. J. (eds.) *Functional Tissue Engineering.* New York: Springer.

BUTLER, D. L., GUAN, Y., KAY, M. D., CUMMINGS, J. F., FEDER, S. M. & LEVY, M. S. 1992. Location-dependent variations in the material properties of the anterior cruciate ligament. *Journal of Biomechanics,* 25**,** 511-8.

CAILLIET, R. 1992. *Knee pain and disability,* Philadelphia, F.A Davis company.

CAPLAN, A. I. 1991. Mesenchymal stem cells. *Journal of Orthopaedic Research,* 9**,** 641-650.

CARTMELL, J. S. & DUNN, M. G. 2000. Effect of chemical treatments on tendon cellularity and mechanical properties. *Journal of Biomedical Materials Research,* 49**,** 134-40.

CAVIGGIOLI, F., KLINGER, F. M., LISA, A., MAIONE, L., FORCELLINI, D., VINCI, V., CODOLINI, L. & KLINGER, M. 2014. Matching biological mesh and negative pressure wound therapy in reconstructing an open abdomen defect. *Case reports in medicine,* 2014**,** 235930-235930.

CEBOTARI, S., TUDORACHE, I., JAEKEL, T., HILFIKER, A., DORFMAN, S., TERNES, W., HAVERICH, A. & LICHTENBERG, A. 2010. Detergent decellularization of heart valves for tissue engineering: toxicological effects of residual detergents on human endothelial cells. *Artificial organs,* 34**,** 206-210.

CHADDERTON, T., WILSON, C., BEWICK, M. & GLÜCK, S. 1997. Evaluation of three rapid RNA extraction reagents: relevance for use in RT-PCR's and measurement of low level gene expression in clinical samples. *Cellular and molecular biology (Noisy-le-Grand, France),* 43**,** 1227-1234.

CHANG, J. 2012. Studies in Flexor Tendon Reconstruction: Biomolecular Modulation of Tendon Repair and Tissue Engineering. *The Journal of Hand Surgery,* 37**,** 552-561.

CHEN, C. C., CHUEH, J. Y., TSENG, H., HUANG, H. M. & LEE, S. Y. 2003a. Preparation and characterization of biodegradable PLA polymeric blends. *Biomaterials,* 24**,** 1167-73.

CHEN, C. S., MRKSICH, M., HUANG, S., WHITESIDES, G. M. & INGBER, D. E. 1997. Geometric control of cell life and death. *Science,* 276**,** 1425-1428.

CHEN, J., ALTMAN, G. H., KARAGEORGIOU, V., HORAN, R., COLLETTE, A., VOLLOCH, V., COLABRO, T. & KAPLAN, D. L. 2003b. Human bone marrow stromal cell and ligament fibroblast responses on RGD-modified silk fibers. *Journal of Biomedical Materials Research. Part A,* 67**,** 559-70.

CHEN, J. C. & JACOBS, C. R. 2013. Mechanically induced osteogenic lineage commitment of stem cells. *Stem Cell Research & Therapy,* 4**,** 1-10.

CHEN, X., YIN, Z., CHEN, J.-L., SHEN, W.-L., LIU, H.-H., TANG, Q.-M., FANG, Z., LU, L.-R., JI, J. & OUYANG, H.-W. 2012. Force and scleraxis synergistically promote the commitment of human ES cells derived MSCs to tenocytes. *Scientific reports,* 2**,** 977.

CHENG, A. W., ABBAS, M. A. & TEJIRIAN, T. 2014a. Outcome of Abdominal Wall Hernia Repair with Biologic Mesh: Permacol (TM) versus Strattice (TM). *American Surgeon,* 80**,** 999-1002.

CHENG, C. W., SOLORIO, L. D. & ALSBERG, E. 2014b. Decellularized tissue and cell-derived extracellular matrices as scaffolds for orthopaedic tissue engineering. *Biotechnology Advances,* 32**,** 462-484.

CHIQUET-EHRISMANN, R., OREND, G., CHIQUET, M., TUCKER, R. P. & MIDWOOD, K. S. 2014. Tenascins in stem cell niches. *Matrix Biology,* 37**,** 112-123.

CHIQUET, M., GELMAN, L., LUTZ, R. & MAIER, S. 2009. From mechanotransduction to extracellular matrix gene expression in fibroblasts. *Biochimica et Biophysica Acta (BBA) - Molecular Cell Research,* 1793**,** 911-920.

CHIQUET, M., SARASA-RENEDO, A. & TUNÇ-CIVELEK, V. 2004. Induction of tenascin-C by cyclic tensile strain versus growth factors: distinct contributions by Rho/ROCK and

MAPK signaling pathways. *Biochimica et Biophysica Acta (BBA) - Molecular Cell Research,* 1693**,** 193-204.

CHRISTIAN, C. A. & INDELICATO, P. A. 1993. Allograft anterior cruciate ligament reconstruction with patellar tendon: An endoscopic technique. *Operative Techniques in Sports Medicine,* 1**,** 50-57.

CHUAN, W., LIN, H., LEI, Z., PING, Y., JOHN, F. M., ZAC, V., YAXI, C. & XIONG, Z. R. 2014. *Primers for semiquantitative PCR.*

CHUE, W.-L., CAMPBELL, G. R., CAPLICE, N., MUHAMMED, A., BERRY, C. L., THOMAS, A. C., BENNETT, M. B. & CAMPBELL, J. H. 2004. Dog peritoneal and pleural cavities as bioreactors to grow autologous vascular grafts. *Journal of Vascular Surgery,* 39**,** 859-867.

CICIONE, C., DÍAZ-PRADO, S., MUIÑOS-LÓPEZ, E., HERMIDA-GÓMEZ, T. & BLANCO, F. J. 2010. Molecular profile and cellular characterization of human bone marrow mesenchymal stem cells: Donor influence on chondrogenesis. *Differentiation,* 80**,** 155-165.

CLANCY, W. G., NARECHANIA, R., ROSENBERG, T., GMEINER, J., WISNEFSKE, D. & LANGE, T. 1981. Anterior and posterior cruciate ligament reconstruction in rhesus monkeys. *J Bone Joint Surg Am,* 63**,** 1270-1284.

CONRAD, E. U., GRETCH, D. R., OBERMEYER, K. R., MOOGK, M. S., SAYERS, M., WILSON, J. J. & STRONG, D. M. 1995. Transmission of the hepatitis-C virus by tissue transplantation. *Journal of Bone & Joint Surgery - American Volume,* 77**,** 214-24.

COONS, D. A. & BARBER, F. A. 2006. Tendon graft substitutes-rotator cuff patches. *Sports Medicine and Arthroscopy Review,* 14**,** 185-190.

COOPER, R. R. & MISOL, S. 1970. Tendon and ligament insertion. A light and electron microscopic study. *Journal of Bone & Joint Surgery - American Volume,* 52**,** 1-20.

COPPÉ, J.-P., DESPREZ, P.-Y., KRTOLICA, A. & CAMPISI, J. 2010. The senescence-associated secretory phenotype: the dark side of tumor suppression. *Annual review of pathology,* 5**,** 99.

CRAPO, P. M., GILBERT, T. W. & BADYLAK, S. F. 2011. An overview of tissue and whole organ decellularization processes. *Biomaterials,* 32**,** 3233-3243.

DAHLIN, L. B., HANFF, G. & MYRHAGE, R. 1991. Healing of ligaments in synovial fluid: an experimental study in rabbits. *Scandinavian journal of plastic and reconstructive surgery and hand surgery,* 25**,** 97-102.

DALE, W., BAER, E., KELLER, A. & KOHN, R. 1972. On the ultrastructure of mammalian tendon. *Experientia,* 28**,** 1293-1295.

DANIEL, D. M. & STONE, M. L. 1988. Diagnosis of knee ligament injury: tests and measurements of laxity. *In:* FEAGIN, J. A. (ed.) *The cruciate ligaments.* New York: Churchill-Livingstone.

DANYLCHUK, K. D. M. S., FINLAY, J. B. P. D. & KRCEK, J. P. M. S. 1978. *Microstructural Organization of Human and Bovine Cruciate Ligaments. [Miscellaneous],* Clinical Orthopaedics & Related Research March/April 1978;131:294-298.

DAVIS, L. G., KUEHL, W. M. & BATTEY, J. F. 1994. *Basic methods in molecular biology,* Norwalk, Conn, Appleton & Lange.

DEEKEN, C. R., WHITE, A. K., BACHMAN, S. L., RAMSHAW, B. J., CLEVELAND, D. S., LOY, T. S. & GRANT, S. A. 2011. Method of preparing a decellularized porcine tendon using tributyl phosphate. *Journal of Biomedical Materials Research. Part B, Applied Biomaterials,* 96**,** 199-206.

DENHARDT, D. T., NODA, M., O'REGAN, A. W., PAVLIN, D. & BERMAN, J. S. 2001. Osteopontin as a means to cope with environmental insults: regulation of inflammation, tissue remodeling, and cell survival. *The Journal of clinical investigation,* 107**,** 1055-1061.

DERWIN, K. A., BAKER, A. R., SPRAGG, R. K., LEIGH, D. R. & IANNOTTI, J. P. 2006. Commercial extracellular matrix scaffolds for rotator cuff tendon repair -

Biomechanical, biochemical, and cellular properties. *Journal of Bone and Joint Surgery-American Volume,* 88A**,** 2665-2672.

DIMRI, G. P., LEE, X., BASILE, G., ACOSTA, M., SCOTT, G., ROSKELLEY, C., MEDRANO, E. E., LINSKENS, M., RUBELJ, I. & PEREIRA-SMITH, O. 1995. A biomarker that identifies senescent human cells in culture and in aging skin in vivo. *Proceedings of the National Academy of Sciences,* 92**,** 9363-9367.

DM, M., BS, T., L, S., MJ, F. & SL-Y, W. 1993. Prosthetic replacement for the anterior cruciate ligament. *In:* JACKSON, D. W. (ed.) *The anterior cruciate ligament: current and future concepts.* New York: Raven Press Ltd.

DOMINICI, M., LE BLANC, K., MUELLER, I., SLAPER-CORTENBACH, I., MARINI, F., KRAUSE, D., DEANS, R., KEATING, A., PROCKOP, D. & HORWITZ, E. 2006. Minimal criteria for defining multipotent mesenchymal stromal cells. The International Society for Cellular Therapy position statement. *Cytotherapy,* 8**,** 315-317.

DOROSKI, D. M., BRINK, K. S. & TEMENOFF, J. S. 2007. Techniques for biological characterization of tissue-engineered tendon and ligament. *Biomaterials,* 28**,** 187-202.

DOROSKI, D. M., LEVENSTON, M. E. & TEMENOFF, J. S. 2010. Cyclic tensile culture promotes fibroblastic differentiation of marrow stromal cells encapsulated in poly(ethylene glycol)-based hydrogels. *Tissue engineering,* Part A.. 16, 3457-66.

DU, L. & WU, X. 2011. Development and Characterization of a Full-Thickness Acellular Porcine Cornea Matrix for Tissue Engineering. *Artificial Organs,* 35**,** 691-705.

DUTHON, V., BAREA, C., ABRASSART, S., FASEL, J., FRITSCHY, D. & MENETREY, J. 2006. Anatomy of the anterior cruciate ligament. *Knee Surgery, Sports Traumatology, Arthroscopy,* 14**,** 204-213.

DYE, S. F. & BOLL, D. A. 1986. Radionuclide imaging of the patellofemoral joint in young adults with anterior knee pain. *Orthopedic Clinics of North America,* 17**,** 249-62.

DYE, S. F., VAUPEL, G. L. & DYE, C. C. 1998. Conscious neurosensory mapping of the internal structures of the human knee without intraarticular anesthesia. *American Journal of Sports Medicine,* 26**,** 773-7.

EDOM-VOVARD, F., SCHULER, B., BONNIN, M.-A., TEILLET, M.-A. & DUPREZ, D. 2002. Fgf4 positively regulates scleraxis and tenascin expression in chick limb tendons. *Developmental Biology,* 247**,** 351-366.

EKWALL, B. 1983. Screening of toxic compounds in mammalian cell cultures. *Annals of the New York Academy of Sciences,* 407**,** 64-77.

ELMER, P. 2013. ATPlite Luminescence ATP detection assay system. Waltham, USA: PerkinElmer Ltd.

ERGUN, S., KARAHAN, M., AKGUN, U. & KAOCAOGLU, B. 2008. A case of multiple congenital anomalies including agenesis of the anterior cruciate ligament. *Acta Orthop Traumatol Turc,* 42**,** 373-376.

ESPOSITO, I., PENZEL, R., CHAIB- HARRIRECHE, M., BARCENA, U., BERGMANN, F., RIEDL, S., KAYED, H., GIESE, N., KLEEFF, J. & FRIESS, H. 2006. Tenascin C and annexin II expression in the process of pancreatic carcinogenesis. *The Journal of pathology,* 208**,** 673-685.

EUGENE, B. 2000. Tissue Engineering in Perspective. *In:* ROBERT, P. L., ROBERT, L., JOSEPH VACANTIA2 - ROBERT P. LANZA, R. L. & JOSEPH, V. (eds.) *Principles of Tissue Engineering (Second Edition).* San Diego: Academic Press.

FEAGIN, J. A. J. M. D. C. & CURL, W. W. M. D. M. 1996. *Isolated Tear of the Anterior Cruciate Ligament: 5-Year Followup Study. [Miscellaneous],* Clinical Orthopaedics & Related Research April 1996;325:4-9.

FERRARI, G., ANGELIS, D., COLETTA, M., PAOLUCCI, E., STORNAIUOLO, A., COSSU, G. & MAVILIO, F. 1998. Muscle regeneration by bone marrow-derived myogenic progenitors. *Science,* 279**,** 1528-1530.

FILISETTI, C., COSTANZO, S., MARINONI, F., VELLA, C., KLERSY, C. & RICCIPETITONI, G. 2016. Effectiveness and properties of the biological prosthesis Permacol™ in pediatric surgery: A large single center experience. *Annals of Medicine and Surgery,* 7**,** 48-54.

FRANCE, E. P., PAULOS, L. E., JAYARAMAN, G. & ROSENBERG, T. D. 1987. The biomechanics of lateral knee bracing. Part II: Impact response of the braced knee. *American Journal of Sports Medicine,* 15**,** 430-8.

FRANK, C., WOO, S. L., AMIEL, D., HARWOOD, F., GOMEZ, M. & AKESON, W. 1985. Medial collateral ligament healing. A multidisciplinary assessment in rabbits. *American Journal of Sports Medicine,* 11**,** 379-89.

FREY, J. W., FARLEY, E. E., O'NEIL, T. K., BURKHOLDER, T. J. & HORNBERGER, T. A. 2009. Evidence that mechanosensors with distinct biomechanical properties allow for specificity in mechanotransduction. *Biophysical journal,* 97**,** 347-56.

FREYMAN, T. 2005. DECELLULARIZED BONE MARROW EXTRACELLULAR MATRIX. WO Patent 2,005,009,498.

FRIDLYANSKAYA, I., ALEKSEENKO, L. & NIKOLSKY, N. 2015. Senescence as a general cellular response to stress: A mini-review. *Experimental Gerontology,* 72**,** 124-128.

FRIEDENSTEIN, A. J., CHAILAKHYAN, R. K., LATSINIK, N. V., PANASYUK, A. F. & KEILISS-BOROK, I. V. 1974. Stromal cells responsible for transferring the microenvironment of the hemopoietic tissues: cloning in vitro and retransplantation in vivo. *Transplantation,* 17**,** 331-340.

FU, F. H. & SCHULTE, K. R. 1996. Anterior Cruciate Ligament Surgery 1996: State of the Art? *Clinical orthopaedics and related research,* 325**,** 19-24.

FUHRMANN, W., FUHRMANN-RIEGER, A. & DE SOUSA, F. 1980. Poly-, syn- and oligodactylyl, aplasia or hypoplasia of fibula, hypoplasia of pelvis and bowing of femora in three sibs--a new autosomal recessive syndrome. *European Journal of Pediatrics,* 133**,** 123-9.

GALLAGHER, S. R. & DESJARDINS, P. R. 2001. Quantitation of DNA and RNA with Absorption and Fluorescence Spectroscopy. *Current Protocols in Human Genetics.* John Wiley & Sons, Inc.

GALLAGHER, S. R. & DESJARDINS, P. R. 2008. Quantitation of DNA and RNA with absorption and fluorescence spectroscopy. *Current Protocols in Protein Science***,** A. 4K. 1-A. 4K. 21.

GAO, K., CHEN, S., WANG, L., ZHANG, W., KANG, Y., DONG, Q., ZHOU, H. & LI, L. 2010. Anterior Cruciate Ligament Reconstruction With LARS Artificial Ligament: A Multicenter Study With 3- to 5-Year Follow-up. *Arthroscopy: The Journal of Arthroscopic & Related Surgery,* 26**,** 515-523.

GARDNER, E. 1948. The innervation of the knee joint. *The Anatomical Record,* 101**,** 109.

GARDNER, E. & O'RAHILLY, R. 1968. The early development of the knee joint in staged human embryos. *Journal of Anatomy,* 102**,** 289-99.

GARVIN, J., QI, J., MALONEY, M. & BANES, A. J. 2003. Novel system for engineering bioartificial tendons and application of mechanical load. *Tissue engineering,* 9**,** 967-79.

GHALAYINI, S. R. A., HELM, A. T., BONSHAHI, A. Y., LAVENDER, A., JOHNSON, D. S. & SMITH, R. B. 2010a. Arthroscopic anterior cruciate ligament surgery: Results of autogenous patellar tendon graft versus the Leeds-Keio synthetic graft Five year follow-up of a prospective randomised controlled trial. *Knee,* 17**,** 334-339.

GHALAYINI, S. R. A., HELM, A. T., BONSHAHI, A. Y., LAVENDER, A., JOHNSON, D. S. & SMITH, R. B. 2010b. Arthroscopic anterior cruciate ligament surgery: Results of autogenous patellar tendon graft versus the Leeds-Keio synthetic graft: Five year follow-up of a prospective randomised controlled trial. *The Knee,* 17**,** 334-339.

GIANOTTI, S. M., MARSHALL, S. W., HUME, P. A. & BUNT, L. 2009. Incidence of anterior cruciate ligament injury and other knee ligament injuries: a national population-based study. *Journal of Science & Medicine in Sport,* 12**,** 622-7.

GILBERT, T. W., SELLARO, T. L. & BADYLAK, S. F. 2006a. Decellularization of tissues and organs. *Biomaterials,* 27**,** 3675-3683.

GILBERT, T. W., SELLARO, T. L. & BADYLAK, S. F. 2006b. Decellularization of tissues and organs. *Biomaterials,* 27**,** 3675-83.

GLOUSMAN, R., SHIELDS, C., JR., KERLAN, R., JOBE, F., LOMBARDO, S., YOCUM, L., TIBONE, J. & GAMBARDELLA, R. 1988. Gore-Tex prosthetic ligament in anterior cruciate deficient knees. *American Journal of Sports Medicine,* 16**,** 321-6.

GLOVER, J. 2010. *The effects of high power ultrasound on acellular patellar tendon.* PhD, University of Leeds.

GOBBI, A., BATHAN, L. & BOLDRINI, L. 2009. Primary repair combined with bone marrow stimulation in acute anterior cruciate ligament lesions: results in a group of athletes. *American Journal of Sports Medicine,* 37**,** 571-8.

GOTTIPAMULA, S., MUTTIGI, M. S., CHAANSA, S., ASHWIN, K. M., PRIYA, N., KOLKUNDKAR, U., SUNDARRAJ, S., MAJUMDAR, A. S. & SEETHARAM, R. N. 2016. Large-scale expansion of pre-isolated bone marrow mesenchymal stromal cells in serum-free conditions. *Journal of Tissue Engineering and Regenerative Medicine,* 10**,** 108-119.

GRATZER, P. F., HARRISON, R. D. & WOODS, T. 2006. Matrix alteration and not residual sodium dodecyl sulfate cytotoxicity affects the cellular repopulation of a decellularized matrix. *Tissue engineering,* 12**,** 2975-2983.

GRAY, D. J. & GARDNER, E. 1950. Prenatal development of the human knee and superior tibiofibular joints. *American Journal of Anatomy,* 86**,** 235-87.

GREENFIELD, L. 1993. *Lymphatic system disorders,* Philadelphia, JB Lippincott.

GRENIER, G., RÉMY-ZOLGHADRI, M., LAROUCHE, D., GAUVIN, R., BAKER, K., BERGERON, F., DUPUIS, D., LANGELIER, E., RANCOURT, D. & AUGER, F. A. 2005. Tissue reorganization in response to mechanical load increases functionality. *Tissue engineering,* 11**,** 90-100.

GUIDOIN, M.-F., MAROIS, Y., BEJUI, J., PODDEVIN, N., KING, M. W. & GUIDOIN, R. 2000. Analysis of retrieved polymer fiber based replacements for the ACL. *Biomaterials,* 21**,** 2461-2474.

GUILLARD, R. R. & SIERACKI, M. S. 2005. Counting cells in cultures with the light microscope. *Algal culturing techniques***,** 239-252.

HAINES, R. W. 1953. The early development of the femoro-tibial and tibio-fibular joints. *Journal of Anatomy,* 87**,** 192-206.

HAMIDO, F., MISFER, A. K., AL HARRAN, H., KHADRAWE, T. A., SOLIMAN, A., TALAAT, A., AWAD, A. & KHAIRAT, S. 2011. The use of the LARS artificial ligament to augment a short or undersized ACL hamstrings tendon graft. *The Knee,* 18**,** 373-378.

HANSEN, K. A., WEISS, J. A. & BARTON, J. K. 2002. Recruitment of tendon crimp with applied tensile strain. *Journal of Biomechanical Engineering,* 124**,** 72-77.

HARRISON, R. D. & GRATZER, P. F. 2005. Effect of extraction protocols and epidermal growth factor on the cellular repopulation of decellularized anterior cruciate ligament allografts. *Journal of Biomedical Materials Research Part A,* 75**,** 841-854.

HAYFLICK, L. & MOORHEAD, P. S. 1961. The serial cultivation of human diploid cell strains. *Experimental Cell Research,* 25**,** 585-621.

HERBERT, A., BROWN, C., ROONEY, P., KEARNEY, J., INGHAM, E. & FISHER, J. 2016. Bi-linear mechanical property determination of acellular human patellar tendon grafts for use in anterior cruciate ligament replacement. *Journal of Biomechanics,* 49**,** 1607-1612.

HERBERT, A., JONES, G. L., INGHAM, E. & FISHER, J. 2015. A biomechanical characterisation of acellular porcine super flexor tendons for use in anterior cruciate ligament replacement: Investigation into the effects of fat reduction and bioburden reduction bioprocesses. *Journal of Biomechanics,* 48**,** 22-29.

HERON, D., BONNARD, C., MORAINE, C. & TOUTAIN, A. 2001. Agenesis of cruciate ligaments and menisci causing severe knee dysplasia in TAR syndrome. *Journal of Medical Genetics,* 38**,** E27.

HEY GROVES, E. 1917. OPERATION FOR THE REPAIR OF THE CRUCIAL LIGAMENTS. *The Lancet,* 190**,** 674-676.

HIGUCHI, H., SHIRAKURA, K., KIMURA, M., TERAUCHI, M., SHINOZAKI, T., WATANABE, H. & TAKAGISHI, K. 2006. Changes in biochemical parameters after anterior cruciate ligament injury. *International Orthopaedics,* 30**,** 43-7.

HILBERT, S. L., YANAGIDA, R., SOUZA, J., WOLFINBARGER, L., JONES, A. L., KRUEGER, P., STEARNS, G., BERT, A. & HOPKINS, R. A. 2004. Prototype anionic detergent technique used to decellularize allograft valve conduits evaluated in the right ventricular outflow tract in sheep. *Journal of Heart Valve Disease,* 13**,** 831-40.

HILTON, J. 1891. *Rest and pain, a course of lecture,* Cincinnati, P. W. Garfield.

HING, E., CHERRY, D. K. & WOODWELL, D. A. 2006. National Ambulatory Medical Care Survey: 2004 summary. *Advance data***,** 1-33.

HODDE, J. & HILES, M. 2002. Virus safety of a porcine- derived medical device: Evaluation of a viral inactivation method. *Biotechnology and bioengineering,* 79**,** 211-216.

HOLMES, P. F., JAMES, S. L., LARSON, R. L., SINGER, K. M. & JONES, D. C. 1991. Retrospective direct comparison of three intraarticular anterior cruciate ligament reconstructions. *American Journal of Sports Medicine,* 19**,** 596-9; discussion 599-600.

HOLMES, T. C. 2002. Novel peptide-based biomaterial scaffolds for tissue engineering. *TRENDS in Biotechnology,* 20**,** 16-21.

HORNER, G. & DELLON, A. L. 1994. Innervation of the human knee joint and implications for surgery. *Clinical Orthopaedics & Related Research***,** 221-6.

HORWITZ, E. M., LE BLANC, K., DOMINICI, M., MUELLER, I., SLAPER-CORTENBACH, I., MARINI, F. C., DEANS, R. J., KRAUSE, D. S. & KEATING, A. 2005. Clarification of the nomenclature for MSC: The International Society for Cellular Therapy position statement. *Cytotherapy,* 7**,** 393-395.

HSU, S.-M. & SOBAN, E. 1982. Color modification of diaminobenzidine (DAB) precipitation by metallic ions and its application for double immunohistochemistry. *Journal of Histochemistry & Cytochemistry,* 30**,** 1079-1082.

HUANG, Q., INGHAM, E., ROONEY, P. & KEARNEY, J. 2013a. Production of a sterilised decellularised tendon allograft for clinical use. *Cell and tissue banking***,** 1-10.

HUANG, Q., INGHAM, E., ROONEY, P. & KEARNEY, J. N. 2013b. Production of a sterilised decellularised tendon allograft for clinical use. *Cell and tissue banking,* 14**,** 645-654.

HUANG, T. F., CHEN, Y. T., YANG, T. H., CHEN, L. L., CHIOU, S. H., TSAI, T. H., TSAI, C. C., CHEN, M. H., MA, H. L. & HUNG, S. C. 2008. Isolation and characterization of mesenchymal stromal cells from human anterior cruciate ligament. *Cytotherapy,* 10**,** 806-814.

HUBBEL, J. A. 2000. Matrix effects. *In:* LANZA, R. P., LANGER, R. & VACANTI, J. (eds.) *Principle of Tissue engineering.* 2nd ed. San Diego, USA: Elsiever.

HUGGETT, J. F., FOY, C. A., BENES, V., EMSLIE, K., GARSON, J. A., HAYNES, R., HELLEMANS, J., KUBISTA, M., MUELLER, R. D. & NOLAN, T. 2013. The digital MIQE guidelines: minimum information for publication of quantitative digital PCR experiments. *Clinical chemistry,* 59**,** 892-902.

HUNG, S.-C., CHANG, C.-F., MA, H.-L., CHEN, T.-H. & LOW-TONE HO, L. 2004. Gene expression profiles of early adipogenesis in human mesenchymal stem cells. *Gene,* 340**,** 141-150.

HYNES, R. O. 1999. Cell adhesion: old and new questions. *Trends in Biochemical Sciences,* 24**,** M33-M37.

INGRAM, J., KOROSSIS, S., FISHER, J. & INGHAM, J. 2006. Development of an Acellular Scaffold Capable of Recellularisation for USE in Tissue Engineering of the ACL. *Journal of Bone & Joint Surgery, British Volume,* 88**,** 390-390.

INGRAM, J. H., KOROSIS, S., FISHER, J. & INGHAM, E. Decellularisation and recellularisation of porcine patella tendon for ACL reconstruction. Transactions - 7th World Biomaterials Congress, May 17, 2004 - May 21, 2004, 2004 Sydney, Australia. Biomaterials 2004 Congress Managers, 1007.

INGRAM, J. H., KOROSSIS, S., HOWLING, G., FISHER, J. & INGHAM, E. 2007. The use of ultrasonication to aid recellularization of acellular natural tissue scaffolds for use in anterior cruciate ligament reconstruction. *Tissue engineering,* 13**,** 1561-1572.

JAALOUK, D. E. & LAMMERDING, J. 2009. Mechanotransduction gone awry. *Nature reviews Molecular cell biology,* 10**,** 63-73.

JAMESON, S. S., DOWEN, D., JAMES, P., SERRANO-PEDRAZA, I., REED, M. R. & DEEHAN, D. 2012. Complications following anterior cruciate ligament reconstruction in the English NHS. *The Knee,* 19**,** 14-19.

JARVINEN, T. A., JOZSA, L., KANNUS, P., JARVINEN, T. L., KVIST, M., HURME, T., ISOLA, J., KALIMO, H. & JARVINEN, M. 1999. Mechanical loading regulates tenascin-C expression in the osteotendinous junction. *Journal of Cell Science,* 112 Pt 18**,** 3157-66.

JENKINS, D. H. 1978. The repair of cruciate ligaments with flexible carbon fibre. A longer term study of the induction of new ligaments and of the fate of the implanted carbon. *Journal of Bone & Joint Surgery - British Volume,* 60-B**,** 520-2.

JENKINS, D. H. & MCKIBBIN, B. 1980. The role of flexible carbon-fibre implants as tendon and ligament substitutes in clinical practice. A preliminary report. *Journal of Bone & Joint Surgery - British Volume,* 62-B**,** 497-9.

JONES, P. L. & JONES, F. S. 2000. Tenascin-C in development and disease: gene regulation and cell function. *Matrix Biology,* 19**,** 581-596.

KADER, D., SAXENA, A., MOVIN, T. & MAFFULLI, N. 2002. Achilles tendinopathy: some aspects of basic science and clinical management. *British Journal of Sports Medicine,* 36**,** 239-249.

KANNUS, P. 2000. Structure of the tendon connective tissue. *Scandinavian journal of medicine & science in sports,* 10**,** 312-320.

KAPANDJI 1970. *The physiology of the joints: annotated diagrams of the mechanics of the human joints,* London, Chirchill Livingstone.

KAPOOR, B., CLEMENT, D. J., KIRKLEY, A. & MAFFULLI, N. 2004. Current practice in the management of anterior cruciate ligament injuries in the United Kingdom. *British Journal of Sports Medicine,* 38**,** 542-4.

KASIMIR, M. T., RIEDER, E., SEEBACHER, G., SILBERHUMER, G., WOLNER, E., WEIGEL, G. & SIMON, P. 2003. Comparison of different decellularization procedures of porcine heart valves. *International Journal of Artificial Organs,* 26**,** 421-7.

KASTELEIN, M., WAGEMAKERS, H. P. A., LUIJSTERBURG, P. A. J., VERHAAR, J. A. N., KOES, B. W. & BIERMA-ZEINSTRA, S. M. A. 2008. Assessing Medial Collateral Ligament Knee Lesions in General Practice. *The American Journal of Medicine,* 121**,** 982-988.e2.

KASTELIC, J., GALESKI, A. & BAER, E. 1978. The multicomposite structure of tendon. *Connective Tissue Research,* 6**,** 11-23.

KEARNEY, E., PRENDERGAST, P. & CAMPBELL, V. 2008. Mechanisms of strain-mediated mesenchymal stem cell apoptosis. *Journal of Biomechanical Engineering,* 130**,** 061004.

KEMP, P. D. 1995. Peracetic acid sterilization of collagen or collagenous tissue. Google Patents.

KENNEDY, J. C., ALEXANDER, I. J. & HAYES, K. C. 1982. Nerve supply of the human knee and its functional importance. *American Journal of Sports Medicine,* 10**,** 329-35.

KENNEDY, J. C., WEINBERG, H. W. & WILSON, A. S. 1974. The anatomy and function of the anterior cruciate ligament. As determined by clinical and morphological studies. *Journal of Bone & Joint Surgery - American Volume,* 56**,** 223-35.

KIELTY, C. M. & GRANT, M. E. 2003. The collagen family: structure, assembly, and organization in the extracellular matrix. *Connective Tissue and Its Heritable Disorders: Molecular, Genetic, and Medical Aspects, Second Edition***,** 159-221.

KILLIAN, M. L., CAVINATTO, L., GALATZ, L. M. & THOMOPOULOS, S. 2012. The role of mechanobiology in tendon healing. *Journal of Shoulder and Elbow Surgery,* 21**,** 228-237.

KIM, S.-J., JEONG, J.-H. & KO, Y.-G. 2003. Synovitic cyclops syndrome caused by a Kennedy ligament augmentation device. *Arthroscopy,* 19**,** E38.

KITAYAMA, S., ONODERA, S., KONDO, E., KOBAYASHI, T., MIYATAKE, S., KITAMURA, N., TOHYAMA, H. & YASUDA, K. 2011. Deficiency of macrophage migration inhibitory factor gene delays healing of the medial collateral ligament: A biomechanical and biological study. *Journal of Biomechanics,* 44**,** 494-500.

KOMDEUR, P., POLLO, F. E. & JACKSON, R. W. 2002. Dynamic knee motion in anterior cruciate impairment: a report and case study. *Proceedings (Baylor University. Medical Center),* 15**,** 257-259.

KOMORI, T. 2009. Regulation of osteoblast differentiation by Runx2. *Osteoimmunology.* Springer.

KOPEN, G. C., PROCKOP, D. J. & PHINNEY, D. G. 1999. Marrow stromal cells migrate throughout forebrain and cerebellum, and they differentiate into astrocytes after injection into neonatal mouse brains. *Proceedings of the National Academy of Sciences,* 96**,** 10711-10716.

KOSHINO, T. 1991. Stage classifications, types of joint destruction, and bone scintigraphy in Charcot joint disease. *Bulletin of the Hospital for Joint Diseases Orthopaedic Institute,* 51**,** 205-17.

KOUTSOPOULOS, S. 2012. Molecular fabrications of smart nanobiomaterials and applications in personalized medicine. *Advanced Drug Delivery Reviews,* 64**,** 1459-1476.

KRUKHAUG, Y., MOLSTER, A., RODT, A. & STRAND, T. 1998. Lateral ligament injuries of the knee. *Knee Surgery, Sports Traumatology, Arthroscopy,* 6**,** 21-5.

KRYGER, G. S., CHONG, A. K. S., COSTA, M., PHAM, H., BATES, S. J. & CHANG, J. 2007. A Comparison of Tenocytes and Mesenchymal Stem Cells for Use in Flexor Tendon Tissue Engineering. *The Journal of Hand Surgery,* 32**,** 597-605.

KURIOKA, A., YAMAZAKI, M. & HIRANO, H. 1999. Primary structure and possible functions of a trypsin inhibitor of Bombyx mori. *European Journal of Biochemistry,* 259**,** 120-6.

KWAN, M. K., LIN, T. H. & WOO, S. L. 1993. On the viscoelastic properties of the anteromedial bundle of the anterior cruciate ligament. *Journal of biomechanics,* 26**,** 447-452.

LAGASSE, E., CONNORS, H., AL-DHALIMY, M., REITSMA, M., DOHSE, M., OSBORNE, L., WANG, X., FINEGOLD, M., WEISSMAN, I. L. & GROMPE, M. 2000. Purified hematopoietic stem cells can differentiate into hepatocytes in vivo. *Nature medicine,* 6**,** 1229-1234.

LANDRY, J., BERNIER, D., OUELLET, C., GOYETTE, R. & MARCEAU, N. 1984. Spheroidal aggregate culture of rat liver cells: histotypic reorganization, biomatrix deposition, and maintenance of functional activities. *Journal of Cell Biology,* 101**,** 914-23.

LARSON, R. L. 1993. (iv) Principles of replacement reinforcement. *Current Orthopaedics,* 7**,** 94-100.

LAURENCIN, C. T., AMBROSIO, A., BORDEN, M. & COOPER JR, J. A. 1999. Tissue engineering: orthopaedic applications. *In:* ML, Y., DILLER, K. & TONER, M. (eds.) *Annual review of biomechanical engineering.* Palo Alto, CA: Annual Riviews.

LAURENCIN, C. T. & FREEMAN, J. W. 2005. Ligament tissue engineering: An evolutionary materials science approach. *Biomaterials,* 26**,** 7530-7536.

LEE, D., ASSOKU, E. & DOYLE, V. 1998. A specific quantitative assay for collagen synthesis by cells seeded in collagen-based biomaterials using sirius red F3B precipitation. *Journal of Materials Science: Materials in Medicine,* 9**,** 47-51.

LEGNANI, C., VENTURA, A., TERZAGHI, C., BORGO, E. & ALBISETTI, W. 2010. Anterior cruciate ligament reconstruction with synthetic grafts. A review of literature. *International Orthopaedics,* 34**,** 465-71.

LEVIN, M. 2007. Gap junctional communication in morphogenesis. *Progress in Biophysics and Molecular Biology,* 94**,** 186-206.

LEVY, B. A. 2010. Is early reconstruction necessary for all anterior cruciate ligament tears? *New England Journal of Medicine,* 363**,** 386-8.

LEWIN, P. 1952a.

*The Knee and related structure; injuries- deformities- diseases- disabilities,* America, All right reserved

LEWIN, P. 1952b. Patient's history and symptoms, Physical examination of the knee, Rontgen ray findings in disorders of the knee, Laboratory procedures of diagnostic value *The Knee and related structures; injuries, deformities, diseases and disabilities.* London: Henry Kimpton.

LI, R., CHEN, B., WANG, G., YU, B., REN, G. & NI, G. 2011. Effects of mechanical strain on oxygen free radical system in bone marrow mesenchymal stem cells from children. *Injury,* 42**,** 753-757.

LIU, H., ZHANG, C., ZHU, S., LU, P., ZHU, T., GONG, X., ZHANG, Z., HU, J., YIN, Z., HENG, B. C., CHEN, X. & OUYANG, H. W. 2015. Mohawk Promotes the Tenogenesis of Mesenchymal Stem Cells Through Activation of the TGF beta Signaling Pathway. *Stem cells,* 33**,** 443-455.

LIU, S. H., AL-SHAIKH, R., PANOSSIAN, V., YANG, R. S., NELSON, S. D., SOLEIMAN, N., FINERMAN, G. A. & LANE, J. M. 1996. Primary immunolocalization of estrogen and progesterone target cells in the human anterior cruciate ligament. *Journal of Orthopaedic Research,* 14**,** 526-33.

LIU, S. H., AL-SHAIKH, R. A., PANOSSIAN, V., FINERMAN, G. A. & LANE, J. M. 1997. Estrogen affects the cellular metabolism of the anterior cruciate ligament. A potential explanation for female athletic injury. *American Journal of Sports Medicine,* 25**,** 704-9.

LIU, Y.-P., LI, S.-Z., YUAN, F., XIA, J., YU, X., LIU, X. & YU, G.-R. 2011. Infrapatellar fat pad may be with tendon repairing ability and closely related with the developing process of patella Baja. *Medical Hypotheses,* 77**,** 620-623.

LOHBERGER, B., KALTENEGGER, H., STUENDL, N., PAYER, M., RINNER, B. & LEITHNER, A. 2014. Effect of cyclic mechanical stimulation on the expression of osteogenesis genes in human intraoral mesenchymal stromal and progenitor cells. *BioMed research international,* 2014.

LOMAS, R. J., CRUSE-SAWYER, J. E., SIMPSON, C., INGHAM, E., BOJAR, R. & KEARNEY, J. N. 2003. Assessment of the biological properties of human split skin allografts disinfected with peracetic acid and preserved in glycerol. *Burns,* 29**,** 515-525.

LOMAS, R. J., JENNINGS, L. M., FISHER, J. & KEARNEY, J. N. 2004. Effects of a peracetic acid disinfection protocol on the biocompatibility and biomechanical properties of human patellar tendon allografts. *Cell & Tissue Banking,* 5**,** 149-60.

LOPEZ-VAZQUEZ, E., JUAN, J. A., VILA, E. & DEBON, J. 1991. Reconstruction of the anterior cruciate ligament with a Dacron prosthesis. *Journal of Bone & Joint Surgery - American Volume,* 73**,** 1294-300.

LOUBOUTIN, H., DEBARGE, R., RICHOU, J., SELMI, T. A. S., DONELL, S. T., NEYRET, P. & DUBRANA, F. 2009. Osteoarthritis in patients with anterior cruciate ligament rupture: A review of risk factors. *The Knee,* 16**,** 239-244.

LUKIANOV, A. V., RICHMOND, J. C., BARRETT, G. R. & GILLQUIST, J. 1989. A multicenter study on the results of anterior cruciate ligament reconstruction using a Dacron ligament prosthesis in" salvage" cases. *The American journal of sports medicine,* 17**,** 380-386.

MACKIE, E. J. 1997. Tenascin-C. *The International Journal of Biochemistry & Cell Biology,* 29**,** 1133-1137.

MACLEAN, S. B. A. & GRATZER, P. F. 2011. Effect of basic fibroblast growth factor on the cellular repopulation of decellularized anterior cruciate ligament allografts. *Journal Of Tissue Engineering & Regenerative Medicine,* 5**,** 201-9.

MACNICOL, M. F., PENNY, I. D. & SHEPPARD, L. 1991. Early results of the Leeds-Keio anterior cruciate ligament replacement. *Journal of Bone & Joint Surgery - British Volume,* 73**,** 377-80.

MAEDA, E., FLEISCHMANN, C., MEIN, C. A., SHELTON, J. C., BADER, D. L. & LEE, D. A. 2010a. Functional analysis of tenocytes gene expression in tendon fascicles subjected to cyclic tensile strain. *Connective tissue research,* 51**,** 434-444.

MAEDA, E., SHELTON, J. C., BADER, D. L. & LEE, D. A. 2009. Differential regulation of gene expression in isolated tendon fascicles exposed to cyclic tensile strain in vitro. *Journal of Applied Physiology,* 106**,** 506-512.

MAEDA, E., TOHYAMA, H., NOGUCHI, H., YASUDA, K. & HAYASHI, K. 2010b. Effects of maturation on the mechanical properties of regenerated and residual tissues in the rabbit patellar tendon after resection of its central one-third. *Clinical Biomechanics,* 25**,** 953-958.

MAIER, S., LUTZ, R., GELMAN, L., SARASA-RENEDO, A., SCHENK, S., GRASHOFF, C. & CHIQUET, M. 2008. Tenascin-C induction by cyclic strain requires integrin-linked kinase. *Biochimica et Biophysica Acta (BBA) - Molecular Cell Research,* 1783**,** 1150-1162.

MAJEWSKI, M., BETZ, O., OCHSNER, P. E., LIU, F., PORTER, R. M. & EVANS, C. H. 2008. Ex vivo adenoviral transfer of bone morphogenetic protein 12 (BMP-12) cDNA improves Achilles tendon healing in a rat model. *Gene Therapy,* 15**,** 1139-46.

MAREDDY, S., CRAWFORD, R., BROOKE, G. & XIAO, Y. 2007. Clonal isolation and characterization of bone marrow stromal cells from patients with osteoarthritis. *Tissue engineering,* 13**,** 819-829.

MARQUIS, R., RUTHERFORD, G., FARACI, M. & SHIN, S. 1995. Sporicidal action of peracetic acid and protective effects of transition metal ions. *Journal of industrial microbiology,* 15**,** 486-492.

MARTÍNEZ DE ALBORNOZ TORRENTE, P. & FORRIOL, F. 2012. Changes in synovial fluid in different knee-joint diseases. *Revista Española de Cirugía Ortopédica y Traumatología (English Edition),* 56**,** 140-148.

MARUMO, K., KUMAGAE, Y., TANAKA, T. & FUJII, K. 2000. Long-term results of anterior cruciate ligament reconstruction using semitendinosus and gracilis tendons with Kennedy ligament augmentation device compared with patellar tendon autografts. *Journal of Long-Term Effects of Medical Implants,* 10**,** 251-65.

MASCARENHAS, R. & MACDONALD, P. B. 2008. Anterior cruciate ligament reconstruction: a look at prosthetics - past, present and possible future. *Mcgill J Med,* 11**,** 29-37.

MCBEATH, R., PIRONE, D. M., NELSON, C. M., BHADRIRAJU, K. & CHEN, C. S. 2004. Cell shape, cytoskeletal tension, and RhoA regulate stem cell lineage commitment. *Developmental Cell,* 6**,** 483-495.

MCNEILLY, C., BANES, A., BENJAMIN, M. & RALPHS, J. 1996. Tendon cells in vivo form a three dimensional network of cell processes linked by gap junctions. *Journal of anatomy,* 189**,** 593.

MEHR, D., PARDUBSKY, P. D., MARTIN, J. A. & BUCKWALTER, J. A. 2000. Tenascin-C in tendon regions subjected to compression. *Journal of Orthopaedic Research,* 18**,** 537-45.

MENG, H., WANG, Z., WANG, W., LI, W., WU, Q., LEI, X., OUYANG, X. & LIANG, Z. 2014. Effect of osteopontin in regulating bone marrow mesenchymal stem cell treatment of skin wounds in diabetic mice. *Diabetes/Metabolism Research Reviews,* 30**,** 457-66.

MILLER, M. D., PETERS, C. L. & ALLEN, B. 2006. Early Aseptic Loosening of a Total Knee Arthroplasty Due to Gore-Tex Particle–Induced Osteolysis. *The Journal of Arthroplasty,* 21**,** 765-770.

MIRALLES, F., POSERN, G., ZAROMYTIDOU, A.-I. & TREISMAN, R. 2003. Actin dynamics control SRF activity by regulation of its coactivator MAL. *Cell,* 113**,** 329-42.

MIRZA, F., MAI, D. D., KIRKLEY, A., FOWLER, P. J. & AMENDOLA, A. 2000. Management of injuries to the anterior cruciate ligament: results of a survey of orthopaedic surgeons in Canada. *Clinical Journal of Sport Medicine,* 10**,** 85-8.

MIYASAKA, K. C., DANIEL, D. M., STONE, M. L. & HIRSHMAN, P. 1991. The incidence of knee ligament injuries in the general population *American Journal of Knee Surgery,* 4**,** 3-8.

MOYEN, B., JENNY, J., MANDRINO, A. & LERAT, J. 1992. Comparison of reconstruction of the anterior cruciate ligament with and without a Kennedy ligament-augmentation device. A randomized, prospective study. *JOURNAL OF BONE AND JOINT SURGERY-AMERICAN VOLUME-,* 74**,** 1313-1313.

MUREN, O., DAHLSTEDT, L. & DALEN, N. 1995. Reconstruction of old anterior cruciate ligament injuries. No difference between the Kennedy LAD-method and traditional patellar tendon graft in a prospective randomized study of 40 patients with 4-year follow-up. *Acta Orthopaedica Scandinavica,* 66**,** 118-22.

MURRAY, A. W. & MACNICOL, M. 2004. 10–16 year results of Leeds-Keio anterior cruciate ligament reconstruction. *The Knee,* 11**,** 9-14.

MURRAY, M. M. & SPECTOR, M. 1999. Fibroblast distribution in the anteromedial bundle of the human anterior cruciate ligament: the presence of alpha-smooth muscle actin-positive cells. *Journal of Orthopaedic Research,* 17**,** 18-27.

NAU, T., LAVOIE, P. & DUVAL, N. 2002. A new generation of artificial ligaments in reconstruction of the anterior cruciate ligament. Two-year follow-up of a randomised trial. *Journal of Bone & Joint Surgery - British Volume,* 84**,** 356-60.

NEBELUNG, W. & WUSCHECH, H. 2005. Thirty-five years of follow-up of anterior cruciate ligament-deficient knees in high-level athletes. *Arthroscopy,* 21**,** 696-702.

NEREM, R. M. 2000. The challange of imitating nature. *In:* LANZA, R. P., LANGER, R. & VACANTI, J. (eds.) *Principles of tissue engineering.* 2nd ed. San Diego: Academic press.

NOLAN, T., HANDS, R. E. & BUSTIN, S. A. 2006. Quantification of mRNA using real-time RT-PCR. *Nature protocols,* 1**,** 1559-1582.

NOMURA, E., INOUE, M. & SUGIURA, H. 2005. Histological evaluation of medial patellofemoral ligament reconstructed using the Leeds–Keio ligament prosthesis. *Biomaterials,* 26**,** 2663-2670.

NORDIN, M. A. F., VICTOR H. (ed.) 2001a. *Basic Biomechanics of the Musculoskeletal System,* Philadelphia: Lippincott Williams & Wilkins.

NORDIN, M. L., TOBIAS. CAMPELLO, MARCO. 2001b. Tendons and Ligaments. *In:* NORDIN, M. A. F., VICTOR H. (ed.) *Basic Biomechanics of the Musculoskeletal System.* 3rd ed. Philadelphia: Lippincott Williams & Wilkins.

NOURISSAT, G., BERENBAUM, F. & DUPREZ, D. 2015. Tendon injury: from biology to tendon repair. *Nature Reviews Rheumatology,* 11**,** 223-233.

NOYES, F. R., MANGINE, R. E. & BARBER, S. 1987. Early knee motion after open and arthroscopic anterior cruciate ligament reconstruction. *The American journal of sports medicine,* 15**,** 149-160.

O'BRIEN, M., OKRAGLY, A., WARNER, T., KALIL, R. & WOLSWIJK, G. 1998. DeadEndTM Colorimetric Apoptosis Detection System: Applications in Pathology. *Promega Notes,* 69**,** 2-5.

O'CONNOR, B. L., VISCO, D. M., BRANDT, K. D., MYERS, S. L. & KALASINSKI, L. A. 1992. Neurogenic acceleration of osteoarthrosis. The effects of previous neurectomy of the articular nerves on the development of osteoarthrosis after transection of the anterior cruciate ligament in dogs. *Journal of Bone & Joint Surgery - American Volume,* 74**,** 367-76.

O'DONOGHUE, D. O. N. H., FRANK, G. R., JETER, G. L., JOHNSON, W., ZEIDERS, J. W. & KENYON, R. 1971. Repair and Reconstruction of the Anterior Cruciate Ligament in Dogs FACTORS INFLUENCING LONG-TERM RESULTS. *The Journal of Bone and Joint Surgery (American),* 53**,** 710-718.

OATIS, C. A. (ed.) 2004. *Kinesiology : the mechanics and pathomechanics of human movement,* Philadelphia: Lippincott William & Wilkins.

ODENSTEN, M. & GILLQUIST, J. 1985. Functional anatomy of the anterior cruciate ligament and a rationale for reconstruction. *Journal of Bone & Joint Surgery - American Volume,* 67**,** 257-62.

OGILVIE-HARRIS, D. J. & GIDDENS, J. 1994. Hoffa's disease: Arthroscopic resection of the infrapatellar fat pad. *Arthroscopy: The Journal of Arthroscopic & Related Surgery,* 10**,** 184-187.

OLSON, E. J., KANG, J. D., FU, F. H., GEORGESCU, H. I., MASON, G. C. & EVANS, C. H. 1988. The biomechanical and histological effects of artificial ligament wear particles: in vitro and in vivo studies. *Am J Sports Med,* 16**,** 558-70.

OMAE, H., ZHAO, C., SUN, Y. L., AN, K. N. & AMADIO, P. C. 2009. Multilayer tendon slices seeded with bone marrow stromal cells: a novel composite for tendon engineering. *Journal of Orthopaedic Research,* 27**,** 937-942.

ORR, A. W., HELMKE, B. P., BLACKMAN, B. R. & SCHWARTZ, M. A. 2006. Mechanisms of mechanotransduction. *Developmental cell,* 10**,** 11-20.

PAPAGEORGIOU, C. D., KOSTOPOULOS, V. K., MOEBIUS, U. G., PETROPOULOU, K. A., GEORGOULIS, A. D. & SOUCACOS, P. N. 2001. Patellar fractures associated with medial-third bone-patellar tendon-bone autograft ACL reconstruction. *Knee Surgery, Sports Traumatology, Arthroscopy,* 9**,** 151-4.

PAS, J., WYSZKO, E., ROLLE, K., RYCHLEWSKI, L., NOWAK, S., ŻUKIEL, R. & BARCISZEWSKI, J. 2006. Analysis of structure and function of tenascin-C. *The International Journal of Biochemistry & Cell Biology,* 38**,** 1594-1602.

PERDIKOGIANNI, C., DIMITRIOU, H., STIAKAKI, E., MARTIMIANAKI, G. & KALMANTI, M. 2008. Could cord blood be a source of mesenchymal stromal cells for clinical use? *Cytotherapy,* 10**,** 452-459.

PEREIRA, R. F., HALFORD, K. W., O'HARA, M. D., LEEPER, D. B., SOKOLOV, B. P., POLLARD, M. D., BAGASRA, O. & PROCKOP, D. J. 1995. Cultured adherent cells from marrow can serve as long-lasting precursor cells for bone, cartilage, and lung in irradiated mice. *Proceedings of the National Academy of Sciences,* 92**,** 4857-4861.

PETERSEN, W. & LAPRELL, H. 2000. Insertion of autologous tendon grafts to the bone: a histological and immunohistochemical study of hamstring and patellar tendon grafts. *Knee Surgery, Sports Traumatology, Arthroscopy,* 8**,** 26-31.

PETERSEN, W. & TILLMANN, B. 1999. Blood and lymph supply of the anterior cruciate ligament: a cadaver study. *Knee Surgery, Sports Traumatology, Arthroscopy,* 7**,** 42-50.

PETRONILLI, V., MIOTTO, G., CANTON, M., BRINI, M., COLONNA, R., BERNARDI, P. & DI LISA, F. 1999. Transient and Long-Lasting Openings of the Mitochondrial Permeability Transition Pore Can Be Monitored Directly in Intact Cells by Changes in Mitochondrial Calcein Fluorescence. *Biophysical journal,* 76**,** 725-734.

PHINNEY, D. G. & PROCKOP, D. J. 2007. Concise Review: Mesenchymal Stem/Multipotent Stromal Cells: The State of Transdifferentiation and Modes of Tissue Repair—Current Views. *STEM CELLS,* 25**,** 2896-2902.

PIRJALI, T., AZARPIRA, N., AYATOLLAHI, M., AGHDAIE, M. H., GERAMIZADEH, B. & TALAI, T. 2013. Isolation and Characterization of Human Mesenchymal Stem Cells Derived from Human Umbilical Cord Wharton's Jelly and Amniotic Membrane. *International journal of organ transplantation medicine,* 4**,** 111-6.

PITTENGER, M. F., MACKAY, A. M., BECK, S. C., JAISWAL, R. K., DOUGLAS, R., MOSCA, J. D., MOORMAN, M. A., SIMONETTI, D. W., CRAIG, S. & MARSHAK, D. R. 1999. Multilineage potential of adult human mesenchymal stem cells. *Science,* 284**,** 143-147.

POLLARD, C. D., BRAUN, B. & HAMILL, J. 2006. Influence of gender, estrogen and exercise on anterior knee laxity. *Clinical Biomechanics,* 21**,** 1060-1066.

POLLARD, T. D., EARNSHAW, W. C. & LIPPINCOTT-SCHWARTZ, J. 2008. Cell of extra cellular matrix and immune system. *Cell Biology.* Philadelphia: Saunders Elsiever.

PRADHAN, S. M., KATTI, K. S. & KATTI, D. R. 2012. Structural hierarchy controls deformation behavior of collagen. *Biomacromolecules,* 13**,** 2562-9.

PRIDGEN, B. C., WOON, C. Y. L., KIM, M., THORFINN, J., LINDSEY, D., PHAM, H. & CHANG, J. 2011. Flexor tendon tissue engineering: acellularization of human flexor tendons with preservation of biomechanical properties and biocompatibility. *Tissue Engineering Part C: Methods,* 17**,** 819-828.

PRUSS, A., BAUMANN, B., SEIBOLD, M., KAO, M., TINTELNOT, K., VON VERSEN, R., RADTKE, H., DORNER, T., PAULI, G. & GOBEL, U. B. 2001. Validation of the sterilization procedure of allogeneic avital bone transplants using peracetic acid-ethanol. *Biologicals,* 29**,** 59-66.

PRUSS, A., KAO, M., KIESEWETTER, H., VON VERSEN, R. & PAULI, G. 1999. Virus safety of avital bone tissue transplants: evaluation of sterilization steps of spongiosa cuboids using a peracetic acid–methanol mixture. *Biologicals,* 27**,** 195-201.

QI, J., CHI, L., BYNUM, D. & BANES, A. J. 2011. Gap junctions in IL-1β-mediated cell survival response to strain. *Journal of Applied Physiology,* 110**,** 1425-1431.

QI, M. C., HU, J., ZOU, S. J., CHEN, H. Q., ZHOU, H. X. & HAN, L. C. 2008. Mechanical strain induces osteogenic differentiation: Cbfa1 and Ets-1 expression in stretched rat mesenchymal stem cells. *Int J Oral Maxillofac Surg,* 37.

QIAGEN 2012a. RNeasy Mini Handbook. June 2012 ed.

QIAGEN 2012b. RNeasy mini handbook 06/2012 ed.: Qiagen.

RABENSTEIN, M., HUCKLENBROICH, J., WILLUWEIT, A., LADWIG, A., FINK, G. R., SCHROETER, M., LANGEN, K.-J. & RUEGER, M. A. 2015. Osteopontin mediates survival, proliferation and migration of neural stem cells through the chemokine receptor CXCR4. *Stem Cell Research & Therapy,* 6**,** 99.

RAGHAVAN, S. S., WOON, C. Y. L., KRAUS, A., MEGERLE, K., CHOI, M. S. S., PRIDGEN, B. C., PHAM, H. & CHANG, J. 2012. Human flexor tendon tissue engineering: decellularization of human flexor tendons reduces immunogenicity in vivo. *Tissue engineering. Part A.,* 18**,** 796-805.

RASHID, S., SALACINSKI, H., BUTTON, M., FULLER, B., HAMILTON, G. & SEIFALIAN, A. 2004. Cellular Engineering of Conduits for Coronary and Lower Limb Bypass Surgery: Role of Cell Attachment Peptides and Pre-conditioning in Optimising Smooth Muscle Cells (SMC) Adherence to Compliant Poly (carbonate–urea) urethane (MyoLink™) Scaffolds. *European Journal of Vascular and Endovascular Surgery,* 27**,** 608-616.

RASINI, V., DOMINICI, M., KLUBA, T., SIEGEL, G., LUSENTI, G., NORTHOFF, H., HORWITZ, E. M. & SCHÄFER, R. 2013. Mesenchymal stromal/stem cells markers in the human bone marrow. *Cytotherapy,* 15**,** 292-306.

RASMUSSEN, T. J., FEDER, S. M., BUTLER, D. L. & NOYES, F. R. 1994. The effects of 4 Mrad of gamma irradiation on the initial mechanical properties of bone-patellar tendon-bone grafts. *Arthroscopy,* 10**,** 188-97.

REDICK, S. D. & SCHWARZBAUER, J. E. 1995. Rapid intracellular assembly of tenascin hexabrachions suggests a novel cotranslational process. *Journal of Cell Science,* 108**,** 1761-1769.

RILEY, G. 2004. The pathogenesis of tendinopathy. A molecular perspective. *Rheumatology,* 43**,** 131-142.

ROBAYO, L. M., MOULIN, V. J., TREMBLAY, P., CLOUTIER, R., LAMONTAGNE, J., LARKIN, A.-M., CHABAUD, S., SIMON, F., ISLAM, N. & GOULET, F. 2011. New ligament healing model based on tissue-engineered collagen scaffolds. *Wound Repair & Regeneration,* 19**,** 38-48.

ROBERTS, T. S., DREZ, D., JR., MCCARTHY, W. & PAINE, R. 1991. Anterior cruciate ligament reconstruction using freeze-dried, ethylene oxide-sterilized, bone-patellar tendon-bone allografts. Two year results in thirty-six patients.[Erratum appears in Am J Sports Med 1991 May-Jun;19(3):272]. *American Journal of Sports Medicine,* 19**,** 35-41.

ROBSON, A. M. 1903. VI. Ruptured Crucial Ligaments and their Repair by Operation. *Annals of Surgery,* 37**,** 716.

RODRIGUEZ, M. L., MCGARRY, P. J. & SNIADECKI, N. J. 2013. Review on Cell Mechanics: Experimental and Modeling Approaches. *Applied Mechanics Reviews,* 65.

ROSKELLEY, C. D., SREBROW, A. & BISSELL, M. J. 1995. A hierarchy of ECM-mediated signalling regulates tissue-specific gene expression. *Current Opinion in Cell Biology,* 7**,** 736-47.

ROSS, S. E., HEMATI, N., LONGO, K. A., BENNETT, C. N., LUCAS, P. C., ERICKSON, R. L. & MACDOUGALD, O. A. 2000. Inhibition of adipogenesis by Wnt signaling. *Science,* 289**,** 950-953.

RUSHTON, N., DANDY, D. & NAYLOR, C. 1983. The clinical, arthroscopic and histological findings after replacement of the anterior cruciate ligament with carbon-fibre. *J. Bone Joint Surg. Br,* 65**,** 308.

RUSSELL, B., MOTLAGH, D. & ASHLEY, W. W. 2000. Form follows function: how muscle shape is regulated by work. *Journal of Applied Physiology,* 88**,** 1127-1132.

SABISTON, P., FRANK, C., LAM, T. & SHRIVE, N. 1990. Allograft ligament transplantation. A morphological and biochemical evaluation of a medial collateral ligament complex in a rabbit model. *American Journal of Sports Medicine,* 18**,** 160-8.

SACHS, D. H. 1994. The pig as a potential xenograft donor. *Veterinary Immunology and Immunopathology,* 43**,** 185-191.

SAHOO, S., ANG, L.-T., CHO-HONG GOH, J. & TOH, S.-L. 2010. Bioactive nanofibers for fibroblastic differentiation of mesenchymal precursor cells for ligament/tendon tissue engineering applications. *Differentiation,* 79**,** 102-10.

SAKANE, M., FOX, R. J., WOO, S. L., LIVESAY, G. A., LI, G. & FU, F. H. 1997. In situ forces in the anterior cruciate ligament and its bundles in response to anterior tibial loads. *Journal of Orthopaedic Research,* 15**,** 285-93.

SALGADO, A. J., COUTINHO, O. P. & REIS, R. L. 2004. Bone tissue engineering: state of the art and future trends. *Macromolecular Bioscience,* 4**,** 743-65.

SALTZMAN, W. M. 2000. Cells interactions with polymers. *In:* LANZA, R. P., LANGER, R. & VACANTI, J. P. (eds.) *Principles of tissue engineering.* 2nd ed. San Diego: Elsiever.

SARASA-RENEDO, A., TUNÇ-CIVELEK, V. & CHIQUET, M. 2006. Role of RhoA/ROCK-dependent actin contractility in the induction of tenascin-C by cyclic tensile strain. *Experimental Cell Research,* 312**,** 1361-1370.

SCHEFFLER, S., TRAUTMANN, S., SMITH, M., KALUS, U., VON VERSEN, R., PAULI, G. & PRUSS, A. 2007. No influence of collagenous proteins of Achilles tendon, skin and cartilage on the virus-inactivating efficacy of peracetic acid-ethanol. *Biologicals,* 35**,** 355-9.

SCHINDHELM, K., ROGERS, G. J., MILTHORPE, B. K., HALL, P. J., HOWLETT, C. R., SEKEL, R., GOLDBERG, J. & VIGLIONE, W. 1991. Autograft and Leeds-Keio reconstructions of the ovine anterior cruciate ligament. *Clinical Orthopaedics & Related Research***,** 278-93.

SCHNEIDER, P. R. A., BUHRMANN, C., MOBASHERI, A., MATIS, U. & SHAKIBAEI, M. 2011. Three- dimensional high- density co- culture with primary tenocytes induces tenogenic differentiation in mesenchymal stem cells. *Journal of Orthopaedic Research,* 29**,** 1351-1360.

SCHUTTE, M. J., DABEZIES, E. J., ZIMNY, M. L. & HAPPEL, L. T. 1987. Neural anatomy of the human anterior cruciate ligament. *Journal of Bone & Joint Surgery - American Volume,* 69**,** 243-7.

SCHWEITZER, R., CHYUNG, J. H., MURTAUGH, L. C., BRENT, A. E., ROSEN, V., OLSON, E. N., LASSAR, A. & TABIN, C. J. 2001. Analysis of the tendon cell fate using Scleraxis, a specific marker for tendons and ligaments. *Development,* 128**,** 3855-3866.

SEGAWA, H., OMORI, G. & KOGA, Y. 2001. Long-term results of non-operative treatment of anterior cruciate ligament injury. *Knee,* 8**,** 5-11.

SERBAN, M. A., LIU, Y. & PRESTWICH, G. D. 2008. Effects of extracellular matrix analogues on primary human fibroblast behavior. *Acta biomaterialia,* 4**,** 67-75.

SETHE, S., SCUTT, A. & STOLZING, A. 2006. Aging of mesenchymal stem cells. *Ageing Research Reviews,* 5**,** 91-116.

SHARROCKS, A. 1994. *PCR technology, current innovations,* Florida, CRC press.

SILVAGGIO, V. J., FU, F. H., GEORGESCU, H. I. & EVANS, C. H. 1993. The induction of IL-1 by freeze-dried ethylene oxide-treated bone-patellar tendon-bone allograft wear particles: an in vitro study. *Arthroscopy,* 9**,** 82-6.

SJÖLANDER, P., JOHANSSON, H. & DJUPSJÖBACKA, M. 2002. Spinal and supraspinal effects of activity in ligament afferents. *Journal of Electromyography and Kinesiology,* 12**,** 167-176.

SMITH, S. A. 1918. The diagnosis and treatment of injuries to the crucial ligaments. *British Journal of Surgery,* 6**,** 176-189.

SNIECINSKI, I. 1991. Use of peripheral stem cells in transplantation. *Transfusion Science,* 12**,** 77-80.

SNOOK, G. A. 1983. A short history of the anterior cruciate ligament and the treatment of tears. *Clinical Orthopaedics and Related Research,* 172**,** 11-13.

SOKAL, R. R. & ROHLF, F. 1981. Biometry (2nd edn). *New York: WH Feeman and Company,* 668.

SOKAL, R. R. A. R., F. JAMES 1995. *Biometry, the principles and practice of statistics in biological research,* New York, W.H. Freeman and company.

SONG, L., WANG, L., SHAH, P. K., CHAUX, A. & SHARIFI, B. G. 2010. Bioengineered vascular graft grown in the mouse peritoneal cavity. *Journal of Vascular Surgery,* 52**,** 994-1002.e2.

STEHLE, J., WEBER, M., HEYMER, A., SCHÜTZE, N., JAKOB, F., EULERT, J. & NÜTH, U. 2006. Effects of cyclic stretching on anterior cruciate ligament-constructs fabricated from human MSCs and collagen type I gels. *Journal of Biomechanics,* 39, Supplement 1**,** S60.

STEINERT, A. F., WEBER, M., KUNZ, M., PALMER, G. D., NOTH, U., EVANS, C. H. & MURRAY, M. M. 2008. In situ IGF-1 gene delivery to cells emerging from the injured anterior cruciate ligament. *Biomaterials,* 29**,** 904-16.

STONE, K. R., WALGENBACH, A. W., TUREK, T. J., SOMERS, D. L., WICOMB, W. & GALILI, U. 2007. Anterior cruciate ligament reconstruction with a porcine xenograft: a serologic, histologic, and biomechanical study in primates. *Arthroscopy: The Journal of Arthroscopic & Related Surgery,* 23**,** 411-419. e1.

SUN, K., ZHANG, J., WANG, Y., XIA, C., ZHANG, C., YU, T. & TIAN, S. 2011. Arthroscopic anterior cruciate ligament reconstruction with at least 2.5 years' follow-up comparing hamstring tendon autograft and irradiated allograft. *Arthroscopy,* 27**,** 1195-202.

TAMADA, Y. & IKADA, Y. 1994. Fibroblast growth on polymer surfaces and biosynthesis of collagen. *Journal of Biomedical Materials Research,* 28**,** 783-9.

THELLIN, O., ZORZI, W., LAKAYE, B., DE BORMAN, B., COUMANS, B., HENNEN, G., GRISAR, T., IGOUT, A. & HEINEN, E. 1999. Housekeeping genes as internal standards: use and limits. *Journal of Biotechnology,* 75**,** 291-295.

THOMOPOULOS, S., ZAMPIAKIS, E., DAS, R., SILVA, M. J. & GELBERMAN, R. H. 2008. The effect of muscle loading on flexor tendon- to- bone healing in a canine model. *Journal of Orthopaedic Research,* 26**,** 1611-1617.

THOMSON, L. A., HOULTON, J. E. F., ALLEN, M. J. & RUSHTON, N. 1994. Replacement of the anterior cruciate ligament with a coated carbon fibre prosthesis: a biomechanical study in goats. *The Knee,* 1**,** 139-145.

THORNTON, G. A. F., CB AND SHRIVE, NG 2006. Ligament. *In:* NIGG, B. M. H., WALTER (ed.) *Biomechanics of the Musculo-skeletal System.* 3rd ed. Calgary, Alberta, Canada: John Wiley & Sons.

TRINKHAUS, J. P. 1984. *Cells into organs. The Forces that shape the embryo*

New Jersey, Prentice-Hall, Englewood Cliffs, N.J.

TROJANI, C., SANÉ, J. C., COSTE, J. S. & BOILEAU, P. 2009. Four-strand hamstring tendon autograft for ACL reconstruction in patients aged 50 years or older. *Orthopaedics & Traumatology: Surgery & Research,* 95**,** 22-27.

TSUZAKI, M., YAMAUCHI, M. & BANES, A. J. 1993. Tendon Collagens: Extracellular Matrix Composition in Shear Stress and Tensile Components of Flexor Tendons. *Connective Tissue Research,* 29**,** 141-152.

TUCKER, R. P. & CHIQUET-EHRISMANN, R. 2015. Tenascin-C: Its functions as an integrin ligand. *The International Journal of Biochemistry & Cell Biology,* 65**,** 165-168.

VACANTI, J. P. & LANGER, R. 1993. Tissue Engineering. *Science,* 260**,** 920-932.

VACANTI, J. P. & LANGER, R. 1999. Tissue engineering: the design and fabrication of living replacement devices for surgical reconstruction and transplantation. *Lancet,* 354 Suppl 1**,** SI32-4.

VALENTIN, J. E., BADYLAK, J. S., MCCABE, G. P. & BADYLAK, S. F. 2006. Extracellular matrix bioscaffolds for orthopaedic applications - A comparative histologic study. *Journal of Bone and Joint Surgery-American Volume,* 88A**,** 2673-2686.

VASSILIS, V. 2013. *Development of methods for the attachment of soft-tissues to implants.* PhD, University of Leeds.

VENTURA, A., TERZAGHI, C., LEGNANI, C., BORGO, E. & ALBISETTI, W. 2010. Synthetic grafts for anterior cruciate ligament rupture: 19-year outcome study. *Knee,* 17**,** 108-113.

VIEIRA, A. C., GUEDES, R. M. & MARQUES, A. T. 2009. Development of ligament tissue biodegradable devices: a review. *Journal of Biomechanics,* 42**,** 2421-30.

VIMALRAJ, S., ARUMUGAM, B., MIRANDA, P. J. & SELVAMURUGAN, N. 2015. Runx2: Structure, function, and phosphorylation in osteoblast differentiation. *International Journal of Biological Macromolecules,* 78**,** 202-208.

WAGGETT, A. D., BENJAMIN, M. & RALPHS, J. R. 2006. Connexin 32 and 43 gap junctions differentially modulate tenocyte response to cyclic mechanical load. *European Journal of Cell Biology,* 85**,** 1145-1154.

WALTERS, W. A., CAPORASO, J. G., LAUBER, C. L., BERG-LYONS, D., FIERER, N. & KNIGHT, R. 2011. PrimerProspector: de novo design and taxonomic analysis of barcoded polymerase chain reaction primers. *Bioinformatics,* 27**,** 1159-1161.

WANG, I. N. E., MITROO, S., CHEN, F. H., LU, H. H. & DOTY, S. B. 2006. Age-dependent changes in matrix composition and organization at the ligament-to-bone insertion. *Journal of Orthopaedic Research,* 24**,** 1745-55.

WATANABE, R. S. 1974. Embryology of the human hip. *Clinical Orthopaedics & Related Research***,** 8-26.

WEST, D. C., HAMPSON, I. N., ARNOLD, F. & KUMAR, S. 1985. Angiogenesis induced by degradation products of hyaluronic acid. *Science,* 228**,** 1324-6.

WIIG, M. E., AMIEL, D., VANDEBERG, J., KITABAYASHI, L., HARWOOD, F. L. & ARFORS, K. E. 2005. The early effect of high molecular weight hyaluronan (hyaluronic acid) on anterior cruciate ligament healing: an experimental study in rabbits. *Journal of Orthopaedic Research,* 8**,** 425-434.

WINTER, J. 2016. Main procedures and interventions: summary. *2015-2016.* England: NHS Digital, Hospital episode statistics for England.

WOO, S. L., GOMEZ, M. A., SITES, T. J., NEWTON, P. O., ORLANDO, C. A. & AKESON, W. H. 1987. The biomechanical and morphological changes in the medial collateral ligament of the rabbit after immobilization and remobilization. *Journal of Bone & Joint Surgery - American Volume,* 69**,** 1200-11.

WOO, S. L., HOLLIS, J. M., ADAMS, D. J., LYON, R. M. & TAKAI, S. 1991. Tensile properties of the human femur-anterior cruciate ligament-tibia complex. The effects of specimen age and orientation. *American Journal of Sports Medicine,* 19**,** 217-25.

WOO, S. L. Y., ABRAMOWITCH, S. D., KILGER, R. & LIANG, R. 2006. Biomechanics of knee ligaments: injury, healing, and repair. *Journal of Biomechanics,* 39**,** 1-20.

WOO, S. L. Y., FISHER, M. B. & FEOLA, A. J. 2008. Contribution of biomechanics to management of ligament and tendon injuries. *Molecular & Cellular Biomechanics: MCB,* 5**,** 49-68.

WOON, C. Y., PRIDGEN, B. C., KRAUS, A., BARI, S., PHAM, H. & CHANG, J. 2011. Optimization of human tendon tissue engineering: peracetic acid oxidation for enhanced reseeding of acellularized intrasynovial tendon. *Plastic & Reconstructive Surgery,* 127**,** 1107-17.

YAMADA, K., GRIESEMER, A. & OKUMI, M. 2005. Pigs as xenogeneic donors. *Transplantation Reviews,* 19**,** 164-177.

YAMAMOTO, E., HAYASHI, K. & YAMAMOTO, N. 1999. Mechanical properties of collagen fascicles from stress-shielded patellar tendons in the rabbit. *Clinical Biomechanics,* 14**,** 418-425.

YANG, C., ZHANG, X., GUO, Y., MENG, F., SACHS, F. & GUO, J. 2015. Mechanical dynamics in live cells and fluorescence-based force/tension sensors. *Biochimica et Biophysica Acta (BBA) - Molecular Cell Research,* 1853**,** 1889-1904.

YAZDANI, S. K., WATTS, B., MACHINGAL, M., JARAJAPU, Y. P., VAN DYKE, M. E. & CHRIST, G. J. 2009. Smooth muscle cell seeding of decellularized scaffolds: the importance of bioreactor preconditioning to development of a more native architecture for tissue-engineered blood vessels. *Tissue Engineering Part A,* 15**,** 827-840.

YAZDANSHENAS, H., MADADI, F., MADADI, F., WASHINGTON III, E. R., JONES, K. & SHAMIE, A. N. 2015. Patellar tendon donor-site healing during six and twelve months after Anterior Cruciate Ligament Reconstruction. *Journal of Orthopaedics,* 12**,** 179-183.

YE, J., COULOURIS, G., ZARETSKAYA, I., CUTCUTACHE, I., ROZEN, S. & MADDEN, T. L. 2012. Primer-BLAST: a tool to design target-specific primers for polymerase chain reaction. *BMC bioinformatics,* 13**,** 134.

YE, X., LU, L., KOLEWE, M. E., PARK, H., LARSON, B. L., KIM, E. S. & FREED, L. E. 2013. A biodegradable microvessel scaffold as a framework to enable vascular support of engineered tissues. *Biomaterials,* 34**,** 10007-10015.

YOUNG III, S. D. & TOTH, A. P. 2006. Complications of Allograft Use in Anterior Cruciate Ligament Reconstruction. *Operative Techniques in Sports Medicine,* 14**,** 20-26.

ZAVRAS, T. D., MACKENNEY, R. P. & AMIS, A. A. 1995. The natural history of anterior cruciate ligament reconstruction using patellar tendon autograft. *The Knee,* 2**,** 211-217.

ZHANG, J., LI, Z.-G., SI, Y.-M., CHEN, B. & MENG, J. 2014. The difference on the osteogenic differentiation between periodontal ligament stem cells and bone marrow mesenchymal stem cells under inflammatory microenviroments. *Differentiation,* 88**,** 97-105.

ZHANG, J. & WANG, J. H. C. 2010. Mechanobiological response of tendon stem cells: implications of tendon homeostasis and pathogenesis of tendinopathy. *Journal of Orthopaedic Research,* 28**,** 639-643.

ZHANG, L., KAHN, C. J. F., CHEN, H.-Q., TRAN, N. & WANG, X. 2008. Effect of uniaxial stretching on rat bone mesenchymal stem cell: Orientation and expressions of collagen types I and III and tenascin-C. *Cell Biology International,* 32**,** 344-352.

ZHANG, L., MU, X., FU, J. & ZHOU, Z. 2007. In vitro cytotoxicity assay with selected chemicals using human cells to predict target-organ toxicity of liver and kidney. *Toxicology in Vitro,* 21**,** 734-740.

ZHENG, M. H., CHEN, J., KIRILAK, Y., WILLERS, C., XU, J. & WOOD, D. 2005. Porcine small intestine submucosa (SIS) is not an acellular collagenous matrix and contains porcine DNA: Possible implications in human implantation. *Journal of Biomedical Materials Research Part B-Applied Biomaterials,* 73B**,** 61-67.

ZOU, C., SONG, G., LUO, Q., YUAN, L. & YANG, L. 2011. Mesenchymal stem cells require integrin beta1 for directed migration induced by osteopontin in vitro. *In Vitro Cellular & Developmental Biology. Animal,* 47**,** 241-50.